Fall 9-23-2013

DNA Interactions and Photocleavage by Anthracene, Acridine, and Carbocyanine-Based Chromophores

Carla Mapp

DNA INTERACTIONS AND PHOTOCLEAVAGE BY ANTHRACENE, ACRIDINE, AND CARBOCYANINE-BASED CHROMOPHORES

by

CARLA TERRY MAPP

Under the Direction of Dr. Kathryn B. Grant

ABSTRACT

The interaction of small molecules with DNA has been extensively studied and has produced a large catalogue of molecules that non-covalently bind to DNA though groove binding, intercalation, electrostatics, or a combination of these binding modes. Anthracene, acridine, and carbocyanine-based chromophores have been examined for their DNA binding properties and photo-reactivities. Their planar aromatic structures make them ideal chromophores that can be used to probe DNA structural interactions and binding patterns. We have studied DNA binding and photocleavgage properties of a bisacridine chromophore joined by a 2,6-bis(aminomethyl)pyridine copper-binding linker (Chapter II), a series of 9-aminomethyl anthracene chromophores (Chapters III and IV), both under conditions of high and low ionic

strength, as well as a series of pentamethine linked symmetrical carbocyanine dyes (Chapter V). In Chapter II we present data showing that high ionic strength efficiently increases copper(II)-dependent photocleavage of plasmid DNA by the bisacridine based chromophore (419 nm, pH 7.0). In Chapters III and IV, using an pyridine *N*-substituted 9-(aminomethyl)anthracene (Chapter III), a bis-9-(aminomethyl)anthracene, and its mono 9-(aminomethyl)anthracene analogue (Chapter IV), pUC19 plasmid DNA was photo-converted to highly diffuse DNA fragments (350 nm, pH 7.0) in the presence of 150 mM NaCl and 260 mM KCl. Spectroscopic analyses suggest that the combination of salts promotes a change in DNA helical structure that initiate a switch in anthracene binding mode from intercalation to an external or groove binding interactions. The alteration in DNA structure and binding mode leads to an increase in the anthracene-sensitized production of DNA damaging reactive oxygen species. Finally, in Chapter V, pUC19 plasmid DNA is converted to its nicked circular and linear forms following irradiation of a series of pentamethine linked symmetrical carbocyanines (red light, pH 7.0). The data suggest that the relative levels of photocleavage arise from the different substituents on the nitrogen alkyl side chain and the pentamethine linker.

INDEX WORDS: Anthracene, Photocleavage, Acridine, Intercalation, Groove binding, Photodynamic therapy

DNA PHOTCLEAVAGE AND INTERACTIONS BY ANTHRACENE, ACRIDINE, AND CARBOCYANINE BASED CHROMOPHORES

by

CARLA TERRY MAPP

A Dissertation Submitted in Partial Fulfillment of the Requirements for the Degree of

Doctor of Philosophy

in the College of Arts and Sciences

Georgia State University

2013

DNA PHOTCLEAVAGE AND INTERACTIONS BY ANTHRACENE, ACRIDINE, AND CARBOCYANINE BASED CHROMOPHORES

by

CARLA TERRY MAPP

Committee Chair: Dr. Kathryn B. Grant

Committee: Dr. David Wilson

Dr. Donald Hamelberg

Electronic Version Approved:

Office of Graduate Studies

College of Arts and Sciences

Georgia State University

December 2013

DEDICATION

I dedicate this dissertation to my daughter Madison, my little nugget. Always believe in yourself, reach for the stars, and you will achieve your dreams.

ACKNOWLEDGEMENTS

This dissertation would not have been possible without the guidance and the help of several individuals who in one way or another contributed and extended their valuable assistance in the preparation and completion of this study.

To my lab mates, both past and present, it was a pleasure to work with you all. To Orapin, thank you for contributing your hard work and insight for Chapter II. I will never forget our wonderful foodie adventures. To Dominique and Blessing I count myself lucky to to call you colleagues. And I applaud you girls for increasing diversity in the biochemistry industry.

To my parents and brothers, thank you for the love, support and understanding that you have given during the long years of my education.

To my wonderful, generous and very supportive husband, you have been here with me from the start of this journey and somehow kept me sane through it all. Thank you.

To my invaluable network of supportive and loving friends you guys have been absolutely fabulous through this entire journey.

To my committee chair and advisor Dr. Kathy Grant, Thank you for all the years of advice and guidance that you have given me. I count myself very lucky to have worked with you.

To my committee members, Dr. Dixon, Dr. Hamelberg, and Dr. Wilson, for their encouraging words, thoughtful criticism, time and attention during many busy semesters. Dr. Dixon, the advice, both career and research related, that you have given over the years has been invaluable to me. I offer my sincerest thanks to you. To Dr. Wilson, thank you for allowing me to utilize your laboratory space and equipment and most of all your troubleshooting insight.

TABLE OF CONTENTS

LIST OF TABLES

LIST OF FIGURES

LIST OF SCHEMES

CHAPTER 1.

DNA STRUCTURE AND FUNCTION.

The flow of genetic information from DNA to RNA to protein drives the cycle of replication and reproduction. By serving as a carrier of genetic information, DNA is an ideal target for the treatment of a wide variety of diseases ranging from genetic disorders, bacterial and viral infections, to numerous types of cancers. It plays a vital role in all living systems, and since the structural elucidation of the DNA duplex, by James Watson and Francis Crick, the scientific community has advanced at an unimaginable rate in the past 60 years. Their results have provided immeasurable insights and advances, and have created new areas of scientific research.

1.1. The Double Helix: DNA Structure. Using X-ray diffraction patterns acquired by Rosalind Franklin, Watson and Crick were able to deduce the double-helical structure of DNA. They proposed that DNA was composed of two strands oriented in an antiparallel direction with the purine/pyrimidine bases facing inside the helix.[1] While the bases are connected internally by hydrogen bonds, they are connected externally by phosphodiester linkages. Each nucleotide is composed of a purine or pyrimidine base, a deoxyribose sugar, and a phosphate group. The purine bases are adenine and guanine, while the pyrimidine bases are cytosine and thymine. The specific hydrogen bonding patterns that facilitate the pairing of the bases within the helix aid in retaining the fidelity of the sequence. Due to the spatial constraints of the helical structure, purines only hydrogen bond with pyrimidines. Adenine makes two hydrogen bonding contacts with thymine, while guanine makes three hydrogen bonding contacts with cytosine. The bases are joined by one strand from its 5’ hydroxyl group to the 3’ hydroxyl group upon its neighboring base. On the adjacent strand they are oriented in the opposite direction, making the strands antiparallel (Figure 1.1).[1] The arrangement of the duplex in this fashion produces the

biologically prevalent B-Form of DNA. It is characterized by a right handed helix with 10.5 base pairs per turn of the helix, a rise of 3.4 Å between base pairs, and a helical twist angle of 36°.[1] The arrangement of the bases about the helical axis gives rise to grooves in the helix that are classified as major and minor. As their names suggest, the major groove is characterized as wide and deep, with the minor groove being narrow and deep.[2]

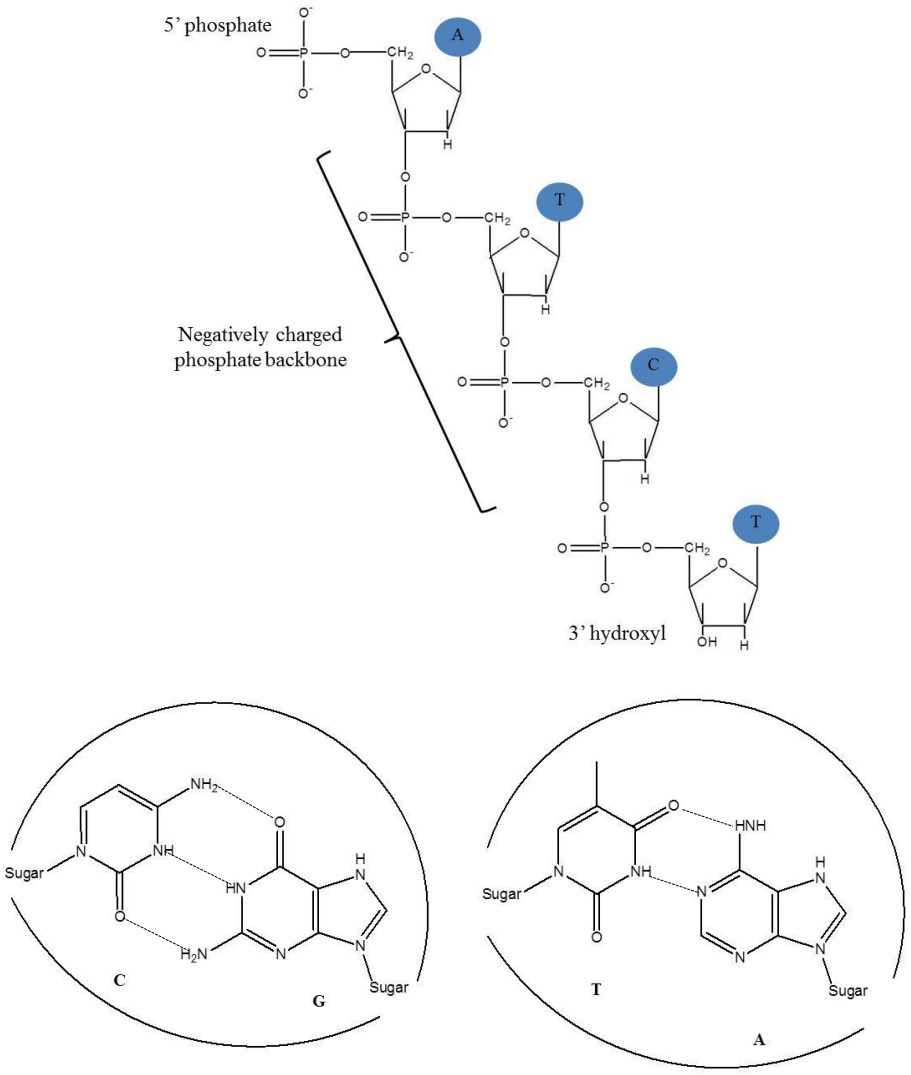

Figure 1.1. Nucleotide phosphodiester linkage and Watson-Crick base pairs show the hydrogen bonding patterns of the bases within the DNA duplex.

1.2. Non-Covalent DNA Molecular Interactions. Small organic molecules interact with DNA thorough a variety of reversible interactions which can be categorized as electrostatic, intercalation or groove binding. Each of these binding modes can be used on their own or tandem in order to achieve a desired mode of interaction by proteins, natural products, or compounds created with specific binding patterns in mind.

1.2.1. Electrostatic Interactions. Electrostatic interactions can be described as an interactive form of binding along the outside of the DNA helix, not within the major or minor grooves. The highly negatively charged phosphate backbone of B-form DNA strongly affects its structural conformations and interactions. In order to achieve stability, the duplex must associate with counter ions from solution. Simple metal cations such as Na^{+}, K^{+} and Mg^{2} interact with DNA through a concept described by Manning and Record as counterion condensation.[3] Counterion condensation theory describes the interaction of the polyanionic structure of DNA and the exchange of cations that occurs within a system. The duplex is described as a linear array of negative point charges characterized by a dimensionless charge density parameter.[4] The atmosphere around this charged linear array is divided into a condensed region, where the counter ions are bound in a well-defined volume around the duplex. In the second region, known as free region, these counterions are treated as a classical Debeye Huckel ion atmosphere. It has been concluded that the exchange of the "condensed" metal cation for the ligand from the duplex increases the entropy of binding for the system and facilitates binding of the ligand to the DNA duplex.[3]

1.2.2. Groove Binding. Groove binding ligands can be divided into two categories, major groove binders and minor groove binders. Due to the differences in hydrogen bonding patterns, steric effects, and spines of hydration, the major and minor grooves are two distinctly different

target environments when designing compounds which interact within these regions. Displacement of water from within the groove and the formation van der Waals contacts with the walls of the grooves are characteristic patterns of groove binding molecules. The recognition of thymine methyl groups in the major groove are specific to major groove binding proteins.[2] A key class of major groove binding proteins possess α-helices in their DNA binding domains. These proteins include helix-turn-helix, zinc-binding, and leucine zipper proteins. Because α-helices can be 16 Å in length or longer, the α-helix is inserted into the major groove at an angle to the helical axis of the duplex as to facilitate binding.[5]

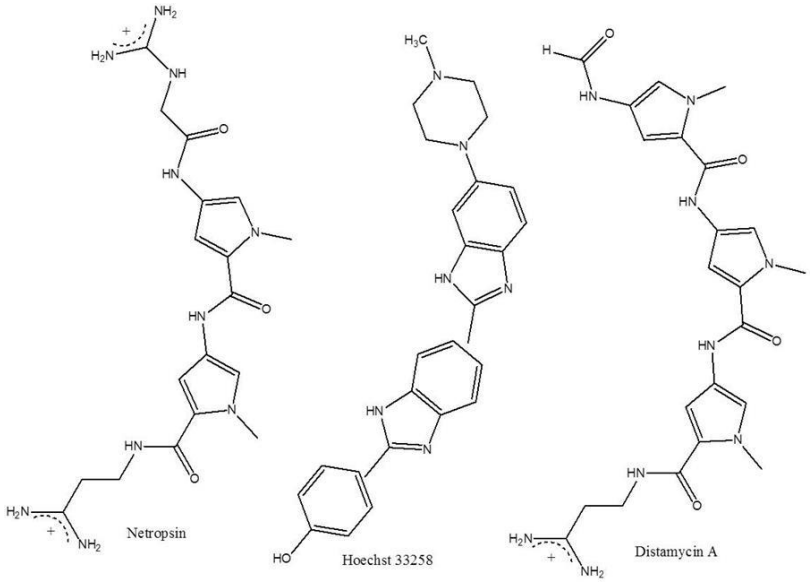

Figure 1.2. Structures of some DNA minor groove binding ligands.

Classical minor groove binding compounds, such as distamycin, netropsin, and the Hoechst dyes, are primarily constructed from unfused aromatic ring systems such as furans and pyroles, which are connected by bonds with rotational freedom that allow for a conformational fit within the minor groove (Figure 1.2). It has been shown that these groups will interact with a minor groove that is created by an A-T rich tract rather than the wider minor groove that is

produced by G-C pairs, which sterically inhibits binding due to the exocyclic amino group (N2) of guanine.[6]

Distamycin A is a crescent shaped molecule which contains three *N*-methlypyrrole amino acid monomers and binds to the minor groove of DNA at A, T tracts four to five base pairs in length.[7] The structure of distamycin A, which reversibly binds to the minor groove of DNA through a combination of hydrogen bonds, van der Waals contacts and electrostatic interactions, has led to the creation of synthetic polyamide ligands which are programmed to recognize Watson-Crick base pairs, of specific DNA sequences, by a series of pairing rules.[7]

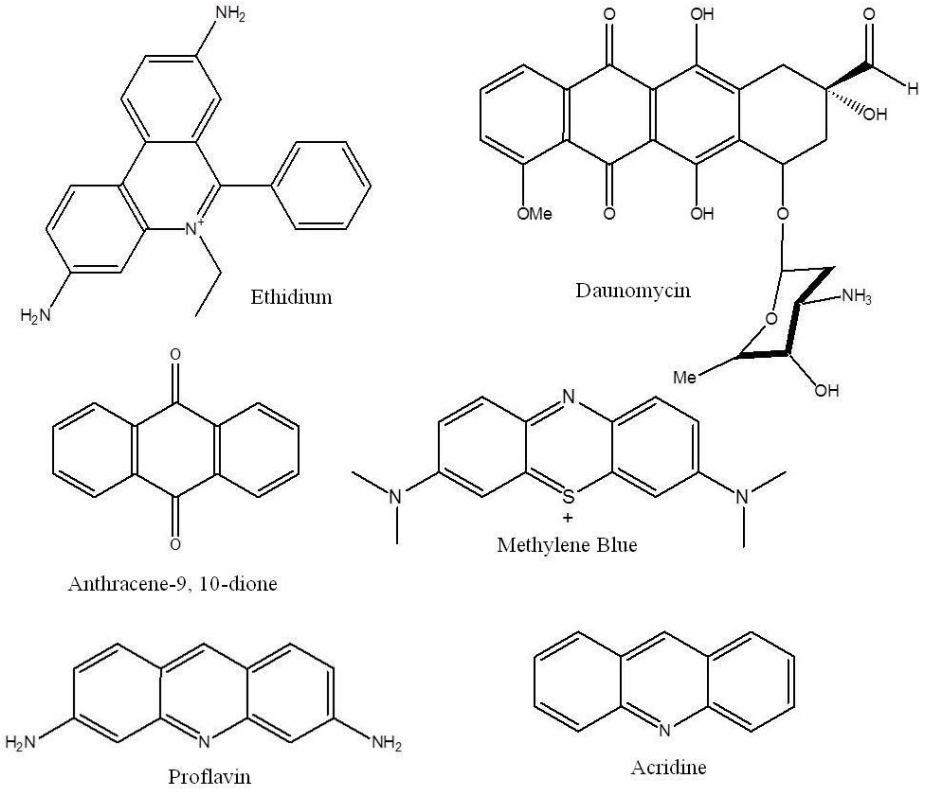

Figure 1.3. Structures of intercalative DNA binders.

1.2.3. Intercalation. Classical intercalators include compounds such as daunomycin, ethidium bromide, acridines, proflavins, and anthracenes (Figure 1.3). Intercalators are described as positively charged, planar, polycyclic aromatic ligands. This class of compounds works by stacking in between the base pairs of DNA and perturbing the hydrogen bonding patterns within the helix. It is thought that the cationic ligands are attracted to the polyionic structure of DNA, and through electrostatic interactions such as those described by the counterion condensation theory, are able to displace counterions such as Mg^{2+} or Na^{+}. This neutralization of charge by the cationic intercalators facilitates its entry between the bases.

Disruption of the hydrogen bonding patterns of the base pairs by intercalators causes alterations in the conformation of the DNA duplex, by increasing the rise per turn of bases, inducing local unwinding of the base pairs, lengthening of the helix and distortion of the helical phosphate backbone. The insertion of the ligand ring system causes the helix to become rigid, due to the stacking of π-electrons of both the ligand and DNA bases.[8] These distortions of the helix can be detected through thermal melting studies, UV/vis spectroscopy, circular dichroism, and also by viscosity measurements. The lengthening and unwinding of the DNA duplex following complexation of an intercalator causes an increase in both DNA viscosity and the melting temperature, and generates changes in the chromophore's absorbance spectrum.

1.3. Photodynamic Therapy and DNA Photocleavage. Photodynamic therapy (PDT) is a current practice that is used to treat a variety of malignancies, ranging from esophageal to basal cell carcinomas and is also used to treat disorders such as age-related wet macular degeneration. PDT involves the administration of a tumor localizing photosensitizing agent followed by excitation of the agent by light of a specific wavelength.[9] This results in a sequence of photochemical processes that cause irreversible damage to tumor tissues in the form of single-

strand DNA breaks and alkali-labile lesions.[9-10] This disrupts the reproduction of cancerous tissues by inhibiting genomic replication. The production of reactive oxygen species (ROS) such as singlet oxygen and hydroxyl radicals also generates cellular damage by initiating necrotic and apoptotic pathways. Following topical or systemic administration, the photosensitizer is taken up metabolically and localized in the diseased tissue.[11] Visible light absorbed by the chromophore, ideally red light in the 600-800 nm wavelength range, is then applied and is able to penetrate tissues and withstand interaction with pigmented molecules within the skin, in order to activate the chromophore.[2]

An ideal photosensitizer has a stable ground state electron configuration known as the singlet state. Upon excitation this singlet state is excited to an energy rich singlet excited state, which undergoes intersystem crossing to a more long lived triplet excited state. The singlet and/or triplet excited states generate pathways of energy and electron transfer that produce the reactive oxygen species which cause damage to the DNA duplex. During this conversion to the triplet state, the intersystem crossing arises when the electrons undergo a spin inversion from the excited singlet state. From this triplet state it, is able to react with oxygen in two ways. In the Type I reaction, electron transfer to molecular oxygen generates the superoxide anion radical which gives rise to hydroxyl radicals and other reactive oxygen species. The Type II reaction is characterized by an energy transfer from the photosensitizer triplet state directly to molecular oxygen, generating singlet oxygen (Figure 1.4).[10, 12]

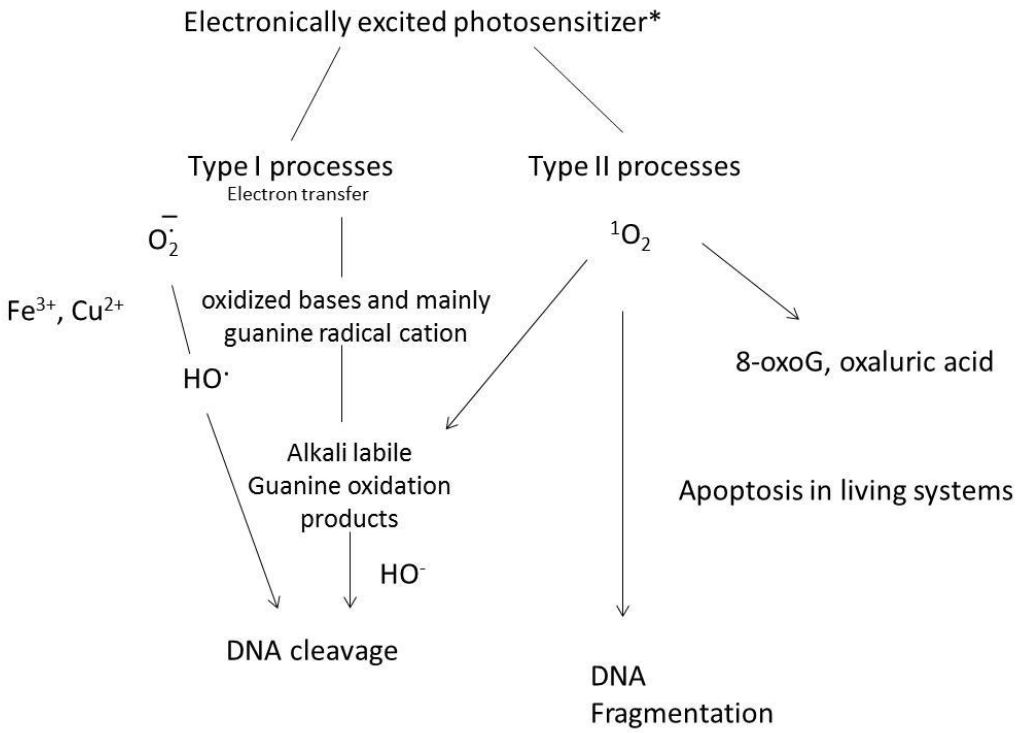

Figure 1.4. Mechanisms of DNA Photocleavage.[14]

The US FDA has approved the use of the drugs Photofrin®, Visudyne®, and Levulan® as PDT photosensitizers. Photofrin® is a hematoporphyrin derivative composed of monomers, dimers and oligermers (Figure 1.5).[13] It is used in the treatment of squamous and basal cell carcinomas, Kaposi sarcoma, and brain, head and neck tumors as well.[13] Red light at 630 nm provides excitation energy needed for therapeutic use. Visudyne® is activated by red light at 690 nm and is used in the treatment of age related macular degeneration. In the clinic, this benzoporphyrin derivative has been formulated with liposomes and has been shown to cause vascular disruption, which aids in the treatment of macular degeneration, a disease of the eye and its neovasculature.[13] Levulan® takes advantage of the porphyrin synthetic pathway. It is administered as the prodrug 5-aminolevulinic acid (ALA) and is then enzymatically converted to

protoporphyrin IX. This conversion to protoporhyrin facilitates its use in the treatment of basal and squamous cell carcinomas.

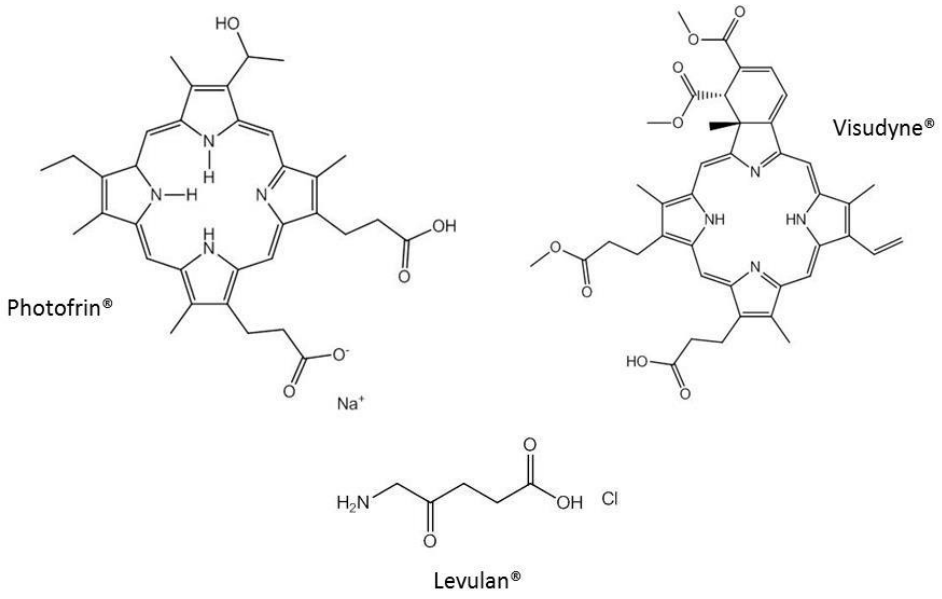

Figure 1.5. Structures of FDA approved Photodynamic Therapy drugs.

1.4. Nucleic Acid Photocleavage

Photochemically activated nucleases target either the deoxyribose or the nucleobase portion of the DNA duplex. By taking advantage of the binding interactions of several types of nucleases, different areas of the duplex can be targeted for use in structural studies or in therapeutics.

1.4.1. Nucleic Acid Strand Scission due to Oxidative Damage of Nucleobases. Damage to the nucleobases has been shown to proceed through three processes: direct electron transfer from the base to the excited state photonuclease, triplet energy transfer from the excited chromophore to molecular oxygen, producing singlet oxygen, and through electron transfer to oxygen and the subsequent formation of base adducts by hydroxyl radicals.[10]

It is believed that over half of all DNA damage inflicted on nucleobases occurs by hydroxyl radical mediated pathways. Hydroxyl radicals typically target nucleobases creating

base radicals. Of the nucleobases, thymine and guanine appear to be the most likely targets (Figure 1.6).[15] Typically modifications of thymine by hydroxyl radicals occur due to binding of the radical at the C_5C_6 double bond of the ring system[16]. It has also been shown that hydrogen abstraction at the methyl group of thymine is a pathway to base degradation.[17] This pathway produces single strand breaks, apurinic, and alkali labile sites.[17,16]

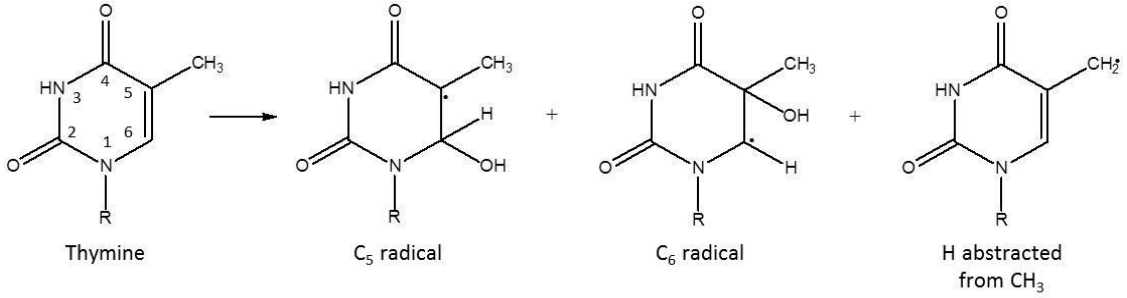

Figure 1.6. Thymine radicals created by hydroxyl radical (·OH) mediated hydrogen abstraction.[16]

Guanine has been shown to be the most easily oxidized of the nucleic acid bases, thereby making it susceptible to oxidation mediated by hydroxyl radicals, singlet oxygen and one-electron oxidants.[18,15] Hydroxyl radicals add to guanine bases through the formation of three intermediates. These hydroxylated adducts occur at the C_4, C_5, and C_8 positions. The adducts formed at the C_4 and C_5 are typically converted back to guanine by gaining an electron from the surrounding system.[19] The C_8 adduct produces the most common types of base mediated DNA damage which are heat and alkali labile. The first of these is the most common, 7,8-dihydro-8-oxoguanine (8-oxo-G). The second, 2, 6-diamino-5-formamido-4-hydroxypyrimidine (FAPy-G), is created by opening of the imidazole ring caused by the gain of both a proton and electron, under reducing conditions (Figure 1.7).[19,16]

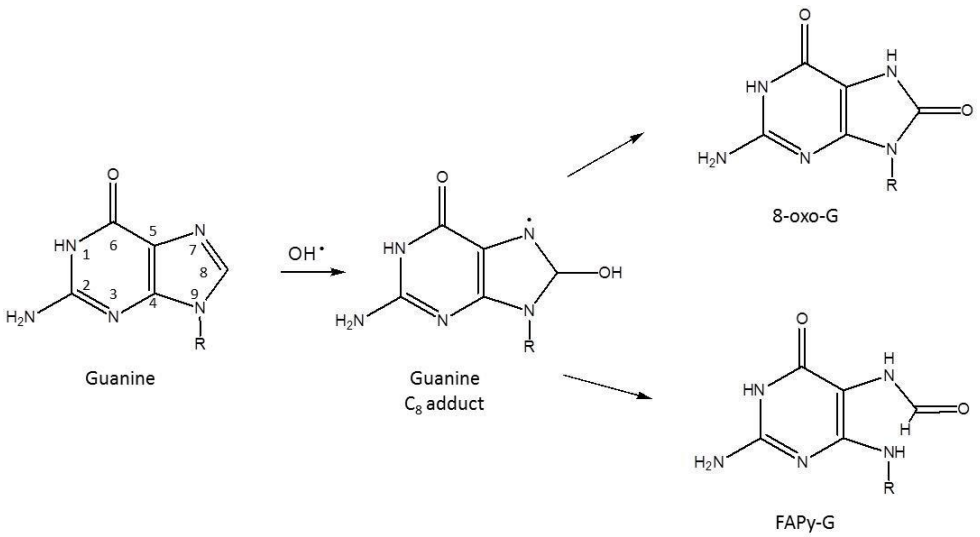

Figure 1.7. Guanine radical adducts produced by hydroxyl radical mediated abstraction.

Studies examining the interaction of DNA with singlet oxygen ($^1O_2$) have shown that it is highly reactive specifically at electron rich guanine bases. Several porphyrin and transition metals complexes have been shown to generate singlet oxygen resulting in oxidized guanine bases.[10,19] Work by Cadet has demonstrated that singlet oxygen oxidizes guanine through a cycloaddition of the imidazole ring forming an unstable 4,8-endoperoxide, which serves as an intermediate in the formation of the final oxidized guanine product 8-oxo-guanine.

1.4.2. Nucleic Acid Strand Scission due to Oxidative Damage of the Deoxyribose Moiety. The majority of DNA strand breaks arise from oxidative processes involving hydrogen abstraction from four of the five carbon atoms in the sugar.[20,18] The presence of heteroatoms at the 1', 3', 4', and 5'carbons makes hydrogen abstraction at these positions thermodynamically favorable.[10,21] The repetition of the deoxyribose unit in the DNA duplex implies that hydrogen abstraction is sequence non-selective. This factor makes it possible to design photonucleases that target specific sequences of the duplex that are capable of cleaving at the deoxyribose. Strand scission is generated at the deoxyribose by exogenous metal complexes as well as a variety of organic compounds.

Metal complexes containing Fe(II), Rh(II), Co(III), Cu(II) and Ru(II) have been extensively studied. It has been found that the metal and the ligand of such complexes play very important roles in cleavage of nucleic acids. The ligand facilitates DNA recognition and binding while the metal bound ligand can aid in photodegredative pathways by undergoing photoinduced electron transfer with the metal ion.

Bleomycin is a glycopeptide antitumor antibiotic and binds to DNA via the bithiazole moiety (Figure 1.8). The metal binding domain has a relatively high affinity for Cu(II) and Fe(III). Upon reduction of the metal, bleomycin proceeds with a cleavage mechanism that involves the abstraction of H at the C_4' position of the deoxyribose, generating 3'-phosphoglycolate, base propenal, and 5'-phosphate cleavage products (Figure 1.9). Baily and Waring noted that the exocyclic amino group of guanine plays an important role in sequence recognition by bleomycin, which is supported by results that show that cleavage most often occurs at guanine sequences.

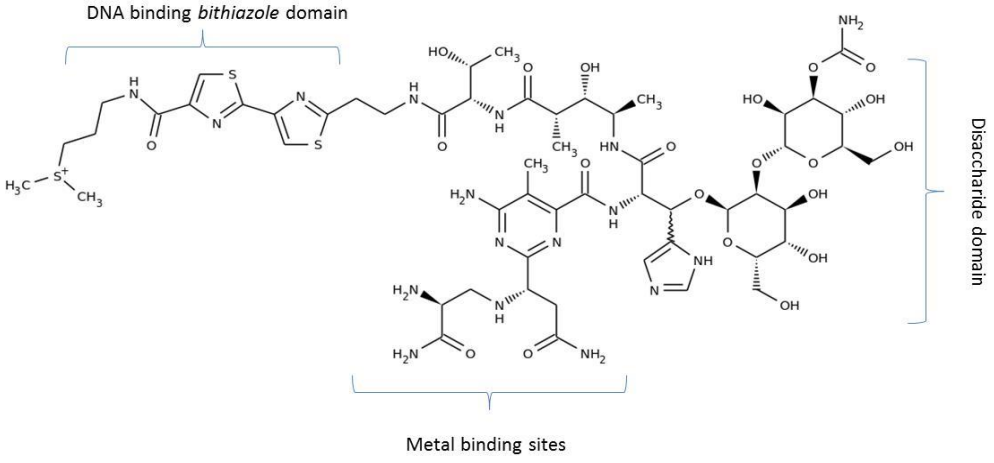

Figure 1.8. Structure of bleomycin A_2.

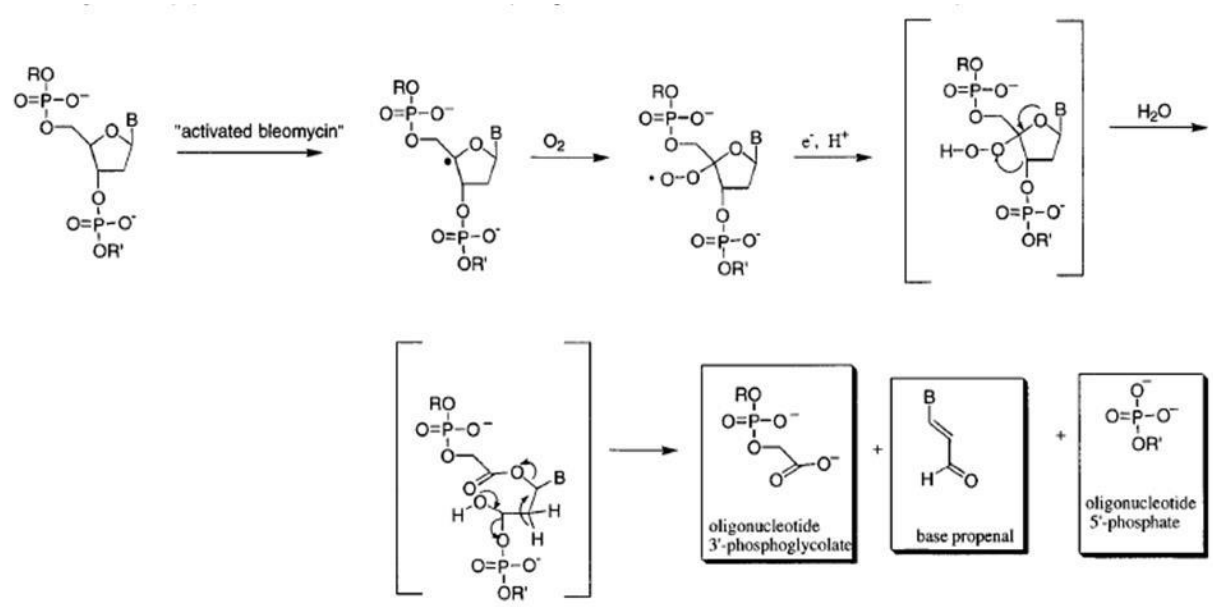

Figure 1.9. Mechanism of oxidative H-4'-Abstraction by reductively activated Fe-BLM.[22]

Barton and coworkers found that irradiation of rhodium (Rh) complexes containing polycyclic aromatic ligands results in photo-oxidative cleavage of the DNA. Primarily their Rh(phi) complexes were found to bind to DNA by intercalation via the major groove. Following photo-activation at 310 – 360 nm, these complexes damage DNA by abstracting a hydrogen from the C_3' atom of the deoxyribose at the intercalation site.[14]

1.5. DNA Interactions with Anthracene, Acridine, and Carbocyanine-based Chromophores. Anthracene-based intercalating chromophores are among the many different biomolecules that are being examined for photoreactivity in PDT. The aromatic, planar, and cationic structure of these anthracenes provides the ideal structural interaction within the helical framework of DNA.[23] "The singlet excited and triplet states of the anthracene fluorophore are photoreactive and provide an opportunity to design photoreactions that induce DNA cleavage at the probe binding site."[5, 23-24] Work by Kumar and coworkers has examined the effects of side chain length and composition at the 9 and/or 10 positions of the anthracene ring system on DNA

interactions (Figure 1.10). They proposed that substituents which possess an increasing number of nitrogen atoms would exhibit a higher DNA binding affinity. Due to the positive charge on the ammonium groups, they proposed that the ligands would help to facilitate potential electrostatic interactions with the double helix.[23, 25]

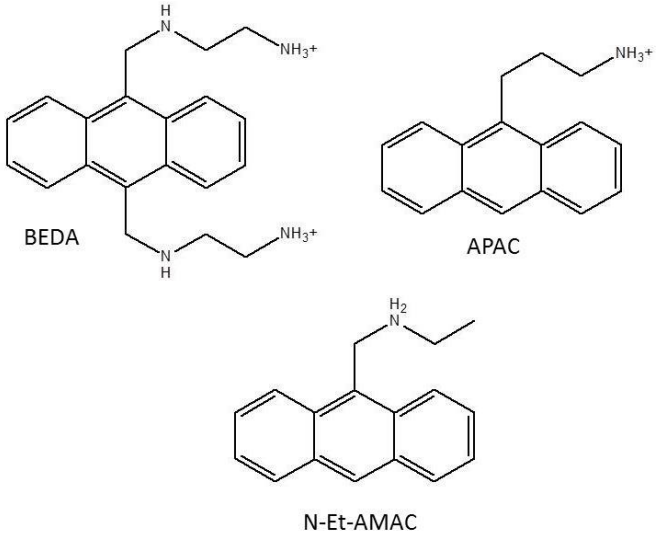

Figure 1.10. Anthracene chromophores used by Kumar et.al.[26]

Anthrycycline derivatives such as anthraquinone, daunomycin, and doxorubicin, have been used at chemotherapeutic agents for several decades and their mechanisms of DNA interaction have been examined by several groups. Daunomycin (Figure 1.3) has been used to treat acute leukemia, as well as a variety of solid tumors. It exerts it effects primarily by inhibiting topoisomerase II activity. Quiqgley and co-workers found that daunomycin intercalates into the DNA duplex with its long axis perpendicular to the long axis of the helix. The cyclopentene ring functions as an anchor is the minor groove by making hydrogen bonding contacts with DNA bases. The daunosamine anchors the structure by making hydrogen bonding contacts with water molecules in the minor groove.[27,28]

Schuester and co-workers examined the interaction and photocleavage capabilities of a class of anthraquinones and found that the observed cleavage patterns were dependent on

anthraquinone side chains as well as the anions in solution (Figure 1.11). They determined that photocleavage was achieved through three possible mechanisms. The first involved sequence specific intercalation of the anthraquinone.[10] Following irradiation and piperidine treatment, damage to the DNA duplex was observed at 5'G of GG sites. Next they determined that with monocationic anthraquinone present in excess, photocleavage occurs due to hydrogen abstraction from the deoxyribose, and this pathway is dependent on the anthraquinone structure.[10] Finally they uncovered a chloride ion assisted photocleavage pathway via a photo-induced electron transfer from the chloride to the quinone, which required no intercalation.[10,29]

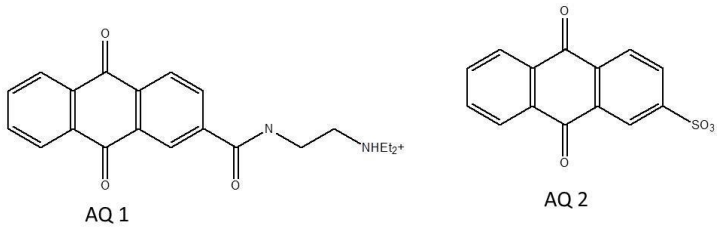

Figure 1.11. Anthraquinone derivatives used by Schuster et.al.[10,29]

Work by L.S. Lerman published in 1961 was the first to show that acridine chromophores (Figure 1.12) bind to DNA by intercalation.[30] Through viscometry, sedimentation studies, and X-ray diffraction patterns, Lerman was able to demonstrate that acridines intercalate into the DNA duplex at an angle that is perpendicular to the helical axis.[31] This work aided in the elucidation of the possible mechanism of action of medically used acridine derivatives.

Since the late 19th and early 20th centuries, acridine based chromophores have been found to possess uses as anti-bacterial and anti-malarial drugs. Beginning in the 1970's, it was discovered that *m*-amsacrine could be used as an anti-cancer agent. Work by Ehrlich and coworkers showed that 10-methyl-3,6-diaminoacridinium chloride (acriflavin) functioned as a trypanocide in the treatment of malaria.[32] The structure activity studies conducted by Alberts, outlined the properties of a) cationic ionization, b) planar molecular surface area, and c) high

ionization potentials.[32] The properties helped to establish that the 3, 6, and 9 positions on the acridine chromophore where important to antibacterial activity. The anticancer properties of acridines can be correlated to the formation of a ternary complex between the acridine, the enzyme topoisomerase II and DNA. It was later discovered that *m*-amsacrine (Figure 1.11) targets topoisomerase II rather than the DNA.

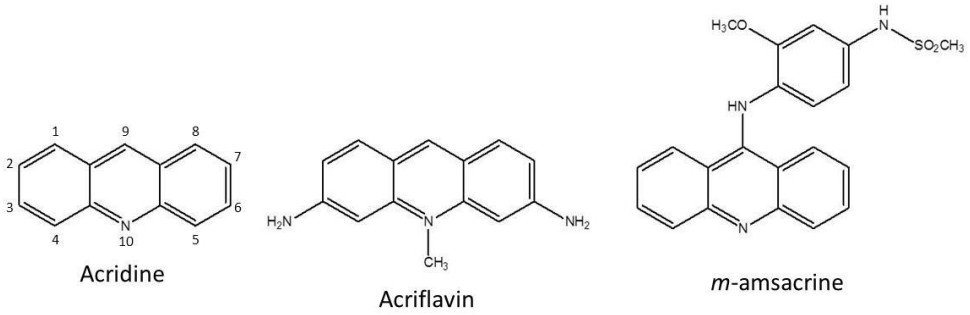

Figure 1.12. Structures of acridine and medically important acridine derivatives.

Cyanine dyes are used as fluorescent probes for proteins, DNA and other macromolecules, where upon binding a significant increase in the observed fluorescence of the cyanine is displayed.[9] This observed increase in fluorescence is attributed to the DNA-cyanine mode of interaction, which is heavily influenced by the cyanine structure and composition.[9] The cyanine dyes are known to bind to DNA and proteins through a combination of intercalation and groove binding, with both binding modes leading to increases in fluorescence yield. Typically cyanines are composed of a heterocyclic region composed of positively charged quinolone, indole, benzoxazole and benxothiazole groups that facilitate intercalation, while the polymethine linker may aid in binding to the minor groove (Figure 1.13).[9] They can be classified as either symmetrical, with the same heterocyclic subunit on each side of the polymethine linker, or unsymmetrical with different heterocyclic subunits on either side of the linker.[33] The thermodynamic interactions of these chromophores have been examined by several research groups and found to vary greatly depending on the composition of the cyanine

chromophore.[34,35,36,37] The knowledge that synthetic cyanine chromophores possess absorbance and fluorescence maxima ranging from 400 – 1000 nm coupled with their modes of DNA interaction, carbocyanines constitute an ideal class of compounds to explore for applications in photodynamic therapy.

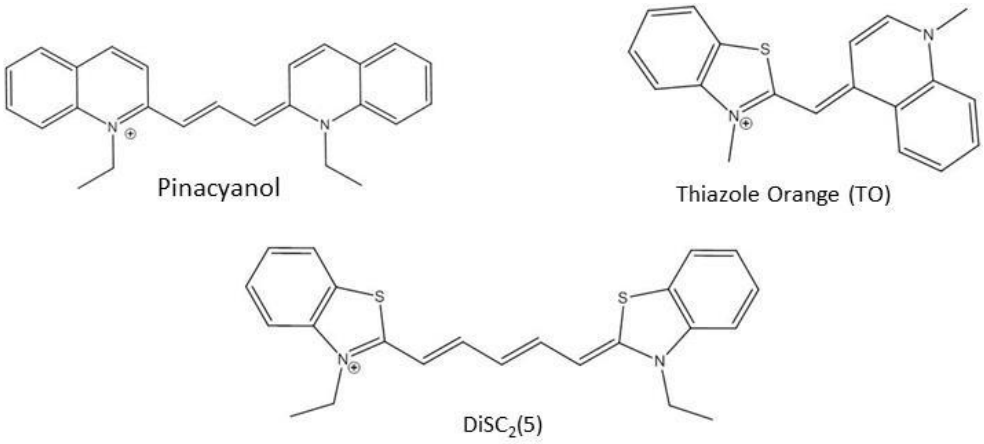

Figure 1.13. Structures of symmetrical and unsymmetrical cyanine dyes.

1.6. Specific Aims

The analysis of the photocleavage and DNA interactions of anthracene, acridine, and carbocyanine based chromophores was the overall objective of the research described in this dissertation. Each group of compounds was chosen because of their optical activity and DNA complex forming abilities. With the knowledge that genomic DNA is found in the nucleus, we set out to mimic the concentrations of NaCl and KCl found in this organelle. By using pUC19 plasmid DNA in photocleavage studies, we were able to examine the photo-conversion of the supercoiled plasmid to its nicked and linear forms that arises from cleavage of one or both strands of the duplex, respectively.

Each group of chromophores was examined for a) photo-reactivity in the presence of pUC19 plasmid DNA and/or b) photo-reactivity under physiological concentrations of NaCl and

KCl and finally c) using UV-visible spectroscopy, fluorescence spectroscopy, circular dichroism, and/or thermal denaturation and viscometric titrations, their mode of interaction with calf thymus DNA (CT DNA).

Side chains attached to the acridine and anthracene chromophores (Chapters 2, 3, and 4) were chosen due to their metal binding properties, in the hopes of taking advantage of the biologically available metals in the cell nucleus to fine tune photocleavage. The cationic heterocyclic subunits of carbocyanines are known for intercalating or stacking in the minor groove within the DNA duplex. They absorb light in the near IR region, which encompasses the 600 – 800 nm therapeutic absorbance range, ideal PDT for chromophores. (Chapter 5). By taking advantage of the above listed properties we, were able to elucidate the DNA binding and photocleaving characteristics of three known classes of DNA binding ligands.

1.7. Dissertation Summary

Chapter 1 provides a review of DNA structure and function. It describes in detail the nature of DNA interaction with small molecules that non covalently bind to its helical structure. Within this chapter is an introduction to the oxidative mechanisms of DNA damage through both the nucleobases and the deoxyribose moiety of the DNA duplex. Finally this dissertation contains a description of acridine, anthracene and carbocyanine chromophores and their known DNA interactions.

The work outlined in Chapter 2 describes the copper (II) dependent photocleavage enhancement of supercoiled pUC19 plasmid DNA by a 2, 6-bis(aminoethyl) pyridine linked bis-acridine chromophore, **3** (Figure 1.14). It was found that **3** binds to Cu(II) and in the presence of physiological concentrations of NaCl and KCl (150 mM and 260 mM respectively) significantly

enhances the photodegredation of pUC19 plasmid DNA compared to the previously examined bis-acridine **4**.

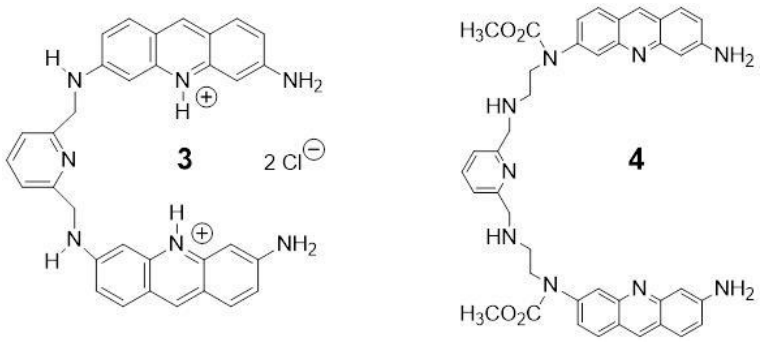

Figure 1.14. Structures of bis-acridine chromophores discussed in Chapter 2.

In Chapters 3 and 4 we examined the photocleaving properties of 9-aminomethyl substituted anthracene chromophores. In the presence of physiological concentrations of NaCl and KCl, we found that the N-substituted pyridinylpolyamine anthracene **4** (Figure 1.15) converted supercoiled, nicked circular and linear forms of pUC19 plasmid DNA to diffuse DNA fragments of high electrophoretic mobility. Spectroscopic data suggests that in the presence of the combination of salts the binding mode of the chromophore is changed from intercalation to a possible external interaction that facilitates the observed photocleavage enhancement. In Chapter 4 we found that the 9-aminomethylbisanthracene **4** and its mono anthracene analogue **5**, (Figure 1.16), also converted pUC19 plasmid DNA to high mobility fragments in the presence of physiological NaCl and KCl concentrations. Spectroscopic data indicated that the photocleavage enhancement can be attributed to a change in binding mode from intercalation to groove binding.

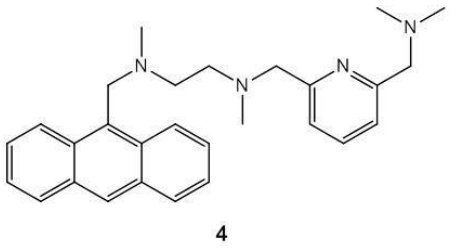

Figure 1.15. Structure of 9-aminomethyl anthracene chromophore described in Chapter 3.

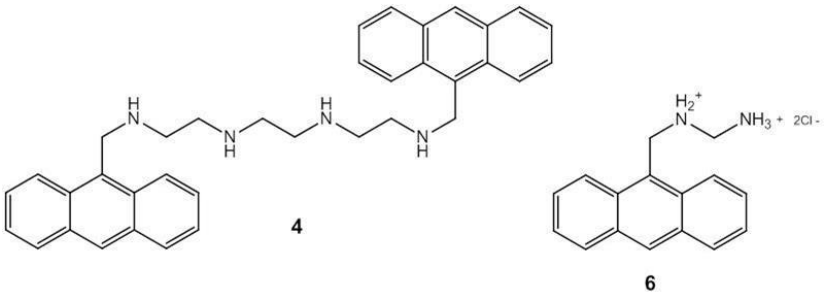

Figure 1.16. 9-aminomethyl bis-anthracene and its mono anthracene analogue described in Chapter 4.

Chapter 5 describes a series of novel symmetrical pentamethine linked carbocyanine dyes, **9** – **15**, were synthesized and examined for their DNA interaction properties (Figure 1.17). Photocleavage analyses show that the halogenated analogues **10**, **11**, **13**, and **14** efficiently converted supercoiled plasmid DNA to its nicked circular and linear forms following irradiation at 575, 588, 620, and 700 nm. Uv-visible and fluorescence spectroscopy studies support the formation of a carbocyanine DNA complex that supports and facilitates the efficient photocleavage of the supercoiled plasmid DNA.

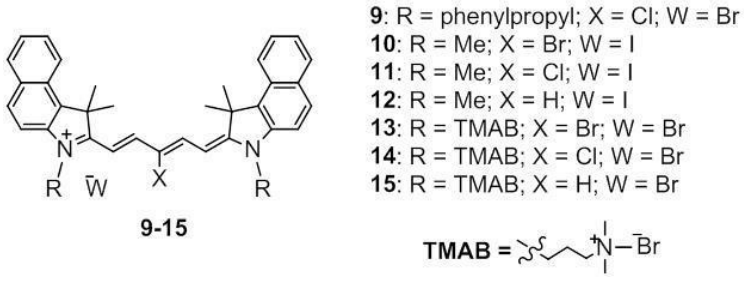

Figure 1.17. Structures of the carbocyanine dyes described in Chapter 5.

1.8. References

1. Watson, J. D.; Crick, F. H. C., A structure for deoxyribose nucleic acid. *Nature* **1953,** *171* (4356), 737-738.

2. Wing, R.; Drew, H.; Takano, T.; Broka, C.; Tanaka, S.; Itakura, K.; Dickerson, R. E., Crystal structure analysis of a complete turn of b-DNA. *Nature* **1980,** *287* (5789), 755-758.

3. Manning, G. S., The molecular theory of polyelectrolyte solutions with applications to the electrostatic properties of polynucleotides. *Q. Rev. Biophys* **1978,** *11* (02), 179-246.

4. Sharp, K. A.; Honig, B., Salt effects on nucleic acids. *Curr. Opin. Struct. Biol.* **1995,** *5* (3), 323-328.

5. Xiong, Y.; Sundaralingam, M., Protein–nucleic acid interaction: Major groove recognition determinants. In *Encyclopedia of life sciences*, John Wiley & Sons, Ltd: Chichester, 2001; pp 1-8.

6. Goodsell, D.; Dickerson, R. E., Isohelical analysis of DNA groove-binding drugs. *J. Med. Chem.* **1986,** *29* (5), 727-733.

7. Dervan, P. B., Molecular recognition of DNA by small molecules. *Biorg. Med. Chem.* **2001,** *9* (9), 2215-2235.

8. Long, E. C.; Barton, J. K., On demonstrating DNA intercalation. *Acc. Chem. Res.* **1990,** *23* (9), 271-273.

9. Armitage, B. A., Cyanine dye–DNA interactions: Intercalation, groove binding, and aggregation. In *DNA binders and related subjects*, Waring, M.; Chaires, J., Eds. Springer Berlin Heidelberg: 2005; Vol. 253, pp 55-76.

10. Armitage, B., Photocleavage of nucleic acids. *Chem. Rev.* **1998,** *98* (3), 1171-1200.

11. Becker, H. D., Unimolecular photochemistry of anthracenes. *Chem. Rev.* **1993,** *93* (1), 145-172.

12. (a) Fernandez, M. J.; Wilson, B.; Palacios, M.; Rodrigo, M. M.; Grant, K. B.; Lorente, A., Copper-activated DNA photocleavage by a pyridine-linked bis-acridine intercalator. *Bioconjugate Chem.* **2007,** *18* (1), 121-129; (b) Wilson, B.; Gude, L.; Fernandez, M. J.; Lorente, A.; Grant, K. B., Tunable DNA photocleavage by an acridine-imidazole conjugate. *Inorg. Chem.* **2005,** *44* (18), 6159-6173.

13. Allison, R. R.; Downie, G. H.; Cuenca, R.; Hu, X.-H.; Childs, C. J.; Sibata, C. H., Photosensitizers in clinical pdt. *Photodiagn. Photodyn.* **2004,** *1* (1), 27-42.

14. Da Ros, T.; Spalluto, G.; Boutorine, A. S.; Bensasson, R. V.; Prato, M., DNA-photocleavage agents. *Curr. Pharm. Design* **2001,** *7* (17), 1781-1821.

15. Steenken, S., Purine bases, nucleosides, and nucleotides: Aqueous solution redox chemistry and transformation reactions of their radical cations and e- and oh adducts. *Chem. Rev.* **1989,** *89* (3), 503-520.

16. Paillous, N.; Vicendo, P., Mechanisms of photosensitized DNA cleavage. *J. Photochem. Photobiol., B: Biol.* **1993,** *20* (2–3), 203-209.

17. Jovanovic, S. V.; Simic, M. G., Mechanism of oh radical reactions with thymine and uracil derivatives. *J. Am. Chem. Soc.* **1986,** *108* (19), 5968-5972.

18. Cadet, J.; Delatour, T.; Douki, T.; Gasparutto, D.; Pouget, J.-P.; Ravanat, J.-L.; Sauvaigo, S., Hydroxyl radicals and DNA base damage. *Mutat. Res-Fund Mol M* **1999,** *424* (1–2), 9-21.

19. Burrows, C. J.; Muller, J. G., Oxidative nucleobase modifications leading to strand scission. *Chem. Rev.* **1998,** *98* (3), 1109-1152.

20. Zhou, X.; Liberman, R. G.; Skipper, P. L.; Margolin, Y.; Tannenbaum, S. R.; Dedon, P. C., Quantification of DNA strand breaks and abasic sites by oxime derivatization and accelerator mass spectrometry: Application to γ-radiation and peroxynitrite. *Anal. Biochem.* **2005,** *343* (1), 84-92.

21. Stochel, G.; Brindell, M.; Macyk, W.; Stasicka, Z.; Szaciłowski, K., Nucleic acid photocleavage and charge transport. In *Bioinorganic photochemistry*, John Wiley & Sons, Ltd: 2009; pp 227-246.

22. Pogozelski, W. K.; Tullius, T. D., Oxidative strand scission of nucleic acids: Routes initiated by hydrogen abstraction from the sugar moiety. *Chem. Rev.* **1998,** *98* (3), 1089-1108.

23. Kumar, C. V.; Punzalan, E. H. A.; Tan, W. B., Adenine-thymine base pair recognition by an anthryl probe from the DNA minor groove. *Tetrahedron* **2000,** *56* (36), 7027-7040.

24. Suh, D.; Chaires, J. B., Criteria for the mode of binding of DNA binding agents. *Biorg. Med. Chem.* **1995,** *3* (6), 723-728.

25. Modukuru, N. K.; Snow, K. J.; Perrin, B. S.; Thota, J.; Kumar, C. V., Contributions of a long side chain to the binding affinity of an anthracene derivative to DNA. *J. Phys. Chem. B* **2005,** *109* (23), 11810-11818.

26. Modukuru, N. K.; Snow, K. J.; Perrin, B. S.; Bhambhani, A.; Duff, M.; Kumar, C. V., Tuning the DNA binding modes of an anthracene derivative with salt. *J. Photochem. Photobiol., A Chem.* **2006,** *177* (1), 43-54.

27. Chaires, J. B.; Satyanarayana, S.; Suh, D.; Fokt, I.; Przewloka, T.; Priebe, W., Parsing the free energy of anthracycline antibiotic binding to DNA. *Biochemistry* **1996,** *35* (7), 2047-2053.

28. Quigley, G. J.; Wang, A. H.; Ughetto, G.; van der Marel, G.; van Boom, J. H.; Rich, A., Molecular structure of an anticancer drug-DNA complex: Daunomycin plus d(cpgptpapcpg). *P. Natl. Acad. Sci.* **1980,** *77* (12), 7204-7208.

29. Armitage, B.; Schuster, G. B., Anthraquinone photonucleases: A surprising role for chloride in the sequence-neutral cleavage of DNA and the footprinting of minor groove-bound ligands. *Photochem. Photobiol.* **1997,** *66* (2), 164-170.

30. Lerman, L. S., Structural considerations in the interaction of DNA and acridines. *J. Mol. Biol.* **1961,** *3* (1), 18-IN14.

31. Lerman, L. S., The structure of the DNA-acridine complex. *P. Natl. Acad. Sci.* **1963,** *49* (1), 94-102.

32. Wainwright, M., Acridine—a neglected antibacterial chromophore. *J. Antimicrob. Chemother.* **2001,** *47* (1), 1-13.

33. Armitage, B., Cyanine dye–nucleic acid interactions. In *Heterocyclic polymethine dyes*, Strekowski, L., Ed. Springer Berlin Heidelberg: 2008; Vol. 14, pp 11-29.

34. Biver, T.; De Biasi, A.; Secco, F.; Venturini, M.; Yarmoluk, S., Cyanine dyes as intercalating agents: Kinetic and thermodynamic studies on the DNA/cyan40 and DNA/ccyan2 systems. *Biophys. J.* **2005,** *89* (1), 374-383.

35. Cao, R.; Venezia, C. F.; Armitage, B. A., Investigation of DNA binding modes for a symmetrical cyanine dye trication: Effect of DNA sequence and structure. *J. Biomol. Struct. Dyn.* **2001,** *18* (6), 844-857.

36. Ihmels, H.; Otto, D., Intercalation of organic dye molecules into double-stranded DNA -- general principles and recent developments. In *Supermolecular dye chemistry*, Würthner, F., Ed. Springer Berlin Heidelberg: 2005; Vol. 258, pp 161-204.

37. Nordén, B.; Tjerneld, F., Optical studies on complexes between DNA and pseudoisocyanine. *Biophys. Chem.* **1976,** *6* (1), 31-45.

CHAPTER 2.

SYNTHESIS AND DNA PHOTOCLEAVAGE BY A PYRIDINE-LINKED BIS-ACRIDINE CHROMOPHORE IN THE PRESENCE OF COPPER(II): IONIC STRENGTH EFFECTS

(This is verbatim as it appears in Grant, K. B.; Terry, C. A.; Gude, L.; Fernández, M.-J.; Lorente, A., *Bioorg. Med. Chem. Lett*. **2011**, 21 (3), 1047-1051. The initial syntheses were conducted by Drs. Gude, Fernandez and Lorente. The contributions by the author of this dissertation are conception and execution of the biochemical, biophysical and photochemical experiments and revisions of the manuscript. The manuscript was written by and revised by Dr. Grant and all of the coauthors). http://www.sciencedirect.com/science/article/pii/S0960894X10017634

2.1. Abstract

We report the synthesis of photonuclease **3** consisting of two acridine rings joined by a 2,6-bis(aminomethyl)pyridine copper-binding linker. In reactions containing micromolar concentrations of **3**, irradiation at 419 nm produces efficient, copper(II)-dependent cleavage of plasmid DNA in the presence of the high concentrations of salt that exist in the cell nucleus (150 mM NaCl and 260 mM KCl). The DNA interactions of **3** are compared to an analogous bis-acridine (**4**) containing a more flexible 2,6-bis{[(methoxycarbonylamino)-ethyl]methylaminomethyl}pyridine unit.

2.1. Introduction

In recent years, there has been increasing interest in the development of copper(II) complexes that cleave DNA.[1] These reagents are important as potential chemotherapeutic drugs for a number of reasons.[1a,c] Amounts of tissue, and/or serum copper show a significant elevation in cancer patients compared to healthy control subjects.[1a] Other studies demonstrate that tissue and/or serum samples taken from cancer patients have significantly lower levels of zinc, iron, and selenium and 2 to 3 fold higher levels of copper compared to normal control samples.[1a] In living systems, copper is closely associated with nucleic acids and chromosomes.[1a,2] While the

majority of copper is tightly bound by these and other macromolecules,[3] the kinetically labile nature of this metal enables it to be mobilized by external metal chelating agents.[1a,3a] Thus, a chemotherapeutic agent that binds to copper has the potential to be of great utility in living systems.

As early as 1979, Sigman and co-workers showed that mixtures of 1,10-phenanthroline and copper(II) sulfate could oxidatively cleave DNA in the presence of the external reducing agent 3-mercaptopropionic acid.[4] Hecht and Oppenheimer generated DNA strand scission by adding dithiothreitol to solutions containing the anticancer antibiotic bleomycin A_2 and copper(II) acetate.[5] Notwithstanding, the addition of an external reducing agent to copper is not necessarily required for efficient oxidative cleavage of DNA. A good alternative is to use light to trigger nuclease activity.[6] An early example is the copper(II) complex of the anticancer alkaloid camptothecin: oxidative DNA cleavage was achieved upon irradiation of the drug/DNA complex at 365 nm.[6h]

In a previous paper, we reported the synthesis of bis-acridine **4**, containing a flexible copper-binding 2,6-bis{[(methoxycarbonylamino)-ethyl]methylaminomethyl} pyridine linking unit.[6d] Oxidative photocleavage of plasmid DNA was markedly enhanced when 50 μM of **4** was irradiated in the presence of one mol equiv of copper(II) chloride (419 nm, 22 °C, pH 7.0).[6d] In the present study, we describe the synthesis and DNA interactions of pyridine-linked bis-acridine photonuclease **3**, equipped with a more compact 2,6-bis(aminomethyl)pyridine unit. By comparison to **4**, herein we show that bis-acridine **3** produces superior levels of photocleavage (50 μM to 2 μM dye, 419 nm, 22 °C, pH 7.0). The addition of one mol equiv of copper(II) chloride to 20 μM to 2 μM of **3** inhibits DNA photocleavage under the standard, low salt conditions used in many *in vitro* DNA reactions (0 mM NaCl).[5, 6b,d,e,f,g,h] Alternatively, the

addition of one mol equiv of Cu(II) to 30 μM to 10 μM of **3** enhances photocleavage under the conditions of high ionic strength that exist in the cell nucleus (~ 150 mM Na(I) and 260 mM K(I)).[7]

2.3. Results and Discussion

2.3.1. Synthesis. Synthesis of bis-acridine **3** was carried out by reaction of (6-amino-3-acridinyl)carbamic acid tert-butyl ester (**1**),[8] as a sodium salt, with 2,6-bis(bromomethyl)pyridine in DMF to afford the bis-acridine **2** with good yield (Scheme 1).[9] The *tert*-butoxycarbonyl protecting groups were then easily removed by treating **2** with hydrochloric acid, affording compound **3** (95%) as a dihydrochloride derivative. The structures of **2** and **3** were confirmed by ^{1}H and ^{13}C-NMR, 2D-NMR, mass spectra, and microanalytical data.[9] Bis-acridine **4** was prepared using a previously reported procedure.[6d]

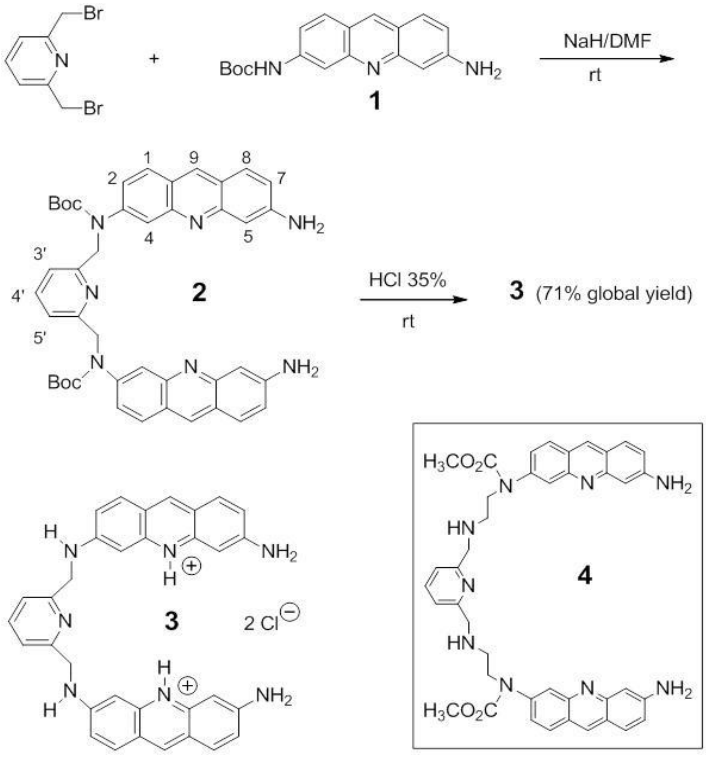

Scheme 2.1. Synthetic route of the pyridine-linked bis-acridine dye **3**. Pyridine-linked bis-acridine dye **4** is inset.

2.3.2. Photocleavage Experiments. In photocleavage experiments, 50 μM to 2 μM concentrations of a bis-acridine (**3** or **4)** were equilibrated with 38 μM bp of pUC19 plasmid DNA and 10 mM sodium phosphate buffer pH 7.0, in the absence and presence of one mol equiv of $CuCl_2$, 150 mM of NaCl, and/or 260 mM of KCl (Fig. 1). The samples were irradiated for 50 min at 419 nm and 22 °C and then electrophoresed on a 1.0% or a 1.5% non-denaturing agarose gel. The conversion of uncleaved supercoiled plasmid DNA (S) to its nicked (N) and linear (L) forms was visualized by ethidium bromide staining. Minimal levels of DNA cleavage were observed in parallel control reactions in which 38 μM bp of pUC19 plasmid, 50 μM of $CuCl_2$, and/or 50 μM of bis-acridine **3** or **4** were kept in the dark for 60 min (no hν**:** Fig. 2.1, Lane C3; Fig. 2.S1, Supplementary data; for compound **4**, Fig. 4, Lanes 11 and 12, in Fernández et al., 2007)[6d].

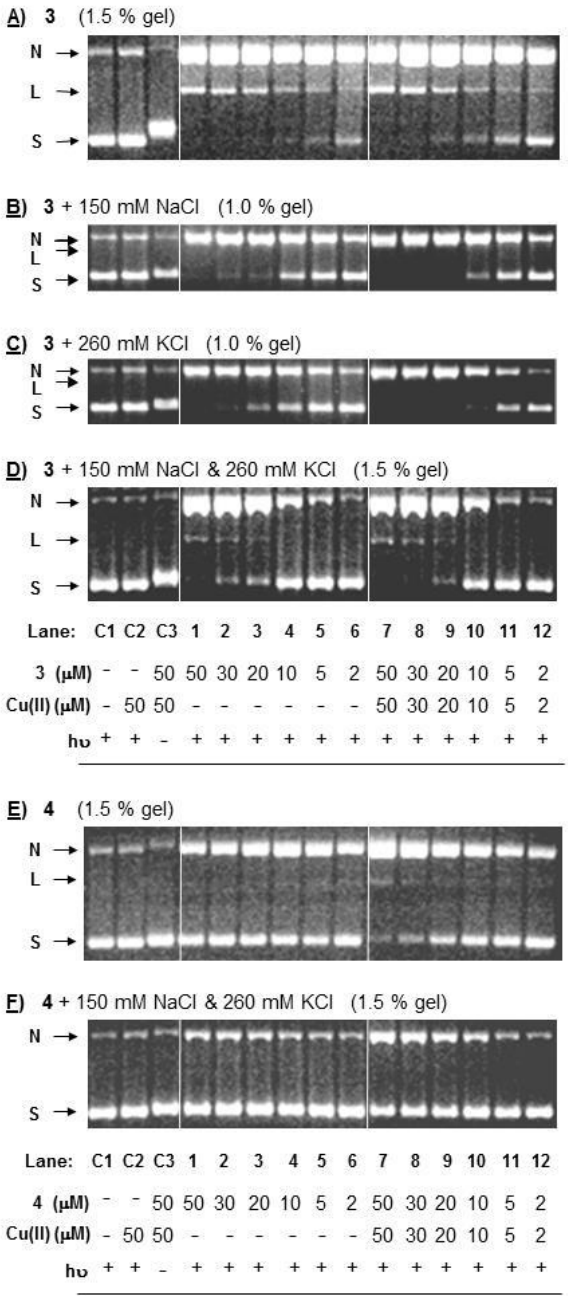

Figure 2.1. Photographs of 1.0 % and 1.5% nondenaturing agarose gels showing photocleavage of pUC19 plasmid DNA by bis-acridine **3** with **A)** no salt, **B)** 150 mM NaCl, **C)** 260 mM KCl, **D)** 150 mM NaCl and 260 mM KCl; and by bis-acridine **4** with **E)** no salt, **F)** 150 mM NaCl and 260 mM KCl. Samples contained 10 mM sodium phosphate buffer pH 7.0, 38 μM bp DNA, and 50 μM to 2 μM concentrations of **3** or **4** without (**Lanes 1** to **6)** and with (**Lanes 7** to **12)** 50 μM to 2 μM of $CuCl_2$ (total volume 40 μL). Prior to photocleavage, the reactions were pre-equilibrated for 1 h in the dark at 22 ºC. The samples in Lanes **C1**, **C2**, and **1** to **12** were then irradiated for 50 min at 22 °C in 1.7 mL microcentrifuge tubes in an aerobically ventilated Rayonet Photochemical Reactor fitted with nine RPR-4190 Å lamps.

The bis-acridine reactions in 10 mM sodium phosphate buffer pH 7.0 (no NaCl and no KCl) were studied first. From an examination of the gels in Figures 1A and 1E, it is evident that, when copper(II) is absent, compound **3** produces significantly more DNA photocleavage than compound **4** (Fig. 1A, Lanes 1 to 6 vs. Fig. 1E, Lanes 1 to 6). Notably, irradiation of concentrations of **3** as low as 10 μM results in the near-complete conversion of the plasmid DNA to its nicked and linear forms (Fig. 1A, Lane 4). Upon the addition of one mol equiv of copper(II) chloride, different trends were observed: DNA photocleavage by **3** was decreased **(**20 μM to 2 μM concentrations of dye; Fig. 1A, Lanes 9 to 12 vs. Lanes 3 to 6), while photocleavage by **4** was enhanced **(**50 μM to 20 μM concentrations of dye; Fig. 1E, Lanes 7 to 9 vs. Lanes 1 to 3). Notwithstanding, in the presence of Cu(II), **3** was still the more reactive compound (Fig. 1A, Lanes 7 to 12 vs. Fig. 1E, Lanes 7 to 12): a total of 20 μM of **3** and 50 μM of **4** were needed for near-complete photo-degradation of DNA, respectively (Fig. 1A, Lane 9 vs. Fig. 1E, Lane 7).

2.3.3. Inhibition of DNA Photocleavage. In order to account for the opposing trends produced by copper(II) chloride, we conducted cleavage inhibition experiments in which 38 μM bp of pUC19 plasmid DNA was equilibrated with the singlet oxygen ($^1O_2$) scavenger sodium azide or with the hydroxyl radical (•OH) scavenger sodium benzoate. The scavengers were added prior to photocleavage by 10 μM of **3** or by 50 μM of **4** in the presence and absence of one mol equiv of $CuCl_2$ (no NaCl and no KCl). When compared to parallel photocleavage reactions run in the absence of the scavengers, sodium azide and sodium benzoate reduced DNA photocleavage by **3** and **4** to a significant degree. The percent inhibition data in Table S1 (Supplementary data) show that, depending on the reaction conditions, the scavengers either inhibited the formation of linear DNA, so that more nicked DNA was produced in the photocleavage reaction, or reduced the amounts of the linear and/or nicked plasmid forms.

These results indicate that hydroxyl radicals and singlet oxygen contribute to DNA photocleavage by **3** and by **4**. In the case of compound **4**, sodium benzoate produces slightly more inhibition than sodium azide, with the percent inhibition values of both scavengers being higher when one mol equiv of Cu(II) is present in the photocleavage reaction. This result indicates that the addition of Cu(II) increases the production of hydroxyl radicals and singlet oxygen and is consistent with our observation that bis-acridine **4** generates more DNA photocleavage in the presence of one mol equiv of Cu(II). In the case of compound **3**, sodium azide causes more inhibition than sodium benzoate, with the percent inhibition value of sodium azide being significantly higher when Cu(II) is omitted from the photocleavage reaction. This result indicates that the addition of Cu(II) decreases the production of singlet oxygen and is consistent with our finding that bis-acridine **3** generates less DNA photocleavage in the presence of one mol equiv of Cu(II).

2.3.4. Ionic Strength Effects. The bis-acridine photocleavage reactions containing 150 mM NaCl and 260 mM KCl were studied next (Figs. 1D and 1F). These NaCl and KCl concentrations were selected in order to simulate the conditions of high ionic strength that exist in the cell nucleus where genomic DNA is contained.[7] Sodium(I), potassium(I), and other cations can induce the dissociation of ligands from DNA in two ways. By decreasing phosphate-phosphate repulsion between DNA strands, counter cations decrease minor groove width, decrease effective helical diameter, and in the case of supercoiled DNA, increase negative writhe.[10] Cations can also directly compete with positively charged ligands for DNA binding sites.[11] As expected, the gel images show that the combination of 150 mM NaCl and 260 mM KCl lowered overall photocleavage yields, both in the presence and absence of Cu(II) (Fig. 1D vs. 1A for **3**; Fig. 1F vs. 1E for **4**). It was also evident that compound **3** continued to produce

more DNA photocleavage than **4 (**Figs. 1D vs. 1F). Considered next were the effects of adding one mol equiv of copper(II) chloride to the bis-acridine reactions. In the presence of 150 mM NaCl and 260 mM KCl, levels of DNA photocleavage by **3** and **4** were both increased (30 μM to 10 μM of **3**, Fig. 1D, Lanes 8 to 10 vs. Lanes 2 to 4; 50 μM to 10 μM of **4**, Fig. 1F, Lanes 7 to 10 vs. Lanes 1 to 4). However, as discussed in the previous section, when NaCl and KCl were omitted from photocleavage reactions, copper(II) produced an enhancement in cleavage only for bis-acridine **4**. In the case of bis-acridine **3**, cleavage was reduced.

In order to better document the differential effects of Cu(II) as a function of ionic strength, the individual salts, either 150 mM of NaCl (Fig. 1B) or 260 mM of KCl (Fig. 1C) were tested against **3**. It was found that the addition of one mol equiv of Cu(II) increased DNA photocleavage by **3** under both sets of reaction conditions (Fig. 1B, Lanes 8 to 10 vs. Lanes 2 to 4 for 150 mM NaCl; Fig. 1C, Lanes 9 to 10 vs. Lanes 3 to 4 for 260 mM KCl). An overall comparison could then be made of the bis-acridine **3** photocleavage reactions run in the presence of copper (Figs. 1A to 1D, Lanes 7 to 12) to those run in the absence of copper (Figs. 1A to 1D, Lanes 1 to 6). Four sets of reaction conditions were considered: no salt (Fig. 1A); 150 mM NaCl (Fig. 1B); 260 mM KCl (Fig. 1C); 150 mM NaCl and 260 mM KCl, (Fig. 1D). The addition of one mol equiv of Cu(II) was found to alter DNA photocleavage yields differentially, according to salt composition: 260 mM KCl (Fig. 1C; increased cleavage in Lanes 9 and 10 vs. Lanes 3 and 4) > 150 mM NaCl and 260 mM KCl (Fig. 1D; increased cleavage in Lanes 7 to 10 vs. 1 to 4) > 150 mM NaCl (Fig. 1B; increased cleavage in Lanes 8 to 10 vs. Lanes 2 to 4) >>>> no salt (Fig. 1A; decreased cleavage in Lanes 9 to 12 vs. Lanes 3 to 6). In the presence of 260 mM of KCl, concentrations of **3** and copper(II) as low as 10 μM produced near-complete conversion of the plasmid DNA to its nicked and linear forms (Fig. 1C, Lane 10).

2.3.5. UV-visible Spectral Analysis. UV-visible spectra were acquired next, in order to examine the interactions of **3** and **4** with DNA (Fig. 2). A total of 38 μM bp of calf thymus DNA (CT DNA) was added to a set of solutions containing a bis-acridine (**3** or **4**) and one mol equiv of copper(II) chloride as well as to a second set of solutions containing **3** or **4,** one mol equiv of copper(II) chloride, and 260 mM KCl. The concentrations of **3** and **4** were set at 10 μM and 50 μM, respectively, due to the large cleavage enhancements produced by copper(II) (Fig. 1C, Lane 10 vs. Lane 4 for **3**; Fig. 1E, Lane 7 vs. Lane 1 for **4**). Chromicity was then quantitated by measuring each curve area from 330 nm to 520 nm, where there is minimal overlap with DNA absorption (Fig. 2). This analysis showed that, within each bis-acridine series, the ordering of DNA photocleavage yields corresponded with the relative bis-acridine chromicity produced by the addition of CT DNA: **3**/Cu(II)/KCl strong cleavage (Fig. 1C, Lane 10) and 40% hyperchromicity > **3**/Cu(II) moderately strong cleavage (Fig. 1A, Lane 10) and 1% hypochromicity; **4**/Cu(II) moderately strong cleavage (Fig. 1E, Lane 7) and 35% hypochromicity > **4**/Cu(II)/KCl moderate cleavage (Fig. 1F, Lane 7) and 4% hypochromicity. Taken together, these data suggest that the addition of KCl to solutions of bis-acridine and one mol equiv of copper(II) increases DNA interactions in the case of **3**, but decreases interactions in the case of **4**. It is conceivable that KCl induces a structural change in the nucleic acid duplex that differentially alters the DNA binding of the two bis-acridine ligands. Experiments aimed at testing this hypothesis will be the subject of future research in our laboratories.

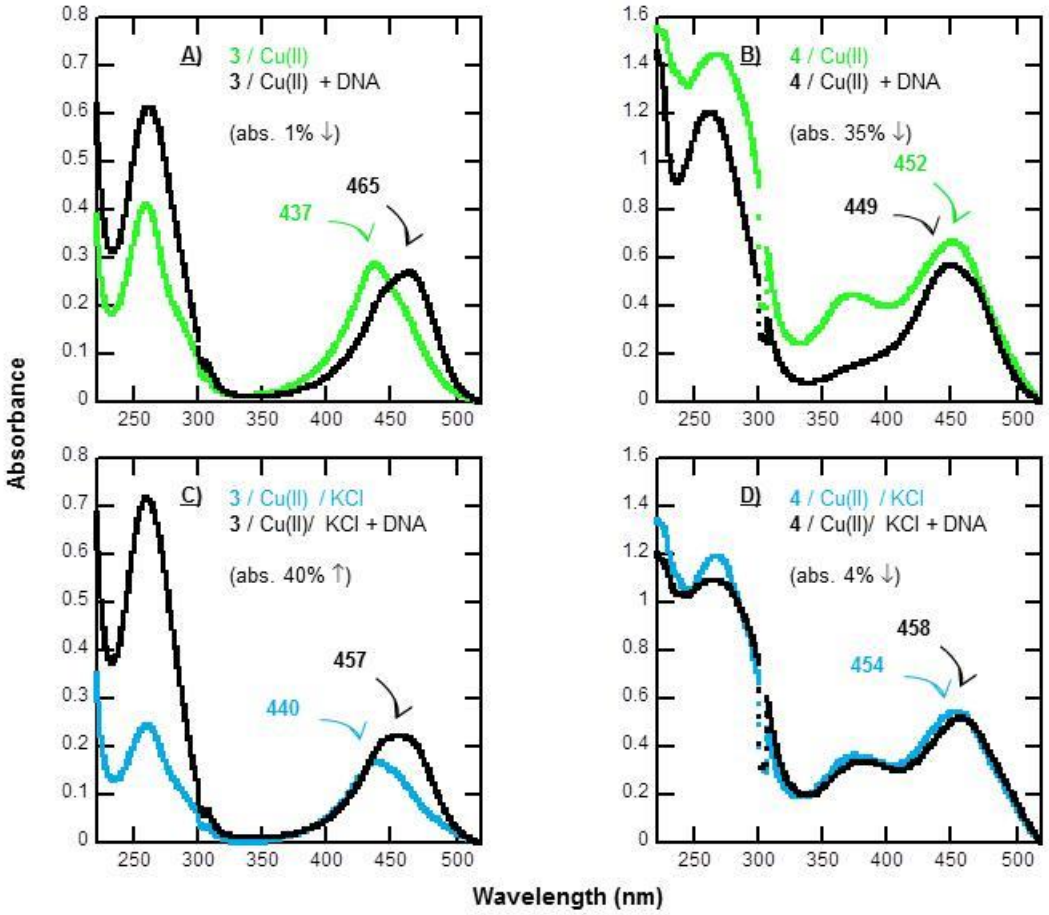

Figure 2.2. UV-visible absorbance spectra recorded at 22 ºC in 10 mM sodium phosphate buffer pH 7.0 of pyridine-linked bis-acridine dyes **3** (10 μM, left panels) and **4** (50 μM, right panels) in the presence of: **A)** and **B)** one mol equiv Cu(II) (green), one mol equiv Cu(II) + 38 μM bp CT DNA (black); **C)** and **D)** one mol equiv Cu(II) + 260 mM KCl (blue), one mol equiv Cu(II) + 260 mM KCl + 38 μM bp CT DNA (black). Individual samples consisted of a total volume of 700 μL. Before absorbance was measured, the samples were pre-equilibrated for 1 h in the dark at 22 ºC. Arrows indicate λ_{max}. The chromicity (% change in absorbance from 330 nm to 520 nm) produced by the addition of DNA appears in parenthesis. Chromicity = [(Total Abs $_{\text{with DNA}}$ – Total Abs $_{\text{without DNA}}$)/ (Total Abs $_{\text{without DNA}}$)] x 100.

2.3.6. Thermal Melting Studies. Our data have shown that bis-acridine **3** consistently produces significantly more photocleavage than bis-acridine **4** (Fig. 1A vs. 1E; Fig. 1D vs. 1F). In order to account for this result, DNA melting isotherms were recorded from 25 °C to 95 °C (no NaCl and no KCl). Melting assays provide a straightforward way of comparing the relative

binding affinities of compounds that interact with double-helical DNA. The π–π, van der Waals, electrostatic, and hydrogen bonding interactions arising from intercalation and/or groove binding stabilize helical DNA. These interactions increase the DNA binding affinity of the ligand, and increase the melting temperature of the DNA-ligand complex compared to the unbound duplex.[12] Melting isotherms of 15 μM bp calf thymus DNA in 20 mM sodium phosphate buffer pH 7.0 were recorded in the presence and absence of 10 μM of bis-acridine **3** and/or copper(II) (Fig. 2.S2 in Supplementary data). In our previous paper, isotherms acquired under identical conditions showed that 10 μM of **4** increased the melting temperature (T_m) of calf thymus DNA by 4 °C and 10 °C in the absence and presence of 10 μM of Cu(II), respectively (Fig. 3, in Fernández et al., 2007)[6d]. Compared to compound **4**, the DNA melting isotherms of **3** were shifted to higher temperatures (Fig. 2.S3 in Supplementary data). Furthermore, the absence of any inflection points in the isotherms of **3** indicated that the DNA was not completely melted up to the maximum recordable temperature in the experiment (95 °C). (Inflection points and T_m values could only be obtained by lowering the concentrations of compound **3** and Cu(II) from 10 μM to 2.5 μM (Fig. 2.S4).) These data indicate that, in the presence and absence of one mol equiv of Cu(II), compound **3** binds to DNA with significantly higher affinity than compound **4**. Thus, the data are consistent with our observation that compound **3** produces higher levels of photocleavage.

2.4. Conclusion

An ideal DNA photosensitizer for therapeutic applications should function optimally under the conditions of ionic strength that exist in the cell nucleus (~150 mM of Na(I) and 260 mM of K(I)).[7] Here we have shown that DNA photocleavage by chromophore **3**, consisting of two acridine rings joined by a compact 2,6-bis(aminomethyl)pyridine copper-binding linker, is

superior to bis-acridine **4**, equipped with a more flexible 2,6-bis{[(methoxycarbonylamino)-ethyl]methylaminomethyl} pyridine unit. In the presence of 150 mM of NaCl and 260 mM of KCl, DNA photocleavage by micromolar concentrations of **3** is enhanced by Cu(II), an ion that is closely associated with genomic DNA and chromosomes and is elevated in serum and tissue samples taken from cancer patients.[1a,2] Thus, the insights gained from the study of copper-binding acridine ligands may give rise to the development of new agents for use in photodynamic cancer therapy.

2.5. References and notes

1. For review: (a) Hadi, S.M.; Ullah, M.F.; Azmi, A.S.; Ahmad, A.; Shamim, U.; Zubair, H.; Khan, H.Y. *Pham. Res.* **2010**, *27,* 979; (b) François, J.-C.; Faria, M.; Perrin, D.; Giovannangeli, C. *Nucleic Acid. Mol. Biol.* **2004**, *13,* 223; (c) Manderville, R.A. *Curr. Med. Chem.: Anti-Cancer Agents* **2001**, *1*, 195.
2. (a) Bryan, S.E.; Vizard, D.L.; Beary, D.A.; LaBiche, R.A.; Hardy, K.J. *Nucleic Acids Res.* **1981**, *9,* 5811; (b) Cantor, K.P.; Hearst, J.E. *Proc. Natl. Acad. Sci. U.S.A.* **1966**, *55,* 642; (c) Wacker, W.E.C.; Vallee, B.L. *J. Biol. Chem.* **1959**, *234,* 3257.
3. (a) Peña, M.M.; Lee, J.; Thiele, D.J. *J. Nutr.* **1999**, *129*, 1251; (b) Linder, M.C. In *Biochemistry of Copper*; Plenum Press: New York, 1991; (c) Halliwell, B.; Gutteridge, J.M.C. *Biochem. J.* **1984,** *219,* 1.
4. Sigman, D.S.; Graham, D.R.; D'Aurora, V.; Stern, A.M. *J. Biol. Chem.* **1979**, *254*, 12269.
5. Ehrenfeld, G.M.; Rodriguez, L.O.; Hecht, S.M.; Chang, C.; Basus, V.J.; Oppenheimer, N.J. *Biochemistry* **1985**, *24,* 81.
6. (a) Patra, A.K.; Bhowmick, T.; Roy, S.; Ramakumar, S.; Chakravarty, A.R. *Inorg. Chem.* **2009,** 48, 2932; (b) González-Álvarez, M.; Arias, M.-S.; Fernández, M.-J.; Gude, L.; Lorente, A.; Alzuet, G.; Borras, J. *Bioorg. Med. Chem. Lett.* **2008**, *18,* 3286; (c) Maity, B.; Roy, M.; Chakravarty, A.R. *J. Organomet. Chem.* **2008**, *693*, 1395; (d) Fernández, M.-J.; Wilson, B.; Palacios, M.; Rodrigo, M.-M.; Grant, K.B.; Lorente, A. *Bioconjugate Chem.* **2007**, *18*, 121; (e) Gude, L.; Fernández, M.J.; Grant, K.B.; Lorente, A. *Org. Biomol. Chem.* **2005,** *3,* 1856; (f) Benites, P.J.; Holmberg, R.C.; Rawat, D.S.; Kraft, B.J.; Klein, L.J.; Peters, D.G.; Thorp, H.H.; Zaleski, J.M. *J. Am. Chem. Soc.* **2003**, *125,* 6434;

(g) Eppley, H.J.; Lato, S.M.; Ellington, A.D.; Zaleski, J.M. *Chem. Commun.* **1999**, 2405; (h) Kuwahara, J.; Suzuki, T.; Funakoshi, K.; Sugiura, Y. *Biochemistry* **1986**, *25,* 1216.

7. (a) Hooper, G.; Dick, D.A.T. *J. Gen. Physiol.* **1976**, *67,* 469; (b) Moore, R.D.; Morrill, G.A. *Biophys. J.* **1976**, *16,* 527; (c) Billett, M.A.; Barry, J.M. *Eur. J. Biochem.* **1974**, *49,* 477; (d) Naora, H.; Naora, H.; Izawa, M.; Allfrey, V.G.; Mirsky, A.E. *Proc. Natl. Acad. Sci. U.S.A.* **1962**, *48,* 853.

8. Lorente, A.; Vázquez, Y.G.; Fernández, M.-J.; Ferrández, A, *Bioorg. Med. Chem.*, **2004**, *12*, 4307.

9. ([a) [2,6-p]yridinediylbis(methylene)]bis[(6-amino-3-acridinyl)]carbamic acid di-tert-butyl ester (**2**). To a suspension of 80% NaH (26 mg, 0.86 mmol) in dry DMF (20 mL) under argon, (6-amino-3-acridinyl)carbamic acid tert-butyl ester (**1**) (240 mg, 0.77 mmol) was added. The mixture was stirred at rt for 20 min and then 2,6-bis(bromomethyl)pyridine (104 mg, 0.39 mmol) was transferred to the reaction. After 2 h, the solvent was evaporated *in vacuo* and the crude product purified by flash column chromatography (diameter: 3 cm) using silica gel as adsorbent and ethyl acetate-acetone-triethylamine (5:5:1) as eluent. The resulting oily product was dissolved in CH2Cl2 (5 mL) and precipitated by addition of hexane (40 mL). The solid thus obtained was filtered and dried, affording 209 mg (75%) of **2**, mp 145-150 °C. 1H-NMR (DMSO-*d6*): δ 1.32 (s, 18H, CO2tBu), 5.02 (s, 4H, CH2), 6.19 (br s, 4H, NH2), 6.83 (d, 2H, *J*= 1,98 Hz, H-5 acridine), 7.04 (dd, 2H, *J*= 9.06, *J'*= 1.98 Hz, H-7 acridine), 7.32 (d, 2H, *J*= 7.58 Hz, H-3',5'), 7.38 (dd, 2H, *J*= 9.06, *J'*= 1.98 Hz, H-2 acridine), 7.68 (d, 2H, *J*= 1.98 Hz, H-4 acridine), 7.74 (d, 2H, *J*= 9.06 Hz, H-8 or H-1 acridine), 7.75 (d, 2H, *J*= 9.06 Hz, H-1 or H-8 acridine), 7.79 (t, 1H, *J*= 7.58 Hz, H-4'), 8.52 (s, 2H, H-9 acridine). 13C-NMR (DMSO-*d6*): δ□157.62, 153.77, 151.49, 144.42, 137.67, 135.25, 129.71, 128.32, 123.36, 121.63, 120.85, 119.42, 102.15, 80.51, 55.18, 27.97. FAB MS: *m/z*= 722 [(M+H)1+, 61%]. *Anal.*

Calcd for C43H43N7O4: C, 71.55; H, 6.0; N, 13.58. Found: C, 71.23; H, 6.14; N, 13.87. (b) *N,N'*-bis(6-amino-3-acridinyl)-2,6-pyridinedimethanamine dihydrochloride (**3**). A solution of **2** (100 mg, 0.14 mmol) in 35% HCl (5 mL) was stirred at rt for 5 min. Then, the solvent was concentrated *in vacuo* and the resulting residue was triturated with CH_2Cl_2. The solid thus obtained was filtered and dried over NaOH. Yield: 95%; mp > 300 °C. ^{1}H-NMR (DMSO-d_6): δ 4.72 (s, 4H, CH_2), 6.82 (br s, 2H, H-5 acridine), 6.89 (br s, 2H, H-4 acridine), 6.99 (dd, 2H, *J*= 9.06, *J'*= 1.81 Hz, H-7 or H-2 acridine), 7.21 (dd, 2H, *J*= 9.06, *J'*= 1.81 Hz, H-2 or H-7 acridine), 7.46 (d, 2H, *J*= 7.91, H-3',5'), 7.81 (d, 2H, *J*= 9.23 Hz, H-1 or H-8 acridine), 7.82 (d, 2H, *J*= 9.23, H-8 or H-1 acridine), 7.94 (t, 1H, *J*= 7.91 Hz, H-4'), 8.75 (s, 2H, H-9 acridine), 14.34 (s, 2H, N^+-H). ^{13}C-NMR (DMSO-d_6): δ 156.63, 156.39, 154.27, 142.77, 142.53, 140.63, 131.94, 131.27, 121.15, 118.39, 117.02, 116.66, 93.63, 46.98. ESI-TOF HRMS obsd 522.2583, calcd 522.2406 [$(M+H)^+$, M= $C_{33}H_{27}N_7$]; obsd 261.6321, calcd 261.6242 [$(M+2H)^{2+}$, M= $C_{33}H_{27}N_7$]. *Anal.* Calcd for $C_{33}H_{29}N_7Cl_2$: C, 66.67; H, 4.92; N, 16.49. Found: C, 66.25; H, 4.81; N, 16.21.

10. (a) Hamelberg, D.; Williams, L.D.; Wilson, W.D. *J. Am. Chem. Soc.,* **2001**, *123*, 7745; (b) Bednar J.; Furrer P.; Stasiak A.; Dubochet J.; Egelman E.H.; Bates A.D. *J. Mol. Biol.* **1994**, *235,* 825.
11. Schelhorn, T.; Kretz, S.; Zimmermann, H.W. *Cell. Mol. Biol.* **1992**, *38,* 345.
12. Wilson, W. D.; Tanious, F. A.; Fernández-Saiz, M. In *Drug-DNA Interaction Protocols*; Fox, K. R., Ed.; Humana Press: New Jersey, 1997; pp 219-240.

2.6. Supplementary Data

Parallel Control Reactions Kept in the Dark. Figure 2.S1 shows a series of negative control reactions that were not irradiated. In this experiment, 50 µM concentrations of a bis-acridine 3 were pre-equilibrated for 1 h at 22 ºC with 38 µM bp of pUC19 plasmid DNA and 10 mM sodium phosphate buffer pH 7.0, in the absence and presence of one mol equiv of $CuCl_2$, 150 mM of NaCl, and/or 260 mM of KCl. The samples were kept in the dark for an additional 60 min at 22 °C and then electrophoreses on a 1.5 % non-denaturing agarose gel. (Fig.2.S1)

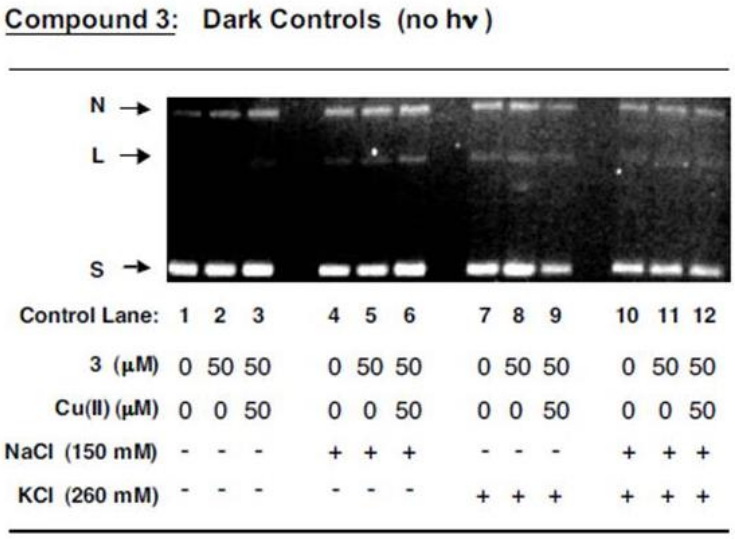

Figure 2.S1. Photograph of a 1.5% nondenaturing agarose gel showing pUC19 plasmid DNA which was equilibrated in the presence and absence of bis-acridine 3 (no hv): Lanes 1-3, no salt; Lanes 4-6, 150 mM NaCl; Lanes 7-9, 260 mM KCl; Lanes 10-12, 150 mM NaCl and 260 mM KCl. The samples contained 10 mM of sodium phosphate buffer pH 7.0, 38 µM bp DNA, and 0 µM of 3 (Lanes 1, 4, 7, and 10) or 50 µM of 3 without (Lanes 2, 5, 8, and 11) and with (Lanes 3, 6, 9, and 12) 50 µM of $CuCl_2$ (total volume 40 µL). The reactions were equilibrated for 1 h and 60 min in the dark (22 ºC).

Inhibition of DNA Photocleavage. In an attempt to identify possible reactive oxygen species (ROS) that contribute to DNA photocleavage, the following experiments were conducted using the singlet oxygen ($^1O_2$) scavenger sodium azide and the hydroxyl radical (•OH) scavenger sodium benzoate. Forty μL reactions containing 10 mM of sodium phosphate buffer pH 7.0, 38 μM bp pUC19 plasmid DNA, 10 μM of $CuCl_2$ and/or 10 μM of 3 or 50 μM of $CuCl_2$ and/or 50 μM of 4, in the presence and absence of either 100 mM of sodium azide or 100 mM of sodium benzoate were pre-equilibrated in the dark for 1 h at 22 ºC. The samples were then irradiated for 60 min at 22 °C in an aerobically ventilated Rayonet Photochemical Reactor fitted with nine RPR-4190 Å lamps. Reaction products were resolved on 1.5% non-denaturing agarose gels stained with ethidium bromide (0.5 μg/mL final concentration). The DNA on each gel was visualized on a transilluminator set at 302 nm, photographed, and then quantitated using ImageQuant v. 5.2 software (Amersham Biosciences). For each lane on the gel, the percent totals of supercoiled, nicked, and linear plasmid DNAs within the lane were calculated. The percent inhibition of DNA photocleavage by 100 mM of sodium azide and by 100 mM of sodium benzoate could then be determined based on a comparison to the parallel reactions run in the absence of scavenger (Table S1). The following formulae were used.

Percent Inhibition of Nicked DNA = [(% Total of Nicked DNA $_{\text{without scavenger}}$ – % Total of Nicked DNA $_{\text{with scavenger}}$)/(% Total of Nicked DNA $_{\text{without scavenger}}$)] x 100

Percent Inhibition of Linear DNA = [(% Total of Linear DNA $_{\text{without scavenger}}$ – % Total of Linear DNA $_{\text{with scavenger}}$)/(% Total of Linear DNA $_{\text{without scavenger}}$)] x 100

Overall Percent of Photocleavage Inhibition = [(% Total of Linear and Nicked DNA $_{\text{without scavenger}}$ – % Total of Linear and Nicked DNA $_{\text{with scavenger}}$)/(% Total of Linear and Nicked DNA $_{\text{without scavenger}}$)] x 100

Table 2.S1. Percent inhibition of DNA photocleavage by the reactive oxygen species (ROS) scavengers sodium azide and sodium benzoate [a]

Scavenger	ROS Targeted	Compound	Percent Inhibition of Nicked DNA	Percent Inhibition of Linear DNA	Overall Percent of Photocleavage Inhibition
sodium benzoate	•OH	3	-10	91	0
sodium azide	$^1O_2$	3	29	80	34
sodium benzoate	•OH	3 + Cu(II)	-7	88	0
sodium azide	$^1O_2$	3 + Cu(II)	-1	82	5
sodium benzoate	•OH	4	42	na [b]	42
sodium azide	$^1O_2$	4	31	na [b]	31
sodium benzoate	•OH	4 + Cu(II)	61	100	63
sodium azide	$^1O_2$	4 + Cu(II)	53	67	54

[a] Individual photocleavage reactions consisting of 38 μM bp of pUC19 plasmid DNA in 10 mM sodium phosphate buffer pH 7.0 were pre-equilibrated with: (i) 10 μM of $CuCl_2$ and/or 10 μM of 3 or (ii) 50 μM of $CuCl_2$ and/or 50 μM of 4, in the presence and absence of 100 mM of sodium benzoate or 100 mM of sodium azide for 1 h at 22 ºC. The reactions were then irradiated at 419 nm for 60 min in an aerobically ventilated Rayonet Photochemical Reactor.

[b] na = not applicable: no linear DNA was produced in the absence and presence of scavenger.

Thermal Melting Studies. Series of 1 mL solutions were prepared using 15 μM bp of calf thymus DNA (Invitrogen Cat. #15633-019) in 20 mM sodium phosphate buffer pH 7.0 or in 20 mM sodium phosphate buffer pH 7.0 with 10 μM or 2.5 of μM of 3 and/or 1 mol equiv $CuCl_2$ (Figs. S2, S3, S4). The solutions were placed in 1 mL (1 cm) quartz cuvettes (Starna) and were allowed to equilibrate in the dark for 1 h at 22 ºC. The calf thymus DNA was then denatured by changing the temperature from 25 °C to 95 °C at a rate of 0.5 °C min^{-1}, while monitoring absorbance at 260 nm with a Cary-100 Bio UV-visible spectrophotometer (Varian). KaleidaGraph™ Version 4.0 software was used to calculate the first derivative of $\Delta A_{260}/\Delta T$ vs temperature, where the T_m value for each melting isotherm was indicated by the maximum of the first derivative plot.

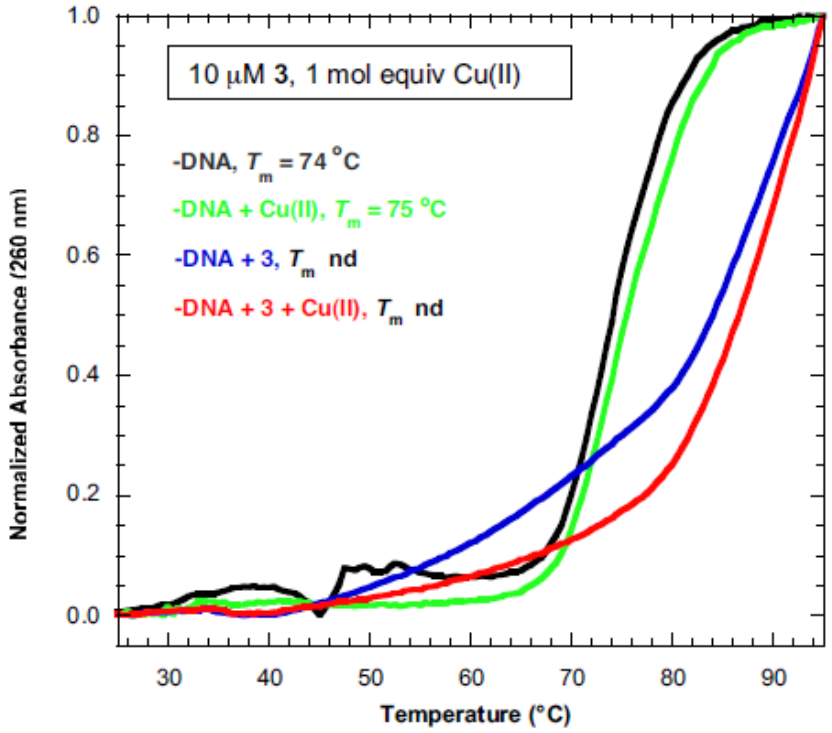

Figure 2.S2. Thermal melting curves and T_m values of 15 μM bp calf thymus DNA in the absence and presence of 10 μM 3 and/or 10 μM $CuCl_2$ (20 mM sodium phosphate buffer pH 7.0). nd = not determined: no inflection point in isotherm and no maximum in corresponding first derivative plot.

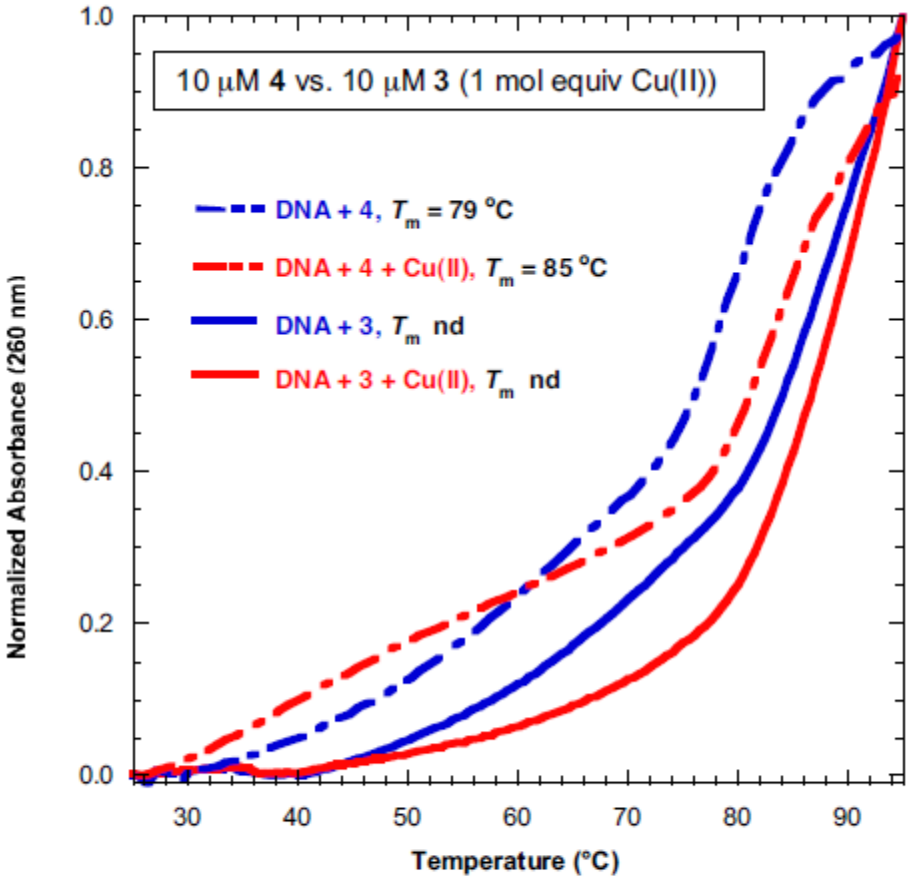

Figure 2.S3. Thermal melting curves and Tm values of 15 μM bp calf thymus DNA in the presence of 10 μM CuCl2 and/or 10 μM 4 or 10 μM 3 (20 mM sodium phosphate buffer pH 7.0). nd = not determined: no inflection point in isotherm and no maximum in corresponding first derivative plot. Compound 4 isotherms are from Fig.3, in Fernández et al., 2007.[1] Compound 3 isotherms are from Fig.2.S2, in this Supplementary data section.

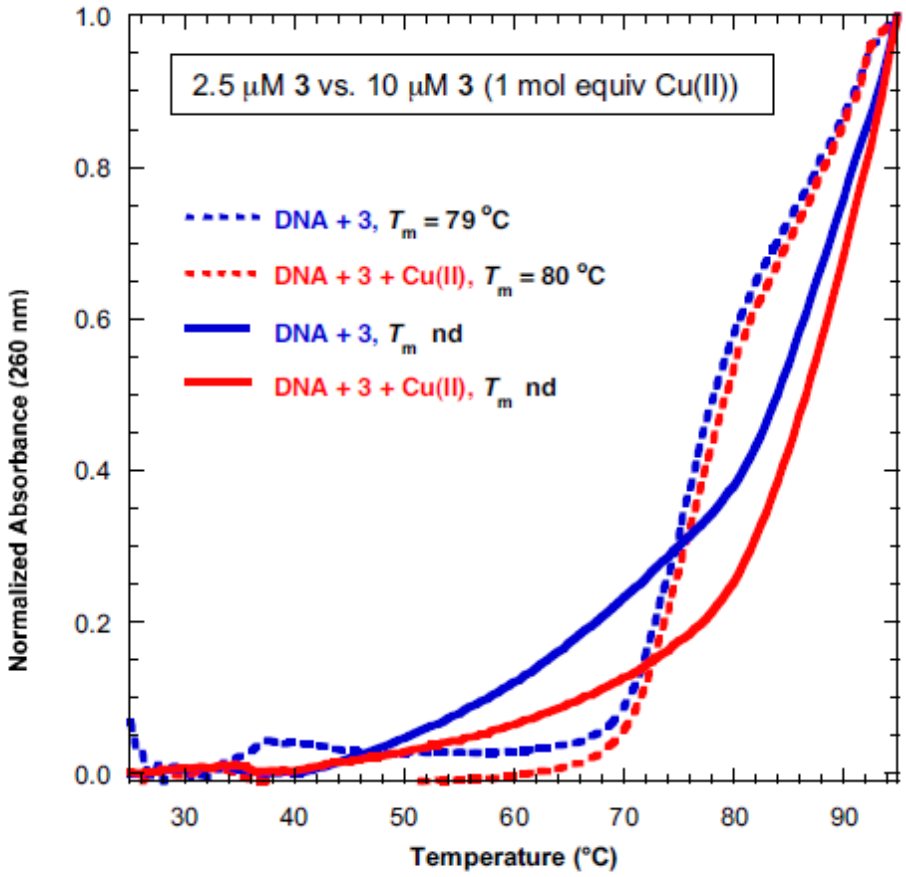

Figure 2.S4. Thermal melting curves and T_m values of 15 μM bp calf thymus DNA in the presence of 1 mol equiv of $CuCl_2$ and/or 2.5 μM 3 (dashed lines) or 10 μM 3 (solid lines; 20 mM sodium phosphate buffer pH 7.0). nd = not determined: no inflection point in isotherm and no maximum in corresponding first derivative plot. The 10 μM Compound 3 isotherms are from Fig.2.S2, in this Supplementary data section.

CHAPTER 3.

PHYSIOLOGICALLY RELEVANT CONCENTRATIONS OF NaCl AND KCl INCREASE DNA PHOTOCLEAVAGE BY *N*-SUBSTITUTED 9-AMINOMETHYLANTHRACENE DYE

(This is verbatim as it appears in Terry, C. A.; Fernández, M.-J.; Gude, L.; Lorente, A.; Grant, K. B., *Biochemistry* **2011**, 50 (47), 10375-10389. The initial syntheses were conducted by Drs. Gude, Fernandez and Lorente and written portions of the experimental section that pertain to the organic synthesis of **1 - 4**. The original manuscript was prepared by Dr. Grant. The contributions by the author of this dissertation are conception and execution of all biochemical, biophysical and photochemical experiments and minor revisions to the manuscript. The manuscript was revised by all of the coauthors). http://pubs.acs.org/doi/abs/10.1021/bi200972c

3.1 Abstract

This paper describes the synthesis of a new 9-aminomethylanthracene dye *N*-substituted with a pyridinylpolyamine side chain (**4**). The effects of NaCl and KCl on anthracene / DNA interactions were then studied, with the goal of simulating the conditions of high ionic strength that a DNA photosensitizer might encounter in the cell nucleus (~150 mM of NaCl and 260 mM of KCl). As exemplified by methylene blue (**5**), the expected effect of increasing ionic strength is to decrease DNA binding and photocleavage yields. In contrast, the addition of 150 mM of NaCl in combination with 260 mM of KCl to photocleavage reactions containing micromolar concentrations of **4** triggers the conversion of supercoiled, nicked, and linear forms of pUC19 plasmid into a highly degraded band of DNA fragments (350 nm hν, pH 7.0). Circular dichroism spectra point to a correlation between salt-induced unwinding of the DNA helix and the increase in DNA photocleavage yields. The results of circular dichroism, UV-visible absorption, fluorescence emission, thermal denaturation, and photocleavage inhibition experiments suggest that the combination of salts causes a change in the DNA binding mode of **4** from intercalation to

an external interaction. This in turn leads to an increase in the anthracene-sensitized production of DNA damaging reactive oxygen species.

3.2. Introduction

Anthracene dyes are aromatic hydrocarbons consisting of three fused six-membered rings. These versatile chromophores have been used as semi-conducting materials[1], in light-emitting diodes[2], and as fluorescent sensors for analyte detection.[3, 4] In biological systems, anthracenes bind avidly to DNA [5, 6], where they interact by intercalative and by groove-binding modes.[7-9] This has constituted the basis for their use as chemotherapeutic agents.[5, 6] Thus, the anthracene derivatives mitoxantrone and/or bisantrene have been utilized in the treatment of metastatic breast cancer[10], non-Hodgkin lymphoma[11], acute lymphoblastic leukaemia[12], and metastatic prostate cancer.[13]

Upon the absorption of long wave ultraviolet light (UVA; 320 nm to 400 nm), anthracene dyes produce singlet oxygen ($^1O_2$) and hydroxyl radicals (·OH) [14, 15], reactive oxygen species (ROS)[1] that cause extensive photo-oxidative damage to DNA and to other macromolecules in living systems.[16] As a result, anthracene-based intercalators are among the different DNA photosensitizers that have displayed activity in photo-therapeutic applications.[14, 17] In the laboratory, anthracenes produce efficient degradation of DNA under the standard, low salt conditions routinely used in *in vitro* photocleavage reactions (0 mM NaCl to 50 mM NaCl). [8, 15, 18-21] Results were very favorable and in several cases, near complete photo-conversion of supercoiled plasmid DNA (S)[1] to its nicked (N)[1] and linear (L)[1] forms was observed.[8, 15, 20, 21]

Within the cell nucleus where genomic DNA is contained, the average concentrations of NaCl and KCl are considerably higher (approximately 150 mM and 260 mM, respectively)[22-25] compared to the standard *in vitro* concentrations (0 mM NaCl to 50 mM NaCl).[8, 15, 18-21] Thus, in

photo-therapeutic applications, an ideal DNA photosensitizer should continue to function optimally under the conditions of ionic strength that exist in the cell nucleus. This goal is formidable, however. Ligands that bind to double-helical DNA, either through intercalation and/or association with the DNA grooves, typically loose their binding affinity as ionic strength is increased.[8, 26, 27, 28] According to Manning's polyelectrolyte theory, monovalent cations such as Na^+ and K^+ interact with DNA through condensation and screening effects that stabilize the polyanionic duplex.[29] Although positively charged DNA ligands contribute to charge neutralization, they can be displaced by a competitive salt effect in which high concentrations of Na^+ and K^+ cations effectively compete for negatively charged binding sites.[26] It has also been proposed that the decrease in phosphate-phosphate repulsion that occurs under conditions of high ionic strength can promote ligand dissociation from DNA[8] by triggering structural changes[30-33] that include alterations in helical diameter[32], and minor groove width.[33] In the case of DNA photosensitizing agents, the reduction in binding that occurs under conditions of high ionic strength has been shown to decrease DNA photocleavage yields.[8, 34-37]

In this report, we describe the synthesis of a 9-aminomethylanthracene dye *N*-substituted with a pyridinylpolyamine side chain (**4** in Scheme 1). The effects of high ionic strength on anthracene / DNA interactions are then studied. We have found that **4** is a very good DNA photocleaver, but that cleavage efficiency is markedly enhanced upon the addition of 150 mM of NaCl and 260 mM of KCl to the DNA reactions. In the presence of the combination of chloride salts, near-complete photo-degradation of pUC19 plasmid is observed at concentrations of **4** as low as 2.5 μM (350 nm, pH 7.0, 22 °C). We present evidence that the increase in DNA photocleavage is accompanied by a salt-induced change in anthracene interaction from

intercalation to non-intercalative binding. This triggers an increase in the anthracene-sensitized production of DNA-damaging reactive oxygen species.

3.3. Experimental Procedures

3.3.1. Materials and Methods. Deionized, distilled water was utilized in the preparation of all buffers and aqueous solutions. Reagents were of the highest available purity and were used without further purification unless otherwise noted. Methlylene blue chloride (99.99%, **5**) was purchased from Fluka and (9-anthracenylmethyl)trimethylammonium chloride (**6**) was from Aldrich^{CPR}. Sodium phosphate dibasic and sodium phosphate monobasic came from J.T. Baker and Fisher Scientific, respectively. Calf thymus DNA (CT DNA)[1] was obtained from Invitrogen (Lot No. 15633-019, 10 mg/mL, average size ≤ 2000 bp). The DNA oligonucleotide 5'-CACTGGTCTCTACCAGTG-3' was purchased from Integrated DNA Technologies and then desalted using an Illustra NAP-25 column packed with Sephadex G-25 DNA grade resin (GE Healthcare). All other chemicals including copper^{2+} chloride dihydrate, iron^{3+} chloride hexahydrate, sodium chloride (99.999%), potassium chloride (99.999%), ethidium bromide, dimethyl sulfoxide (DMSO;[1] > 99.9%), sodium azide, sodium benzoate, D-mannitol, and deuterium oxide (99 atom % D) were from Sigma-Aldrich. The starting material 2-bromomethyl-6-hydroxymethylpyridine (**1**) was prepared according to a reported procedure.[38]

Established literature protocols were used to transform *E. coli* competent cells (Stratagene, XL-1 blue) with pUC19 plasmid DNA (Sigma-Aldrich) and to clone the plasmid in bacterial cultures.[39] Purification of the DNA was accomplished with a Quiagen Plasmid Mega Kit.

Thin layer chromatography was performed on pre-coated aluminum silica gel plates (Machery-Nagel F_{254} 0.2 mm). Merck silica gel 60 (70-230 ASTM mesh) was utilized for flash column chromatography. An FT-IR Perkin-Elmer 2000 spectrophotometer was used to plot infrared spectra. ^{1}H- and ^{13}C-NMR spectra were recorded at 300 MHz on Varian UNITY-300 and Varian Mercury-VX-300 instruments. The residual peaks of chloroform (δ 7.26 and 77.0 ppm) were employed as an internal NMR reference. An Automass Multi GC/API/MS Finnigan spectrometer was utilized to acquire ESI (electrospray ionization)[1] mass spectra. UV-visible and fluorescence spectra were recorded with a UV-2401 PC spectrophotometer and an RF-1501 spectrofluorometer, respectively (Shimadzu Scientific Instruments). A Cary 300 Bio UV-visible spectrophotometer fitted with a Cary temperature controller was utilized to plot thermal melting curves. Circular dichroism (CD)[1] and induced circular dichroism (ICD)[1] spectra were acquired using a Jasco J-810 spectropolarimeter. Photocleavage reactions were run in an aerobically ventilated Rayonet Photochemical Reactor fitted with either ten RPR-3500 Å lamps or eight RPR-5750 Å lamps (The Southern New England Ultraviolet Company). Elemental analyses (CHN) were done on a Perkin-Elmer 240-B analyzer.

3.3.2. Synthesis of (6-((methyl(2-(methylamino)ethyl)amino)methyl)pyridin-2-yl)methanol (2). *N,N´*-dimethylethylenediamine (1.5 mL, 20 mmol) and anhydrous potassium carbonate (400 mg, 2.9 mmol) were transferred to dry acetonitrile (25 mL). To this suspension, a solution of 2-bromomethyl-6-hydroxymethylpyridine (**1**; *38*; 300 mg, 1.48 mmol) in dry acetonitrile (20 mL) was added dropwise for 3 h. The reaction mixture was stirred at rt for 90 min and then concentrated to dryness *in vacuo*. The white residue thus obtained was treated with distilled water (10 mL) and with an aqueous saturated sodium chloride solution (5 mL). The resulting suspension was extracted with dichloromethane (4 x 10 mL) and the combined organic

extracts were dried with magnesium sulfate, filtered, and concentrated under reduced pressure to afford 340 mg (90%) of an oily product (**2**): ^{1}H-NMR ($CDCl_3$) δ 2.27 (s, 3H, NH$\underline{CH_3}$), 2.41 (s, 3H, N$\underline{CH_3}$), 2.57 (t, *J*= 5.9 Hz, 2H, $CH_2\alpha$), 2.67 (t, *J*=5.9 Hz, 2H, $CH_2\beta$), 3.67 (s, 2H, Py$\underline{CH_2}$N), 4.71 (s, 2H, Py$\underline{CH_2}$OH), 7.10 (d, *J*= 7.7 Hz, 1H, H-3'), 7.25 (d, *J*= 7.7 Hz, 1H, H-5'), 7.63 (t, *J*= 7.7 Hz, 1H, H-4') ppm; ^{13}C-NMR ($CDCl_3$) δ 36.3, 42.6, 49.2, 56.6, 63.7, 64.0, 118.7, 121.4, 137.0, 158.3, 158.5 ppm; MS (ESI) *m/z* 210 $[M+H]^+$ (calcd for $C_{11}H_{20}N_3O$ 210.2). Anal. calcd. for $C_{11}H_{19}N_3O$: C, 63.13; H, 7.64; N, 20.08. Found: C, 63,41; H, 7.56; N, 19.82.

3.3.3. Synthesis of (6-(((2-((anthracen-9-ylmethyl)(methyl)amino)ethyl)(methyl)amino)methyl)pyridin-2-yl)methanol (3).

Compound **2** (104 mg, 0.5 mmol) and anhydrous potassium carbonate (100 mg, 0.72 mmol) were suspended in dry acetonitrile (10 mL). Then, a solution of 0.5 mmol (113 mg) of 9-chloromethylanthracene in dry acetonitrile (20 mL) was added dropwise. The reaction mixture was stirred at rt for 48 h and then concentrated *in vacuo* until dry. The resulting white residue was treated with distilled water (10 mL) and an aqueous saturated sodium chloride solution (5 mL). The suspension obtained was extracted with dichloromethane (4 x 10 mL). The combined organic extracts were then dried with magnesium sulfate, filtered, and concentrated under reduced pressure to give a crude product. Purification was achieved by flash column chromatography in silica gel using ethyl acetate and then ethyl acetate-MeOH-triethylamine (10/2/1, v/v/v) as eluents. The combined fractions obtained with the last eluent were concentrated to dryness, affording the desired product **3** as an amber oil in 75% yield: IR (film) υ 2917, 2847, 2364, 1593, 1577, 1453, 1284, 1096 cm^{-1}; ^{1}H-NMR ($CDCl_3$) δ2.21 (s, 3H, βN$\underline{CH_3}$), 2.27 (s, 3H, αN$\underline{CH_3}$), 2.70 (t, *J*= 6.6 Hz, 2H, $CH_2\beta$), 2.79 (t, J= 6.6, 2H, $CH_2\alpha$), 3.64 (s, 2H, $\underline{NCH_2}$Py), 4.46 (s, 2H, $\underline{CH_2}$ Anthr), 4.70 (s, 2H, Py$\underline{CH_2}$OH), 7.04 (d, *J*= 7.6 Hz, 1H, H-3'), 7.14 (d, *J*= 7.6 Hz, 1H, H-5'), 7.53 (t, *J*=7.6 Hz,

1H, H-4'), 7.45 (m, 4H, H-2, H-3, H-6, and H-7), 7.53 (t, *J*=7.6 Hz, 1H, H-4'), 7.98 (dd, *J*= 7.6, 1.8 Hz, 2H, H-4, and H-5), 8.40 (s, 1H, H-10), 8.50 (d, *J*= 8.1 Hz, 2H, H-1 and H-8) ppm; ^{13}C-NMR ($CDCl_3$) d 42.4, 42.8, 54.1, 55.5, 56.0, 63.5, 63.8, 118.4, 121.5, 124.7, 125.1, 125.5, 127.4, 128.9, 130.2, 131.3, 131.4, 136.9, 157.8, 158.4 ppm; MS (ESI) *m/z* 400 $[M+H]^+$ (calcd for $C_{26}H_{30}N_3O$ 400.2). Anal. calcd. for $C_{26}H_{29}N_3O$: C, 78.16; H, 7.32; N, 10.52. Found: C, 77.8; H, 7.49; N, 10.73.

3.3.4. Synthesis of N-(anthracen-9-ylmethyl)-N'-((6-((dimethylamino)methyl)pyridin-2-yl)methyl)-N,N'-dimethylethane-1,2-diamine (4). To a round-bottomed flask with a trap of potassium hydroxide, 150 mg (0.375 mmol) of **3** and thionyl chloride (3 mL) were added. The orange solution was stirred at rt for 12 h. The thionyl chloride was then removed *in vacuo*, affording an orange solid that was dissolved in methanol. A 2 M solution of dimethylamine in methanol (2 mL, 4 mmol) was then added in one portion and the reaction was stirred at room temperature overnight. After the methanol was evaporated under reduced pressure, the oily residue thus obtained was purified by flash column chromatography in silica gel using ethyl acetate and then ethyl acetate-triethylamine (95/5, v/v) as eluents. The combined fractions from the last eluent were concentrated until dryness, affording the desired product **4** (83 mg) as an amber oil in 70% yield: IR (film) υ 2917, 2848, 2360, 2341, 1655, 1591, 1453 cm^{-1}; ^{1}H-NMR ($CDCl_3$) δ 2.21 (s, 3H, βN$\underline{CH_3}$) 2.24 (s, 3H, αN$\underline{CH_3}$), 2.28 (s, 6H, N$\underline{Me_2}$), 2.69 (t, *J*= 6.6 Hz, 2H, CH_2β), 2.80 (t, *J*= 6.6 Hz, 2H, CH_2α), 3.56 (s, 2H, Py$\underline{CH_2}$NMe_2), 3.67 (s, 2H, $\underline{NCH_2}$Py), 4.46 (s, 2H, $\underline{CH_2}$Anthr), 7.18 (d, *J*= 7.6 Hz, 1H, H-3'), 7.23 (d, *J*= 7.6 Hz, 1H, H-5'), 7.45 (m, 4H, H-2, H-3, H-6, and H-7), 7.54 (t, *J*=7.6 Hz, 1H, H-4'), 7.98 (dd, *J*= 7.6, 2.0 Hz, 2H, H-4 and H-5), 8.40 (s, 1H, H-10), 8.50 (d, *J*= 8.1 Hz, 2H, H-1 and H-8) ppm; ^{13}C-NMR ($CDCl_3$) δ 42.3, 42.8, 45.5, 54.1, 55.5, 56.0, 63.9, 65.7, 121.2, 121.3, 124.7, 125.0, 125.6, 127.3, 128.9, 130.2, 131.3,

131.4, 136.6, 158.3, 159.0 ppm; HRMS (ESI) *m/z* 427.2852 $[M+H]^+$ (calcd for $C_{28}H_{35}N_4$ 427.2862). Anal. calcd. for $C_{28}H_{34}N_4$: C, 78.83; H, 8.03; N, 13.13. Found: C, 78.60; H, 8.21; N, 13.22.

3.3.5. Photocleavage of Supercoiled Plasmid DNA. In concentration titration experiments, 10 μM, 5 μM, 2.5 μM, 1.0 μM, 0.5 μM, and 0 μM amounts of a dye, either *N*-substituted 9-aminomethylanthracene **4**, methylene blue (**5**) or (9-anthracenylmethyl)trimethylammonium chloride (**6**), were equilibrated with 38 μM bp of pUC19 plasmid DNA and 10 mM sodium phosphate buffer pH 7.0, in the presence and absence of 150 mM of NaCl in combination with 260 mM of KCl, 150 mM of NaCl, 260 mM of KCl, or 410 mM of NaCl (40 μL total volume). Additional concentration titrations were conducted in which 10 μM to 0 μM amounts of **4** were equilibrated with 38 μM bp of pUC19 plasmid DNA in 150 mM of NaCl, 260 mM of KCl, and 10 mM sodium phosphate buffer pH 7.0, in the presence and absence of 10 μM of $CuCl_2 \cdot 2H_2O$ or 10 μM of $FeCl_3 \cdot 6H_2O$. In the above experiments, samples were kept for 1 h in the dark at 22 ºC and were then irradiated for 60 min in an aerobically ventilated Rayonet Photochemical Reactor fitted with either ten RPR-3500 Å lamps (compounds **4** and **6**) or eight RPR-5750 Å lamps (compound **5**). Parallel control reactions consisting of 10 mM sodium phosphate buffer pH 7.0, 38 μM bp of pUC19, and 10 μM of dye were prepared in the presence and absence of the appropriate amounts of the $copper^{2+}$, $iron^{3+}$, $potassium^{+}$ and $sodium^{+}$ chloride salts. The control reactions were kept in the dark during the 60 min irradiation period (no hν).

In time course experiments, 2.5 μM of *N*-substituted 9-aminomethylanthracene **4** was equilibrated with 38 μM bp of pUC19 plasmid DNA and 10 mM sodium phosphate buffer pH 7.0, in the presence and absence of 150 mM of NaCl in combination with 260 mM of KCl (40

μL total volume). The individual 40 μL reactions were irradiated in the Rayonet Photochemical Reactor for specific time intervals ranging from 5 min to 60 min (350 nm, 22 ºC).

After irradiation, a total of 3 μL of electrophoresis loading buffer (15.0% (w/v) Ficoll, 0.025% (w/v) bromophenol blue) was transferred to each 40 μL cleavage reaction. The samples were then loaded onto 1.5% non-denaturing agarose gels stained with ethidium bromide (0.5 μg/mL, final concentration) and electrophoresed at 160 V using 1 x TAE[1] running buffer in an OWL A1 Large Gel System (Thermo Scientific). Gels were visualized on a transilluminator set at 302 nm and photographed. For time course, scavenger, and D_2O experiments, the gels were quantitated with ImageQuant v. 5.0 software. The data obtained for supercoiled DNA were multiplied by a correction factor of 1.22 in order to account for the decreased binding affinity of ethidium bromide to supercoiled vs. nicked and linear plasmid forms. Photocleavage yields were then calculated according to Formula 1.

Percent Photocleavage = [(Linear + Nicked DNA)/(Linear + Nicked + Supercoiled DNA)] x 100. (1)

3.3.6. Circular Dichroism Analysis. Individual CD samples consisted of 10 mM of sodium phosphate buffer pH 7.0 in the presence and absence of one or more of the following reagents: 10 μM of **4,** 30 μM bp of calf thymus DNA, 150 mM of NaCl, and 260 of mM KCl (700 μL total volume). For ICD spectra, samples contained 10 mM of sodium phosphate buffer pH 7.0, 50 μM of **4,** and/or 150 μM bp of CT DNA in the presence and absence of 150 mM of NaCl and 260 of mM KCl (2000 μL total volume). After equilibration in the dark for 1 h at 22 °C, CD and ICD spectra were collected using 1 mL (0.2 cm) and 3 mL (1.0 cm) quartz cuvettes (Starna), respectively. The following operating parameters were employed: scan rate, 100

nm/min; response time, 1 s; bandwidth, 1 nm; and sensitivity, 100 millidegrees. The final spectra were averaged over 4 acquisitions.

3.3.7. UV-Visible Absorption Titrations. In DNA titration experiments, small volumes of a 2000 μM bp aqueous stock solution of CT DNA were sequentially added to anthracene samples containing 10 mM of sodium phosphate buffer pH 7.0 and 50 μM of compound **4** (500 μL initial volume). Separate titrations were conducted in the absence and presence of 150 mM NaCl in combination with 260 mM KCl. Final concentrations of CT DNA ranged from 0 μM bp up to 300 μM or 400 μM bp. In a third titration, small volumes of neat dimethyl sulfoxide were sequentially added to an anthracene sample containing 10 mM of sodium phosphate buffer pH 7.0, 50 μM of compound **4**, 150 mM NaCl, and 260 mM KCl (500 μL initial volume, no DNA used). The final concentrations of DMSO were from 0% (v/v) to 10% (v/v). After each sequential addition of titrant, the anthracene samples were equilibrated in the dark for 1 h at 22 °C, after which UV-visible absorption spectra were recorded from 800 nm to 200 nm at 22 °C. All absorption spectra were corrected for sample dilution.

3.3.8. Fluorescence Measurements. Samples consisted of 10 mM of sodium phosphate buffer pH 7.0 and 50 μM of **4** in the presence and absence of one or more of the following reagents: 400 μM bp of calf thymus DNA, 150 mM of NaCl, and 260 of mM KCl (2000 μL total volume). After equilibration in the dark for 1 h at 22 °C, the anthracene solutions were excited at 393 nm in a 3 mL (1.0 cm) quartz cuvette (Starna). Fluorescence emission spectra were recorded from 250 nm to 700 nm at 22 °C.

3.3.9. Thermal Denaturation Experiments. DNA thermal melting curves were acquired as a function of increasing anthracene concentration. Solutions contained 0 μM to 54 μM or 72 μM of **4**, 30 μM bp of the 18 mer DNA oligonucleotide 5’-CACTGGTCTCTACCAGTG-3’, and

10 mM sodium phosphate buffer pH 7.0, either in the absence or presence of 150 mM NaCl in combination with 260 mM KCl. Additional solutions consisting of 0 μM to 36 μM concentrations of **4**, 30 μM bp of CT DNA, and 10 mM sodium phosphate buffer pH 7.0 were prepared without the chloride salts. In a third experiment, thermal melting curves were recorded using 30 μM bp of CT DNA and 10 mM sodium phosphate buffer pH 7.0 with a fixed concentration of chromophore, either 0 μM or 10 μM of compound **4** or of methylene blue (**5**), in the presence and absence of individual salts, either 150 mM of NaCl or 150 mM of KCl. The solutions (1 mL total volume) were transferred to a 1.5 mL (1 cm) quartz cuvette (Starna) and were allowed to equilibrate for 1 h at 22 °C. Absorbance at 260 nm was then recorded as the temperature was increased from 25 °C to 95 °C at a heating rate of 0.5 °C /min. KaleidaGraph version 4.0 software was used to curve fit the first derivative of $\delta A_{260}/\delta T$ versus temperature, where the melting temperature (T_m)[1] value was indicated by the maximum of each first derivative plot.

3.3.10. Chemically Induced Changes in DNA Photocleavage. Individual reactions contained compound **4**, 38 mM bp of pUC19 plasmid DNA, 10 mM of sodium phosphate buffer pH 7.0, and 100 mM of the singlet oxygen scavenger sodium azide, 100 mM of the hydroxyl radical scavenger sodium benzoate, 100 mM of the hydroxyl radical scavenger D-mannitol, or 81% (v/v) of D_2O, in the presence and absence of 150 mM NaCl in combination with 260 mM of KCl. The final concentrations of compound **4** in the scavenger and D_2O reactions were 2.5 mM and 0.2 mM, respectively. In a set of parallel controls, sodium azide, sodium benzoate, D-mannitol, and D_2O were replaced by equivalent volumes of ddH_2O. All samples were pre-equilibrated in the dark for 1 h at 22 ºC and then irradiated for 60 min at 22 °C in an aerobically ventilated Rayonet Photochemical Reactor fitted with ten RPR-3500 Å lamps. After irradiation,

cleaved plasmid DNA was electrophoresed on a 1.5% non-denaturing agarose gel stained with ethidium bromide (0.5 mg/mL final concentration). Gels were placed on a transilluminator set at 302 nm, photographed, and then quantitated using ImageQuant v. 5.0 software. The percent totals of supercoiled, nicked, and linear plasmid DNAs within each gel lane were determined. Photocleavage yields were calculated according to Formula 1. In the case of the ROS scavengers, the percent inhibition of DNA photocleavage was calculated using Formula 2.

Percent Photocleavage Inhibition = [(% Total of Linear and Nicked DNA $_{\text{without scavenger}}$ – % Total of Linear and Nicked DNA $_{\text{with scavenger}}$)/(% Total of Linear and Nicked DNA $_{\text{without scavenger}}$)] x 100. (2)

3.4. Results and Discussion

3.4.1. Synthesis of N-Substituted 9-aminomethylanthracene 4. The design of **4** was based on placement of a positively charged pyridinylpolyamine side chain at the 9 position of an anthracene ring. Intercalative binding of anthracene with its long axis superimposed over the long axis of the DNA base pairs would place substituents at this position into one of the two DNA grooves.[9] In the case of **4**, we envisaged that this might allow the positively charged ammonium groups in the side chain to participate in hydrogen bonding and electrostatic interactions with the DNA duplex.[40] Additionally, the incorporation of a potentially tridentate, metal-binding bis((dimethylamino)methyl)pyridine ring into the side chain of **4** might lead to metal complexation and/or to the formation of additional hydrogen bonds between the pyridine nitrogen atom and the 2-amino group of guanine.[41,42]

Synthesis of *N*-substituted 9-aminomethylanthracene **4** was carried out as shown in Scheme 1. Treatment of 2-bromomethyl-6-hydroxymethylpyridine (**1**) [38] with *N*,*N*´-

dimethylethylenediamine in dry acetonitrile afforded compound **2** in 90% yield. *N*-substituted 9-aminomethylanthracene **3** was then obtained by reacting **2** with 9-chloromethylanthracene in dry acetonitrile (75%). Treatment of **3** with neat thionyl chloride gave the corresponding alkyl chloride. Following the removal of the thionyl chloride *in vacuo*, reaction with dimethylamine in methanol afforded *N*-substituted 9-aminomethylanthracene **4** as the final product (70% yield). The structures of **2**, **3**, and **4** were confirmed from analyses of their ^{1}H- and ^{13}C-NMR, IR, ESI-MS spectral, and microanalytical data.

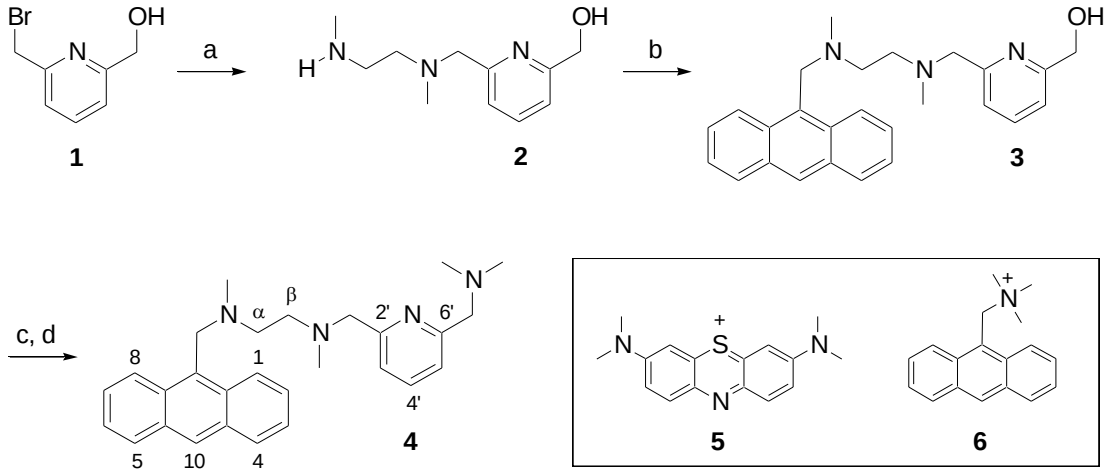

Scheme 3.1. Synthesis of *N*-substituted 9-aminomethylanthracene **4**: (a) to *N*,*N*´-dimethylethylenediamine in CH_3CN, add **1** in CH_3CN dropwise over 3 h, then react 90 min, rt; (b) to **2** in CH_3CN, add 9-chloromethylanthracene in CH_3CN dropwise, then react 48 h, rt; (c) **3** in thionyl chloride, 12 h, rt, then (d) dry *in vacuo* and react with dimethylamine in MeOH, overnight, rt. Inset: structures of methylene blue (**5**) and (9-anthracenylmethyl)trimethylammonium chloride (**6**).

3.4.2. Photocleavage of Plasmid DNA. The effects of salt on DNA photocleavage were studied first. In these experiments, concentrations of NaCl and KCl were set at 150 mM and 260 mM, respectively, in order to simulate the conditions of high ionic strength that exist in the cell nucleus (*22-25*). In a typical reaction, pUC19 plasmid DNA was equilibrated with either 10.0 μM, 5.0 μM, 2.5 μM, 1.0 μM, or 0.5 μM concentrations of **4** in the presence and absence of 150

mM of NaCl and 260 mM of KCl (10 mM of sodium phosphate buffer pH 7.0). For comparison purposes, a parallel set of reactions was conducted using the intercalating dye methylene blue (**5** in Scheme 1). Uncleaved, supercoiled plasmid was changed to its nicked and linear forms by irradiation of the DNA samples (350 nm, 60 min). Reaction products were then resolved on 1.5% non-denaturing agarose gels (Figure 1). As expected, the addition of the combination of salts inhibited DNA photocleavage by methylene blue at all dye concentrations (Lanes 1 to 5 vs. 8 to 12 in Figure 1B). In contrast, the combination of 150 mM NaCl and 260 mM KCl produced a dramatic enhancement in DNA photocleavage by *N*-substituted 9-aminomethylanthracene **4** (Lanes 1 to 5 vs. 8 to 12 in Figure 1A). The increase was evident even at the lowest concentration of **4** tested (0.5 μM), where the inclusion of the salts converted supercoiled and nicked forms of the plasmid to 100% nicked DNA (Lanes 5 vs. 12 in Figure 1A). In the presence of 1.0 μM of **4**, supercoiled and nicked plasmid was changed to nicked and linear (Lanes 4 vs. 11 in Figure 1A). At higher concentrations of **4** (10.0 μM, 5.0 μM, and 2.5 μM), 150 mM NaCl and 260 mM KCl caused complete photo-degradation of the plasmid, into a diffuse band of high mobility DNA fragments (Lanes 1 to 3 vs. 8 to 10 in Figure 1A). No DNA photocleavage occurred when the plasmid was irradiated in the absence of dye (350 nm, 60 min; Lanes 6 and 13 in Figures 1A and 1B), and when the highest concentration of **4** or **5** (10 μM) was reacted with the plasmid in the dark (no hν, 60 min; Lanes 7 and 14 in Figures 1A and 1B).

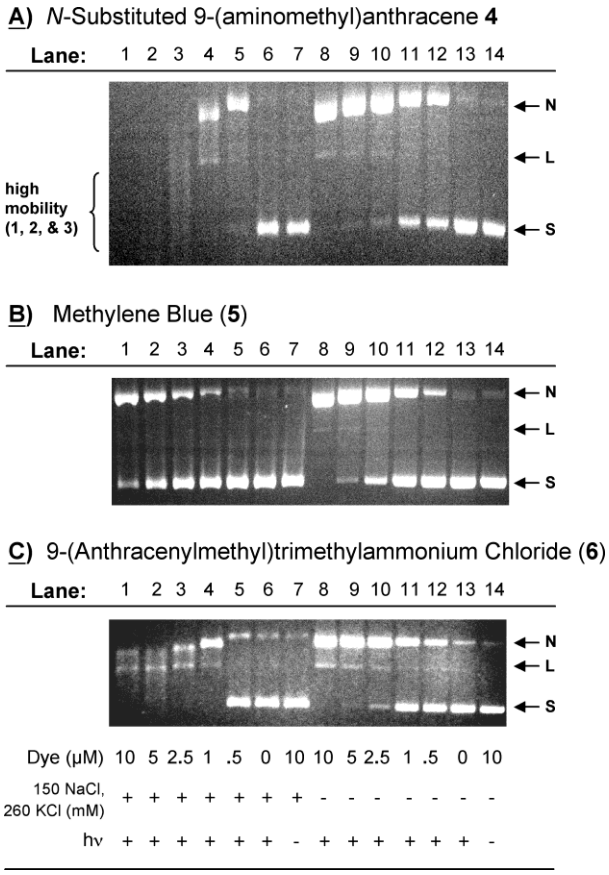

Figure 3.1. Photographs of 1.5% nondenaturing agarose gels showing photocleavage of 38 μM bp of pUC19 plasmid by **A)** *N*-substituted 9-(aminomethyl)anthracene **4**, **B)** methylene blue (**5**), and **C)** (9-anthracenylmethyl)trimethylammonium chloride (**6**). Samples contained 10 mM sodium phosphate buffer pH 7.0 and 38 mM bp DNA. **Lanes 1** to **6**: 10 μM to 0 μM of dye in the presence of 150 mM NaCl and 260 mM KCl. **Lanes 8** to **13**: 10 μM to 0 μM of dye in the absence of 150 mM NaCl and 260 mM KCl. **Lane 7**: 10 μM of dye in the presence of 150 mM NaCl and 260 mM KCl (no hν). **Lane 14**: 10 μM of dye in the absence of 150 mM NaCl and 260 mM KCl (no hν). Prior to photocleavage, the reactions were pre-equilibrated for 1 h in the dark at 22 ºC. The samples in Lanes **1** to **6** and **8** to **13** were irradiated at 350 nm (compounds **4** and **6**) or at 575 nm (compound **5**) for 60 min (22 °C). Abbreviations: **L** = linear; **N** = nicked; **S** = supercoiled.

The aim of our next experiment was to quantitate the amounts of DNA photocleavage produced by 9-aminomethylanthracene **4** as a function of time. Individual reactions contained 2.5 μM of **4**, the lowest concentration of dye to have produced near-complete photo-degradation of the plasmid DNA (Lane 3 in Figure 1A). After the samples were equilibrated in the presence and absence of 150 mM NaCl in combination with 260 mM KCl, they were irradiated at 350 nm for

intervals of time up to 60 min (Figure S1 in Supporting Information). DNA photocleavage yields were then determined by quantitating a photograph of the 1.5% agarose gel (Figure 2). While 2.5 μM of 9-aminomethylanthracene **4** clearly demonstrated time-dependent photo-conversion of supercoiled plasmid to its nicked and linear forms (Figure 2; Lanes 11 to 15 vs. Lanes 3 to 7 in Figure S1), the addition of 150 mM NaCl and 260 mM KCl markedly enhanced cleavage yields at time points ranging from 15 min to 60 min. At t = 30 min of irradiation, the electrophoretic mobilities of the nicked and linear forms of the plasmid began to increase with increasing time (Lanes 5 to 7 in Figure S1). (We presently attribute this effect to photo-induced cross-linking of the anthracene to the DNA). [43, 44] Moreover, the supercoiled plasmid was changed completely into its nicked and linear DNA forms (Figure 2; Lanes 5 to 7 in Figure S1). In the absence of the salts, the highest photocleavage yield to be achieved was 87% of nicked and linear DNA (t = 60 min of hν; Figure 2; Lane 15 in Figure S1). The mobilities of the cleaved DNA bands did not appear to change, even after prolonged irradiation times (Lanes 9 to 16 in Figure S1).

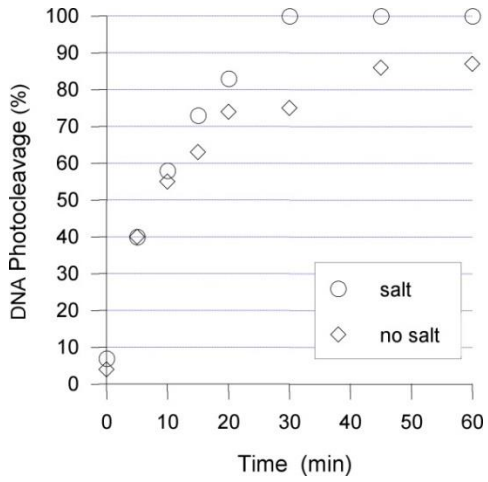

Figure 3.2. Time course plots for DNA photocleavage by *N*-substituted 9-(aminomethyl)anthracene **4**. Samples contained 10 mM sodium phosphate buffer pH 7.0, 38 μM bp of pUC19 plasmid DNA, and 2.5 μM of **4** in the presence (circles) and absence (diamonds) of 150 mM NaCl and 260 mM KCl. Prior to photocleavage, the reactions were pre-equilibrated for 1 h in the dark at 22 ºC. The samples were then irradiated for 0 min, 5 min, 10 min, 15 min, 20 min, 30 min, 45 min, or 60 min at 350 nm (22 °C). Cleaved DNA fragments were resolved on a 1.5% nondenaturing agarose gel (Figure S1 in Supporting Information).

The increase in DNA photocleavage produced by the addition of 150 mM of NaCl and 260 mM of KCl to reactions containing 9-aminomethylanthracene **4** was not anticipated. High concentrations of sodium$^+$, potassium$^+$, and other cations decrease the association of ligands with double-helical DNA in two ways.[8, 26, 27, 28] By interacting with the negatively charged phosphate groups in the DNA backbone, counter cations can alter DNA structure, *e.g.*, by decreasing minor groove width [33] and helical diameter [32], and by increasing helical twist angle. [30, 31] Cations can also effectively compete with positively charged ligands for binding sites on the DNA duplex.[26] As typified by methylene blue (**5** in Figure 1B; *34*), and by other ring systems including cyanine dyes [36], *meso* substituted porphyrins[35], and bis-proflavine[37] and 9,10-bis(aminomethyl)anthracene[8] derivatives, the expected effect of a salt-induced reduction in ligand binding is to decrease DNA photocleavage yields.

In order to account for the salt-dependent reactivity of 9-aminomethylanthracene **4**, two initial hypotheses were considered. In the presence of excess amounts of NaCl and KCl, the pyridinylpolyamine side chain of **4** could conceivably form up to three five-membered chelate rings with the alkali metal cations Na^+ and/or K^+. The change in ligand conformation accompanying complex formation could favor high affinity binding to duplex DNA. Alternatively, the ability of the alkali metal salts to increase DNA photocleavage could arise from a direct interaction between Na^+ and/or K^+ cations and 9-aminomethyl nitrogen lone pair electrons. In 9-aminomethylanthracenes, the nitrogen lone pair quenches the electronically excited state of the anthracene ring by a photo-induced electron transfer mechanism.[45, 46] However, the fluorescence quenching can be reversed by coordination of Na^+ or K^+ to the nitrogen atom. The metal-ligand interaction decreases the oxidation potential of the amine. As a result, electron transfer is prevented and the lifetime of the anthracene ring excited state is

extended. In the context of our experiments, this would be expected to lead to a Na^+ or K^+-induced increase in the production of DNA damaging reactive oxygen species from the photochemically excited singlet or triplet state. In order to test the two hypotheses, DNA photocleavage experiments were repeated utilizing the quaternary amine (9-anthracenylmethyl)trimethylammonium chloride (**6** in Scheme 1), a chromophore that is devoid of nitrogen lone pair electrons. The DNA samples were irradiated in the presence and absence of 150 mM NaCl in combination with 260 mM KCl, and then electrophoresed. As shown in Figure 1C, a significant salt-induced increase in DNA photocleavage was observed at concentrations of **6** ranging from 10.0 μM to 1.0 μM (Lanes 1 to 4 vs. Lanes 8 to 11 in Figure 1C). This result points to an alternate mechanism in which metal-ligand interactions involving Na^+ or K^+ cations and the amine groups in the side chain of **4** do not play a major role in the salt-induced cleavage enhancement.

Acridine-sensitized one electron photo-reduction of Fe^{3+} and of Cu^{2+} results in the production of hydroxyl radicals and/or metal-peroxide species that significantly increase levels of oxidative DNA photocleavage.[47-49] In order to minimize interference from redox active metals, all NaCl and KCl solutions used in our experiments were prepared from deionized, distilled water and 99.999% trace metals basis sodium$^+$ and potassium$^+$ chloride salts (Sigma-Aldrich). Notwithstanding, we considered the possibility that the increase in DNA photocleavage generated by the addition of 150 mM of NaCl and 260 mM of KCl to **4** might be due to contamination of the chloride salt solutions by DNA damaging, redox active iron^{3+} and copper^{2+} ions. In order to test this hypothesis, photocleavage experiments were conducted in which 10 μM to 0.5 μM concentrations of 9-aminomethylanthracene **4** were equilibrated with pUC19 plasmid DNA, 150 mM of NaCl in combination with 260 mM of KCl, in the presence and absence of a

redox active metal salt, either $CuCl_2 \cdot 2H_2O$ or $FeCl_3 \cdot 6H_2O$. As shown in Figure S2 of Supporting Information, the addition of the Cu^{2+} salt inhibited DNA photocleavage (Lanes 1 to 5 vs. Lanes 8 to 12 in Figure S2A), while the Fe^{3+} salt had no discernable effect (Lanes 1 to 5 vs. Lanes 8 to 12 in Figure S2B). This result indicates that contamination by copper^{2+} and/or iron^{3+} ions is not the major cause of the chloride salt-induced photocleavage enhancement observed in our experiments.

In order to evaluate the effects of individual chloride salts, pUC19 plasmid DNA was equilibrated with 10.0 μM to 0.5 μM concentrations of **4** in the presence and absence of either 150 mM of NaCl, 260 mM of KCl, or 410 mM of NaCl. The gel images in Figure S3 show that, when present in combination, 150 mM NaCl and 260 mM KCl (Figures 1A and S3A) produce a much more dramatic enhancement in anthracene-sensitized DNA photocleavage compared to either 150 mM NaCl, 260 mM KCl, or 410 mM NaCl (Figures S3B to S3D). The addition of the salts altered photocleavage in the following order: 150 mM NaCl and 260 mM KCl (major enhancement, Lanes 1 to 5 vs. Lanes 8 to 12 in Figure S3A) > 410 mM NaCl (enhancement, Lanes 4 and 5 vs. Lanes 11 and 12 in Figure S3D), ≅ 260 mM KCl (enhancement, Lanes 1 to 3 vs. Lanes 8 to 10 and inhibition, Lane 5 vs. Lane 12 in Figure S3C) > 150 mM NaCl (minor amounts of photocleavage inhibition, Lanes 4 and 5 vs. Lanes 11 and 12 in Figure S3B). Taken together, the results of these experiments indicate that potassium^{+} cations play a more significant role than sodium^{+} and chloride^{-} anions in the observed photocleavage increase.

3.4.3. Circular Dichroism Analysis. Monovalent and divalent cations that bind to nucleic acids bring about a number of changes to the secondary structure of double-helical DNA.[30-33] In particular, the helical twist angle of the duplex is increased, causing the DNA helix to be less tightly wound. This salt-induced alteration in twist angle is characterized by a

significant reduction in the positive DNA CD signal at 275 nm, making CD a useful tool to monitor helical unwinding.[30, 31]Towards this end, we recorded CD spectra of calf thymus DNA under the conditions of ionic strength employed in the preceding DNA photocleavage experiments (no hμ; Figure 3). The addition of 150 mM of NaCl did not produce a significant change in the overall shape and intensity of the CD spectrum of the CT DNA. Alternatively, the amplitude of the 275 nm band was markedly decreased by 260 mM KCl and by 260 mM KCl in combination with 150 mM of NaCl. Taken together with the results of the DNA photocleavage experiments (Figures 1A, S3A, S3B, and S3C), the CD data suggest that there may be a correlation between salt-induced changes in DNA structure and cleavage yields. The conditions of ionic strength that favor unwinding of the DNA duplex (260 mM KCl alone and in combination with 150 mM of NaCl) also increase levels of 9-aminomethylanthracene-sensitized photocleavage. In the absence of KCl, 150 mM of NaCl did not have a significant effect (Figure 3, Figure S3B).

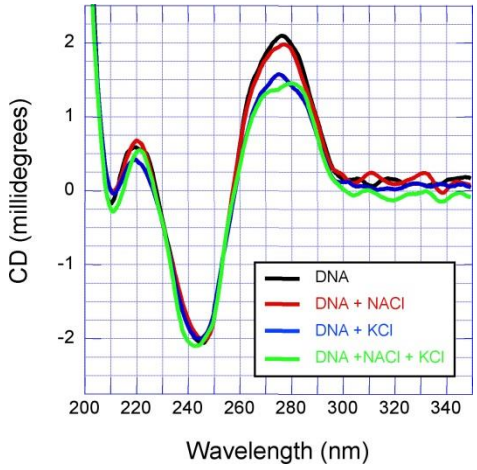

Figure 3.3. CD spectra recorded at 22 °C. Individual samples contained 30 μM bp CT DNA and 10 mM sodium phosphate buffer pH 7.0 (black line); 30 μM bp CT DNA, 10 mM sodium phosphate buffer pH 7.0, and 150 mM NaCl (red line); 30 μM bp CT DNA, 10 mM sodium phosphate buffer pH 7.0, and 260 mM KCl (blue line); 30 μM bp CT DNA, 10 mM sodium phosphate buffer pH 7.0, and 150 mM NaCl, and 260 mM KCl (green line). Prior to recording the spectra, the samples were pre-equilibrated for 1 h in the dark at 22 ºC.

DNA intercalators stack horizontally in between DNA base pairs. Upon binding, the DNA duplex unwinds in order to allow adjacent DNA base pairs to physically separate and make room for the intercalator.[50] As a result, intercalation significantly decreases the intensity of the positive DNA CD signal at 275 nm. (Because anthracene chromophores display relatively weak absorption at this wavelength, the DNA CD signal at 275 nm has been used as a sensitive probe for intercalative binding by anthracene derivatives (*51*).) Towards this end, we recorded the CD spectra of a series of solutions containing CT DNA, and/or 10.0 μM of **4** in the presence and absence of 150 mM of NaCl in combination with 260 mM of KCl (Figure 4). Under the low ionic strength conditions, the addition of compound **4** caused the CT DNA CD signal at 275 nm to decrease in intensity (Figure 4A). It can therefore be inferred from the CD spectra that 9-aminomethylanthracene derivative **4** may be engaging in DNA intercalation (*51*). Alternatively, there were no anthracene-induced variations in the CT DNA CD signal when 150 mM of NaCl and 260 mM KCl were present (Figure 4B). Because 10.0 μM of the anthracene produced significant photo-degradation of plasmid DNA under equivalent conditions of ionic strength (150 mM of NaCl in combination with 260 mM KCl), the data suggest that **4** is interacting with DNA by a non-intercalative binding mode that does not make substantial changes to DNA secondary structure.

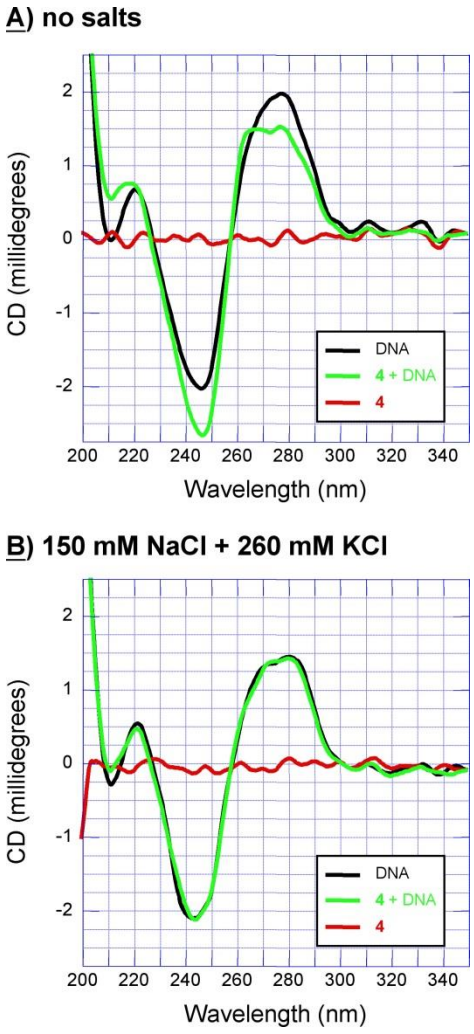

Figure 3.4. CD spectra recorded at 22 °C **A)** in the absence of 150 mM NaCl and 260 mM KCl and **B)** in the presence of 150 mM NaCl and 260 mM KCl. Individual samples contained 30 µM bp CT DNA and 10 mM sodium phosphate buffer pH 7.0 (black line); and 10 µM of **4**, 30 µM bp CT DNA, and 10 mM sodium phosphate buffer pH 7.0 (green line); and 10 µM of **4** and 10 mM sodium phosphate buffer pH 7.0 (red line). Prior to recording the spectra, the samples were pre-equilibrated for 1 h in the dark at 22 ºC.

3.4.4. Absorption Titration and Induced Circular Dichroism Data. UV-visible spectrophotometry was utilized in order to further study anthracene / DNA interactions. Our first DNA titration experiment was conducted in the absence of 150 mM NaCl and 260 mM KCl. Small volumes of CT DNA were sequentially added to a solution containing 50 mM of **4** (Figure 5A). An isosbestic point at 393 nm was observed, indicating that the titration produced a

transition between two spectroscopically distinct anthracene species. Notably, saturating amounts of CT DNA (250 μM bp and 300 μM bp) induced significant hypochromicity and a significant bathochromic shift in the peak positions of the anthryl vibronic absorption bands. These spectral features are hallmarks of anthracene intercalation and are consistent with the decrease in the 275 nm CT DNA CD signal that compound **4** produces in the absence of NaCl and KCl (Figure 4A).[8, 9, 51, 52] Thus, one of the two spectroscopic species revealed by the absorption titration spectra may arise from intercalative binding of the anthracene chromophore to the DNA.

In a second titration experiment, CT DNA was added to 9-aminomethylanthracene **4** in the presence of 150 mM NaCl and 260 mM KCl. In contrast to the data shown in Figure 5A, the wavelengths and intensities of the three most prominent anthryl vibronic absorption maxima were not appreciably altered (Figure 5B). This result suggests that 9-aminomethylanthracene **4** is no longer engaging in intercalation. In the case of intercalative DNA binding, the strong hypochromism and red-shifts in the absorption spectrum of the chromophore are produced by electronic effects involving π–π stacking and dipole-dipole interactions with DNA base pairs. The strength of these electronic interactions is inversely proportional to the cube of the distance separating the chromophore and the bases.[53] Thus, when compared to intercalation, the absorption spectra of groove-binding anthracene derivatives show minimal if any red-shifting and intermediate amounts of hypochromism.[8, 9, 52]

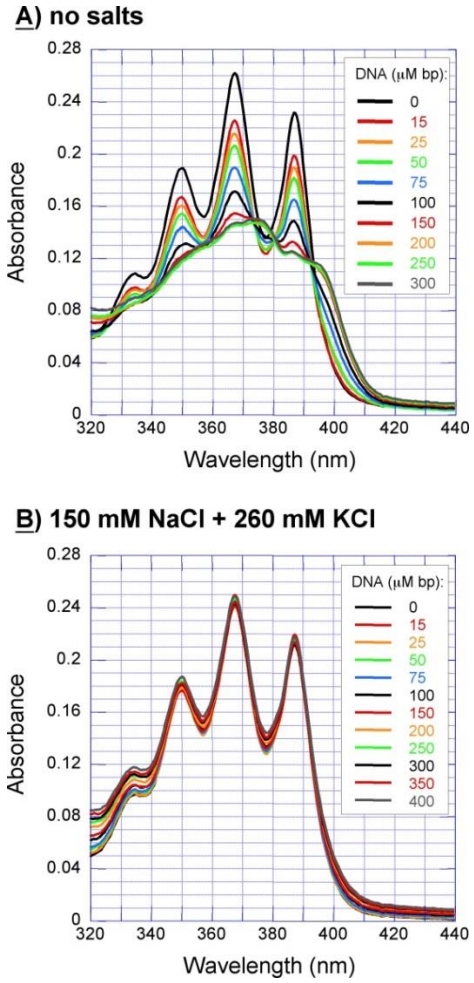

Figure 3.5. UV-visible absorption titration spectra of 50 μM of **4** recorded at 22 °C **A)** in the absence of 150 mM NaCl and 260 mM KCl and **B)** in the presence of 150 mM NaCl and 260 mM KCl. Individual samples contain 10 mM sodium phosphate buffer pH 7.0 and increasing concentrations of CT DNA (0 mM bp to 300 μM bp or 400 μM bp). Following each sequential DNA addition, the solution was allowed to equilibrate for 1 h in the dark before the UV-visible spectrum was recorded. All absorption spectra have been corrected for sample dilution.

Self-stacking of aromatic chromophores in aqueous solution can lead to the formation of dimers and higher order aggregates.[54, 55] In general, the absorption of the aggregate is hypochromic with respect to the absorption of the corresponding monomer. Taking this into account, we considered a scenario in which chromophore self-stacking in the absence of DNA might produce hypochromicity in the absorption spectrum of compound **4** (0 μM bp DNA;

Figure 5B). This interaction could then conceal changes in chromicity caused by subsequent DNA binding. In order to investigate this possibility, UV-visible spectra of a solution containing 50 μM of **4**, 150 mM of NaCl, and 260 mM of KCl (no DNA) were recorded in the presence of 0% (v/v) to 10% (v/v) concentrations of dimethyl sulfoxide, a reagent that is routinely used to disrupt intermolecular stacking of aromatic chromophores (*56;* Figure S4 in Supporting Information). Upon the addition of the DMSO, anthryl chromicity was unchanged, indicating that compound **4** was not self-stacking under the experimental conditions employed in the preceding DNA titration experiment (Figure 5B). It is therefore reasonable to hypothesize that when compound **4** is in the presence of 150 mM NaCl and 260 mM KCl, its anthryl ring is associated with DNA by an external interaction. At a significant distance from the chromophore, the DNA base pairs would be expected to have minimal influence on anthracene absorption (Figure 5B).

In order to study of effects of individual salts on absorption spectra, 50 μM of compound **4** was equilibrated with saturating amounts of DNA in the presence of 150 mM NaCl, 260 mM KCl, or 150 mM NaCl and 260 mM of KCl (Figure S5 of Supporting Information). The intensities of the vibronic bands of **4** were found to decrease according to salt conditions in the following order: 150 mM NaCl and 260 mM of KCl > 260 mM of KCl > 150 NaCl. This trend is in good general agreement with the relative levels of DNA photocleavage produced in the presence of equivalent concentrations of the chloride salts: 150 mM NaCl and 260 mM KCl (large salt-induced DNA photocleavage enhancement observed) > 260 mM KCl (intermediate enhancement) > 150 mM NaCl (minor amount of DNA photocleavage cleavage inhibition observed) (Figure S3 in Supporting Information). Because the strength of π–π stacking and dipole-dipole electronic interactions with DNA is proportional to anthracene hypochromicity and

is inversely proportional to separation between the DNA base pairs and the chromophore (*53*), the ability of compound **4** to photocleave DNA may increase as a function of increasing distance from the DNA bases.

In Figure 6 are the complete set UV-visible absorption spectra of 50 μM of **4** before and after the addition of saturating amounts of CT DNA (400 μM bp). In the absence of the chloride salts, the DNA produced strong hypochromicity accompanied by respective 8 nm and 7 nm red-shifts in the 0-1 and 0-0 vibronic bands of **4**, spectral features that are characteristic of anthracene intercalation (Figure 6A).[9, 51] In the presence of the individual salts, either 150 mM of NaCl (Figure 6B) or 260 mM KCl (Figure 6C), evidence of groove-binding was indicated by intermediate hypochromicity and minimal bathochromicity, with a significantly more pronounced effect being exhibited by 150 mM of NaCl.[8, 9, 52] In the case of the combination of salts (150 mM NaCl and 260 mM KCl), the vibronic absorption maxima of the two spectra were nearly superimposable (Figure 6D), consistent with our hypothesis that compound **4** is associated with the DNA helix through a mode in which the anthracene ring of the chromophore is external to the DNA base pairs.

In order to corroborate the absorption data shown in Figure 6, we recorded induced circular dichroism spectra of 50 μM of **4** equilibrated with CT DNA (150 μM bp). In the absence of the chloride salts, we observed positive ICD bands with peak positions closely resembling the red-shifted vibronic bands in the absorption spectrum of DNA-bound **4** (Figure 6A; Figure S6 of Supporting Information). This ICD signature is typical of 9-aminomethylanthracene derivatives and is thought to arise from an intercalative binding mode in which the long axis of the anthracene is perpendicular to the long axis of the DNA base pairs.[8, 9, 19, 51, 52] The addition of 150 mM NaCl and 260 mM KCl to the anthracene solutions caused the ICD signal of DNA-bound **4**

to become significantly attenuated (Figure S6). In general, a major reduction in ICD signal intensity is displayed when anthracene chromophores undergo a change in binding from

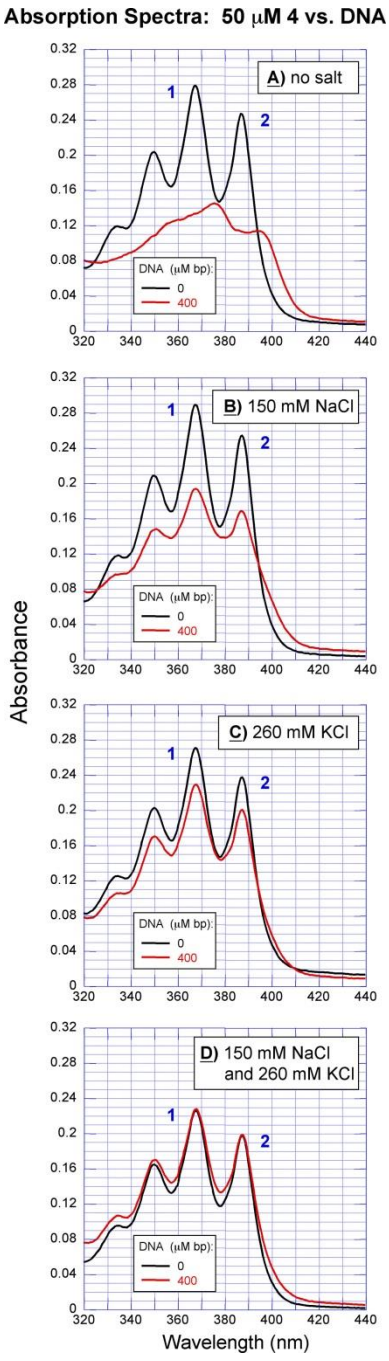

Figure 3.6. UV-visible absorption spectra of: 50 mM of **4** equilibrated in the absence (black line) and presence (red line) of 400 mM bp CT DNA (10 mM sodium phosphate buffer pH 7.0): **A)** no salt, Dl_{max1} = 8 nm, Dl_{max2} = 7 nm; **B)** 150 mM NaCl, Dl_{max1} = 0 nm, Dl_{max2} = -0.5 nm; **C)** 260 mM KCl, Dl_{max1} = 0.5 nm, Dl_{max2} = 0 nm; **D)** 150 mM NaCl and 260 mM KCl, Dl_{max1} = 0 nm, Dl

$_{max2}$ = 0 nm. Note: Peak 1 = 0-1 transition; Peak 2 = 0-0 transition; $Dl_{max\ n}$ = (l_{max} of peak n in the presence of DNA - l_{max} of peak n in the absence of DNA).

intercalation to a non-intercalative mode (*e.g.,* groove binding).[8, 9] Furthermore, the ICD peak positions of **4** were found to be dissimilar to the anthryl vibrational bands of the corresponding absorption spectrum recorded in the presence of the chloride salts (Figures S6 and 6D). This suggests that the ICD spectra may arise from a secondary binding interaction, (*e.g.*, residual intercalation), that is unrelated to the principal, non-intercalative binding mode indicated by the absorption data (Figures S6 and 6D).[9] Notwithstanding, the absorption and ICD data support the hypothesis that the addition of the chloride salts to the DNA solution disrupts the intercalative binding of compound **4**.[9]

3.4.5. Fluorescence Spectroscopy. DNA intercalation of 9-aminomethylanthracene derivatives results in strong fluorescence quenching of the anthryl fluorophore's vibronic emission bands.[8, 19, 52, 57] In some cases, this is accompanied by a change in relative band intensities and in red-shifting of their peak positions.[8, 19, 57] The quenching produced by intercalation is dependent on DNA sequence in the following order: d(GC) > CT DNA >> d(AT) >> d(A)-d(T).[57] Because the oxidation potential of guanine is the lowest of the four DNA bases, it has been suggested that an electron transfer pathway is responsible.[19] (The singlet energies of the DNA bases are significantly higher than that of anthracene, making energy transfer to DNA an unlikely alternative).[19, 57] Upon switching a DNA-bound anthracene from an intercalative to a groove-binding mode, the fluorescence quenching can be partially reversed.[8] In the case of electrostatic interaction of anthracenes with anionic media (*e.g.,* poly(sodium 4-styrenesulfonate) and sodium dodecyl sulfate), an increase (rather than decrease) in anthryl emission intensity is observed.[57] Thus, in order to obtain additional insights into the nature of

the interactions of 9-aminomethylanthracene **4** with DNA, we recorded a complete set of fluorescence emission spectra before and after the addition of saturating amounts of CT DNA (Figure 7; 50 μM of **4**, 400 μM bp CT DNA; 150 mM of NaCl and/or 260 mM of KCl). The samples were excited at 393 nm, a wavelength at which absorbance was found to relatively independent of DNA concentration and ionic strength (Figure 6). In the absence of the chloride salts, the addition of the CT DNA produced significant fluorescence quenching and red-shifting of the anthryl vibronic bands, consistent with intercalative binding (Figure 7A). As the chloride salt concentration was increased up to 150 mM NaCl and 260 mM KCl, the CT DNA caused a progressive reduction in: (i) red-shifting of the emission spectra, and (ii) quenching of the low energy 0-1 and, to a greater extent, the high energy 0-0 anthryl bands (Peaks 2 and 1 in Figure 7). The latter changes in relative peak intensity may arise from differences in the equilibrium geometries of the ground states and excited vibronic states of the free vs. DNA-bound anthracene.[19] Notwithstanding, a considerable increase in anthryl fluorescence emission intensity was produced by the addition of the CT DNA to the solution containing the combination of chloride salts (150 mM NaCl and 260 mM KCl; Figure 7D). This result points to a non-intercalative interaction between compound **4** and the CT DNA.[57] The ability of the chloride salts to induce significant spectral changes to the emission spectrum of free **4** (no CT DNA) is consistent with literature reports in which metal chelating 9-aminomethylanthracene fluorophores have been used to detect Na^+ and K^+ cations in aqueous and non-aqueous media (Figures 7B, 7C, and 7D vs. Figure 7A).[45, 46]

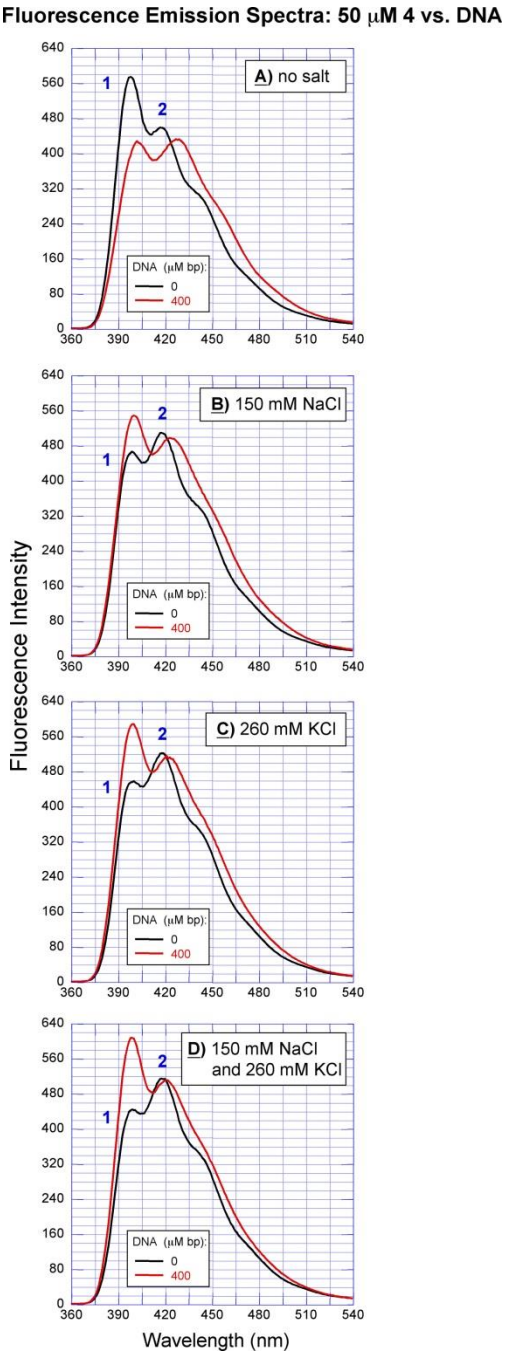

Figure 3.7. Fluorescence emission spectra with excitation at 393 nm of: 50 mM of **4** equilibrated in the absence (black line) and presence (red line) of 400 μM bp CT DNA (10 mM sodium phosphate buffer pH 7.0): **A)** no salt, Dl_{max1} = 4 nm, Dl_{max2} = 10 nm; **B)** 150 mM NaCl, Dl_{max1} = 1 nm, Dl_{max2} = 6 nm; **C)** 260 mM KCl, Dl_{max1} = 0 nm, Dl_{max2} = 2 nm; **D)** 150 mM NaCl and 260 mM KCl, Dl_{max1} = 0 nm, Dl_{max2} = 3 nm. Note: Peak 1 = 0-0 transition; Peak 2 = 0-1 transition; $Dl_{max\ n}$ = (l_{max} of peak n in the presence of DNA - l_{max} of peak n in the absence of DNA).

3.4.6. Thermal Melting of DNA. Ligands that preferentially interact with double-helical DNA stabilize the nucleic acid duplex and, as a result, increase the helical melting temperature. Alternatively, preferred association with single-stranded DNA can lead to duplex destabilization and a concomitant reduction in T_m.[58] In this regard, DNA melting temperature trends can reveal important information regarding the effects of ligand interactions on the dynamics of DNA structure. In our first set of thermal melting experiments, DNA isotherms were recorded in the absence and presence of 150 mM NaCl and 260 mM KCl, at dye to DNA bp molar ratio values (**r**)[1] ranging from 0 to 2.4 (Figure 8). The 18 mer hairpin duplex sequence 5'-CACTGGTCTCTACCAGTG-3' was used as an alternative to calf thymus DNA, in order to avoid exceeding the maximum recordable temperature of our instrumentation (95 °C) when working under high chloride salt concentrations. Shown in Figure 8A are the normalized melting curves generated in the absence of NaCl and KCl. (Reprentative, un-normalized and first derivative melting curves are in Figure S7A of Supporting Information.) Under these conditions, the T_m value obtained for the 18 mer hairpin duplex was 60 °C. Upon the addition of 9-aminomethylanthracene derivative **4**, the T_m was increased to a maximum of 66 °C at DNA saturation (**r** $\geq$ 1.5). Intercalative binding of anthracene chromophores enhances duplex stability and substantially increases DNA melting temperature.[8, 9, 19, 52] In the case of groove-binding anthracenes, changes in melting temperature are generally not observed.[9] Thus, in the absence of salts, the high T_m values produced by compound **4** are consistent with intercalative binding. Interestingly, the increase in melting temperature at each **r** value was accompanied by a progressive broadening of the 18 mer hairpin duplex melting curve (Figure 8A).

In our next experiment, melting curves of the 18 mer hairpin duplex were recorded in the presence of 150 mM of NaCl in combination with 260 mM of KCl (Figure 8B; Figure S7B). The

inclusion of the chloride salts raised the T_m value of the duplex from 60 °C (**r** = 0 in Figure 8A) to 71 °C (**r** = 0 in Figure 8B). Compound **4** was then added at **r** values of 0.3 up to 2.4. This resulted in an additional, progressive broadening of the DNA melting curves accompanied by an incremental shift of each curve to a lower temperature range. At DNA saturation (**r** ≥ 0.9), the melting temperature of the duplex was reduced from 71 °C to 68 °C.

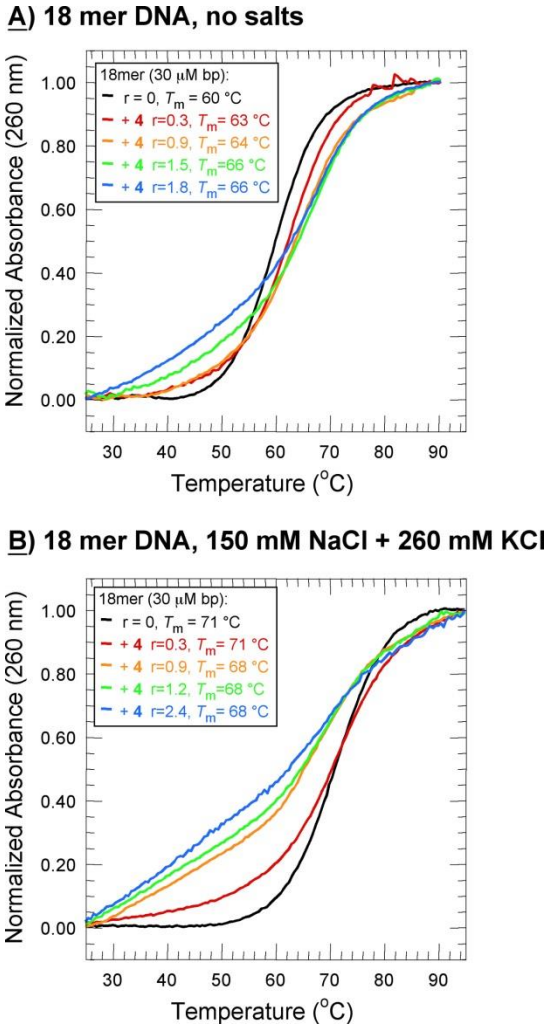

Figure 3.8. Normalized melting isotherms of 30 μM bp of 18 mer hairpin duplex 5'-CACTGGTCTCTACCAGTG-3' in 10 mM sodium phosphate buffer pH 7.0 without and with compound **4.** Melting curves were recorded **A)** in the absence of 150 mM NaCl and 260 mM KCl (**r** = 0 to 1.8), and **B)** in the presence of 150 mM NaCl and 260 mM KCl (**r** = 0 to 2.4). Abbreviation: **r** = [dye]/[DNA bp].

The majority of DNA ligands increase, rather than decrease, the T_m of double-helical DNA (*58*). Therefore, in order to confirm the preceding results, an additional set of melting isotherms was obtained using sonicated CT DNA. In the absence of the chloride salts, compound **4** (**r** = 0.3 in Figure 9A), and a positive control, the classical intercalating dye methylene blue (**5**; **r** = 0.3 in Figure 9B), each raised the T_m value of the duplex DNA from 68 °C to 75 °C, with the isotherm of **4** melting over a broader range than the isotherm of **5** (Figure 9). We then recorded a complete set of thermal melting curves in which CT DNA was pre-equilibrated with compound **4** at **r** values of 0 to 1.2 (no chloride salts; Figure S8 of Supporting Information). The magnitude of the ΔT_m value obtained at DNA saturation (12 °C; **r** $\geq$ 1.0) is characteristic of intercalative binding of anthracene derivatives to DNA.[8, 9, 19, 52]

Individual chloride salts, either 150 mM of NaCl or 150 mM of KCl, were then added to DNA solutions. The T_m value of the calf thymus DNA was raised from 68 °C to 85 °C and 88 °C by NaCl and KCl, respectively (**r** = 0 in Figure 9). The inclusion of the methylene blue (**5**) did not significantly alter the CT DNA melting curves (**r** = 0.3 in Figure 9B). In contrast, 9-aminomethylanthracene **4** broadened and shifted the melting curves to a lower temperature range (**r** = 0.3 in Figure 9A). In the case of 150 mM of NaCl, the 85 °C melting temperature was not changed. Alternatively, when 150 mM of KCl was present, compound **4** lowered the T_m of the CT DNA from 88 °C to 86 °C (**r** = 0.3 in Figure 9A).

Taken together, the 18 mer hairpin duplex and CT DNA data support our hypothesis that compound **4** engages in DNA intercalation under conditions of low ionic strength (Figures 8A, 9A, and S9). In DNA samples containing high concentrations of KCl, alone and in combination with NaCl, the addition of **4** to DNA decreases T_m. These findings suggest that intercalation has been disrupted in favor of a binding mode that does not confer appreciable stabilization onto the

DNA duplex (Figures 8B and 9A). The majority of ligands that lower DNA melting temperature are metal salts or compounds that form destabilizing adducts with DNA bases.[59-61] Interactions between anthracenes and DNA are primarily non-covalent in nature.[43, 44] Although long wave UV irradiation of anthracene-DNA complexes can initiate covalent binding of the hydrocarbon to DNA bases, precautions were taken to protect our melting temperature samples from prolonged exposure to light. Therefore, the question remains as to why, under conditions of high ionic strength, compound **4** appears to exert a destabilizing effect that reduces DNA melting temperature. In the presence of anthracene derivative **4**, the DNA melting curves also exhibited a significant degree of transition broadening (Figures 8, 9A, and S8). This phenomenon normally occurs when a given ligand stabilizes (or destabilizes) specific regions or sequences within a DNA duplex to a greater degree than other regions.[58]

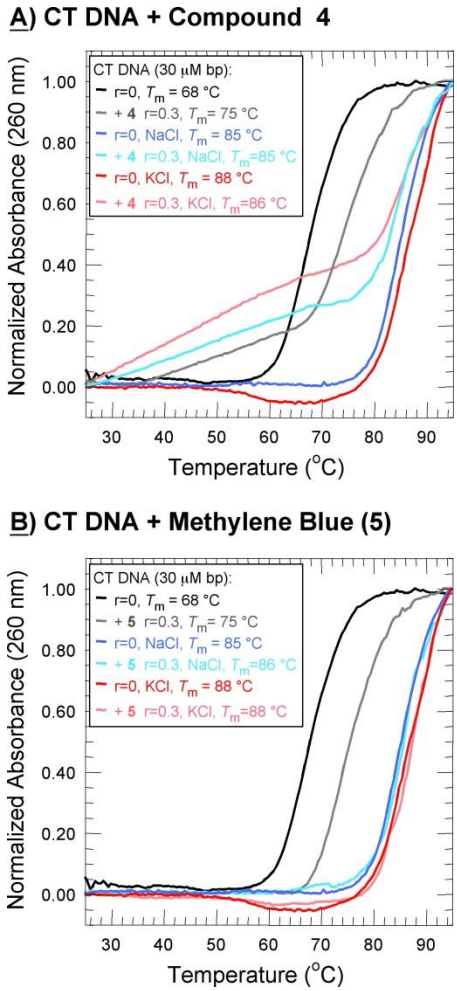

Figure 3.9. Normalized melting isotherms of 30 μM bp of CT DNA in 10 mM sodium phosphate buffer pH 7.0: without chloride salts (black / grey lines), with 150 mM of NaCl (blue / cyan lines), or with 150 mM of KCl (red / pink lines). Melting curves were recorded in the absence (**r** = 0; light lines) and presence (**r** = 0.3; dark lines) of **A)** 10 μM of compound **4**, and **B)** 10 μM of methylene blue (**5**). Abbreviation: **r** = [dye]/[DNA bp].

3.4.7. Chemically Induced Changes in DNA Photocleavage. As a test for reactive oxygen species, we used the singlet oxygen ($^1O_2$) scavenger sodium azide and the hydroxyl radical (·OH) scavengers sodium benzoate and D-mannitol. Individual samples contained pUC19 plasmid DNA and 9-aminomethylanthracene derivative **4** in the presence and absence of 150 mM of NaCl in combination with 260 mM of KCl. The percent of total photocleavage inhibited by each of the scavengers is shown in Table 1. Sodium azide, sodium benzoate, and D-mannitol

produced a considerable inhibitory effect, indicating that singlet oxygen and hydroxyl radicals contribute to DNA photocleavage. Moreover, higher levels of photocleavage inhibition occurred in the reactions containing the combination of chloride salts. The most significant result was produced by sodium azide. Using this $^1O_2$ scavenger, yields of DNA photocleavage were respectively reduced by 83$\pm$6% and by 27$\pm$1% in the presence and absence of 150 mM NaCl and 260 mM of KCl (Table 1). These data suggest that there is a sharp increase in the production of singlet oxygen under conditions of high ionic strength. The salt-dependent involvement of singlet oxygen was then confirmed using deuterium oxide, a solvent that increases the lifetime of $^1O_2$ (Figure S9 in Supporting Information).[62] In the presence of the combination of chloride salts, the average percent yields of DNA photocleavage increased from 67$\pm$10% in ddH_2O to 100$\pm$0% in D_2O. In contrast, deuterium oxide had little effect in the absence of the chloride salts, where the average yields of cleaved DNA were 42$\pm$2% and 40$\pm$2% in ddH_2O and D_2O, respectively (Figure S9).

In a study of DNA photocleavage by cyanine dyes, Åckerman and Tuite found that externally bound cyanines produced more DNA photocleavage than when the same dyes were engaged in DNA intercalation.[36] Scavenger experiments showed that, when bound externally, the cyanine dyes generated DNA cleavage by photosensitizing the production of singlet oxygen. However, when the dyes were intercalated, there was no evidence of the involvement of singlet or ground state triplet oxygen in the photocleavage reactions. This finding was considered to be consistent with a general phenomenon in which the microenvironment of the DNA intercalation pocket prevents fluorescent dyes from freely interacting with ground state triplet oxygen and other quenching agents.[36, 63] The same principle may be used to explain why levels of DNA photocleavage are increased when the combination of 150 mM of NaCl and 260 mM of KCl is

added to 9-aminomethylanthracene **4**. The presence of the chloride salts appears to trigger a change in anthracene binding from intercalation to an external mode in which the anthracene chromophore may be considerably more accessible to dissolved oxygen. This in turn may lead to an increase the anthracene-sensitized production of DNA damaging singlet oxygen and hydroxyl radicals.

Table 3.1. Average % Inhibition of DNA Photocleavage by ROS Scavengers [a]

Scavenger	ROS	Percent Inhibition, No Salt [b]	Percent Inhibition, Salt [c]
sodium azide	$^1O_2$	27±1	83±6
sodium benzoate	·OH	21±5	55±7
D-mannitol	·OH	2±1	17±4

[a] Photocleavage inhibition reactions consisted of 38 μM bp of pUC19 plasmid DNA equilibrated with 2.5 μM of **4**, 100 mM of scavenger, and 10 mM sodium phosphate buffer pH 7.0, in the absence [b] and presence [c] of 150 mM NaCl in combination with 260 mM KCl. Samples were aerobically irradiated for 60 min at 350 nm. Percent inhibition data were averaged over three to four trials with error reported as standard deviation.

3.5. Summary and General Discussion

In this paper, we describe the synthesis and DNA interactions of a new 9-aminomethylanthracene dye *N*-substituted with a pyridinylpolyamine side chain (**4** in Scheme 1). We found that the levels of DNA photocleavage produced by compound **4** were enhanced when 150 of mM NaCl and 260 of mM KCl were added to cleavage reactions (0.5 to 10 mM of **4**, 350 nm, pH 7.0, 22 °C; Figures 1A, 2, S1, and S3A). This finding was quite unexpected. Because conditions of high ionic strength typically decrease the association of DNA photosensitizers and other ligands with double-helical DNA, it is anticipated that photocleavage yields will be

substantially decreased (Figure 1B) [8, 27, 28, 34-37] Therefore, a major goal of the research described in this paper was to determine why DNA photocleavage was enhanced upon the addition of 150 mM of NaCl and 260 mM of KCl to 9-aminomethylanthracene **4** cleavage reactions. In preliminary experiments, the inclusion of micromolar concentrations of $CuCl_2 \cdot 2H_2O$ or $FeCl_3 \cdot 6H_2O$ in chloride salt solutions did not add to photocleavage yields, ruling against contamination by redox active Cu^{2+} and Fe^{3+} ions (Figure S2). Alternatively, DNA photocleavage was enhanced upon the addition of 150 mM and 260 mM KCl to the quaternary amine (9-anthracenylmethyl)trimethylammonium chloride (**6**) (Figure 1C), ruling out a major involvement of the amine group lone pair electrons in the side chain of **4**. When the chloride salts were tested in combination and individually, the largest photocleavage enhancement was produced by 150 mM of NaCl in combination with 260 mM of KCl, followed by 410 mM of NaCl and 260 mM of KCl (Figures 1 and S3). Thus, potassium$^+$ cations were shown to play a significant role. A correlation between K^+-induced helical unwinding and an increase in cleavage yields was then indicated by CD spectrometry (Figure 3).

Our next experiments were focused on determining if the salt-induced increase in DNA photocleavage was related to a change in anthracene binding mode. In the absence of the chloride salts, intercalative binding of **4** was indicated by the following lines of evidence. The addition of **4** to CT DNA caused the DNA CD signal at 275 nm to decrease in intensity (Figure 4A).[51] The addition of CT DNA to **4** produced (i) significant hypochromicity and bathochromicity in the anthracene's vibronic absorption bands (Figures 5A and 6A) [9, 51]; (ii) a relatively strong, corresponding, positive induced CD signal (Figure S6) [8, 9, 19, 51, 52]; and (iii) significant fluorescence quenching and red-shifting of the anthryl vibronic emission spectrum (Figure 7A; *19, 57*). Finally, compound **4** at DNA saturation produced helical stabilization that

was associated with a significant increase in the T_m values of an 18 mer hairpin duplex (Figure 8A) and calf thymus DNA (Figure S8). [8, 9, 19, 52]

Evidence obtained in the presence of the combination of chloride salts (150 mM NaCl and 260 mM KCl) pointed to a non-intercalative binding mode. The addition of **4** to CT DNA did not alter the intensity of the DNA CD signal at 275 nm (Figure 4B). The addition of CT DNA to **4** produced (i) minimal changes to the wavelengths and intensities of the major anthryl vibronic band absorption maxima (Figures 5B and 6D); (ii) a very weak, positive induced CD signal (Figure S6); [8, 9] and (iii) enhanced fluorescence emission accompanied by minimal red-shifting of the anthryl vibronic peak positions (Figure 7D; *57*). Lastly, compound **4** at DNA saturation shifted the melting curves of DNA to a lower temperature range, generating a decrease in the T_m of the 18 mer hairpin duplex consistent with helical destabilization (Figure 8B)[58] The addition of **4** to solutions containing the individual salts (either 150 mM of NaCl or 150 mM of KCl) also shifted the melting curves of CT DNA to lower temperatures (Figure 9A). This effect was more pronounced in the case of 150 mM of KCl, where compound **4** exhibited a destabilizing effect that lowered T_m (Figure 9A).

All in all, the preceding data indicate that the increase in anthracene-sensitized photocleavage that is produced by the addition of 150 mM NaCl and 260 mM KCl to the DNA reactions is likely to be accompanied by a salt-induced change in anthracene binding from intercalation to a non-intercalative mode. While unraveling the precise nature of the interactions between DNA and compound **4** will rest on high-resolution structural analyses, the evidence presented in this paper points to external binding. In the presence of the chloride salts, the addition of saturating amounts of CT DNA does not alter the positions and intensities of the major vibronic absorption maxima of **4**, indicating that there is a significant distance separating

the anthracene chromophore from the DNA base pairs. Secondly, the sharp increase in singlet oxygen production that occurs under conditions of high ionic strength is consistent with a binding mode in which the anthracene chromophore is relatively accessible to ground state triplet oxygen.[36, 63]

3.6. Conclusions

Within the cell nucleus where genomic DNA is contained, average concentrations of NaCl and KCl are ~ 150 mM and 260 mM, respectively.[22 - 25] Thus, in photodynamic cancer therapy, an ideal DNA photosensitizer should function optimally under conditions of high ionic strength. Towards this end, we have shown that the addition of 150 mM of NaCl and 260 mM of KCl to 9-aminomethylanthracene **4** reactions produces a significant and unexpected increase in anthracene-sensitized DNA photocleavage (350 nm, pH 7.0). In the presence of micromolar concentrations of **4**, the combination of chloride salts triggers the photo-degradation of supercoiled, nicked, and linear forms of pUC19 plasmid into a diffuse band of high mobility DNA fragments (Lanes 1 to 3 vs. Lanes 8 to 10 in Figure 1A). Our data point to a salt-induced change in DNA binding mode from intercalation to an external interaction that efficiently promotes the formation of reactive oxygen species. Helical unwinding by monovalent potassium cations may play an important role in this process. We envisage that the insights gained from this research will contribute to the development of new and structurally diverse photo-therapeutic agents that function optimally in the ionic environment of the cell nucleus.

3.7. Supporting Information

The following Figures and Discussion: **Figure S1**, agarose gel showing time-dependent photocleavage of pUC19 plasmid by *N*-substituted 9-(aminomethyl)anthracene **4**; **Figure S2**, agarose gels showing photocleavage of pUC19 plasmid by **4** in the presence and absence of A) $CuCl_2 \cdot 2H_2O$, and B) $FeCl_3 \cdot 6H_2O$; **S2** Discussion; **Figure S3**, agarose gels showing photocleavage of pUC19 plasmid by **4** in the presence and absence of A) 150 mM of NaCl and 260 mM of KCl, B) 150 mM of NaCl, C) 260 mM of KCl, and D**)** 410 mM of NaCl; **Figure S4,** UV-visible absorption titration spectra of **4** with 150 mM NaCl and 260 mM KCl in the presence of increasing concentrations of DMSO; **Figure S5,** UV-visible absorption spectra of **4** with CT DNA in the presence of 150 mM NaCl in combination with 260 mM KCl, 260 mM KCl, or 150 mM NaCl; **Figure S6**, double y-axis plot of A) ICD spectra and B) UV-visible absorption spectra of **4** and/or CT DNA; **Figure S7**, un-normalized and corresponding first derivative melting isotherms an 18 mer hairpin duplex in the absence and presence of **4** (**r** = 0 and 0.3); **Figure S8**, normalized thermal melting curves of CT DNA in the absence and presence of **4** (**r** = 0 to 1.2). **Figure S9**, agarose gels showing photocleavage of pUC19 plasmid by **4** in the presence of ddH_2O or D_2O.

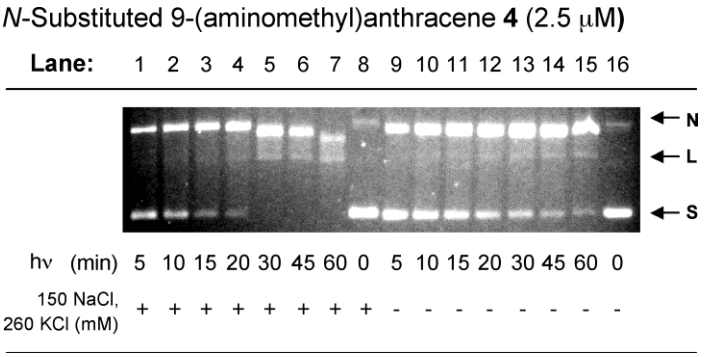

Figure 3.S1. Photograph of a 1.5% nondenaturing agarose gel showing photocleavage of pUC19 plasmid by *N*-substituted 9-(aminomethyl)anthracene **4** (0.5 mg/mL of ethidium bromide). Samples contained 10 mM sodium phosphate buffer pH 7.0, 38 mM bp DNA, and 2.5 mM of **4** in the presence (Lanes 1 to 8) and absence (Lanes 9 to 14) of 150 mM NaCl and 260 mM KCl (total volume 40 mL). Prior to photocleavage, the reactions were pre-equilibrated for 1 h in the dark at 22 ºC. The samples were then irradiated for 0 min, 5 min, 10 min, 15 min, 20 min, 30 min, 45 min, or 60 min at 22 °C in an aerobically ventilated Rayonet Photochemical Reactor fitted with ten RPR-3500 Å lamps. After electrophoresis, yields of DNA photocleavage in each lane were determined by quantitating the DNA bands on the gel using the following formula: DNA photocleavage (%) = [(nicked DNA + linear DNA)/(nicked DNA + linear DNA + supercoiled DNA)] x 100 (Figure 2). Abbreviations: **L** = linear; **N** = nicked; **S** = supercoiled. Data correspond to time course plot in Figure 2 of the Main Manuscript.

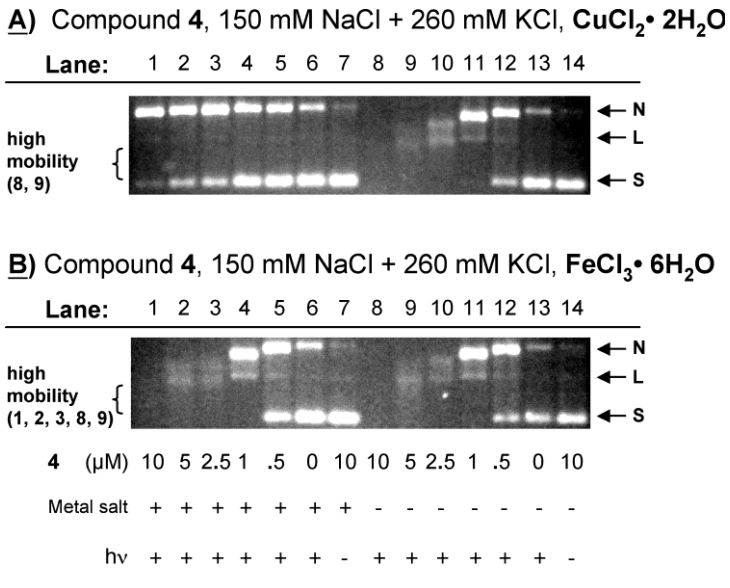

Figure 3.S2. Photographs of 1.5% nondenaturing agarose gels showing photocleavage of pUC19 plasmid by *N*-substituted 9-(aminomethyl)anthracene **4** in the presence and absence of **A)** 10 mM of $CuCl_2 \cdot 2H_2O$, and **B)** 10 mM of $FeCl_3 \cdot 6H_2O$ (0.5 mg/mL of ethidium bromide). Samples contained 38 mM bp DNA, and 150 mM of NaCl and 260 mM of KCl in 10 mM sodium phosphate buffer pH 7.0 (total volume 40 mL). **Lanes 1** to **6**: 10 mM to 0 mM of dye in the presence of metal salt. **Lanes 8** to **13**: 10 mM to 0 mM of dye in the absence of metal salt. **Lane 7**: 10 mM of dye in the presence of metal salt (no hn). **Lane 14**: 10 mM of dye in the absence of metal salt (no hn). Prior to photocleavage, the reactions were pre-equilibrated for 1 h in the dark

at 22 ºC. The samples in Lanes **1** to **6** and **8** to **13** were irradiated for 60 min at 22 °C in 1.7 mL microcentrifuge tubes in an aerobically ventilated Rayonet Photochemical Reactor fitted with ten RPR-3500 Å lamps. Abbreviations: **L** = linear; **N** = nicked; **S** = supercoiled.

3.7.1. Discussion In the photocleavage experiments shown in Figure S2, 10 μM to 0.5 μM concentrations of 9-aminomethylanthracene **4** were equilibrated with pUC19 plasmid DNA, 150 mM of NaCl in combination with 260 mM of KCl, in the presence and absence of $CuCl_2 \cdot 2H_2O$ or $FeCl_3 \cdot 6H_2O$. The data show that the addition of the Cu^{2+} salt inhibited DNA photocleavage (Lanes 1 to 5 vs. Lanes 8 to 12 in Figure S2A), while the Fe^{3+} salt had no effect (Lanes 1 to 5 vs. Lanes 8 to 12 in Figure S2B). This result indicates that contamination by copper^{2+} and/or iron^{3+} ions is not the major cause of the chloride salt-induced photocleavage enhancement observed in our experiments (Figures 1, 2, S1, and S3). Notwithstanding, it is of interest to consider possible causes underlying the differential effects of Cu^{2+} and Fe^{3+} on DNA photocleavage yields (Figure S2). The dissociation constants of Cu^{2+} and Fe^{3+} binding to CT DNA are in the micromolar range (*1, 2, 3*). While Cu^{2+} and Fe^{3+} bind to mixed nitrogen and oxygen sites on duplex DNA, the metal ions have different donor preferences (*2, 4*). The hard acid Fe^{3+} binds more favorably to the oxygen atoms of backbone phosphate groups (*5*), and in general leaves the conformation of B-form DNA unperturbed (*2*). Alternatively, the borderline acid Cu^{2+} interacts strongly with the nitrogen atoms in the DNA bases (*4, 5*). Thus, significant interaction with Cu^{2+} can disrupt Watson-Crick hydrogen bonding and base stacking interactions, causing the DNA to undergo a structural change (*4, 6*). It is therefore conceivable that the lower levels of DNA photocleavage we observed upon the inclusion of Cu^{2+} arise from the consequences of a direct interaction of this metal ion with DNA bases (Figure S2A). A second possible explanation involves the metal-binding bis((dimethylamino)methyl)pyridine ring

attached to the pyridinylpolyamine side chain of **4**. Amino-*N*-substituted analogs of the ligand 2,6-bis(aminomethyl)pyridine form stable 1:1 complexes with Cu^{2+} (*7, 8*). Thus, the preference of Cu^{2+} for nitrogen donors may lead to the formation of a strong Cu^{2+}/9-aminomethylanthracene complex. If the complex were to have reduced affinity for DNA compared to free **4**, then photocleavage inhibition would be observed. Because Fe^{3+} is oxophilic, it would be expected to interact with **4** less avidly. This would explain why the addition of the Fe^{3+} salt to DNA photocleavage reactions had no effect on cleavage yields.

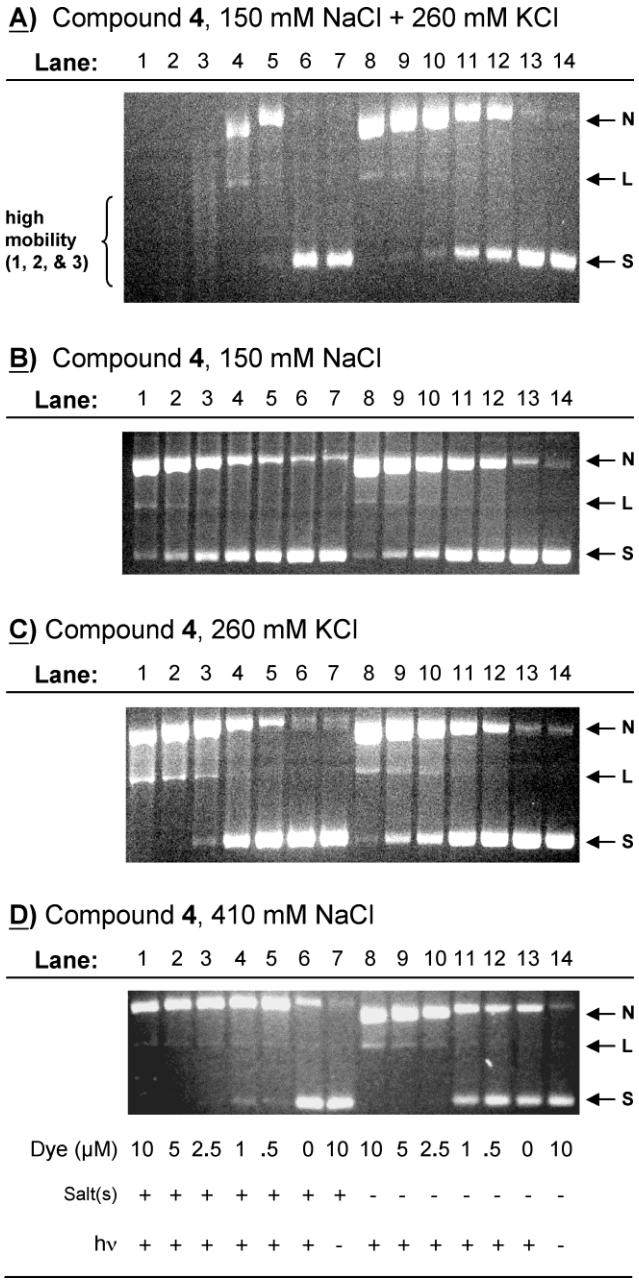

Figure 3.S3. Photographs of 1.5% nondenaturing agarose gels showing photocleavage of pUC19 plasmid by *N*-substituted 9-(aminomethyl)anthracene **4** in the presence and absence of **A)** 150 mM of NaCl and 260 mM of KCl, **B)** 150 mM of NaCl, **C)** 260 mM of KCl, and **D)** 410 mM of NaCl (0.5 mg/mL of ethidium bromide). Samples contained 10 mM sodium phosphate buffer pH 7.0 and 38 mM bp DNA (total volume 40 mL). **Lanes 1** to **6**: 10 mM to 0 mM of dye in the presence of salt(s). **Lanes 8** to **13**: 10 mM to 0 mM of dye in the absence of salt(s). **Lane 7**: 10 mM of dye in the presence of salt(s) (no hn). **Lane 14**: 10 mM of dye in the absence of salt(s) (no hn). Prior to photocleavage, the reactions were pre-equilibrated for 1 h in the dark at 22 ºC. The samples in Lanes **1** to **6** and **8** to **13** were irradiated for 60 min at 22 °C in 1.7 mL microcentrifuge tubes in an aerobically ventilated Rayonet Photochemical Reactor fitted with ten RPR-3500 Å lamps. Abbreviations: **L** = linear; **N** = nicked; **S** = supercoiled.

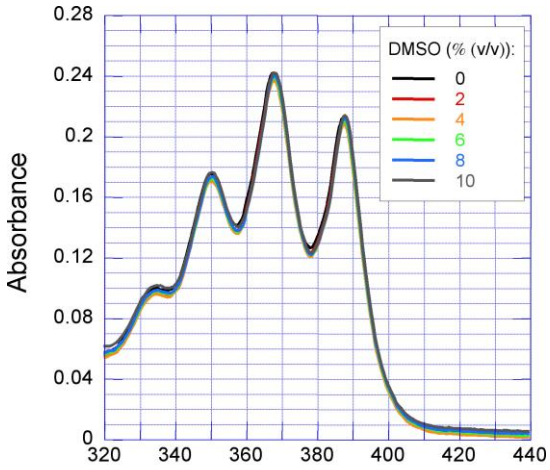

Figure 3.S4. UV-visible absorption spectra of 50 µM of **4** recorded at 22 °C in the presence of 150 mM NaCl and 260 mM KCl (no DNA). Individual samples contain 10 mM sodium phosphate buffer pH 7.0 and increasing concentrations of DMSO (0% to 10% (v/v)). The absorption spectra have been corrected for sample dilution.

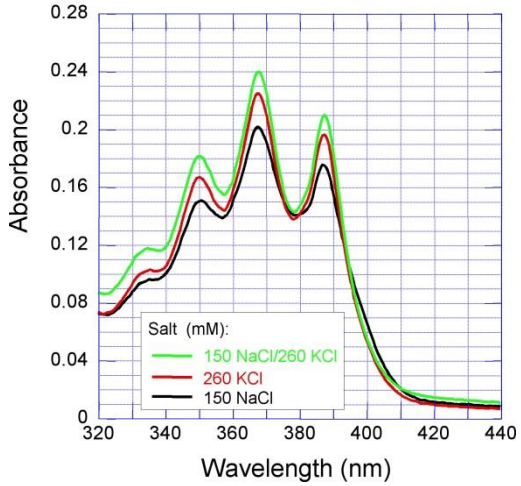

Figure 3.S5. UV-visible absorption titration spectra of 50 µM of **4** recorded at 22 °C in the presence of 350 mM bp CT DNA. Individual samples contain 10 mM sodium phosphate buffer pH 7.0 and 150 mM NaCl in combination with 260 mM KCl, 260 mM KCl, and 150 mM NaCl.

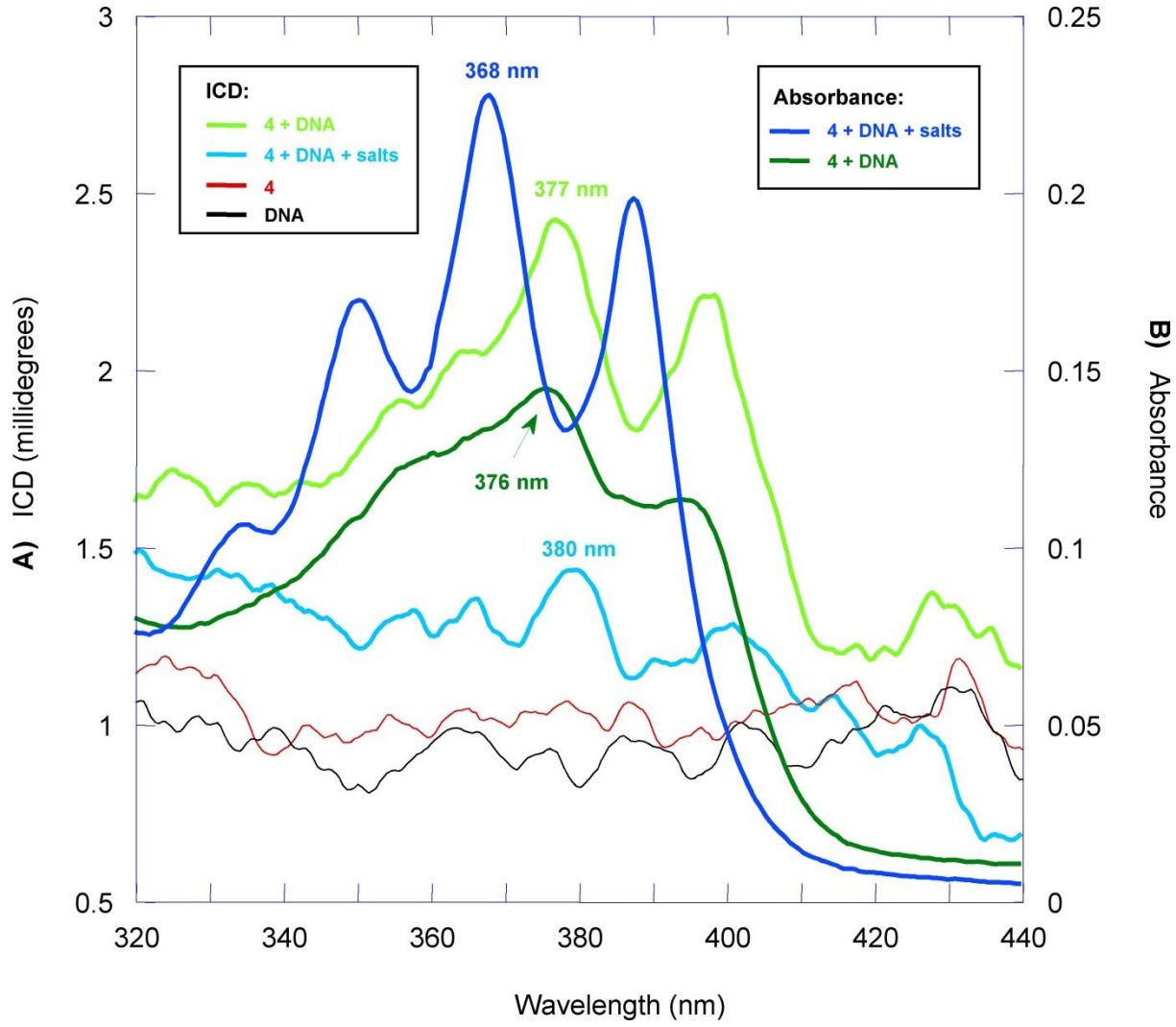

Figure 3.S6. Double y-axis plot of **A**) induced circular dichroism (ICD) spectra and **B)** UV-visible absorption spectra recorded at 22 °C in the absence and presence of salts (150 mM NaCl in combination with 260 mM KCl). Individual samples contained 10 mM sodium phosphate buffer pH 7.0, 50 µM of **4**, and/or CT DNA (400 mM bp for absorption spectra; 150 mM bp for ICD spectra). Prior to recording the spectra, the samples were equilibrated in the dark for 1 h at 22 °C. The l_{max} of the 0-1 anthryl band is indicated. UV-visible absorption spectra are from Figures 6A and 6D of the Main Manuscript.

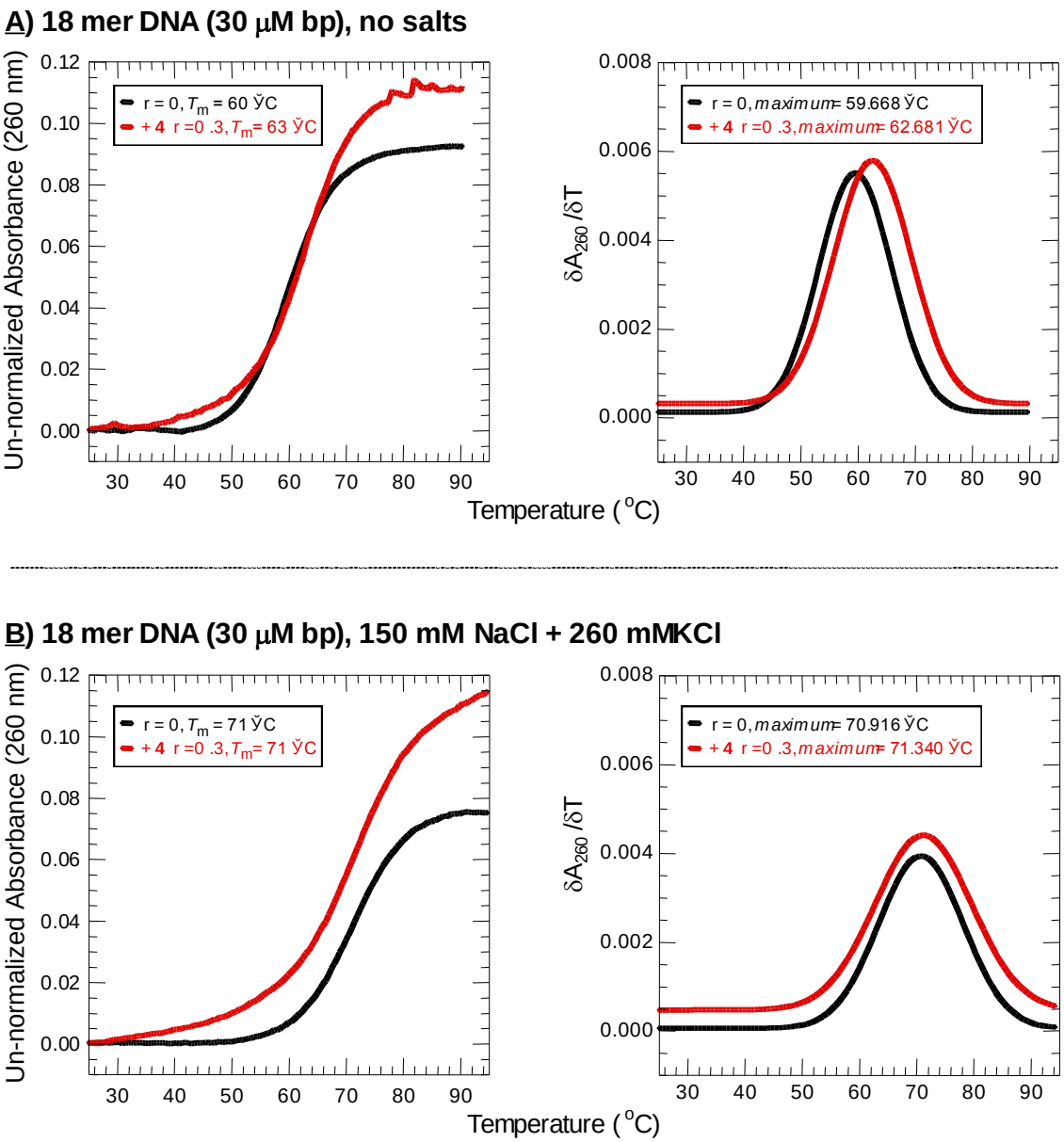

Figure 3.S7. Un-normalized and corresponding first derivative melting isotherms of 30 μM bp of 18 mer hairpin duplex 5'-CACTGGTCTCTACCAGTG-3' in 10 mM sodium phosphate buffer pH 7.0 without and with 10 mM of compound **4.** Melting curves were recorded **A)** in the absence of 150 mM NaCl and 260 mM KCl (**r** = 0.0 and 0.3), and **B)** in the presence of 150 mM NaCl and 260 mM KCl (**r** = 0 and 0.3). Individual solutions were allowed to pre-equilibrate for 1 h in the dark before the isotherms were acquired. Abbreviation: **r** = [dye]/[DNA bp]. Data correspond to normalized melting isotherms in Figures 8A and 8B of the Main Manuscript.

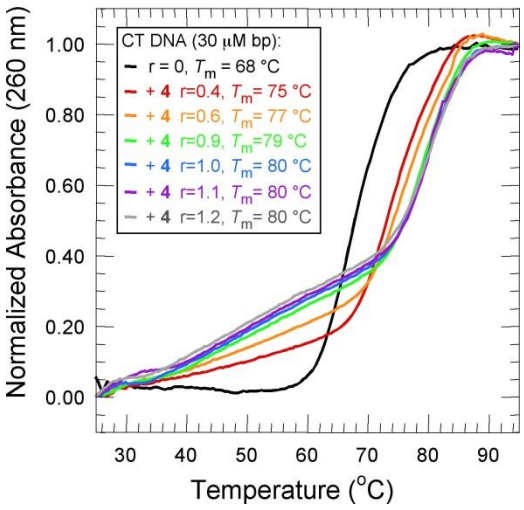

Figure 3.S8. Normalized thermal melting curves of 30 mM bp CT DNA in the absence of NaCl and KCl. The DNA was pre-equilibrated in 10 mM sodium phosphate buffer pH 7.0 and 0 mM to 36 mM of compound **4** (**r** = 0 to 1.2). Abbreviation: **r** = [dye]/[DNA bp].

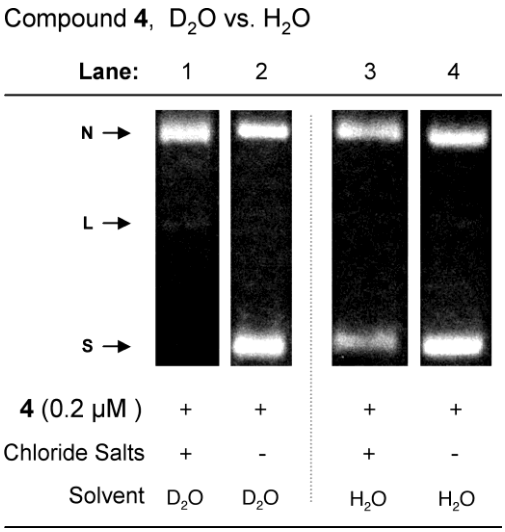

Figure 3.S9. Representative 1.5% nondenaturing agarose gels showing photocleavage of pUC19 plasmid by *N*-substituted 9-(aminomethyl)anthracene **4** in the presence and absence of D_2O (0.5 mg/mL of ethidium bromide). Samples contained 38 mM bp pUC19 plasmid DNA, 0.2 mM of **4**, and 10 mM sodium phosphate buffer pH 7.0, with and without 150 mM NaCl and 260 mM KCl (total volume 40 mL). The solvents employed were 81% (v/v) D_2O (**Lanes 1** and **2**) and 100% (v/v) ddH_2O (**Lanes 3** and **4**). Prior to photocleavage, samples were pre-equilibrated for 1 h in the dark at 22 ºC and then irradiated for 60 min at 22 °C in 1.7 mL microcentrifuge tubes in an aerobically ventilated Rayonet Photochemical Reactor fitted with ten RPR-3500 Å lamps. Abbreviations: **L** = linear; **N** = nicked; **S** = supercoiled. Note: the above reactions were run over three trials. The average % yields of cleaved DNA appear in the Main Manuscript. Errors are reported as standard deviation.

3.8. References

1. Zhang, Y., and Galoppini, E. (2010) Organic polyaromatic hydrocarbons as sensitizing model dyes for semiconductor nanoparticles. *ChemSusChem 3,* 410-428.

2. Jarikov, V.V. (2008) Quantum efficiency improvement in anthracene-based organic light-emitting diodes codoped with a hole-trapping material. *Appl. Phys. Lett. 92*, 244103/1-244103/3.

3. Gunnlaugsson, T., Ali, H.D.P., Glynn, M., Kruger, P.E., Hussey, G.M., Pfeffer, F.M., Santos, C.M.G., and Tierney, J. (2005) Fluorescent photoinduced electron transfer (PET) sensors for anions; from design to potential application. *J. Fluoresc. 15,* 287-299.

4. Lodeiro, C., Lippolis, V., and Mameli, M. (2010) From Macrocyclic Ligands to Fluorescent Molecular Sensors for Metal Ions: Recent Results and Perspectives, in *Macrocyclic Chemistry: New Research Developments* (Fitzpatrick, D.W. and Ulrich, H.J., Eds) pp 159-212, Nova Publishers, Hauppauge N.Y.

5. Bowden, G.T., Roberts, R., Alberts, D.S., Peng, Y.M., and Garcia, D. (1985) Comparative molecular pharmacology in leukemic L1210 cells of the anthracene anticancer drugs mitoxantrone and bisantrene. *Cancer Res. 45,* 4915-4920.

6. Iyengar, B.S., Dorr, R.T., Alberts, D.S., Sólyom, A.M., Krutzsch, M., and Remers, W.A. (1997) 1,4-disubstituted anthracene antitumor agents. *J. Med. Chem. 40,* 3734-3738.

7. Wilson, W.D., Wang, Y.H., Kusuma, S., Chandrasekaran, S., and Boykin, D.W. (1986) The effect of intercalator structure on binding strength and base-pair specificity in DNA interactions. *Biophys. Chem. 24,* 101-109.

8. Modukuru, N.K., Snow, K.J., Perrin, Jr., B.S., Bhambhani, A., Duff, M., and Kumar, C.V. (2006) Tuning the DNA binding modes of an anthracene derivative with salt. *J. Photochem. Photobiol. A 177,* 43-54.

9. Tan, W.B., Bhambhani, A., Duff, M.R., Rodger, A., and Kumar, C.V. (2006) Spectroscopic identification of binding modes of anthracene probes and DNA sequence recognition. *Photochem. Photobiol. 82,* 20-30.

10. Holmes, F.A., Esparza, L., Yap, H.Y., Buzdar, A.U., Blumenschein, G.R., and Hortobagyi, G.N. (1986) A comparative study of bisantrene given by two dose schedules in patients with metastatic breast cancer. *Cancer Chemother. Pharmacol. 18,* 157-161.

11. Morschhauser, F., Mounier, N., Sebban, C., Brice, P., Solal-Celigny, P., Tilly, H., Feugier, P., Fermé, C., Copin, M.C., and Lamy, T. (2010) Efficacy and safety of the combination of rituximab, fludarabine, and mitoxantrone for rituximab-naive, recurrent/refractory follicular non-Hodgkin lymphoma with high tumor burden: a multicenter phase 2 trial by the Groupe d'Etude des Lymphomes de l'Adulte (GELA) and Groupe Ouest Est des Leucémies et Autres Maladies du Sang (GOELAMS). *Cancer 116,* 4299-4308.

12. Parker, C., Waters, R., Leighton, C., Hancock, J., Sutton, R., Moorman, A.V., Ancliff, P., Morgan, M., Masurekar, A., Goulden, N., Green, N., Révész, T., Darbyshire, P., Love, S., and Saha, V. (2010) Effect of mitoxantrone on outcome of children with first relapse of acute lymphoblastic leukaemia (ALL R3): an open-label randomised trial. *Lancet 376,* 2009-2017.

13. de Bono, J.S., Oudard, S., Ozguroglu, M., Hansen, S., Machiels, J.P., Kocak, I., Gravis, G., Bodrogi, I., Mackenzie, M.J., Shen, L., Roessner, M., Gupta, S., and Sartor, A.O. (2010)

Prednisone plus cabazitaxel or mitoxantrone for metastatic castration-resistant prostate cancer progressing after docetaxel treatment: a randomised open-label trial. *Lancet 376,* 1147-1154.

14. Tuveson, R.W., Wang, G.R., Wang, T.P., and Kagan, J. (1990) Light-dependent cytotoxic reactions of anthracene. *Photochem. Photobiol. 52,* 993-1002.

15. Huang, Y., Zhang, Y., Zhang, J., Zhang, D.W., Lu, Q.-S., Liu, J.-L., Chen, S.-Y., Lin, H.-H., and Yu, X.-Q. (2009) Synthesis, DNA binding and photocleavage study of novel anthracene-appended macrocyclic polyamines. *Org. Biomol. Chem. 7,* 2278-2285.

16. Bernal, M.E., Varon, J., Acosta, P., and Montagnier, L. (2010) Oxidative stress in critical care medicine. *Int. J. Clin. Pract. 64,* 1480-1488.

17. Rai, S., Kasturi, C., Grayzar, J., Platz, M.S., Goodrich, R.P., Yerram, N.R., Wong, V., and Tay-Goodrich, B.H. (1993) Dramatic improvements in viral inactivation with brominated psoralens, naphthalenes and anthracenes. *Photochem. Photobiol. 58,* 59-65.

18. Kumar, C.V., Tan, W.B., and Betts, P.W. (1997) Hexamminecobalt(III) chloride assisted, visible light induced, sequence dependent cleavage of DNA. *J. Inorg. Biochem. 68,* 177-181.

19. Kumar, C.V., Punzalan, E.H.A., and Tan, W.B. (2000) Adenine-thymine base pair recognition by an anthryl probe from the DNA minor groove. *Tetrahedron 56,* 7027-7040.

20. Gude, L., Fernández, M.-J., Grant, K.B., and Lorente, A. (2002) Anthracene and naphthalene (2,2'-bipyridine)platinum(II) conjugates: synthesis and DNA photocleavage. *Tet. Lett. 43,* 4723-4727.

21. Gude, L., Fernández, M.-J., Grant, K.B., and Lorente, A. (2005) Syntheses and copper(II)-dependent DNA photocleavage by acridine and anthracene 1,10-phenanthroline conjugate systems. *Org. Biomol. Chem. 3,* 1856-1862.

22. Naora, H., Naora, H., Izawa, M., Allfrey, V.G., and Mirsky, A.E. (1962) Some observations on differences in composition between the nucleus and cytoplasm of the frog oocyte. *Proc. Natl. Acad. Sci. U.S.A. 48,* 853-859.

23. Billett, M.A., and Barry, J.M. (1974) Role of histones in chromatin condensation. *Eur. J. Biochem. 49,* 477-484.

24. Hooper, G., and Dick, D.A.T. (1976) Nonuniform distribution of sodium in the rat hepatocyte. *J. Gen. Physiol. 67,* 469-474.

25. Moore, R.D., and Morrill, G.A. (1976) A possible mechanism for concentrating sodium and potassium in the cell nucleus. *Biophys. J. 16,* 527-533.

26. Schelhorn, T., Kretz, S., and Zimmermann, H.W. (1992) Reinvestigation of the binding of proflavine to DNA. Is intercalation the dominant binding effect? *Cell. Mol. Biol. 38,* 345-365.

27. Bhattacharya, S., and Mandal, S.S. (1997) Interaction of surfactants with DNA. Role of hydrophobicity and surface charge on intercalation and DNA melting. *Biochim. Biophys. Acta 1323,* 29-44.

28. Haq, I., Ladbury, J.E., Chowdhry, B.Z., Jenkins, T.C., and Chaires, J.B. (1997) Specific binding of Hoechst 33258 to the d(CGCAAATTTGCG)$_2$ duplex: calorimetric and spectroscopic studies. *J. Mol. Biol. 271,* 244-257.

29. Manning, G.S. (1972) Application of polyelectrolyte "limiting laws" to the helix-coil transition of DNA. I. Excess univalent cations. *Biopolymers 11,* 937-949.

30. Baase, W.A., and Johnson, W.C. (1979) Circular dichroism and DNA secondary structure. *Nucleic Acids Res. 6,* 797-813.

31. Belintsev, B.N., Gagua, A.V., and Nedospasov, S.A. (1979) The effect of the superhelicity on the double helix twist angle in DNA. *Nucleic Acids Res. 6,* 983-992.

32. Bednar, J., Furrer, P., Stasiak, A., Dubochet, J., Egelman, E.H., and Bates, A.D. (1994) The twist, writhe and overall shape of supercoiled DNA change during counterion-induced transition from a loosely to a tightly interwound superhelix. Possible implications for DNA structure in vivo. *J. Mol. Biol. 235,* 825-847.

33. Hamelberg, D., Williams, L.D., and Wilson, W.D. (2001) Influence of the dynamic positions of cations on the structure of the DNA minor groove: sequence-dependent effects. *J. Am. Chem. Soc. 123,* 7745-7755.

34. OhUigin, C., McConnell, D.J., Kelly, J.M., and van der Putten, W.J. (1987) Methylene blue photosensitised strand cleavage of DNA: effects of dye binding and oxygen. *Nucleic Acids Res. 15,* 7411–7427.

35. Munson, B., and Fiel, R.J. (1992) DNA intercalation and photosensitization by cationic meso substituted porphyrins. *Nucleic Acids Res. 24,* 1080–1090.

36. Åckerman, B., and Tuite, E. (1996) Single- and double-strand photocleavage of DNA by YO, YOYO and TOTO. *Nucleic Acids Res. 20,*1315-1319.

37. Grant, K.B., Terry, C.A., Gude, L., Fernández, M.-J., and Lorente, A. (2011) Synthesis and DNA photocleavage by a pyridine-linked bis-acridine chromophore in the presence of copper(II): ionic strength effects. *Bioorg. Med. Chem. Lett, 21,* 1047-1051.

38. Newcomb, M., Timko, J.M., Walba, D.M. and Cram, D.J. (1977) Host-guest complexation. 3. Organization of pyridyl binding sites. *J. Am. Chem. Soc. 99,* 6392-6398.

39. Sambrook, J., Fritsch, E. F., and Maniatis, T. (1989) *Molecular Cloning: A Laboratory Manual 2nd ed.,* Cold Spring Harbor Laboratory, Cold Spring Harbor, New York.

40. Schmid, N., and Behr, J.P. (1991) Location of spermine and other polyamines on DNA as revealed by photoaffinity cleavage with poly(amino)benzenediazonium salts. *Biochemistry 30,* 4357–4361.

41. Vedernikov, A.N., Wu, P., Huffman, J.C., and Caulton, K.G. (2002) Cu(I) and Cu(II) complexes of a pyridine-based pincer ligand. *Inorg. Chim. Acta 330,* 103-110.

42. Dwyer, T.J., Geierstanger, B.H., Mrksich, M., Dervan, P.B., and Wemmer, D.E. (1993) Structural analysis of covalent peptide dimers, bis(pyridine-2-carboxamidonetropsin)$(CH_2)_{3-6}$, in complex with 5'-TGACT-3' sites by two-dimensional NMR. *J. Am. Chem. Soc. 115,* 9900–9906.

43. Blackburn, G.M., and Taussig, P.E. (1975) The photocarcinogenicity of anthracence: photochemical binding to deoxyribonucleic acid in tissue culture. *Biochem. J. 149,* 289-291.

44. Sinha, B.K., and Chignell, C.F. (1983) Binding of anthracene to cellular macromolecules in the presence of light. *Photochem. Photobiol. 37,* 33-37.

45. de Silva, A.P., and de Silva, S.A. (1986) Fluorescent signalling crown ethers; ‘switching on’ of fluorescence by alkali metal ion recognition and binding *in situ*. *J. Chem. Soc., Chem. Commun.* 1709-1710.

46. Kubo K., Sakurai, T., and Mori, A. (1999) Complexation and fluorescence behavior of 9,10-bis[bis(beta-hydroxyethyl)aminomethyl]anthracene. *Talanta 50*, 73-77.

47. Wilson, B., Gude, L., Fernández, M.-J., Lorente, A., and Grant, K.B. (2005) Tunable DNA photocleavage by an imidazole-acridine conjugate. *Inorg. Chem. 44*, 6159-6173.

48. Fernández, M.-J., Wilson, B., Palacios, M., Rodrigo, M.M., Grant, K.B., and Lorente, A. (2007) Copper-activated DNA photocleavage by a pyridine-linked bis-acridine intercalator. *Bioconjugate Chem. 18*, 121-129.

49. Oikawa, S., and Kawanishi, S. (1998) Distinct mechanisms of site-specific DNA damage induced by endogenous reductants in the presence of iron(III) and copper(II*). Biochim. Biophys. Acta 1399*, 19-30.

50. Sinden, R.R. (1994) *DNA Structure and Function*, pp 109-110, Academic Press, Inc., San Diego.

51. Duff, M., Mudhivarthi, V.M., and Kumar, C.V. (2009) Rational design of anthracene-based DNA binders. *J. Phys. Chem. B 113*, 1710–1721.

52. Modukuru, N.K., Snow, K.J., Perrin, Jr., B.S., Thota, J., and Kumar, C.V. (2005) Contributions of a long side chain to the binding affinity of an anthracene derivative to DNA. *J. Phys. Chem. B 109*, 11810-11818.

53. Cantor, C., and Schimmel, P.R. (1980) *Biophysical Chemistry*, p 398, W.H. Freeman, San Francisco.

54. Tuite, E.M., and Kelly, J.M. (1993) Photochemical interactions of methylene blue and analogues with DNA and other biological substrates. *J. Photochem. Photobiol. B. 21,* 103-124.

55. Dixon, D.W., and Steullet, V. (1998) Dimerization of tetracationic porphyrins: ionic strength dependence. *J. Inorg. Biochem. 69,* 25-32.

56. Bolte, J., Demuynck, C., Lhomme, M.F., Lhomme, J., Barbet, J., and Roques, B.P. (1982) Synthetic models related to DNA intercalating molecules: comparison between quinacrine and chloroquine in their ring-ring interaction with adenine and thymine. *J. Am. Chem. Soc. 104*, 760–765.

57. Kumar, C.V., and Asuncion, E.H. (1993) DNA binding studies and site selective fluorescence sensitization of an anthryl probe. *J. Am. Chem. Soc. 115,* 8547-8553.

58. Wilson, W.D., Tanious, F.A., and Fernández-Saiz, M. (1997) Evaluation of Drug-Nucleic Acid Interactions by Thermal Melting Curves, in *Drug-DNA Interaction Protocols* (Fox, K.R., Ed.) pp 219-240, Humana Press, New Jersey.

59. Gotoh, O., Wada, A., Tada, M., and Tada, M. (1978) Base and base sequence specificity of the binding of 4-hydroxyaminoquinoline 1-oxide to DNA. *Gann 69,* 61-66.

60. Duguid, J.G., Bloomfield, V.A., Benevides, J.M., and Thomas Jr., G.J. (1995) Raman spectroscopy of DNA-metal complexes. II. The thermal denaturation of DNA in the presence of Sr^{2+}, Ba^{2+}, Mg^{2+}, Ca^{2+}, Mn^{2+}, Co^{2+}, Ni^{2+}, and Cd^{2+}. *Biophys. J. 69,* 2623-2641.

61. Novakova, O., Chen, H., Vrana, O., Rodger, A., Sadler, P.J., and Brabec, V. (2003) DNA interactions of monofunctional organometallic ruthenium(II) antitumor complexes in cell-free media. *Biochemistry 42,* 11544-11554.

62. Khan, A.U. (1976) Singlet molecular oxygen. A new kind of oxygen. *J. Phys. Chem. 80,* 2219-2228.

63. Poulos, A.T., Kuzmin, V. and Geacintov, N.E. (1982) Probing the microenvironment of benzo[a]pyrene diol epoxide-DNA adducts by triplet excited state quenching methods. *J. Biochem. Biophys. Meth. 6,* 269-281.

3.9. Supporting Information References

1. Bregadze, V.G. (1996) Metal Ion Interactions with DNA: Considerations of Structure, Stability, and Effects from Metal Ion Binding, in *Metal Ions in Biological Systems, Volume 32* (Sigel, A. and Sigel, H. Eds) pp 419-451, Marcel Dekker, Inc., N.Y.

2. Ouameur, A.A., Arakawa, H., Ahmad, R., Naoui, M., and Tajmir-Riahi, H.A. (2005) A comparative study of Fe(II) and Fe(III) interactions with DNA duplex: major and minor grooves bindings. *DNA Cell Biol. 24,* 394-401.

3. Bregadze, V., Gelagutashvili, E., and Tsakadze, K. (2009) Thermodynamic Models of Metal-Ion-DNA Interactions, in *Metal Complex - DNA Interactions* (Hadjiliadis, N. and Sletten, E. Eds) pp 31-53, John Wiley & Sons, Ltd., Chichester, U.K.

4. Tajmir-Riahi, H.A., Langlais, M., and Savoie, R. (1988) A laser Raman spectroscopic study of the interaction of calf-thymus DNA with Cu(II) and Pb(II) ions: metal ion binding and DNA conformational changes. *Nucleic Acids Res. 16,* 751-762.

5. Sabat, M. (1996) Ternary Metal Ion-Nucleic Acid Base-Protein Complexes, in *Metal Ions in Biological Systems, Volume 32* (Sigel, A. and Sigel, H. Eds) pp 521-555, Marcel Dekker, Inc., N.Y.

6. Duguid, J., Bloomfield, V.A., Benevides, J., and Thomas Jr., G.J. (1993) Raman spectroscopy of DNA-metal complexes. I. Interactions and conformational effects of the divalent cations: Mg, Ca, Sr, Ba, Mn, Co, Ni, Cu, Pd, and Cd. *Biophys. J. 65,* 1916-1928.

7. Couturier, Y., and Petitfaux, C. (1978) Composition and stability of copper complexes and pyridine amine-copper complexes. XI. Comparison of monopyridine mono- and diamines. *Bull. Soc. Chim. France 11-12, Pt. 1,* 435-441.

8. Garcia Basallote, M., and Martell, A. E. (1988) New multidentate ligands. 29. Stabilities of metal complexes of the binucleating macrocyclic ligand BISBAMP and dioxygen affinity of its dinuclear cobalt(II) complex. *Inorg. Chem*. *27*, 4219-4224.

Chapter 4.

Bis- and Mono-9-aminomethylanthracene Dyes: The Effects of Chloride Salts on DNA Interactions and Photocleavage.

(This Chapter is as it appears in the submitted manuscript Grant, K.B.; Sawoo, S.; Mapp, C.T.; Williams, D.E.; Gude, L.; Fernández, M.J.; and Lorente, A., *European Journal of Medicinal Chemistry*. The syntheses were carried out by Drs. Sawoo, Fernández, and Lorente. Dominique Williams and Drs. Fernández and Gude contributed to the structural determination of the synthesized compounds. Dr. Sawoo conducted the photochemical, thermal melting and viscometric experiments. Dr. Grant conducted the UV-visible absorption titrations, prepared the figures and wrote the manuscript. The contributions by the author of this dissertation are the experiments relating to circular dichroism analyses, viscometric titrations. All of the authors assisted in reviewing and revising the manuscript.)

4.1. Abstract

This paper describes the effects of physiologically relevant concentrations of salt (150 mM of NaCl and 260 mM of KCl) on the interactions between double-helical DNA and two 9-aminomethylanthracene dyes. Although the addition of the chloride salts to photocleavage reactions containing bis-anthracene **2** and its mono-anthracene analog **4** reduces their affinity for DNA, levels of DNA photo-oxidative damage are markedly increased at high anthracene to DNA bp molar ratios (**r =** [dye]/[DNA bp]) (350 nm hν, pH 7.0). The photocleavage enhancement is observed at dye concentrations ranging from 10 μM to 0.25 μM for **2** (**r** = 0.26 to 0.007) and 10 μM to 2.5 μM for **4** (**r** = 0.26 to 0.07). At lower **r** values (< 0.007 for **2** and < 0.07 for **4)**, the trend is reversed and the addition of the salts inhibits cleavage. The results of UV-visible absorption, circular dichroism, DNA viscometry, and melting temperature experiments suggest that the photocleavage increase at high **r** values arises from a salt-induced change in anthracene binding mode from intercalation to minor groove interactions.

4.2. Introduction

Photodynamic therapy (PDT) is utilized as a clinical treatment for age-related macular degeneration, actinic keratosis, Barrett's esophagus, and localized cancers that include neoplasms of the esophagus and lung for which surgery is not an option [1-2]. In PDT, an aromatic chromophore called a photosensitizer (PS) is administered systemically or topically. Low-energy visible light precisely targeted to the diseased tissue is then used to activate the PS, through intersystem crossing, to a long-lived triplet state (^{3}PS*). Reaction of the ^{3}PS* with ground state triplet molecular oxygen ($^3O_2$) results in the production of hydroxyl radicals (•OH) and singlet oxygen ($^1O_2$), which are short-lived reactive oxygen species (ROS) that inflict damage that is highly localized to the targeted cells [1-2]. In this regard, PDT has minimal side effects. Additionally, treatment is relatively noninvasive, and unlike high-energy radiation therapy, can be repeated many times at the same site if necessary.

At the sub-cellular level, PDT photosensitizers are taken up by the nucleus and other organelles including lysosomes and mitochondria [1]. Here, the ROS cause extensive photo-oxidative damage to DNA, proteins, lipids, and other macromolecules within the cell [1]. However, the nucleus is the most sensitive organelle [1] and the photo-oxidative damage that is generated quickly leads to cell death [1, 3-6]. Because the photosensitizers are chromophores, they possess aromatic ring systems that have the capacity to interact with nucleic acids by intercalating in between DNA base pairs and/or by binding within the DNA minor groove [7-12]. The DNA in the cell nucleus therefore constitutes a highly desirable target in photodynamic therapy.

Compared to the cell cytoplasm, the concentrations of salt in the nucleus are relatively high (~150 mM NaCl and 260 mM KCl) [13-16]. The monovalent cations sodium(I) and potassium(I) assist in stabilizing nucleic acid structure by neutralizing the opposing, negatively

charged strands of the DNA duplex [17]. It is therefore desirable for DNA photosensitizers to function optimally under conditions of high ionic strength. This is often problematic, however. Na(I) and K(I) cations decrease the association of ligands with DNA in two ways [10, 18-20]. In their interaction with the negatively charged phosphate groups in each DNA strand, the counter cations can alter DNA structure by decreasing helical diameter [21] and minor groove width [22], and by increasing helical twist angle [23-24]. If the photosensitizer is positively charged, it can be displaced by cations that effectively compete for negatively charged binding sites on the DNA duplex [18]. As exemplified by many DNA photosensitizers including those based on *meso* substituted porphyrins [7], cyanine dyes [8], 9,10-bis(aminomethyl)anthracene [10], bis-proflavine [11], and methylene blue [12], the salt-induced reduction in ligand binding affinity decreases levels of photosensitizer-induced DNA damage.

Our research group has explored the effects of high ionic strength on the photodynamic action of a number of DNA photosensitizers [11-12]. In these previously published experiments, 150 mM NaCl and 260 mM KCl were used to approximate the conditions of high ionic strength found in the cell nucleus [13-16]. While DNA photocleavage was inhibited by the salts in the majority of cases, we identified a pyridylpolyamine *N*-substituted 9-aminomethylanthracene dye (**5**) for which cleavage was markedly enhanced (Scheme 1) [11-12]. We found that the salt-induced increase in anthracene-sensitized DNA photocleavage was associated with an increase in the production of singlet oxygen and hydroxyl radicals accompanied by a change in DNA binding mode from intercalation to external binding. In the present report, we compare the effects of 150 mM NaCl and 260 mM KCl on DNA photocleavage by bis-anthracene dye **2** and the mono-anthracene analog **4** (Scheme 1). In both cases, a salt-induced change from intercalation to a groove binding mode was observed at high anthracene to DNA bp molar ratios (**r =** [dye]/[DNA

bp]**)**. Importantly, the addition of the salts increased bis-anthracene **2** photocleavage over a broader range of **r** values compared to mono-anthracene **4**. The lower limit for observing a salt-induced photocleavage enhancement was 0.25 μM for the bis-anthracene compared to 2.5 μM for the mono-anthracene dye (350 nm, pH 7.0, 22 °C).

4.3. Results and Discussion

4.3.1. Preparation of Anthracene Dyes *2* and *4*. The design of bis-anthracene **2** and its monomeric counterpart **4** was guided by a number of factors. In the course of our published experiments with pyridylpolyamine-substituted anthracene **5**, we observed a significant salt-induced DNA photocleavage enhancement in control reactions in which the quaternary amine (9-anthracenylmethyl)trimethylammonium chloride (**6**) was used as a photosensitizing agent (Scheme 4.1) [12]. This result suggested that the pyridine ring of **5** was not an absolute requirement and could be replaced with a simpler design. In preparing anthracene **2**, we selected a straightforward triethylenetetramine linker with four positively charged ammonium groups to promote hydrogen bonding and electrostatic interactions within the DNA minor groove [25]. In order to further increase binding affinity, a second anthracene unit was incorporated. If bisintercalation of bis-anthracene **2** were to be achieved, then its affinity for DNA would be expected to be approximately the square of the binding constant of the monomeric counterpart **4** [26].

Anthracenes **2** and **4** are known compounds. Synthesis of bis-anthracene **2** was performed according to a previously reported procedure by condensation of 9-anthracenecarboxaldehyde with triethylenetetramine in chloroform at reflux, followed by reduction with sodium borohydride in refluxing ethanol and HCl treatment to isolate the product **2** as the tetrahydrochloride salt [27]. Mono-anthracene **4** was prepared by refluxing 9-

chloromethylanthracene with ethylenediamine in DMSO, [28-30] followed by treatment with HCl to yield the dihydrochloride salt **4**.

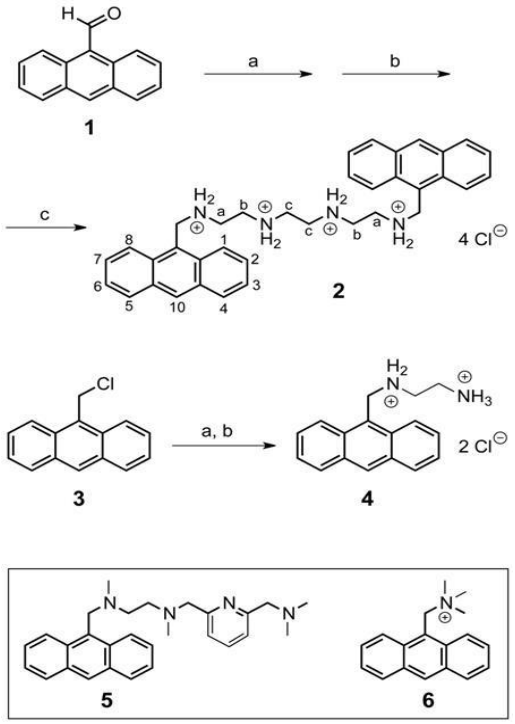

Scheme 4.1. Preparation of **2** and **4**, reagents and conditions. Bis-anthracene **2**: (a) $CHCl_3$, triethylenetetraamine, reflux 2 h; (b) CH_3CH_2OH, $NaBH_4$, reflux 3 h, rt 36 h, (c) excess HCl, 34%. Mono-anthracene **4**: (a) DMSO, K_2CO_3, ethylenediamine, 80 °C 8 h, 79%; (b) CH_3OH, excess HCl, 74%.

4.3.2. DNA Photocleavage. Our first goal was to assess the effects of high ionic strength on anthracene-sensitized photo-oxidative DNA damage. In initial experiments, pUC19 plasmid DNA was equilibrated with either 10.0 µM, 5.0 µM, 2.5 µM, 1.0 µM, 0.5 µM, 0.25 µM, 0.1 µM, or 0.05 µM concentrations of anthracene dyes **2** or **4** in the presence and absence of 150 mM of NaCl and 260 mM of KCl (10 mM of sodium phosphate buffer pH 7.0). Upon irradiating the reactions at 350 nm for 60 min, supercoiled plasmid was photo-cleaved into its nicked and linear DNA forms. Reaction products were then electrophoresed on 1.5% ethidium bromide-stained agarose gels. In the absence of the salts, anthracene dyes **2** and **4** produced approximately the

same amounts of DNA damage (Lanes 1 to 5 in Fig. 4.1; Lanes 1 to 3 in Fig. 4.S1, supplementary data). In contrast, while the addition of 150 mM NaCl and 260 mM KCl to the reactions enhanced DNA photocleavage, the increase was observed over a significantly broader dye concentration range in the case of bis-anthracene **2** (10 µM to 0.25 µM; **r** = 0.26 to 0.007) compared to mono-anthracene **4** (10 µM to 2.5 µM; **r** = 0.26 to 0.07) (Lanes 8 to 12 vs. 1 to 5 in Fig. 4.1A; Lanes 8 to 10 vs. 1 to 3 in Fig. 4.1B; Lane 6 vs. 1 in Fig. 4.S1A). At very low **r** values (< 0.007 for **2** and < 0.07 for **4),** the enhancement effect was reversed and the addition of the salts reduced photocleavage yields (Lanes 11 to 12 vs. 4 to 5 in Fig. 4.1B; Lanes 7 to 9 vs. 2 to 4 in Fig. 4.S1A; Lanes 6 to 9 vs. 1 to 4 in Fig. 4.S1B). Minimal amounts of DNA degradation were observed in dark control reactions containing maximum concentrations of **2** or **4** (10 µM of dye, no hν, 60 min; Lanes 7 and 14 in Fig. 4.1).

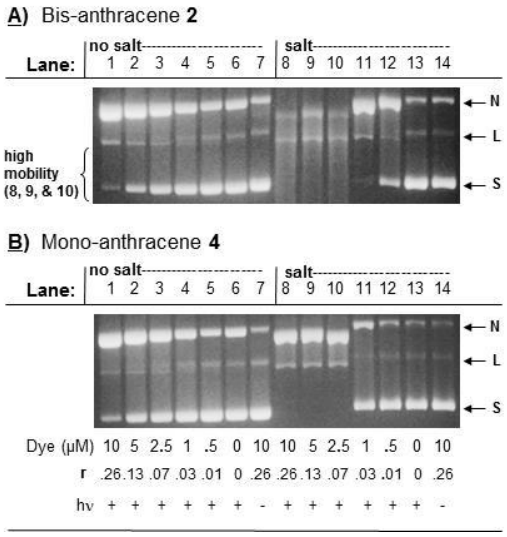

Figure 4.1. Photographs of 1.5% non-denaturing agarose gels showing photocleavage of pUC19 plasmid DNA by **(A)** bis-anthracene **2**, and **(B)** mono-anthracene **4**. Samples contained 10 mM sodium phosphate buffer pH 7.0 and 38 µM bp DNA. **Lanes 1** to **6**: 10 µM to 0 µM of dye in the **absence** of 150 mM NaCl and 260 mM KCl. **Lanes 8** to **13**: 10 µM to 0 µM of dye in the **presence** of 150 mM NaCl and 260 mM KCl. **Lane 7**: 10 µM of dye in the **absence** of 150 mM NaCl and 260 mM KCl (no hν). **Lane 14**: 10 µM of dye in the **presence** of 150 mM NaCl and 260 mM KCl (no hν). Prior to photocleavage, the reactions were pre-equilibrated for 1 h in the dark at 22 ºC. The samples in Lanes **1** to **6** and **8** to **13** were irradiated at 350 nm for 60 min (22 °C). Abbreviations: **L** = linear; **N** = nicked; **S** = supercoiled.

4.3.3. UV-visible Absorption Spectrophotometry. In our next set of experiments, UV-visible absorption titrations were conducted to further study anthracene-DNA interactions. Extensive comparisons of circular dichroism, linear dichroism, and DNA melting temperature data to anthracene absorption spectra have shown that DNA-induced changes in anthracene vibronic fine structure can be utilized to assign DNA binding mode [10, 12, 31-33]. Small volumes of calf thymus (CT) DNA titrant were sequentially added to solutions containing fixed concentrations of **2** or **4** until the titration endpoint was reached, where no additional changes in the absorption of the anthracenes were observed (Fig. 4.2). The first spectrum in each titration represents free anthracene (**2** or **4**). Intermediate spectra arise from the gradual conversion of free to DNA-bound chromophore. At the titration endpoint, all of the dye is fully bound to the DNA and saturation of the chromophore has been attained (Fig. 4.2). In the absence of the chloride salts, the titrations show that bis-anthracene **2** and mono-anthracene **4** reach saturation at approximately the same concentration of CT DNA (297 μM bp, **r** = 0.168), suggesting that the anthracenes bind to the DNA with similar affinities (Figs. 4.2A and 4.2C). This interpretation rules against bis-intercalation as a possible binding mode for **2**, but accounts for the observation that the anthracenes produce similar levels of photocleavage in the absence of the chloride salts (Figs. 4.1 and 4.S1).

As expected, DNA interactions were substantially reduced by 150 mM NaCl and 260 mM KCl (Fig. 4.2B and 4.2D).[10, 18-20] More CT DNA was required to fully bind the anthracene dyes. However, in contrast to the low ionic strength data, bis-anthracene **2** appeared to possess significantly more DNA affinity than **4**, reaching saturation at 645 μM bp CT DNA (**r** = 0.078) compared to 2888 μM bp (**r** = 0.002) for the mono-anthracene analog. In the presence of the

salts, anthracene **2** accordingly produced more photocleavage than **4** over the majority of dye concentrations tested (Lanes 8 to 12 in Fig. 4.1; Lane 6 in Fig. 4.S1).

The final spectrum at the endpoint of each of the four titrations shows that, irrespective of ionic strength, saturating amounts of the CT DNA induced significant hypochromicity and large bathochromic shifts in the peak positions of the anthracene vibronic bands (Fig. 4.2). These spectral features are hallmarks of anthracene intercalation [10, 12, 31-33] and strongly suggest that chromophores **2** and **4** engage in intercalative DNA binding at low **r** (anthracene to DNA bp molar ratio) values approaching the titration endpoint. This binding mode was not expected to predominate in the presence of the chloride salts. The salt concentrations used in the titration experiments (150 mM NaCl and 260 mM KCl) were similar to conditions of high ionic strength that, in previous studies, were shown to disrupt anthracene intercalation in favor of minor groove [10, 31-32] and external [12] DNA binding modes.

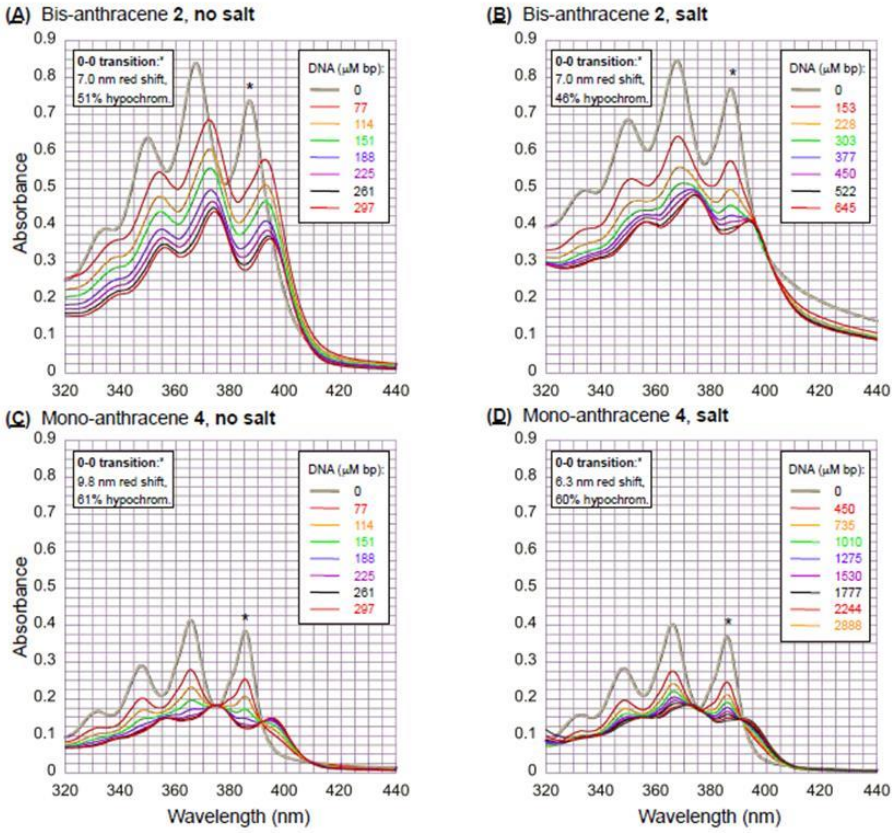

Figure 4.2. Representative UV-visible absorption titration spectra of: 50 μM of bis-anthracene **2** in the **absence** of (**A)** and in the **presence** of (**B)** 150 mM NaCl and 260 mM KCl; 50 μM of mono-anthracene **4** in the **absence** of (**C)** and in the **presence** of (**D)** 150 mM NaCl and 260 mM KCl. Individual samples contained 10 mM sodium phosphate buffer pH 7.0 and increasing concentrations of CT DNA (0 μM bp to 297 μM bp, 645 μM bp or 2888 μM bp). Following each sequential DNA addition, the solutions were allowed to equilibrate for 1 h in the dark before a UV-visible spectrum was recorded (22 ºC). All absorption spectra were corrected for sample dilution and baseline drift. Upper left corner: nm red shift and % hypochromicity of the 0-0 transition (*) at titration endpoint.

In order to account for the apparent inconsistency between the chloride salt data in Figs. 4.2B and 4.2D and the literature findings [10, 12, 31-32], we utilized the anthracene 0-0 transition, the vibrational band in Fig. 4.2 furthest away from DNA absorption (λ_{max} = 260 nm), to plot chromophore red shifting and hypochromicity as a function of CT DNA concentration (Fig. 4.3). While significant hypochromicity and large bathochromic shifts signify anthracene intercalation [10, 12, 31-33], hypochromicity in the absence of red shifting points to a binding mode involving

minor groove interactions [10, 31-32]. Under conditions of low ionic strength, persistent intercalative binding of bis-anthracene **2** was indicated by hypochromicity in the 0-0 vibronic transition accompanied by red-shifting of the peak's position, starting from the initial DNA addition up until the endpoint of the titration (**r** = 0.65 to 0.17, in Fig. 4.3A). In the case of mono-anthracene **4**, hypochromicity without red shifting occurred during the early stages of the titration, suggesting that, at high **r** values (**r** ≥ 0.27, in Fig. 4.3C), the chromophore preferentially interacts within the DNA minor groove. However, at **r** values of 0.22 down to the titration endpoint (**r** = 0.17, in Fig. 4.3C), the hypochromicity is accompanied by considerable bathochromicity. This observation is consistent with a change in binding mode from minor groove interactions to intercalation as the DNA concentration is increased.

Upon the addition of 150 mM NaCl and 260 mM KCl, hypochromicity in the absence of red shifting becomes more extensive, occurring at high bis-anthracene **2** to DNA bp molar ratios (**r** ≥ 0.17, in Fig. 4.3B) and over a wide range of mono-anthracene **4** ratios (**r** ≥ 0.039, in Fig. 4.3D). Similar overall trends were found when the 0-1 transition of each of the anthracene chromophores was used to plot red shifting and hypochromicity as a function of CT DNA concentration (Fig. 4.S2, supplementary data).

Taken together, the data in Figs. 4.2, 4.3, and 4.S2 suggest that, irrespective of ionic strength, **2** and **4** engage in intercalation at low **r** values approaching chromophore saturation at the titration endpoint. At high anthracene to DNA bp molar ratios, the titrations are consistent with the literature data and point to a salt-induced change in 9-aminomethylanthracene DNA binding mode from intercalation to groove binding interactions [10, 12, 31-32].

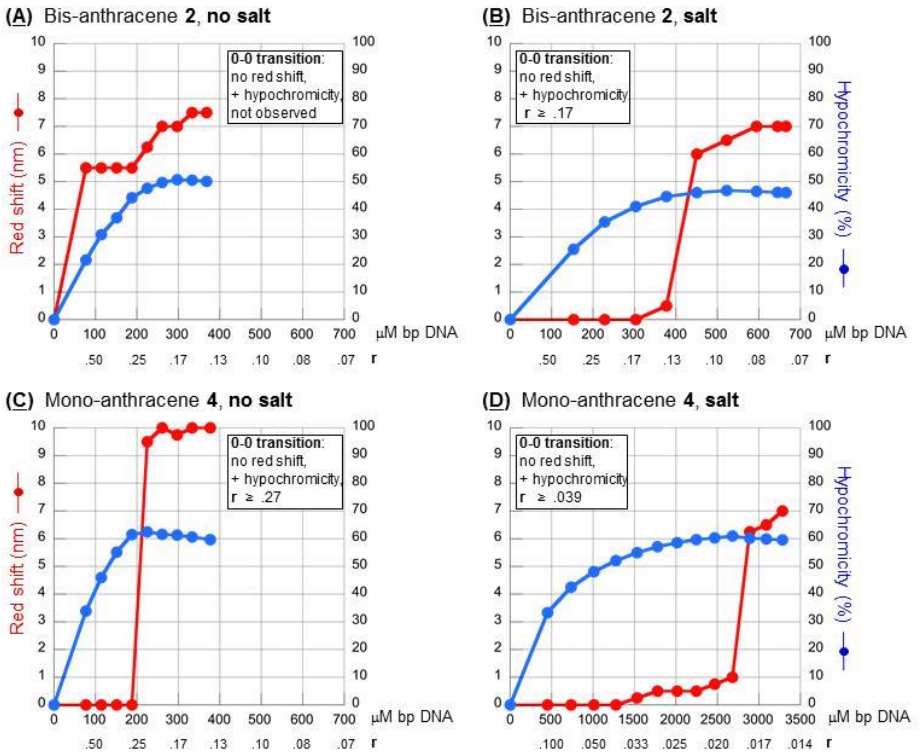

Figure 4.3. Double y-axis graphs of DNA-induced red shifting and DNA-induced hypochromicity plotted as a function of CT DNA concentration for the 0-0 absorption transition (*) of anthracene dyes **2** and **4**. The plots were prepared using the full set of UV-visible absorption titration data corresponding to the experiment in Figure 4.2.

4.3.4. Viscometric Titrations. Before an intercalator can become inserted in between adjacent DNA base pairs, the double-helix must first unwind to create a gap. This increases the contour length of the helix, making the DNA more viscous. In the case of compounds that bind externally or within the DNA grooves however, space between the base pairs is not required. There is little to no DNA unwinding and major viscosity changes are not expected to occur [34]. When the cubed root of relative DNA viscosity $(\eta/\eta_o)^{1/3}$ is plotted as a function of bound ligand to DNA bp molar ratio (**r**), the theory of Cohen and Eisenberg predicts that a straight line will be generated with a slope approximately equal to 0.0 for groove binding compounds and 1.0 for classical monointercalators [35]. In practice, the slopes associated with prototype minor groove

binders such as pentamidine range from -0.3 to 0.2 [36], while those of classical monointercalators such ethidium bromide are from 0.80 to 1.50 [26, 36-38]. In the case of bisintercalation, the slope produced by the ligand is expected to be approximately twice that observed for monointercalation. Typical slopes for bisintercalators range from 1.3 to 2.3 [26, 39-40].

Viscosity measurements were carried out with a fixed concentration of CT DNA in the absence (η_o) and presence (η) of increasing amount of anthracene dye. Low ionic strength conditions were explored first. The UV-visible titration data were utilized to identify anthracene to DNA bp molar ratios likely to promote intercalative binding of bis-anthracene **2** and monomeric **4** to the CT DNA (Figs. 4.3A, 4.3C, 4.S2A, and 4.S2C). The cubed root of the relative viscosity ($(\eta/\eta_o)^{1/3}$) was plotted as a function of **r**. Linear regression analysis was then used to fit the best straight line to the titration data. In the absence of 150 mM NaCl and 260 mM KCl, the slope obtained for mono-anthracene **4** was 0.8, consistent with monofunctional intercalation [26, 36-38], while the slope for bis-anthracene **2** was almost double that amount (1.4), falling within the ranges expected for both mono- and bisintercalators (Fig. 4.4A). While the large increase in DNA viscosity produced by bis-anthracene **2** points to bisintercalation as a possible binding mode, this conclusion is not supported by the UV-visible titration data which indicate that **2** and **4** possess similar DNA binding affinities under conditions of low ionic strength (Figs. 4.2A and 4.2C).

Because anthracene affinity was expected to decrease upon the addition of 150 mM NaCl and 260 KCl, the chloride salt viscosity data were collected using high concentrations of dye (**r** = 0.02 to 1.5 for bis-anthracene **2** and **r** = 0.3 to 1.5 for anthracene **4)**. Corresponding anthracene to DNA bp molar ratios in the UV-visible titration data in Figs. 4.3B, 4.3D, 4.S2B, and 4.S2D point to groove binding for mono-anthracene **4** and, in the case of bis-anthracene **2**, a transition

from intercalation to groove binding at high **r** values (≥ 0.17 to 0.33). In the presence of 150 mM NaCl and 260 mM KCl, the slope of the best straight line obtained for mono-anthracene **4** was 0.2, consistent with groove binding interactions (Fig. 4.4B) [36]. In the case of bis-anthracene **2**, a polynomial function was fit to viscosity data at **r** values from 0.02 to 1.5 (dashed line in Fig. 4.4B). It is evident in this plot that the addition of anthracene **2** causes a large, initial increase in DNA viscosity that levels off at ~ **r** = 0.6, to produce a line with a slope approximately equal to mono-anthracene **4**. When a straight line is fit to bis-anthracene **2** molar ratios of 0.02 up to 0.6 (solid line with circles in Fig. 4.4B), the slope obtained is 1.0, consistent with monofunctional intercalation [26, 36-38]. The viscosity change at ~ **r** = 0.6 could be due to saturation of the CT DNA by the chromophore or, as suggested by the UV-visible titration data in Fig. 4.3, a reduction in the extent of intercalation by a competitive, groove binding mode [41].

The results of the viscosity experiments were found to be in good agreement with the UV-visible absorption data in Figs. 4.2, 4.3, and 4.S2. The viscosity titrations conducted under conditions of low ionic strength confirm that anthracenes **2** and **4** engage in DNA intercalation at low **r** values (Fig. 4.4a). Alternatively, the high **r** value data acquired in the presence of 150 mM NaCl and 260 mM KCl point to the possibility of an interaction (*e.g.*, minor groove binding) that does not cause significant changes to DNA contour length (Fig. 4.4b).

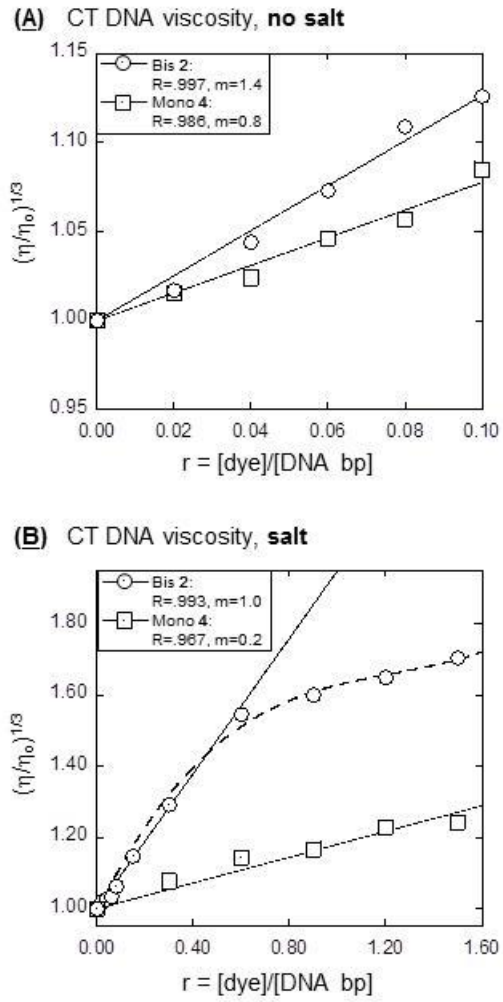

Figure 4.4. Straight line (—) and polynomial (– –) plots of relative DNA viscosity recorded as a function of **r** value **without** (**A)** and **with** (**B)** 150 mM NaCl and 260 mM KCl. The symbol η indicates the DNA viscosity in the presence of bis-anthracene **2** (○) or mono-anthracene **4** (□); η_0 is the viscosity of DNA alone. Individual samples contained 10 mM sodium phosphate buffer pH 7.0, 200 µM bp CT DNA, and increasing concentrations of anthracene dye (0 µM to 20 µM or 300 µM). Following each sequential anthracene addition, the DNA solutions were allowed to equilibrate for 15 to 30 min before viscosity was recorded (25.0 ± 0.2 ºC). Abbreviations: R = correlation coefficient; m = slope.

4.3.5. Circular Dichroism. The unwinding and lengthening of the DNA helix caused by intercalation has been shown to decrease the intensity of the positive DNA CD signal at 280 nm [12, 33, 42]. In contrast, groove binders do not unwind the DNA and do not appreciably change the CD signal at this wavelength [33]. At 280 nm, anthracene chromophores absorb minimally and do

not contribute to an induced CD. The magnitude of the DNA CD signal at 280 can therefore be used to test for intercalative binding by anthracene chromophores [12, 33, 42].

We recorded the CD spectra of a series of CT DNA solutions containing anthracene dye (r = 0.33) in the presence and absence of the chloride salts (150 mM NaCl and 260 mM KCl). The spectra show that anthracenes **2** and **4** have no intrinsic CD signal in the absence of DNA (Fig. 4.5). However, under low ionic strength conditions, the addition of **2** causes the CT DNA CD signal at 280 nm to decrease in intensity by 30.6% (Fig. 4.5A, inset). This suggests that, at r = 0.33, bis-anthracene **2** is binding to DNA by intercalation [33]. Strong interactions between DNA and **2** are indicated by the presence of a very intense bisignate, induced CD (ICD) band between 230 nm and 270 nm, similar in appearance to the ICD signals of other anthracene chromophores that engage in intercalative binding [33, 42-44]. (Anthracenes absorb strongly in this region and can contribute to an induced CD.) While the ICD signal is not customarily used to assign binding mode, it is thought to arise from coupling between anthracene and DNA transitions and from changes in DNA base coupling induced upon anthracene binding [43-44]. The addition of mono-anthracene **4** causes the CT DNA CD signal at 280 nm to decrease in intensity by 5.8% (Fig. 4.5b, inset) compared to 30.6% for compound **2**. Consistent with the viscosity data in Fig. 4a, this observation indicates that bis-anthracene **2** intercalates more efficiently and contributes to DNA unwinding and lengthening to a greater extent than mono-anthracene **4**.

In agreement with the absorption spectra in Fig. 2, the CD data show that the addition of 150 mM NaCl and 260 mM KCl to anthracene solutions lowers the overall affinity of the chromophores for CT DNA (Fig. 4.5). The bisignate 220 nm to 260 nm ICD signal, indicative of DNA interactions, is significantly reduced in intensity, particularly in the case of compound **4**. Additionally, the chloride salts lower the anthracene-induced reduction in the 280 nm CT DNA

CD signal from 30.6% to 8.3 % and from 5.8% to 2.8% for bis-anthracene **2** and mono-anthracene **4**, respectively (**r** = 0.33). Consistent with the absorption (Fig. 4.3) and viscosity data (Fig. 4.4b), the latter observation indicates that the chloride salts greatly reduce intercalative binding. Because the salt-induced decrease in anthracene affinity at **r** = 0.33 coincides with a salt-induced increase in DNA photocleavage at a similar **r** value (10.0 µM of **2** or **4**, **r** = 0.26 in Fig. 4.1), the CD data suggest that NaCl and KCl promote a transition from intercalation to a non-intercalative mode (*e.g.*, groove binding) that enhances photocleavage without unwinding the DNA duplex.

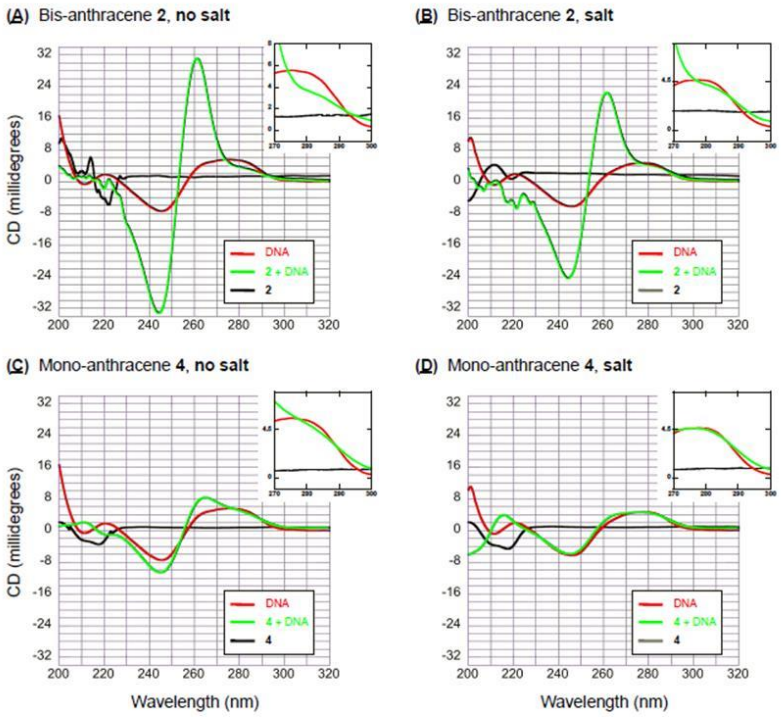

Figure 4.5. Circular dichroism (CD) spectra recorded at 22 ºC of 50 µM of anthracene derivatives **2** or **4**, and/or 150 µM bp of CT DNA in the **absence** (**A**, **C**) and in the **presence** (**B**, **D**) of 150 mM NaCl and 260 mM KCl. Individual samples contained 10 mM sodium phosphate buffer pH 7.0 and: CT DNA (red line); anthracene **2** or **4** and 150 µM bp CT DNA (green line, **r** = 0.33); and anthracene **2** or **4** (black line). Prior to recording the spectra, the samples were pre-equilibrated for 1 h in the dark at 22 ºC. Inset: absorbance from 270 nm to 300 nm.

4.3.6. Thermal Melting Titrations. Ligands that preferentially associate with double-helical DNA shift the equilibrium between the double-stranded and single-stranded DNA states towards the helical form. This increases duplex stability and in turn, raises the melting temperature (T_m) of the helix. In the case of ligands that have greater affinity for single-stranded DNA, equilibrium is shifted in the direction of the single-stranded state. Helical stability is decreased and the T_m of the duplex is lowered [45].

In order to gain additional insight into the nature of the interactions between the anthracene chromophores and DNA, melting temperature experiments were conducted at anthracene to DNA bp molar ratio values ranging from 0.2 to 0.8 (Fig. 4.6). While a T_m increase is expected for most DNA intercalators, some groove binding ligands can also raise melting temperature [44]. In the absence of 150 mM NaCl and 260 mM KCl, the T_m obtained for CT DNA was 61 °C. Upon the addition of mono-anthracene **4**, intermediate levels of duplex stabilization were displayed. The T_m value of CT DNA was increased from 64 °C at **r** = 0.2 to a maximum of 67 °C at **r** = 0.8 (Figs. 4.6B and 4.7). The resulting ΔT_m values of 3 °C to 6 °C are beneath the 7 °C to 21 °C range reported for most anthracene mono-intercalators under conditions of low ionic strength [12, 44, 46-47], but are higher than values in the 0 °C to 2 °C range reported for typical groove-binding anthracenes [32, 39]. In contrast to **4**, the addition of bis-anthracene **2** to the CT DNA produced significant levels of duplex stabilization, giving rise to ΔT_m values of 11 °C up to 22 °C at **r** values of 0.2 to 0.8 (Figs. 4.6A and 4.7). Taken together with the absorption titration data in Figs. 4.2 and 4.3 as well as the CD spectra in Fig. 4.5, the ΔT_m values suggest that, at high anthracene to DNA bp molar ratios (**r** $\geq$ 0.2), mono-anthracene **4** engages in groove binding accompanied by low levels of intercalation. In contrast, bis-anthracene **2** strongly favors intercalative interactions.

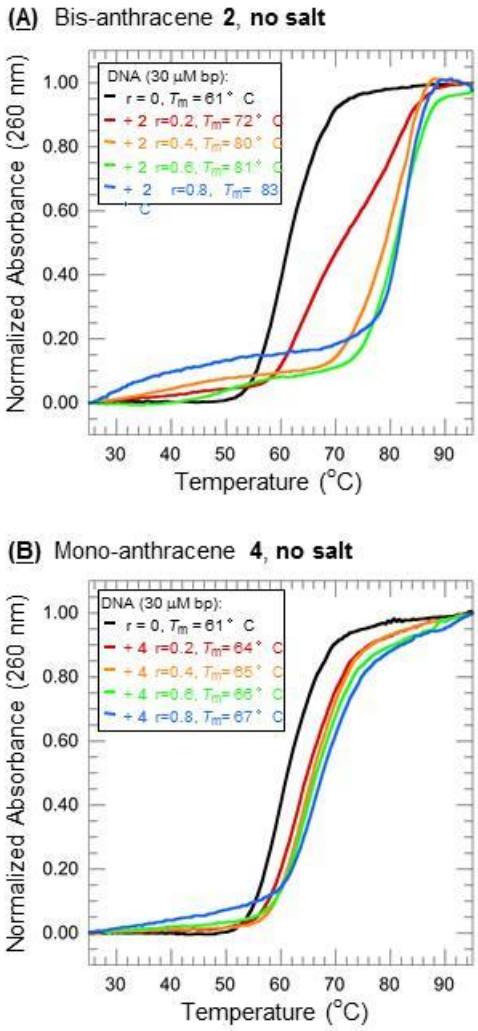

Figure 4.6. Normalized melting isotherms of 30 µM bp of CT DNA in the **absence** of 150 mM NaCl and 260 mM KCl (10 mM sodium phosphate buffer pH 7.0). Melting curves were recorded at **r** values of 0 to 0.8 for bis-anthracene **2 (A)** and mono-anthracene **4 (B)**, where **r** = [dye]/[DNA bp].

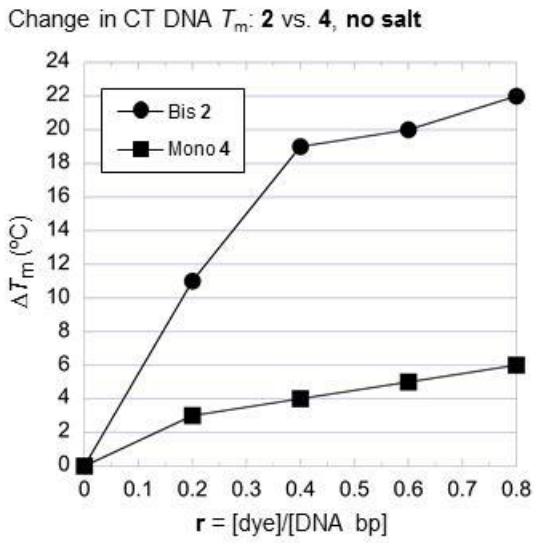

Figure 4.7. ΔT_m of 30 μM bp of CT DNA as a function of **r** value for bis-anthracene **2 (●)** and mono-anthracene **4 (■)**, where ΔT_m equals the T_m of DNA alone subtracted from the T_m of the DNA with anthracene dye (10 mM sodium phosphate buffer pH 7.0 in the **absence** of 150 mM NaCl and 260 mM KCl).

In our next experiment, thermal melting curves were recorded in the presence of 150 mM of NaCl and 260 mM of KCl (Fig. 4.8). As expected, the addition of the salts had a stabilizing effect, raising the T_m of the CT DNA from 61 °C (**r** = 0 in Fig. 4.6) to 89 °C (**r** = 0 in Fig. 4.8). Interestingly, the DNA melting curves were progressively broadened upon each incremental addition of anthracene, but the duplex melting temperatures remained constant (89 °C, **r** = 0.2 to 0.8 in Fig. 4.8). These results suggest that bis-anthracene **2** and mono-anthracene **4** continue to interact with the CT DNA throughout the titrations and that the chloride salts have disrupted intercalative binding in favor of a mode (*e.g.*, groove binding) that does not appreciably stabilize duplex DNA (Fig. 4.8). Similar to **2** and **4**, pyridylpolyamine-substituted anthracene **5** produced a significant degree of transition broadening in the presence of the chloride salts [12]. While the explanation for this behavior is not clear, the usual cause in the case of anthracene chromophores is thought to be related to dye-induced changes in DNA conformation [44].

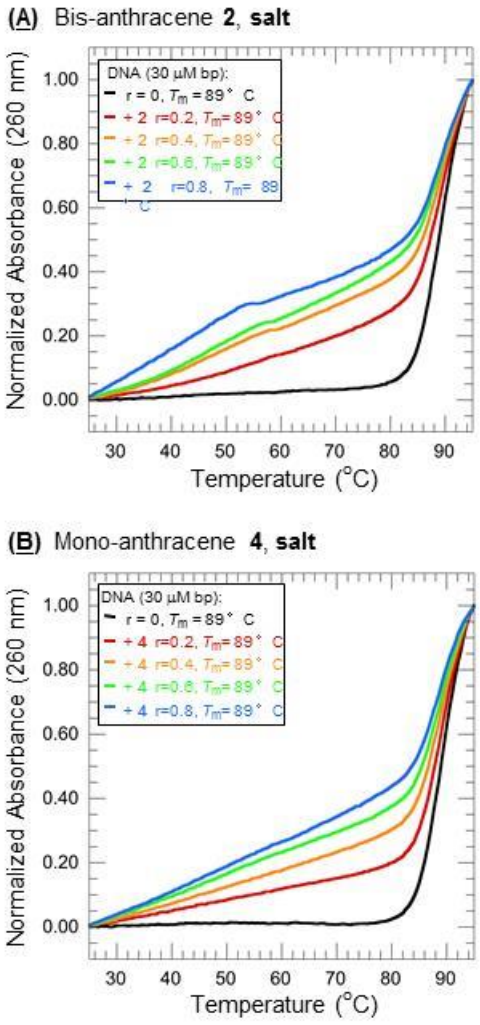

Figure. 4.8. Normalized melting isotherms of 30 μM bp of CT DNA in the **presence** of 150 mM NaCl and 260 mM KCl (10 mM sodium phosphate buffer pH 7.0). Melting curves were recorded at **r** values of 0 to 0.8 bis-anthracene **2 (A)** and mono-anthracene **4 (B)**, where **r** = [dye]/[DNA bp].

4.3.7. Summary and General Discussion. The results presented in this paper complement our previously published work in which the addition of chloride salts to solutions containing pyridylpolyamine anthracene **5** (Scheme 4.1) were shown to produce an increase in anthracene-sensitized DNA photocleavage [12]. Reactions were conducted in the presence and absence of 150 mM NaCl and 260 mM KCl in order to approximate the conditions of high ionic strength that exist in the cell nucleus [13-16]. Using UV-visible spectrophotometry in combination with circular dichroism, fluorimetry, and thermal melting data, we demonstrated that the

photocleavage increase was accompanied by a salt-induced change in DNA binding mode from intercalation to external interactions [12]. In photocleavage reactions containing the ROS scavengers sodium benzoate, D-mannitol, and sodium azide and deuterium oxide, which increases the lifetime of singlet oxygen, we then showed that the addition of the salts triggered a sharp increase in the pyridylpolyamine anthracene-sensitized production of DNA damaging hydroxyl radicals and singlet oxygen [12]. Taken together, the previously published data point to a close relationship between DNA photocleavage, reactive oxygen species, and anthracene binding mode. The microenvironment of the DNA intercalation pocket can prevent chromophores from freely interacting with ground state triplet oxygen [8, 48]. When bound externally [8, 12] or in the DNA minor groove [49] however, anthracene and other chromophores are considerably more accessible to oxygen and have the potential to generate DNA damaging reactive oxygen species more efficiently.

The present work examines the effects of 150 mM NaCl and 260 mM KCl on DNA photocleavage by bis-anthracene dye **2** and its monomeric analog **4**. Several major conclusions can be drawn from this study. Under conditions of low ionic strength, the absorption, viscosity, CD, and thermal melting data presented in this paper indicate that bis-anthracene **2** engages in persistent intercalative binding (Figs. 4.2 through 4.7). In the case of **4** however, the DNA interactions were influenced by the molar ratio of anthracene to DNA bp (**r**). The viscosity and absorption data pointed to intercalation at **r** values less than 0.27 (Figs. 4.3 and 4.4A). At higher molar ratios, the absorption spectra of mono-anthracene **4**, taken together with CD and thermal melting data, suggest that levels of intercalation are decreased and that minor groove interactions predominate (Figs. 4.2C, 4.3C, and 4.4A). The concept of multiple anthracene binding modes was first considered by Rodger and co-workers, who employed circular and linear dichroism to

study the interactions between an anthracene-9-carbonyl derivative of spermine and the polynucleotides $[poly(dA\text{-}dT)]_2$ (AT) and $[poly(dG\text{-}dC)]_2$ (GC) [44, 50]. At low **r** values, intercalation was the dominant binding mode, but at high **r** values, groove-bound anthracene was detected. In the case of GC, intercalation was favored, and groove binding only occurred when the intercalative mode was saturated. In the case of AT however, the intercalative and groove binding modes were competitive [50]. CD data suggested that groove binding might involve anthracene-anthracene stacking interactions [44]. In the UV-visible absorption titrations shown in Fig. 4.2, CT DNA was added to fixed concentrations of anthracene. At initial **r** values, vibronic bands of mono-anthracene **4** display significant hypochromicity in the absence of red shifting, suggesting that groove binding interactions precede intercalation under the conditions of the titration experiment (Figs. 4.2C and 4.3C).

Additional important conclusions drawn from the present study involve the relationship between DNA interactions and ionic strength. The absorption, viscosity, CD, and thermal melting experiments reported in this paper indicate that the addition of 150 mM NaCl in combination with 260 mM of KCl promotes a transition from intercalation to minor groove binding at high bis-anthracene **2** to DNA bp molar ratios ($\mathbf{r} \geq 0.17$) and mono-anthracene **4** molar ratios ($\mathbf{r} \geq 0.039$). Accordingly, Tuite and Nordén have shown that the predominant interaction between the phenothiazinium dye methylene blue and $[poly(dA\text{-}dT)]_2$ (AT) changes from intercalation under conditions of low ionic strength to groove binding with increasing salt concentrations [51]. Using CT DNA, Kumar and co-workers demonstrated that anthracene derivatives substituted at the 10 and/or 9 position exhibit a salt-induced change in binding mode similar to methylene blue [10, 31-32]. Groove binding compounds interact with DNA by making close van der Waals contacts with the walls of the minor groove. Van der Waals interactions are

short-range forces that fall off exponentially as a function of increasing intermolecular distance. As previously mentioned, conditions of high ionic strength decrease the width of the DNA minor groove [22]. It is conceivable that this salt-induced structural change promotes a transition from intercalation to groove binding by enabling anthracenes **2** and **4** to achieve optimal van der Waals contact distances [31]. In lieu of groove binding, we detected external interactions in our published work with compound **5** (Scheme 4.1). This was perhaps due to unfavorable steric interactions between the DNA minor groove and the relatively bulky pyridylpolyamine side chain of the anthracene [12]. While the energies associated with individual van der Waals contacts are very small, even at short intermolecular distances, the large number of contacts within the DNA minor groove makes total van der Waals interactions a major intermolecular force. This points to the importance of shape and size complementarity in the design of minor groove binding ligands [52-53].

The UV-visible absorption titrations in Fig. 4.2 and the CD spectra in Fig. 4.5 suggest that the combination of chloride salts, in addition to changing binding mode, reduces the overall affinity of anthracenes **2** and **4** for DNA. The latter result was expected for the following reasons. When present in high concentrations, sodium(I) and potassium(I) cations reduce the binding of positively charged ligands by effectively competing for negatively charged sites on the DNA [18]. Also, at high concentrations the cations promote duplex unwinding, condensation, and other structural changes that reduce ligand affinity [10, 19-20]. Although the chloride salts lowered overall binding, anthracenes **2** and **4** were affected to different extents. Under conditions of low ionic strength, the UV-visible titration and photocleavage data suggest that **2** and **4** have similar affinities for DNA (Figs. 4.2A and 4.2C). Bis-anthracene **2** and mono-anthracene **4** each reached saturation at approximately the same CT DNA concentration (297 μM bp) and produced similar

levels of photocleavage (Figs. 4.1 and 4.S1). However, in the presence of 150 mM NaCl and 260 mM KCl, bis-anthracene **2** appeared to have significantly more DNA affinity than **4**, reaching saturation at 645 μM bp CT DNA compared to 2888 μM bp for the mono-anthracene and producing more photocleavage at most of the dye concentrations tested (Lanes 8 to 12 in Fig. 4.1; Lane 6 in Fig. 4.S1). As a result, the addition of the chloride salts increased bis-anthracene **2** photocleavage over a broader range of **r** values compared to mono-anthracene **4**. This reduced the lower limit for observing a salt-induced photocleavage enhancement from 2.5 μM for the mono-anthracene dye to 0.25 μM for bis-anthracene **2** (Figs. 4.1 and 4.S1; 350 nm, pH 7.0, 22 °C).

4.3.8. Concluding Remarks. Anthracenes and their derivatives have a number of current and potential medical applications [54]. As an example, the synthetic anthraquinone mitoxantrone is employed in the clinic to treat acute lymphoblastic leukemia [55] and metastatic prostate cancer [56]. It has been suggested that the anti-cancer effects of this drug are related to its ability to interact with double-helical DNA [57]. Confocal microscopic imaging of cancer cells has confirmed that mitoxantrone can enter the cell nucleus [58-59]. Hipericin, a naturally occurring anthracene derivative isolated from St. John's Wort, has been used as a phototherapeutic agent to treat squamous cell carcinoma in animal models [60], and as a photosensitizer to assist in internalizing mitoxantrone into the nuclei of multidrug resistant cancer cell lines [61]. Nucleic acids within the cell nucleus constitute a highly desirable molecular target in photodynamic therapy [1]. It is therefore significant that conditions of high ionic strength similar to those that exist within this organelle promote efficient DNA photocleavage by sub-micromolar concentrations of bis-anthracene **2**.

4.4. Experimental Section

4.4.1. General. Deionized, distilled water was utilized in the preparation of all aqueous solutions. Reagents were of the highest purity available. Sodium phosphate dibasic salt came from J.T. Baker. Sodium phosphate monobasic salt was from Fisher Scientific. Calf thymus DNA was obtained from Invitrogen (10 mg/mL, average size $\leq$ 2000 bp). All other chemicals including sodium chloride (99.999%), potassium chloride (99.999%), and ethidium bromide were from Sigma-Aldrich. PUC19 plasmid DNA was cloned using XL-1 blue *E. coli* competent cells (Stratagene) according to a frequently cited literature procedure [62]. The cloned plasmid was purified with a Qiagen Plasmid Mega Kit.

FT-IR Perkin-Elmer 1725X and FT-IR Perkin-Elmer Spectrum 100 spectrophotometers were used to acquire infrared spectra. ^{1}H- and ^{13}C-NMR spectra were recorded at 300 and 75 MHz, respectively, on a Varian Mercury spectrometer or at 400 MHz and 100 MHz on a Bruker Advance spectrometer. ESI (electrospray ionization) mass spectra were obtained using Automass Multi GC/API/MS Finnigan and API 3200 Triple Quadrupole spectrometers. Melting points were determined in an Electrothermal IA9100 or Electrothermal Mel-Temp 1001 apparatus and were uncorrected. A UV-2401 PC spectrophotometer (Shimadzu Scientific Instruments) was used to record UV-visible spectra. A Cary 300 Bio UV-visible spectrophotometer fitted with a Cary temperature controller was utilized to plot thermal melting curves. CD spectra were acquired using a Jasco J-810 spectropolarimeter. Photocleavage reactions were run in an aerobically ventilated Rayonet Photochemical Reactor fitted with twelve RPR-3500 Å lamps (The Southern New England Ultraviolet Company).

4.4.2. *Synthesis of 1,10-bis(9-anthracenemethyl)-1,4,7,10-tetraazadecane tetrahydrochloride (2).* [27] To a solution of triethylenetetramine (351 mg, 2.4 mmol) in

chloroform (100 mL), 9-anthracenecarboxaldehyde (1 g, 4.85 mmol) and 20 g of freshly activated molecular sieves (3 Å) were added. The reaction mixture was refluxed for 2 h, filtered, and the solid washed with chloroform. The filtrate was concentrated until dryness, affording a yellow residue that was dried *in vacuo*. The solid thus obtained was suspended in ethanol (100 mL) and then sodium borohydride (610 mg, 16 mmol) was added. The reaction mixture was heated at reflux for 3 h and then stirred at room temperature for 36 h. The solvent was removed under reduced pressure and the residue obtained was dissolved in chloroform (75 mL) and then washed with 25 mL and then 100 mL of 1 M sodium hydroxide. The organic phase was acidified with concentrated hydrochloric acid (3 mL), giving rise to a gummy product that, by addition of methanol (20 mL) and stirring at room temperature for 12 h, afforded a yellow precipitate. The solid was filtered and dried *in vacuo* to give 551 mg of **2**. Yield: 34%, mp 232-234 ºC. IR (KBr) ν: 3408, 2953, 2740, 1623, 1579, 1445 cm^{-1}. ^{1}H-NMR (D_2O, 300 MHz) δ (ppm): 3.26 (s, 4H, H-c), 3.30-3.38 (m, 4H, H-b), 3.49-3.56 (m, 4H, H-a), 5.15 (s, 4H, N-CH_2-Anthr), 7.50 (t, *J* 8.9, 6.9 Hz, 4H, H-2, H-7), 7.60 (t, *J* 8.6, 6.9 Hz, 4H, H-3, H-6), 8.00 (d, *J* 8.6 Hz, 4H, H-4, H-5), 8.12 (d, *J* 8.9 Hz, 4H, H-1, H-8), 8.50 (s, 2H, H-10). ^{13}C-NMR (D_2O, 75 MHz) δ (ppm): 43.32, 43.37, 43.49, 43.65, 119.92, 122.41, 125.52, 127.84, 129.45, 130.28, 130.76. MS(ESI): (calcd for $C_{36}H_{38}N_4$, 526.31) m/z 527 (M^++H, 33%), 337 (98), 191 (100).

4.4.3. Synthesis of N-(9-anthracenemethyl) ethylenediamine dihydrochloride (4). [28-30]

9-Chloromethylanthracene (1.13 g, 5.0 mmol) was dissolved in 5 mL of dry DMSO and added to anhydrous K_2CO_3 (3.5 g, 25 mmol) in a round-bottomed flask. Ethylenediamine (0.4 mL, 5 mmol) was then added dropwise and the solution was allowed to stir at 80 °C for 8 h. The progress of the reaction was monitored by thin layer chromatography on pre-coated aluminum silica gel plates (EMD F_{254} 0.2 mm). The reaction mixture was added to chloroform and then

extracted with excess ddH_2O. The organic layer was dried over Na_2SO_4 and concentrated *in vacuo*. The resulting brown sticky product was purified by flash column chromatography using Sigma-Aldrich silica gel 60 Å (100-200 mesh), with 4:96 (v/v) MeOH:chloroform as eluent, to afford a yellow-brown semi-solid as a pure product (980 mg, 79%). In order to obtain the corresponding dihydrochloride salt, 300 mg of the semi-solid were dissolved in MeOH, an excess of dilute HCl was added, and the resulting solution was stirred. The solvent was removed under reduced pressure to afford the dihydrochloride salt, which was recrystallized from MeOH and dried under a vacuum to give 287 mg of **4**. Yield: 74%, mp 242-245 ºC. IR ν: 3396, 3327, 3010, 2975, 2806, 2714, 1625, 1598, 1491, 1450, 1165, 739 cm^{-1}. ^{1}H-NMR (D_2O, 400 MHz) δ (ppm): 3.39 (t, *J* 8.0 Hz, 2H, H-b), 3.64 (t, *J* 8.0 Hz, 2H, H-a), 5.29 (s, 2H, N-CH_2-Anthr), 7.62 (t, *J* 8.0 Hz, 2H, H-2, H-7), 7.73 (t, *J* 8.0 Hz, 2H, H-3, H-6), 8.15 (d, *J* 8.0 Hz, 2H, H-4, H-5), 8.26 (d, *J* 8.0 Hz, 2H, H-1, H-8), 8.67 (s, 1H, H-10). ^{13}C NMR (D_2O, 100 MHz) δ (ppm): 35.54, 43.47, 44.36, 119.76, 122.47, 125.58, 127.86, 129.54, 130.18, 130.70. HR ESI-MS m/z calcd for $C_{17}H_{19}N_2Cl_2$ 321.0928, found 321.0929 (100%).

4.4.4. DNA Photocleavage. In separate reactions, a total of 10 µM, 5 µM, 2.5 µM, 1.0 µM, 0.5 µM, 0.25 µM, 0.1 µM, 0.05 µM, and 0 µM of bis-anthracene **2** or of mono-anthracene **4** was equilibrated with 38 µM bp of pUC19 plasmid DNA and 10 mM sodium phosphate buffer pH 7.0, in the presence and absence of 150 mM of NaCl and 260 mM of KCl (40 µL total volume). Samples were kept for 60 min in the dark at 22 ºC and were then irradiated for 60 min in an aerobically ventilated Rayonet Photochemical Reactor fitted with twelve RPR-3500 Å lamps. Parallel control reactions consisted of 10 µM or 2 µM of each dye, 38 µM bp of pUC19, and 10 mM sodium phosphate buffer pH 7.0 in the presence and absence of 150 mM NaCl and 260 mM KCl (60 min, no hν).

After irradiation, a total of 3 µL of electrophoresis loading buffer (15.0% (w/v) Ficoll, 0.025% (w/v) bromophenol blue) was added to each 40 µL reaction. Twenty µL of each of the samples were then loaded into the wells of 1.5% non-denaturing agarose gels stained with ethidium bromide (0.5 µg/mL, final concentration). The loaded gels were electrophoresed at 160 V using 1 x Tris-acetate-EDTA as running buffer in an OWL A1 Large Gel System (Thermo Scientific). After electrophoresis, the stained gels were visualized and photographed using a 302 nm transilluminator equipped with a digital camera.

4.4.5. UV-visible Absorption Spectrophotometry. In DNA titration experiments, small volumes of an aqueous stock solution of CT DNA were sequentially added to samples containing 50 µM of anthracene **2** or **4** and 10 mM of sodium phosphate buffer pH 7.0 in the presence and absence of 150 mM NaCl and 260 mM KCl (500 µL initial volume). Final concentrations of CT DNA in each sample ranged from 0 µM bp up to 297, 645, or 2888 µM bp. After each sequential addition of titrant, the anthracene samples were equilibrated in the dark for 30 min at 22 °C. UV-visible absorption spectra were then recorded from 800 nm to 200 nm. All absorption spectra were corrected for sample dilution.

4.4.6. Viscometric Titrations. In a total volume of 1000 µL, solutions containing 200 µM bp of CT DNA and 10 mM sodium phosphate buffer pH 7.0 were prepared in the presence and absence of 150 mM NaCl and 260 mL KCl. Sixty µL aliquots of anthracenes **2** and **4** were sequentially added to afford samples that contained final anthracene concentrations ranging from 0 µM to 20 µM and 0 µM to 300 µM. Fifteen to 30 min after each addition, DNA viscosity was measured in a Cannon-Ubbelohde size 75 capillary viscometer immersed in a thermostated water bath maintained at 25.0 ± 0.2 °C. A stopwatch was used over three trials to measure the flow times of the buffer, DNA in buffer, and dye-DNA in buffer. After subtracting the averaged buffer

flow time, DNA (η_0) and dye-DNA (η) averaged flow times were plotted as $(\eta/\eta_o)^{1/3}$ versus the dye to DNA bp molar ratio (**r**). KaleidaGraph version 4.03 software was used to fit straight line and polynomial functions to the titration data.

4.4.7. Circular Dichroism. Individual solutions for CD analysis contained 10 mM of sodium phosphate buffer pH 7.0 in the presence and absence of: 50 μM of anthracene dye (**2** or **4**), 150 μM bp of CT DNA, and 150 mM of NaCl in combination with 260 of mM KCl (500 μL total volume). After a pre-equilibration period of 60 min (22 °C, no hν), spectra were collected from 320 to 190 nm in 1 mL (0.2 cm) quartz cuvettes (Starna) with a scan rate of 100 nm/min and a response time of 4 s. Bandwidth was set at 1 nm and the sensitivity was 100 millidegrees. Final spectra were averaged over 4 acquisitions.

4.4.8. Thermal Melting Titrations. Solutions for thermal melting analysis consisted of 0 μM to 24 μM of anthracene dye (**2** or **4**), 30 μM bp CT DNA, and 10 mM sodium phosphate buffer pH 7.0 in the presence and absence of 150 mM NaCl in combination with 260 mM KCl (1000 μL total volume). After a pre-equilibration period of 60 min at 22 °C (no hν), absorbance at 260 nm was recorded in a 1.5 mL (1 cm) quartz cuvette (Starna) as the temperature was increased from 25.0 °C to 95.0 °C at a heating rate of 0.5 °C/min. The first derivative of $\Delta A_{260}/\Delta T$ versus temperature was curve fit using KaleidaGraph version 4.03 software, where the maximum of the resulting plot indicated the DNA melting temperature (T_m).

4.5. Acknowledgments

We gratefully acknowledge financial support from the Georgia State University Molecular Basis of Disease Program (C.T.M.), the CTQ2011-26822 (A.L.), and the National Science Foundation (CHE-0718634, K.B.G.)

4.6. Appendix A. Supplementary Data

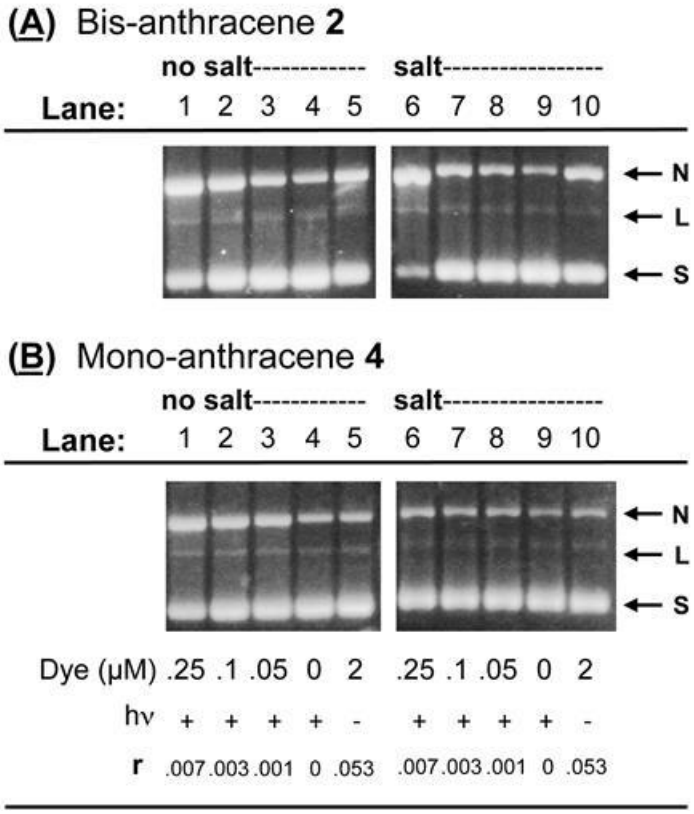

Figure 4.S1. Photographs of 1.5% non-denaturing agarose gels showing photocleavage of pUC19 plasmid DNA by **(A)** bis-anthracene **2**, and **(B)** mono-anthracene **4**. Samples contained 10 mM sodium phosphate buffer pH 7.0 and 38 μM bp DNA. **Lanes 1** to **4**: 0.25 μM to 0 μM of dye in the **absence** of 150 mM NaCl and 260 mM KCl. **Lanes 6** to **9**: 0.25 μM to 0 μM of dye in the **presence** of 150 mM NaCl and 260 mM KCl. **Lane 5**: 2 μM of dye in the **absence** of 150 mM NaCl and 260 mM KCl (no hν). **Lane 10**: 2 μM of dye in the **presence** of 150 mM NaCl and 260 mM KCl (no hν). Prior to photocleavage, the reactions were pre-equilibrated for 1 h in the dark at 22 ºC. The samples in Lanes **1** to **4** and **6** to **9** were irradiated at 350 nm for 60 min (22 °C). Abbreviations: **L** = linear; **N** = nicked; **S** = supercoiled

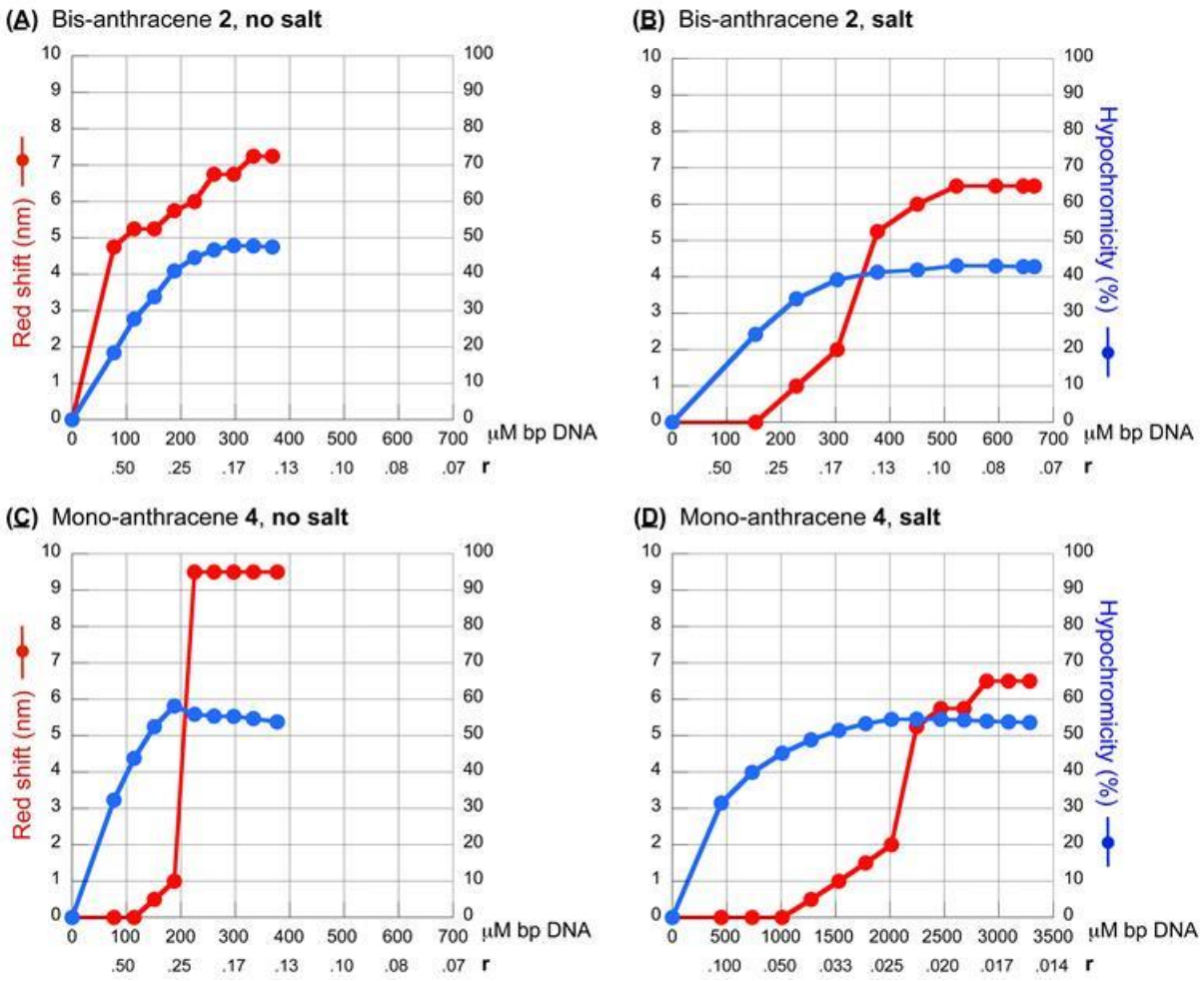

Figure 4.S2. Double y-axis graphs of DNA-induced red shifting and DNA-induced hypochromicity plotted as a function of DNA concentration in the 0-1 absorption transition of anthracene dyes 2 and 4. The plots were prepared using the full set of UV-visible absorption titration data corresponding to the experiment in Figure 4.2 of the main manuscript.

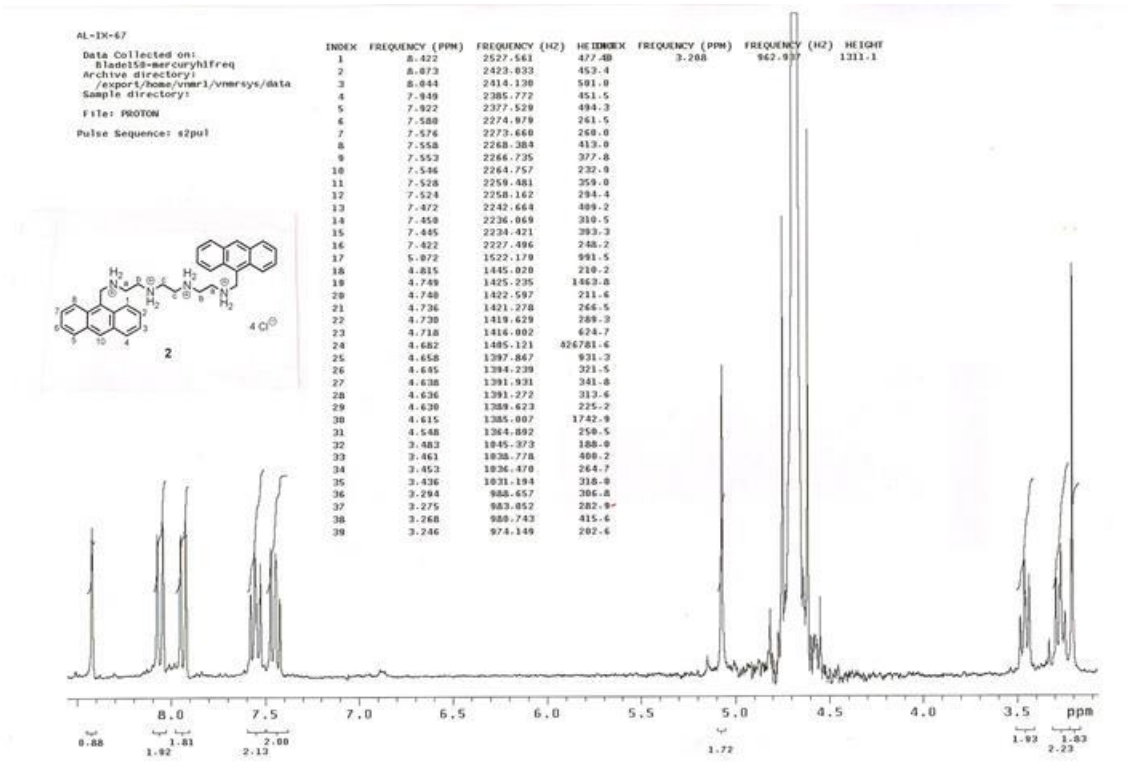

INDEX	FREQUENCY (PPM)	FREQUENCY (HZ)	HEIGHT
1	8.422	2527.561	477.48
2	8.073	2423.033	453.4
3	8.044	2414.130	501.0
4	7.949	2385.772	451.5
5	7.922	2377.529	494.3
6	7.588	2274.979	261.5
7	7.576	2273.660	260.0
8	7.558	2268.384	413.0
9	7.553	2266.735	377.8
10	7.546	2264.757	232.0
11	7.528	2259.481	359.0
12	7.524	2258.162	294.4
13	7.472	2242.664	409.2
14	7.458	2236.069	310.5
15	7.445	2234.421	393.3
16	7.422	2227.496	248.2
17	5.072	1522.170	991.5
18	4.815	1445.020	210.2
19	4.749	1425.235	1463.8
20	4.748	1422.597	211.6
21	4.736	1421.278	266.5
22	4.730	1419.629	289.3
23	4.718	1416.002	624.7
24	4.682	1405.121	826781.6
25	4.658	1397.867	931.3
26	4.645	1394.239	321.5
27	4.638	1391.931	341.8
28	4.636	1391.272	313.6
29	4.630	1389.623	225.2
30	4.615	1385.007	1742.9
31	4.548	1364.892	259.5
32	3.483	1045.373	188.0
33	3.461	1038.778	400.2
34	3.453	1036.470	264.7
35	3.436	1031.194	318.8
36	3.294	988.657	306.8
37	3.275	983.052	282.9
38	3.268	980.743	415.6
39	3.246	974.149	202.6

Figure 4.S3. Bis-anthracene **2,** ^{1}H-NMR (D_2O, 300 MHz) δ (ppm): 3.26 (s, 4H, H-c), 3.30-3.38 (m, 4H, H-b), 3.49-3.56 (m, 4H, H-a), 5.15 (s, 4H, N-CH_2-Anthr), 7.50 (t, *J* 8.9, 6.9 Hz, 4H, H-2, H-7), 7.60 (t, *J* 8.6, 6.9 Hz, 4H, H-3, H-6), 8.00 (d, *J* 8.6 Hz, 4H, H-4, H-5), 8.12 (d, *J* 8.9 Hz, 4H, H-1, H-8), 8.50 (s, 2H, H-10).

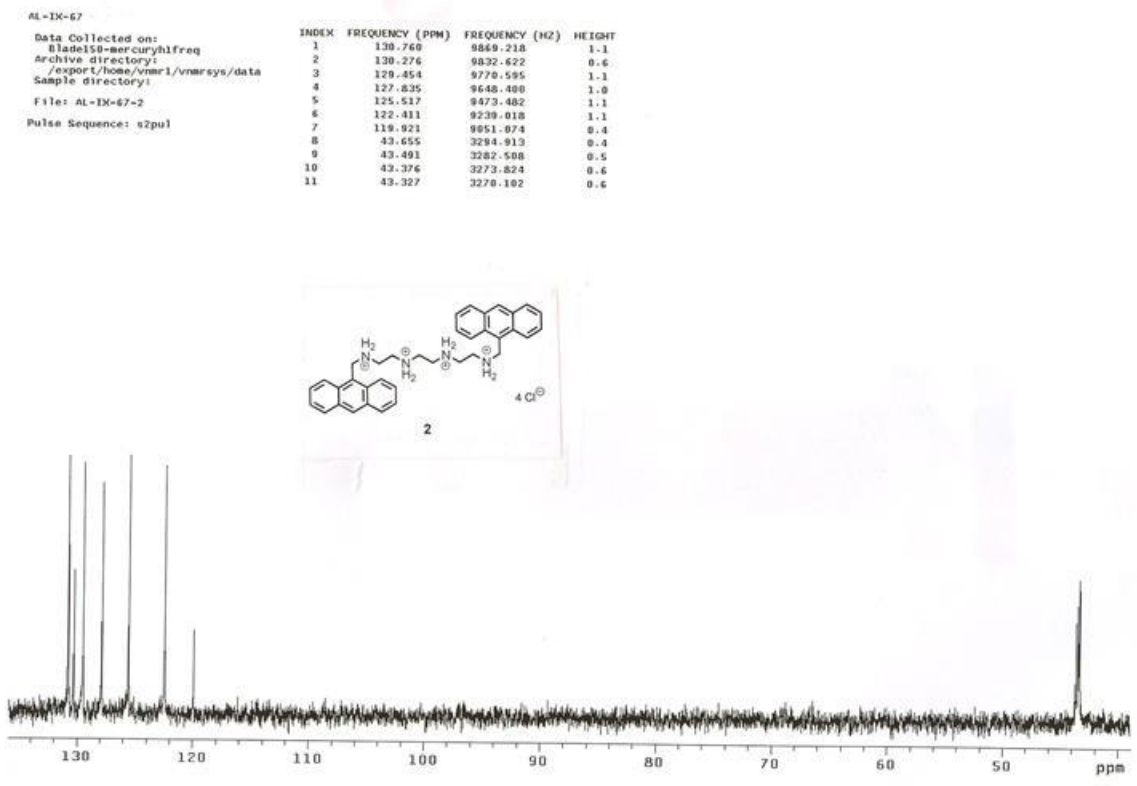

Figure 4.S4. Bis-anthracene **2,** ^{13}C-NMR (D_2O, 75 MHz) δ (ppm): 43.32, 43.37, 43.49, 43.65, 119.92, 122.41, 125.52, 127.84, 129.45, 130.28, 130.76.

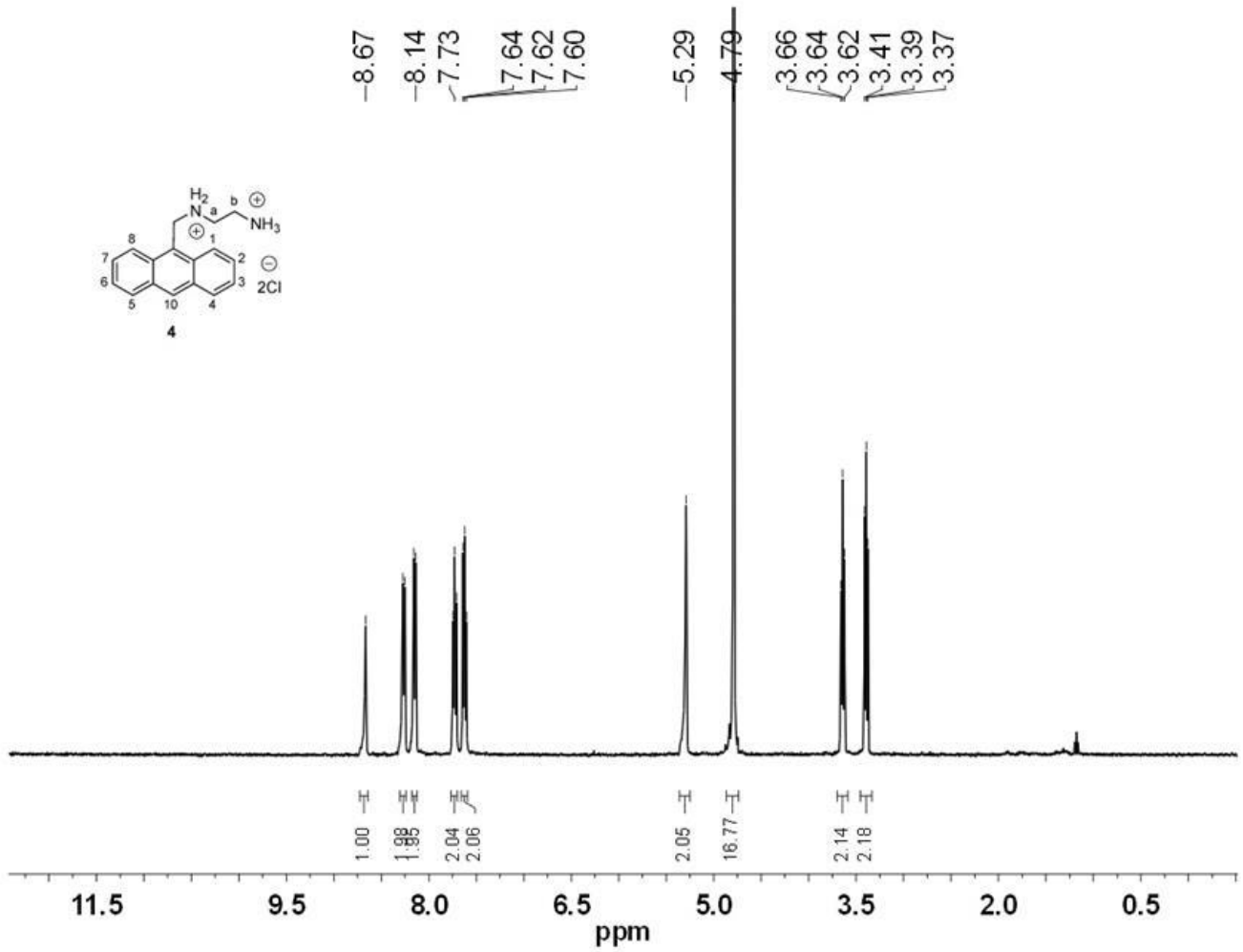

Figure 4.S5. Mono-anthracene **4**, ^{1}H-NMR (D2O, 400 MHz) δ (ppm): 3.39 (t, J 8.0 Hz, 2H, H-b), 3.64 (t, J 8.0 Hz, 2H, H-a), 5.29 (s, 2H, N-CH2-Anthr), 7.62 (t, J 8.0 Hz, 2H, H-2, H-7), 7.73 (t, J 8.0 Hz, 2H, H-3, H-6), 8.15 (d, J 8.0 Hz, 2H, H-4, H-5), 8.26 (d, J 8.0 Hz, 2H, H-1, H-8), 8.67 (s, 1H, H-10).

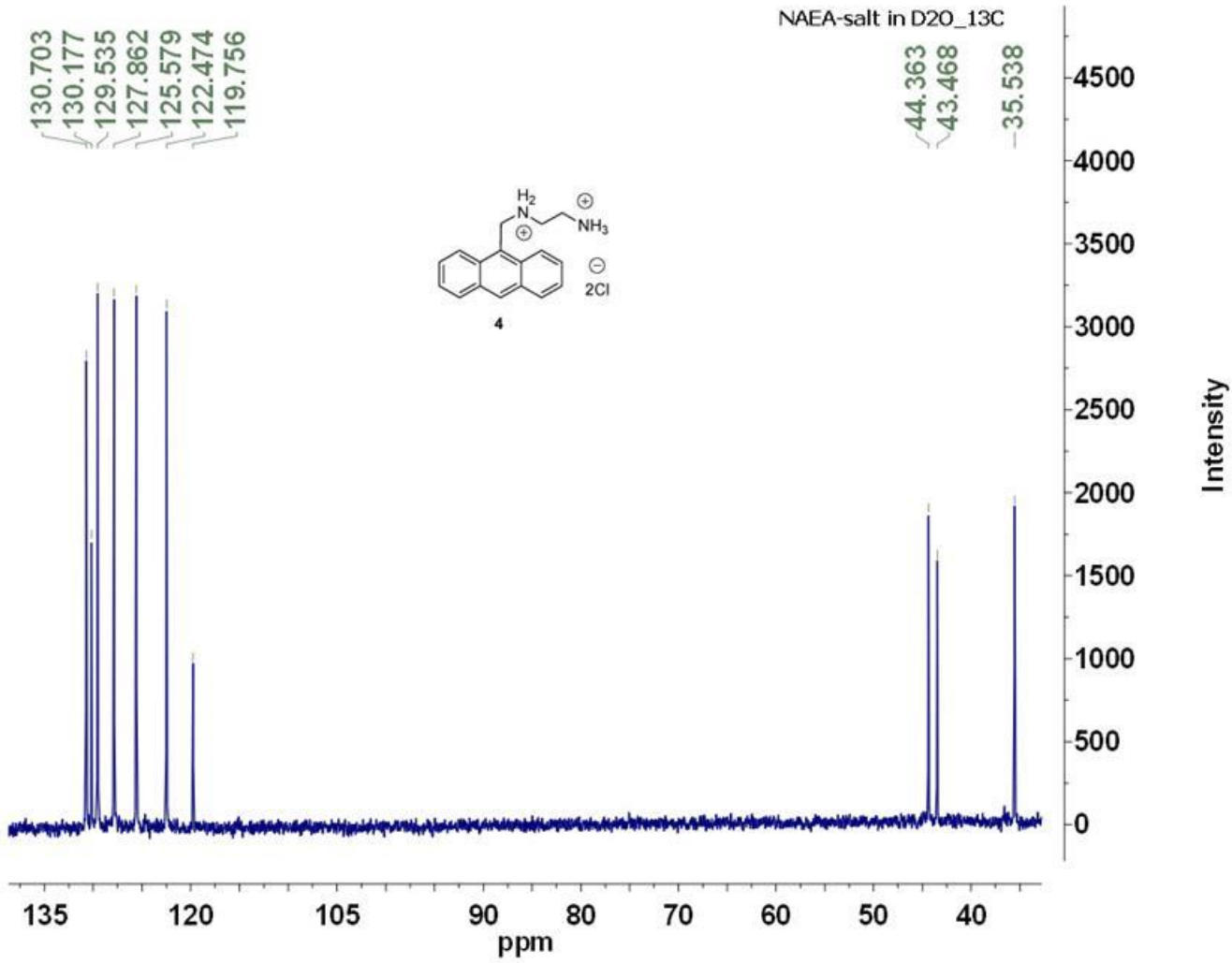

Figure 4.S6. Mono-anthracene **4**, ^{13}C NMR (D2O, 100 MHz) δ (ppm): 35.54, 43.47, 44.36, 119.76, 122.47, 125.58, 127.86, 129.54, 130.18, 130.70.

4.7. References

1. Josefsen, L. B.; Boyle, R. W., Unique diagnostic and therapeutic roles of porphyrins and phthalocyanines in photodynamic therapy, imaging and theranostics. *Theranostics* **2012,** *2* (9), 916-966.

2. Ormond, A. B.; Freeman, H. S., Dye sensitizers for photodynamic therapy. *Materials* **2013,** *6* (3), 817-840.

3. Agarwal, M. L.; Clay, M. E.; Harvey, E. J.; Evans, H. H.; Antunez, A. R.; Oleinick, N. L., Photodynamic therapy induces rapid cell death by apoptosis in L5178Y mouse lymphoma cells. *Cancer Res* **1991,** *51* (21), 5993-6.

4. Dozzo, P.; Koo, M. S.; Berger, S.; Forte, T. M.; Kahl, S. B., Synthesis, characterization, and plasma lipoprotein association of a nucleus-targeted boronated porphyrin. *J Med Chem* **2005,** *48* (2), 357-359.

5. Tada-Oikawa, S.; Oikawa, S.; Hirayama, J.; Hirakawa, K.; Kawanishi, S., DNA damage and apoptosis induced by photosensitization of 5,10,15,20-tetrakis (N-methyl-4-pyridyl)-21H,23H-porphyrin via singlet oxygen generation. *Photochem Photobiol* **2009,** *85* (6), 1391-9.

6. Harris, F.; Chatfield, L. K.; Phoenix, D. A., Phenothiazinium based photosensitisers--photodynamic agents with a multiplicity of cellular targets and clinical applications. *Curr Drug Targets* **2005,** *6* (5), 615-27.

7. Munson, B. R.; Fiel, R. J., DNA intercalation and photosensitization by cationic meso substituted porphyrins. *Nucleic Acids Res* **1992,** *20* (6), 1315-9.

8. Akerman, B.; Tuite, E., Single- and double-strand photocleavage of DNA by YO, YOYO and TOTO. *Nucleic Acids Res* **1996,** *24* (6), 1080-90.

9. Rohs, R.; Sklenar, H., Methylene blue binding to DNA with alternating AT base sequence: minor groove binding is favored over intercalation. *J Biomol Struct Dyn* **2004,** *21* (5), 699-711.

10. Modukuru, N. K.; Snow, K. J.; Perrin, B. S.; Bhambhani, A.; Duff, M.; Kumar, C. V., Tuning the DNA binding modes of an anthracene derivative with salt. *J Photoch Photobio A* **2006,** *177* (1), 43-54.

11. Grant, K. B.; Terry, C. A.; Gude, L.; Fernández, M. J.; Lorente, A., Synthesis and DNA photocleavage by a pyridine-linked bis-acridine chromophore in the presence of copper(II): Ionic strength effects. *Bioorg Med Chem Lett* **2011,** *21* (3), 1047-1051.

12. Terry, C. A.; Fernández, M. J.; Gude, L.; Lorente, A.; Grant, K. B., Physiologically relevant concentrations of NaCl and KCl increase DNA photocleavage by an N-substituted 9-aminomethylanthracene dye. *Biochemistry-Us* **2011,** *50* (47), 10375-10389.

13. Naora, H.; Izawa, M.; Allfrey, V. G.; Mirsky, A. E., Some observations on differences in composition between the nucleus and cytoplasm of the frog oocyte. *Proc Natl Acad Sci U S A* **1962,** *48*, 853-9.

14. Billett, M. A.; Barry, J. M., Role of histones in chromatin condensation. *Eur J Biochem* **1974,** *49* (3), 477-84.

15. Hooper, G.; Dick, D. A., Nonuniform distribution of sodium in the rat hepatocyte. *J Gen Physiol* **1976,** *67* (4), 469-74.

16. Moore, R. D.; Morrill, G. A., A possible mechanism for concentrating sodium and potassium in the cell nucleus. *Biophys J* **1976,** *16* (5), 527-33.

17. Todd, B. A.; Rau, D. C., Interplay of ion binding and attraction in DNA condensed by multivalent cations. *Nucleic Acids Res* **2008,** *36* (2), 501-10.

18. Schelhorn, T.; Kretz, S.; Zimmermann, H. W., Reinvestigation of the binding of proflavine to DNA. Is intercalation the dominant binding effect? *Cell Mol Biol (Noisy-le-grand)* **1992,** *38* (4), 345-65.

19. Bhattacharya, S.; Mandal, S. S., Interaction of surfactants with DNA. Role of hydrophobicity and surface charge on intercalation and DNA melting. *Biochim Biophys Acta* **1997,** *1323* (1), 29-44.

20. Haq, I.; Ladbury, J. E.; Chowdhry, B. Z.; Jenkins, T. C.; Chaires, J. B., Specific binding of Hoechst 33258 to the d(CGCAAATTTGCG)2 duplex: calorimetric and spectroscopic studies. *J Mol Biol* **1997,** *271* (2), 244-57.

21. Bednar, J.; Furrer, P.; Stasiak, A.; Dubochet, J.; Egelman, E. H.; Bates, A. D., The twist, writhe and overall shape of supercoiled DNA change during counterion-induced transition from a loosely to a tightly interwound superhelix. Possible implications for DNA structure in vivo. *J Mol Biol* **1994,** *235* (3), 825-47.

22. Hamelberg, D.; Williams, L. D.; Wilson, W. D., Influence of the dynamic positions of cations on the structure of the DNA minor groove: Sequence-dependent effects. *J Am Chem Soc* **2001,** *123* (32), 7745-7755.

23. Baase, W. A.; Johnson, W. C., Jr., Circular dichroism and DNA secondary structure. *Nucleic Acids Res* **1979,** *6* (2), 797-814.

24. Belintsev, B. N.; Gagua, A. V.; Nedospasov, S. A., The effect of the superhelicity on the double helix twist angle in DNA. *Nucleic Acids Res* **1979,** *6* (3), 983-92.

25. Schmid, N.; Behr, J. P., Location of spermine and other polyamines on DNA as revealed by photoaffinity cleavage with polyaminobenzenediazonium salts. *Biochemistry-Us* **1991,** *30* (17), 4357-61.

26. Chaires, J. B.; Leng, F.; Przewloka, T.; Fokt, I.; Ling, Y. H.; Perez-Soler, R.; Priebe, W., Structure-based design of a new bisintercalating anthracycline antibiotic. *J Med Chem* **1997,** *40* (3), 261-6.

27. Sclafani, J. A.; Maranto, M. T.; Sisk, T. M.; VanArman, S. A., Terminal alkylation of linear polyamines. *J Org Chem* **1996,** *61* (9), 3221-3222.

28. Srivastava, S. K.; Chauhan, P. M. S.; Bhaduri, A. P., A novel strategy for N-alkylation of primary amines. *Synthetic Commun* **1999,** *29* (12), 2085-2091.

29. Salvatore, R. N.; Yoon, C. H.; Jung, K. W., Synthesis of secondary amines. *Tetrahedron* **2001,** *57* (37), 7785-7811.

30. Bag, B.; Bharadwaj, P. K., Perturbation of the PET process in fluorophore-spacer-receptor systems through structural modification: Transition metal induced fluorescence enhancement and selectivity. *J. Phys. Chem. B* **2005,** *109* (10), 4377-4390.

31. Modukuru, N. K.; Snow, K. J.; Perrin, B. S., Jr.; Thota, J.; Kumar, C. V., Contributions of a long side chain to the binding affinity of an anthracene derivative to DNA. *J Phys Chem B* **2005,** *109* (23), 11810-8.

32. Tan, W. B.; Bhambhani, A.; Duff, M. R.; Rodger, A.; Kumar, C. V., Spectroscopic identification of binding modes of anthracene probes and DNA sequence recognition. *Photochem Photobiol* **2006,** *82* (1), 20-30.

33. Duff, M. R.; Mudhivarthi, V. K.; Kumar, C. V., Rational design of anthracene-based DNA binders. *J. Phys. Chem. B* **2009,** *113* (6), 1710-1721.

34. Suh, D.; Chaires, J. B., Criteria for the mode of binding of DNA binding agents. *Bioorg Med Chem* **1995,** *3* (6), 723-8.

35. Cohen, G.; Eisenberg, H., Viscosity and sedimentation study of sonicated DNA-proflavine complexes. *Biopolymers* **1969,** *8*, 45-55.

36. Fairley, T. A.; Tidwell, R. R.; Donkor, I.; Naiman, N. A.; Ohemeng, K. A.; Lombardy, R. J.; Bentley, J. A.; Cory, M., Structure, DNA minor groove binding, and base pair specificity of alkyl- and aryl-linked bis(amidinobenzimidazoles) and bis(amidinoindoles). *J Med Chem* **1993,** *36* (12), 1746-53.

37. Drummond, D. S.; Pritchard, N. J.; Simpson-Gildemeister, V. F. W.; Peacocke, A. R., Interaction of aminoacridines with deoxyribonucleic acid: Viscosity of the complexes. *Biopolymers* **1966,** *4*, 971-87.

38. Kubota, Y.; Hashimoto, K.; Fujita, K.; Wakita, M.; Miyanohana, E.; Fujisaki, Y., Flow dichroism, flow polarized fluorescence and viscosity of the DNA acridine complexes. *Biochim Biophys Acta* **1977,** *478* (1), 23-32.

39. Huang, Y.; Zhang, Y.; Zhang, J.; Zhang, D. W.; Lu, Q. S.; Liu, J. L.; Chen, S. Y.; Lin, H. H.; Yu, X. Q., Synthesis, DNA binding and photocleavage study of novel anthracene-appended macrocyclic polyamines. *Org Biomol Chem* **2009,** *7* (11), 2278-2285.

40. Kokoschka, M.; Bangert, J. A.; Stoll, R.; Sheldrick, W. S., Sequence-selective organoiridium DNA bis-intercalators with flexible dithiaalkane linker chains. *Eur J Inorg Chem* **2010,** (10), 1507-1515.

41. Pasic, L.; Sepcic, K.; Turk, T.; Macek, P.; Poklar, N., Characterization of parazoanthoxanthin A binding to a series of natural and synthetic host DNA duplexes. *Arch Biochem Biophys* **2001,** *393* (1), 132-142.

42. Duff, M. R.; Tan, W. B.; Bhambhani, A.; Perrin, B. S.; Thota, J.; Rodger, A.; Kumar, C. V., Contributions of hydroxyethyl groups to the DNA binding affinities of anthracene probes. *J. Phys. Chem. B* **2006,** *110* (41), 20693-20701.

43. Rodger, A.; Blagbrough, I. S.; Adlam, G.; Carpenter, M. L., DNA-binding of a spermine derivative - spectroscopic study of anthracene-9-carbonyl-N-1-spermine with poly[d(G-C)Center-Dot(d(G-C)] and Poly[d(a-T)Center-Dot-d(a-T)]. *Biopolymers* **1994,** *34* (12), 1583-1593.

44. Rodger, A.; Taylor, S.; Adlam, G.; Blagbrough, I. S.; Haworth, I. S., Multiple DNA-binding modes of anthracene-9-carbonyl-N-1 spermine. *Bioorg Med Chem* **1995,** *3* (6), 861-872.

45. Wilson, W. D.; Tanious, F. A.; Fernandez-Saiz, M.; Rigl, C. T., Evaluation of drug-nucleic acid interactions by thermal melting curves. *Methods Mol Biol* **1997,** *90*, 219-40.

46. Kumar, C. V.; Asuncion, E. H., DNA-binding studies and site-selective fluorescence sensitization of an anthryl probe. *J Am Chem Soc* **1993,** *115* (19), 8547-8553.

47. Kumar, C. V.; Punzalan, E. H. A.; Tan, W. B., Adenine-thymine base pair recognition by an anthryl probe from the DNA minor groove. *Tetrahedron* **2000,** *56* (36), 7027-7040.

48. Poulos, A. T.; Kuzmin, V.; Geacintov, N. E., Probing the microenvironment of benzo[a]pyrene diol epoxide-DNA adducts by triplet excited state quenching methods. *J Biochem Biophys Methods* **1982,** *6* (4), 269-81.

49. Zinger, D.; Geacintov, N. E., Acrylamide and molecular oxygen fluorescence quenching as a probe of solvent-accessibility of aromatic fluorophores complexed with DNA in relation to their conformations: coronene-DNA and other complexes. *Photochem Photobiol* **1988,** *47* (2), 181-8.

50. Adlam, G.; Blagbrough, I. S.; Taylor, S.; Latham, H. C.; Haworth, I. S.; Rodger, A., Multiple binding modes with DNA of anthracene-9-carbonyl-N-1-spermine probed by LD, CD, normal absorption, and molecular modeling compared with those of spermidine and spermine. *Bioorg Med Chem Lett* **1994,** *4* (20), 2435-2440.

51. Tuite, E.; Norden, B., Sequence-specific interactions of methylene-blue with polynucleotides and DNA - a spectroscopic study. *J Am Chem Soc* **1994,** *116* (17), 7548-7556.

52. Czarny, A.; Boykin, D. W.; Wood, A. A.; Nunn, C. M.; Neidle, S.; Zhao, M.; Wilson, W. D., Analysis of van der Waals and electrostatic contributions in the interactions of minor-groove binding benzimidazoles with DNA. *J Am Chem Soc* **1995,** *117* (16), 4716-4717.

53. Shaikh, S. A.; Ahmed, S. R.; Jayaram, B., A molecular thermodynamic view of DNA-drug interactions: a case study of 25 minor-groove binders. *Arch Biochem Biophys* **2004,** *429* (1), 81-99.

54. Ihmels, H.; Otto, D., Intercalation of organic dye molecules into double-stranded DNA general principles and recent developments. *Top Curr Chem* **2005,** *258*, 161-204.

55. Parker, C.; Waters, R.; Leighton, C.; Hancock, J.; Sutton, R.; Moorman, A. V.; Ancliff, P.; Morgan, M.; Masurekar, A.; Goulden, N.; Green, N.; Revesz, T.; Darbyshire, P.; Love, S.; Saha, V., Effect of mitoxantrone on outcome of children with first relapse of acute lymphoblastic leukaemia (ALL R3): an open-label randomised trial. *Lancet* **2010,** *376* (9757), 2009-17.

56. de Bono, J. S.; Oudard, S.; Ozguroglu, M.; Hansen, S.; Machiels, J. P.; Kocak, I.; Gravis, G.; Bodrogi, I.; Mackenzie, M. J.; Shen, L.; Roessner, M.; Gupta, S.; Sartor, A. O., Prednisone plus cabazitaxel or mitoxantrone for metastatic castration-resistant prostate cancer progressing after docetaxel treatment: a randomised open-label trial. *Lancet* **2010,** *376* (9747), 1147-54.

57. Alberts, D. S.; Peng, Y. M.; Bowden, G. T.; Dalton, W. S.; Mackel, C., Pharmacology of mitoxantrone: mode of action and pharmacokinetics. *Invest New Drugs* **1985,** *3* (2), 101-7.

58. Fox, M. E.; Smith, P. J., Subcellular localisation of the antitumour drug mitoxantrone and the induction of DNA damage in resistant and sensitive human colon carcinoma cells. *Cancer Chemother Pharmacol* **1995,** *35* (5), 403-10.

59. Feofanov, A.; Sharonov, S.; Fleury, F.; Kudelina, I.; Nabiev, I., Quantitative confocal spectral imaging analysis of mitoxantrone within living K562 cells: intracellular accumulation and distribution of monomers, aggregates, naphtoquinoxaline metabolite, and drug-target complexes. *Biophys J* **1997,** *73* (6), 3328-36.

60. Head, C. S.; Luu, Q.; Sercarz, J.; Saxton, R., Photodynamic therapy and tumor imaging of hypericin-treated squamous cell carcinoma. *World J Surg Oncol* **2006,** *4*, 87.

61. Adigbli, D. K.; Wilson, D. G.; Farooqui, N.; Sousi, E.; Risley, P.; Taylor, I.; Macrobert, A. J.; Loizidou, M., Photochemical internalisation of chemotherapy potentiates killing of multidrug-resistant breast and bladder cancer cells. *Br J Cancer* **2007,** *97* (4), 502-12.

62. Sambrook, J.; Fritsch, E. F.; Maniatis, T., *Molecular Cloning, A Laboratory Manual*. Cold Spring Harbor Press: Cold Spring Harbor, NY, 1989.

CHAPTER 5.

OXIDATIVE CLEAVAGE OF DNA BY PENTAMETHINE CYANINE DYES WITH LONG-WAVELENGTH VISIBLE LIGHT

(This chapter is as it appears in a preliminary version of the prepared manuscript Mapp, C.T.; Owens, E.A.; Henary, M.; and Grant, K.B., for *Bioorganic &Medicinal Chemistry Letters*. The initial syntheses and writing of the synthetic procedures were conducted by Eric Owens and Dr. Henary. The figures were prepared by Dr. Grant. The contributions by the author of this dissertation are conception and execution of the biochemical and photochemical experiments, preparation and revision of the initial draft. The final manuscript was extensively revised by Dr. Grant).

5.1. Abstract

Here we report the synthesis of seven new symmetrical cyanine dyes in which two N-alkylated benz[*e*]indole rings are joined by a pentamethine bridge appended with a H, Cl, or Br atom at the meso position. In reactions containing micromolar concentrations of dye, irradiation at 575 nm, 588 nm, 623 nm, and 700 nm produce efficient oxidative cleavage of plasmid DNA, especially in the case of the halogenated dyes. UV-visible spectrophotometry indicated that the carbocyanines are capable of interacting with DNA in their aggregated and monomeric forms. Scavenger experiments point to the involvement of singlet oxygen ($^1O_2$) and hydroxyl radicals (•OH) in the photocleavage reactions.

5.2. Introduction

Cyanine dyes serve as sensitizers in photography and have been used as absorbers in ultrafast high energy lasers as well as fluorescent labels for macromolecules such as proteins and nucleic acids.[1-2] Cyanines are typically composed of two positively charged, aromatic ring systems that contain a heterocyclic nitrogen atom that is conjugated to a central polymethine bridge.[2] The positive charge of the cyanine rings is delocalized over the nitrogen via the

polymethine unit.[2] These structural features enable many cyanine dyes to bind to DNA, through intercalative, groove, and/or external modes, depending on the precise nature of the dye.[2-4] The photo-physical properties of the cyanines are directly influenced by the length of the polymethine chain and by the identity of the terminal heterocyclic group(s).[2] Specifically, the absorption maximum of the dye can be red shifted by ~100 nm for every two methine groups added.[5] By adjusting structural variables, we can tune the absorption wavelengths of the cyanines to yield ideal compounds for a variety of purposes.

In photodynamic therapy (PDT), light of a specific wavelength is used to activate a phototherapeutic agent in diseased tissue. The reactive oxygen species (ROS) that are generated cause highly localized oxidative damage to DNA and other macromolecules only within the irradiated cells that contain the photosensitizer (PS). This minimizes the involvement of surrounding healthy tissue and has made PDT a good alternative therapy for age related wet macular degeneration, skin conditions such as actinic keratosis, and localized cancers for which surgery is not an option. [6-7] An ideal PDT agent will absorb light within a "phototherapeutic window" of 600 – 800 nm, wavelengths that are more readily transmitted by biological tissues. [8] This range is well within the region of cyanine absorption. Using *meso*-halogenated pentamethine linkers to bridge two N-alkylated benz[*e*]indole rings, we have synthesized carbocyanines dyes that exhibit good activity in cleaving pUC19 plasmid DNA when irradiated with phototherapeutic wavelengths of light.

A total of seven symmetrical cyanine dyes were synthesized (compounds **9** to **15** in Scheme 5.1). A pentamethine bridge was selected in order to bring absorption maxima of the dyes within the range of the PDT phototherapeutic window.[5] Chlorine (dyes **11** and **14**) and bromine atoms (dyes **10** and **13**) vs. hydrogen (in **12** and **15**) were placed at the *meso*-carbon of

the polymethine bridge to induce a "heavy atom effect". Bromine and other heavy atoms have been shown to heighten ROS production by increasing the efficiency of intersystem crossing from the photosensitizer's singlet excited state to the triplet state.[9] Benz[*e*]indole nitrogen substituents were selected to increase interactions of the dyes with DNA. In dyes **10** to **12**, methyl groups were employed to reduce steric hindrance. In **13** to **15,** positively charged 4-trimethylammoniumbutyryl (TMAB) groups of dyes were used to maximize water solubility and increase electrostatic interactions with the negatively charged DNA. The benz[*e*]indole nitrogen of cyanine dye **9** was derivatized with a bulky phenylpropyl group to afford a negative control with weak DNA binding affinity.

It is well known that cyanine dyes π-stack in aqueous solution to form dimers and higher order aggregates.[2] Monomeric cyanines bind by intercalation and in the DNA minor groove,[2, 10] while H- and J- aggregates engage in minor groove binding and external electrostatic interactions.[2, 4, 11] (DNA intercalation would be inhibited due to a structural perturbation caused by the aromatic rings of the H- and J- aggregates). The addition of substituents that add positive charge[12-13] and/or steric bulk[11, 14] to the polymethine system inhibit cofacial H-stacking in favor of staggered end-to-end J-stacked aggregation. The spectroscopic properties of the H-and J aggregates have been well characterized.[2] The absorption spectra of the cofacial H-band aggregates are hypsochromic with respect to the cyanine monomer, while staggered J absorption bands are bathochromic.[2] In the case of pentamethine cyanines, aggregate binding usually occurs almost exclusively in the minor groove.[5, 10]

Here we present and evaluate the UV-visible absorption, fluorescence emission, DNA photocleavage properties and synthesis, of seven symmetrical pentamethine carbocyanine based dyes.

5.3. Results and Discussion

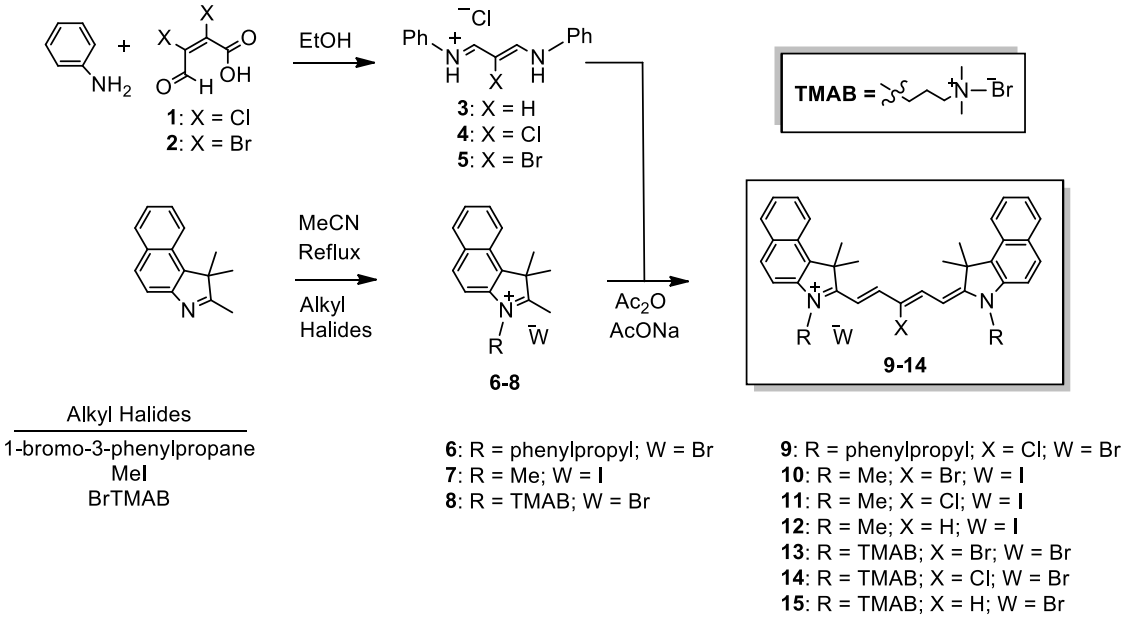

Scheme 5.1. Synthetic route of the pentamethine-linked cyanine dyes **9** through **15**.

5.3.1. UV-visible Absorbance and Fluorescence Analysis. In our first set of experiments, UV-visible spectra were acquired in order to examine the interactions of cyanine dyes **9** to **15** with DNA (Figure 5.1). Solutions contained 0 or 10 µM of dyes **9** to **15**, 38µM bp CTDNA, and 10 mM sodium phosphate buffer pH 7.0. In the absence of DNA, the cyanine dyes display a low intensity hypsochromic band showing maximum absorption between 619 nm and 640 nm and a major, high intensity peak between 670 nm and 707 nm. We respectively ascribe these absorption bands to the presence of H-aggregates and monomeric dye, based on the similarity to the spectral bands of a number of well characterized cyanine dyes including benz[e]indolium polymethine cyanines similar to those synthesized in this study.[4-5, 12, 15] In the case of the tri-cationic TMAB-substituted dyes **13**, **14**, and **15**, the H-band peak heights are suppressed with respect to the H-band heights of mono-cationic methyl-substituted dyes **10** and **11**. This may be the result of the addition positive charge and steric bulk conference by the TMAB group.

Absorption bands characteristic of J-aggregation were not observed in any of the cyanine spectra (Figure 5.1).

Upon the addition of DNA to the cyanine dye samples, the absorption maxima corresponding to the H-aggregated forms of TMAB dyes **13** through **15** are hypochromic and red-shifted by ~ 3 to 4 nm. The intensity of the peaks corresponding to the H-aggregates of **10** through **12** are altered and a new bathochromic peak emerges ~ 580 nm (Figures 5.1B, 5.1C, and 5.1D). The spectra in Figure 5.1 provide strong evidence that the cyanine dyes **10** through **15** are interacting with DNA through their H-aggregated forms. The absorption maxima of the monomeric forms of these dyes are also altered. For cyanines **10** through **15**, moderate to significant hypochromicity of the M band is accompanied by a 4 to 16 nm bathochromic shift. While these trends usually indicate cyanine intercalation,[10, 13-14] some minor groove binding cyanine dyes become hypochromic and red-shifted upon binding to DNA.[5] Although DNA interactions are strongly indicated, the absorption spectra in Figure 5.1 cannot be used to definitively assign cyanine binding mode(s) to the monomeric forms of dyes **10** through **15**. The spectral bands of the phenylpropyl control (**9**) are atypical, undergoing blue-shifting and hypochromicity upon DNA addition.

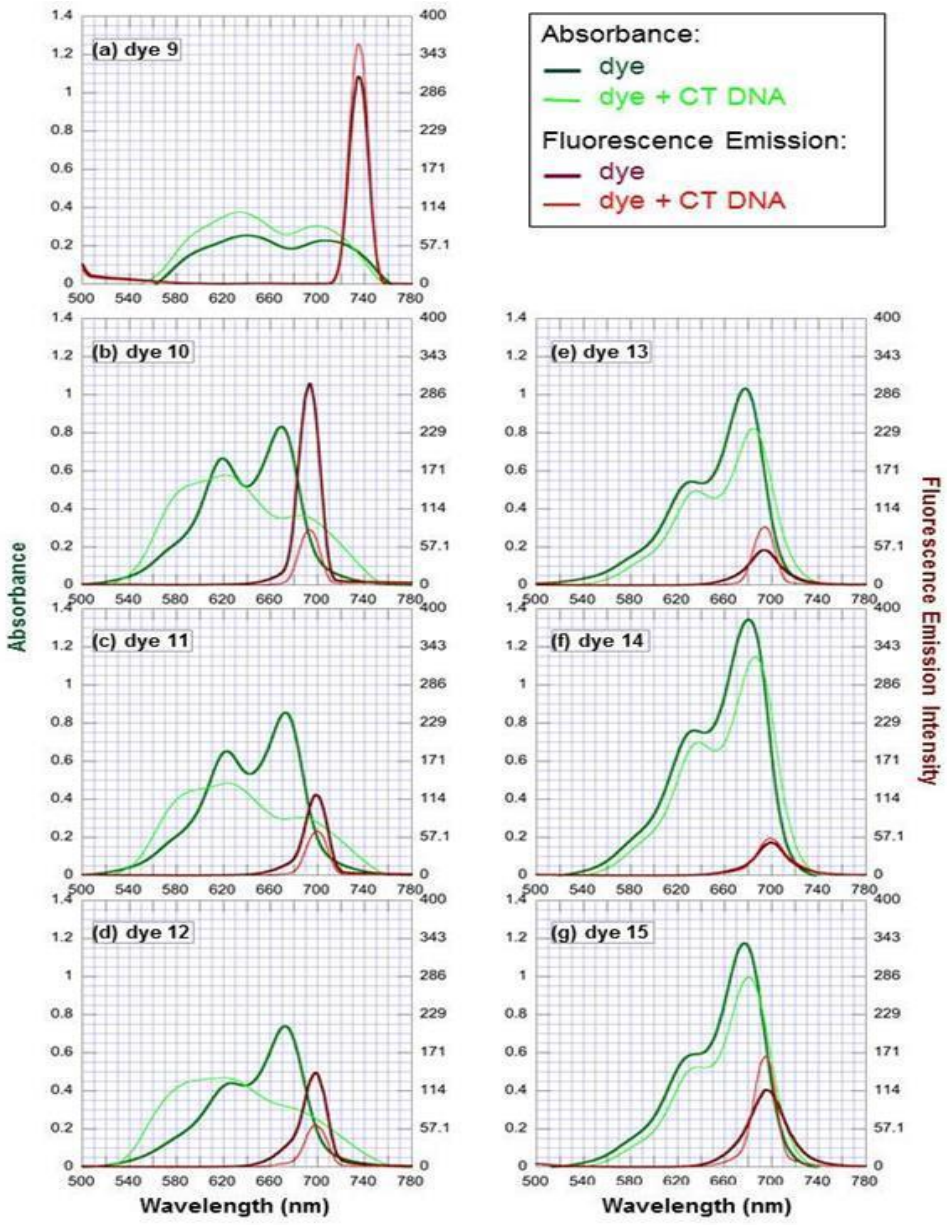

Figure 5.1. Double y-axis plots showing UV-visible absorption spectra (green) and fluorescence emission spectra (red) of 10 μM of cyanine dyes **9** to **15** equilibrated in the absence (dark lines) and presence (light lines) of 38 μM bp CT DNA (10 mM sodium phosphate buffer pH 7.0). For emission spectra, samples were excited at low energy wavelengths at which dye absorbance was unaffected by the addition of DNA: 731 nm (**9**); 689 nm (**10**); 695 nm (**11**), 695 nm (**12**); 689 nm (**13**); 692 nm (**14**), and 690 nm (**15**).

Fluorescence spectra were recorded in order to gain additional insights into the precise DNA binding mode of the cyanine monomers. Individual solutions contained 0 or 10 μM of cyanine dye and 38μM bp CTDNA in 10 mM sodium phosphate buffer pH 7.0. At each of the

excitation wavelengths selected, the H-aggregate contributed minimally and the absorbance of the monomeric band was not changed by the addition of the DNA (Figure 5.1). While the fluorescence of methylated dyes **10** to **12** was partially quenched, DNA addition produced moderate fluorescence enhancements in the case of cyanine control **9** and TMAB derivatized dyes **13** through **15**. In general, cyanine dyes that associate with double-helical DNA by intercalative modes exhibit large florescence enhancements upon binding.[2,13, 16] The fluorescence spectra in Figure 5.1 therefore suggest that the monomeric cyanines may be engaging in non-intercalative binding under the experimental conditions employed.

5.3.2. Photocleavage of Supercoiled Plasmid DNA at 575 nm, 588 nm, 623 nm, and 700 nm. DNA photocleavage by cyanine dyes **9** through **15** was studied next. Reactions consisted of 10 μM of dye, 38 μM bp pUC19 plasmid DNA and 10 mM phosphate buffer, pH 7.0. Individual samples were irradiated for 60 min in a ventilated Rayonet Photochemical Reactor equipped with ten 575 nm broad spectrum fluorescent lamps (spectral output 400-650; power > 21 watts per lamp) or with a single monochromatic, low power light emitting diode (LED; 588 $\pm$ 10 nm, 623 $\pm$ 10 nm, or 700 $\pm$ 10 nm; power = 0.17 to 0.20 watts). The photo-conversion of supercoiled plasmid to its nicked and linear forms was then visualized on 1.5 % nondenaturing agarose gels (Figures 5.2; Figures 5.S1 to 5.S3 in Supplementary Data). As expected, photocleavage yields were higher when the more powerful 21 watt, broad spectrum lamps were used and approached 86% and 91% for bromine-substituted methyl cyanine **10** and chlorine-substituted TMAB cyanine **14**, respectively (Lanes 2 and 6 in Figure 5.2).

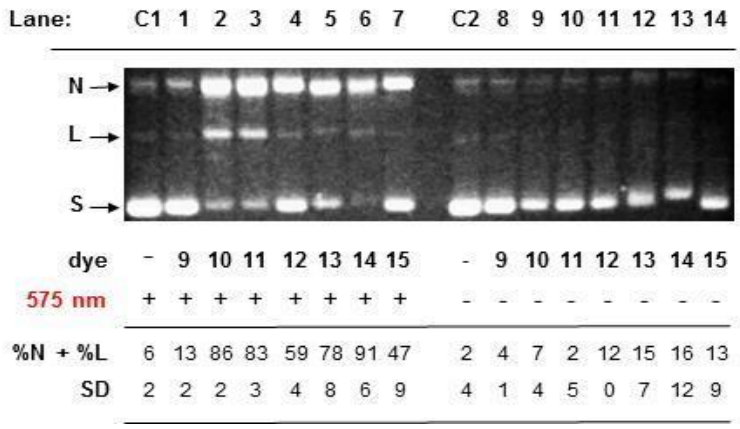

Figure 5.2. A photograph of a 1.5% non-denaturing agarose gel showing photocleavage of 38 μM bp of pUC19 plasmid DNA in the presence of 10 μM of dyes **9** through **15** (22 °C, 10 mM sodium phosphate buffer pH 7.0). **C1** and **C2** correspond to DNA without dye. Reactions in **C1** and **Lanes 1-7** were aerobically irradiated at 575 nm for 60 min in a ventilated Rayonet photochemical reactor equipped with ten 575 nm fluorescent lamps (> 21 watts per lamp, spectral output 400-650 nm). Reactions in **C2** and **Lanes 8** to **14** were kept in the dark for 60 min. DNA photocleavage yields (%**N** + %**L**) were averaged over two trials with errors reported as standard deviation. S, L, and N designate supercoiled, linear, and nicked forms of pUC19 plasmid DNA.

Although lower in power, the three monochromatic LEDs afforded good photocleavage yields. The 623 nm and 700 nm LEDs emit red light within the PDT phototherapeutic window. The best LED results were obtained using 700 diodes in combination with the TMAB-substituted bromine and chlorine dyes (Figure 5.3; Lanes 13 and 14 in Figure 5.S3). Irrespective of the light source, very low levels of photocleavage were produced by phenylpropyl cyanine **9** (Lane 2 in Figure 5.2 and Figures 5.S1 to 5.S3), suggesting cyanine-DNA interactions can be weakened by the placement of bulky substituents on the cyanine benz[*e*]indole hetero atom. Photocleavage levels were also low for plasmid DNA irradiated in the absence of dye (Lane 1 in Figure 5.2 and Figures 5.S1 to 5.S3), and in the dark control reactions (no hν; Lanes C2 to 14).

Upon irradiation with the broad spectrum lamps or with the monochromatic LEDs, the histogram in Figure 5.3 shows that, irrespective of the light source, the halogenated forms (X =

Br or Cl in Scheme 5.1) of the methyl (**10**, **11**) and TMAB (**13**, **14**) carbocyanines dyes consistently produced more photocleavage than their non-halogenated counterparts **12** and **15** (X = H in Scheme 5.1). It is possible that the halogenated cyanine dyes are binding to the DNA with higher affinity. Alternatively, the chlorine and bromine atoms may contribute to the production of DNA damaging ROS by inducing a "heavy atom effect". The heavy atom effect is described as enhancement of intersystem crossing, or the enhancement of the spin-forbidden transition from a singlet excited state molecule to a triplet state in the presence of an atom of high atomic number.[9,17] This heavy atom effect is expected to increase photocleavage levels through the increased generation of singlet oxygen, which is regulated by the efficiency of intersystem crossing between the triplet excited state chromophore and molecular oxygen.

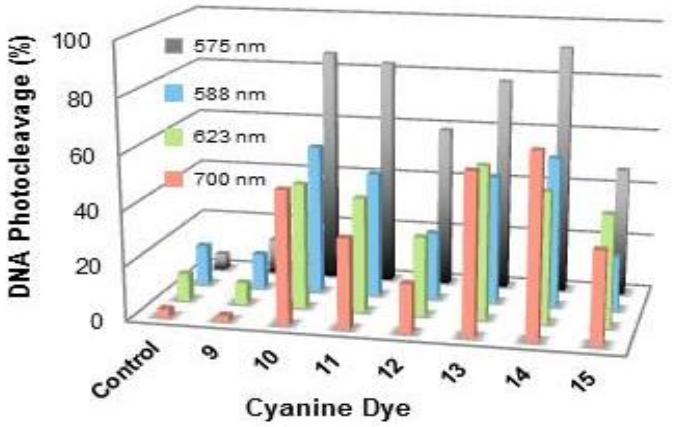

Figure 5.3. Percent DNA photocleavage (% nicked DNA + % linear DNA) plotted as a function of irradiation wavelength for reactions containing 38 μM bp of pUC19 plasmid DNA in the presence of 10 μM of cyanine dye **9**, **10**, **11**, **12**, **13**, **14**, or **15** (60 min irradiation at 22 °C, 10 mM sodium phosphate buffer pH 7.0). Key: control, irradiated DNA, no dye; 575 nm, samples were irradiated in a ventilated Rayonet photochemical reactor equipped with ten 575 nm fluorescent lamps (> 21 watts per lamp, spectral output 400-650 nm); 588 nm, samples were individually irradiated with a 588 nm LED (0.17 watts);623 nm, samples were individually irradiated with a 623 nm LED (0.17 watts); 700 nm, samples were individually irradiated with a 700 nm LED (0.20 watts).

Work by Akerman and Tuite has shown that the asymmetrical cyanine oxazole yellow (YO) and its dimer YOYO generate strand breaks within ΦX174 plasmid DNA when irradiated

using a 150 watt broad spectrum xenon lamp.[16] They observed that photocleavage levels were dependent on the DNA binding mode of the dye. When externally or groove bound,[18] the cyanines sensitized DNA photocleavage more efficiently than when intercalated. In the hydrophobic intercalation pocket, the dyes had restricted access to ground state triplet oxygen ($^3O_2$) and as a result, produced DNA damaging singlet oxygen ($^1O_2$) less efficiently.[16] The spectral output of the 575 nm lamps overlaps with DNA-bound cyanine absorption bands corresponding to the H-aggregate and monomer, while the 588 nm and 700 nm LEDs are more selective for the H-aggregate and monomer, respectively. The 623 nm LED is at an intermediate wavelength. Specifically, the photocleavage data obtained using the monochromatic 588 nm and 700 nm LEDs show that the H-aggregated and monomeric forms of cyanine dyes **10** through **15** produce similar levels of photocleavage (Figure 5.S1 and 5.S3; Figure 5.3). Suppressed cleavage is not observed using the 700 nm LED. This suggests that the monomeric cyanines are engaging in non-intercalative binding similar to the H-aggregated cyanine forms.

5.3.3. Inhibition of DNA Photocleavage. Cleavage inhibition experiments were conducted under conditions identical to initial photocleavage studies. In dye photosensitization, singlet oxygen is generated when the triplet excited state of the dye transfers energy to ground state triplet molecular oxygen. If the triplet or singlet state transfers electrons to $^3O_2$, hydroxyl radicals (•OH) are produced.[19] Both singlet oxygen and hydroxyl radicals are powerful enough to form direct strand breaks in duplex DNA.[19-20] Individual reactions, containing the singlet oxygen scavenger sodium azide, and the hydroxyl radical scavenger sodium benzoate, were irradiated for 60 min with the 575 nm broad spectrum lamps and then compared to parallel photocleavage reactions run in the absence of scavenger. The percent photocleavage inhibition data in Table 5.1 show that sodium azide and sodium benzoate reduce DNA photocleavage to a significant degree.

It can be inferred from these results that hydroxyl radicals and singlet oxygen both contribute substantially to DNA photocleavage by the cyanine dyes, but a clear contribution to photocleavage inhibition of the halogenated dyes is not apparent.

Table 5.1. Percent Inhibition of DNA Photocleavage by ROS Scavengers [a]

	Inhibition (%)	
Cyanine Dye	sodium azide ($^1O_2$)	sodium benzoate (·OH)
10	61	85
11	37	91
12	54	83
13	63	79
14	59	83
15	60	69

[a] Photocleavage inhibition reactions consisting of 38 μM bp of pUC19 plasmid DNA were equilibrated with 10 μM of cyanine dye, 100 mM of scavenger sodium azide or sodium benzoate, and 10 mM sodium phosphate buffer pH 7.0. Samples were then aerobically irradiated for 60 min with ten Rayonet 575 nm fluorescent lamps (spectral output 400-650 nm). ROS are in parenthesis.

5.3.4. DNA Photocleavage Concentration Titration. The effects of cyanine dye concentration on DNA photocleavage were studied next (Figure 5.S4). The reactions were carried out with 38 μM bp pUC19 plasmid DNA and 1.0 μM to 10.0 μM concentrations of the halogenated dyes **10**, **11**, **13**, and **14**. The samples were then aerobically irradiated for 60 min. using the broad spectrum 575 nm lamps. As expected, the amounts of DNA photocleavage produced by **10**, **11**, **13**, and **14** increased linearly as a function of increasing dye concentration from 1.0 μM up until 10 μM of dye.

5.3.5. UV-visible Absorption Titration. UV-visible absorption titrations were conducted in order to further investigate cyanine dye-DNA interactions. This was done by sequentially adding small volumes of CT DNA to solutions containing of 10 μM of cyanine dyes **10** through **15** until dye saturation where no additional changes in cyanine absorption were observed (Figures 5.4 and 5.S5). The first spectrum in each titration represents free cyanine dye. Intermediate spectra arise from the conversion of free to DNA-bound dye. At the titration endpoint, designated by the symbol "**e**", (Figures 5.4 and 5.S5), all of the dye is fully bound to the DNA.

The mono-cationic methyl cyanines **10** through **12** were studied first (Figures 5.4A to 5.4C). As the DNA concentration was increased, the cyanine bands displayed the extensive broadening we observed in our preliminary absorption spectra (Figures 5.1 B to D). The 619 nm to 626 nm absorption maxima corresponding to the free H-aggregate became slightly red-shifted and progressively attenuated as a new ~ 580 nm hypsochromic peak developed. Both cyanine bands are clearly visible at the titration endpoints. The 669 nm to 673 nm peaks corresponding to the monomeric form of the free dyes lost nearly all of their intensity as a new bathochromic peak between 668 nm to 686 nm emerged and then increases in intensity until the titration endpoint. The spectra generated by mono-cationic methyl cyanines **10** through **12** are very similar in overall appearance to those acquired by Kawabe and co-workers for a series of mono-cationic benzo[*d*]oxazole cyanine dyes. Upon DNA addition, new short and long wavelength components gave rise to extensive spectral broadening. Although the precise DNA binding modes of the dyes were not ascertained, the spectral changes were presumed to arise from the formation of irregular aggregates (not determinable as J or H) within or external to the DNA minor groove.[4]

The titrations in Figures 5.4A to 5.4C show that halogen modified cyanines **10** and **11** reach saturation at 5.0 μM bp of CT DNA compared to 16 μM bp for hydrogen modified cyanine **12**. This suggests that **10** and **11** produce more photocleavage than **12** because they bind to DNA with greater affinity (Figs. 5.2A and 5.2C). Although a heavy atom effect may still be contributing to photocleavage, it is not supported by the spectroscopic data.

UV-visible absorption spectra corresponding to tri-cationic TBMA-substituted **13** to **15** were acquired next (Figures 5.4D to 5.4F; Figure 5.S4). With each sequential DNA addition, the 632 nm to 637 nm band corresponding to free H-aggregate became slightly red-shifted and progressively hypochromic. The behavior of the absorption band corresponding to the free monomer was more complex. Sequential additions of CT DNA induced hypochromicity and slight red-shifting of the 677 nm to 681 nm M-band until the absorption at the λ_{max} reached a minimum value designated by the symbol "**m**" in Figure 5.4. After this point, CT DNA addition caused additional red-shifting of the M-band, and a progressive hyperchromicity until the titration endpoint. The ratio of the maximum absorbance intensity of the monomer to the H-aggregate band began to increase, suggests that the DNA was beginning to disassemble the H-aggregate in favor of the monomer formation.[5, 15] Our fluorescence and DNA photocleavage data suggest that, in the monomeric form, the tri-cationic TBMA cyanines **13** to **15** bind to DNA in a non-intercalative fashion.

The chlorine-substituted cyanine **14** and hydrogen-substituted cyanine **15** became saturated at 103 μM bp of CT DNA (Figures 5.4E and 5.4F) compared to 261 μM bp μM bp for brominated analog **13** (Figure 5.S5). This indicates and that the binding affinities of **14** and **15** are roughly equivalent, while cyanine **13** has lower affinity for DNA. Therefore, it is possible

that the halogenated cyanines **13** and **14** produce more photocleavage than **15** due to a heavy atom effect that increases the efficiency of intersystem crossing to the photosensitizers' triplet excited state (Figure 5.1 and 5.2; Figures 5.S1 to 5.S3).

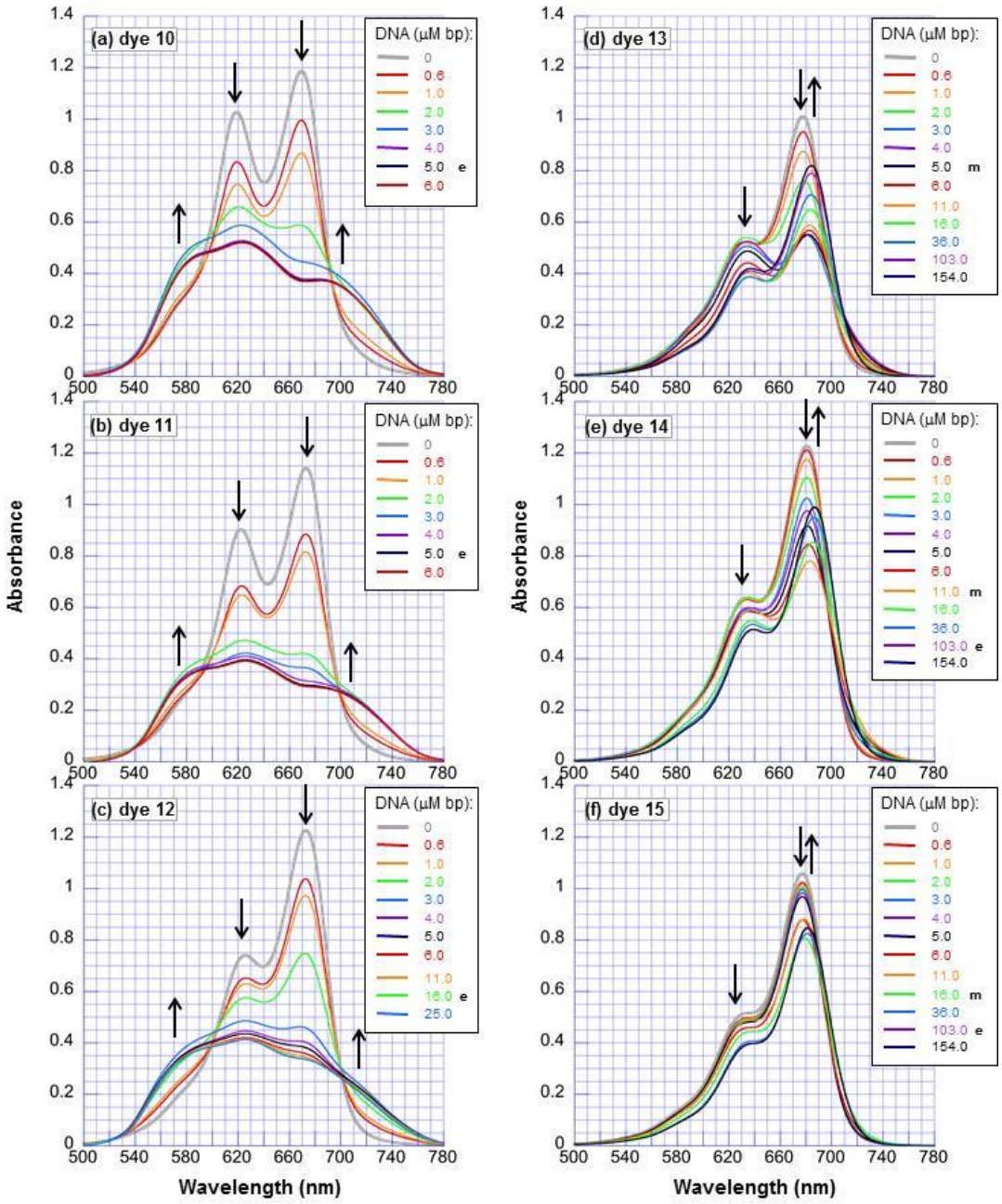

Figure 5.4. UV-visible absorption titration spectra of 10 μM of dye (a) **10**, (b) **11**, (c) **12**, (d) **13**, (e) **14**, or (f) **15** recorded at 22 °C. Individual samples contained 10 mM sodium phosphate buffer pH 7.0 and increasing concentrations of calf thymus DNA (0 μ mM bp to 6 μM bp, 25 μM bp, or 154 μM bp). Following each sequential DNA addition, the solutions were allowed to equilibrate for 15 min in the dark before the UV-visible spectra were recorded. All absorption spectra have been corrected for sample dilution. The letter **m** designates absorption minimum at λ_{max}; **e** designates titration endpoint.

5.4. Conclusion

Though much is known about their binding affinity and photo-reactivity in relation to fluorescence labeling, little is known about the photonuclease properties of symmetrical cyanine dyes compared to asymmetrical dyes. This work demonstrates that carbocyanines **10** – **15** function as efficient DNA photonucleases. Through the production of the reactive oxygen species singlet oxygen and hydroxyl radicals they are able to convert plasmid DNA to circular nicked and linear forms. UV-visible and fluorescence spectroscopy measurements suggest carbocyanine-DNA complex formation that facilitates these observed enhancements in photocleavage levels. Ideally we hope to further explore these mechanisms of interaction through further experimentation and analysis, with the hopes of finding other carbocyanines that functions as DNA photonucleases.

5.5 Supplementary Materials

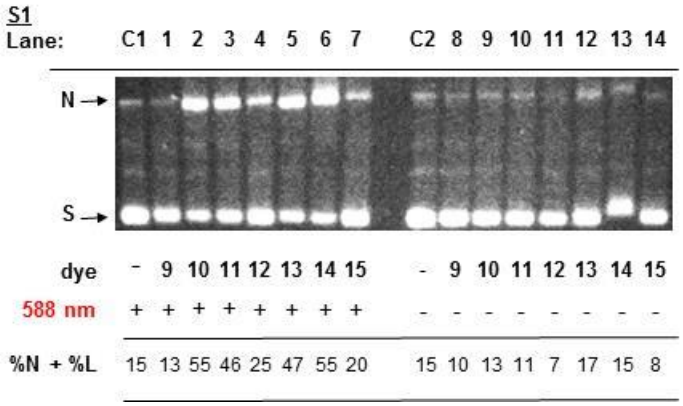

Figure 5.S1. A photograph of a 1.5% non-denaturing agarose gel showing photocleavage of 38 μM bp of pUC19 plasmid DNA in the presence of 10 μM of dyes **9** through **15** (22 °C, 10 mM sodium phosphate buffer pH 7.0). **C1** and **C2** correspond to DNA without dye. Reactions in **C1** and **Lanes 1-7** were individually irradiated for 60 min with a 588 nm LED (0.17 watts). Reactions in **C2** and **Lanes 8** to **14** were kept in the dark for 60 min. S, L, and N designate supercoiled, linear, and nicked forms of pUC19 plasmid DNA.

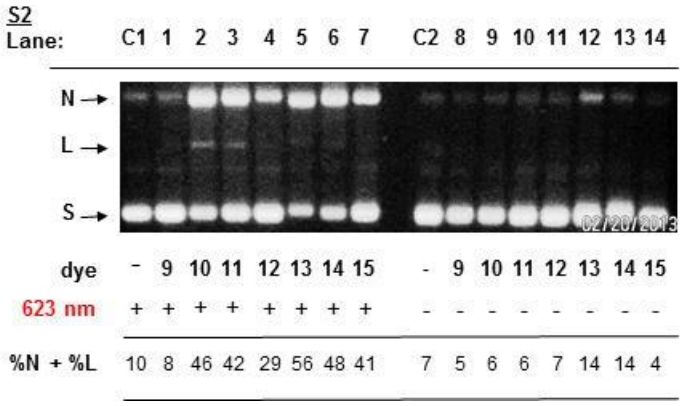

Figure 5.S2. A photograph of a 1.5% non-denaturing agarose gel showing photocleavage of 38 μM bp of pUC19 plasmid DNA in the presence of 10 μM of dyes **9** through **15** (22 °C, 10 mM sodium phosphate buffer pH 7.0). **C1** and **C2** correspond to DNA without dye. Reactions in **C1** and **Lanes 1-7** were individually irradiated for 60 min with a 623 nm LED (0.17 watts). Reactions in **C2** and **Lanes 8** to **14** were kept in the dark for 60 min. S, L, and N designate supercoiled, linear, and nicked forms of pUC19 plasmid DNA.

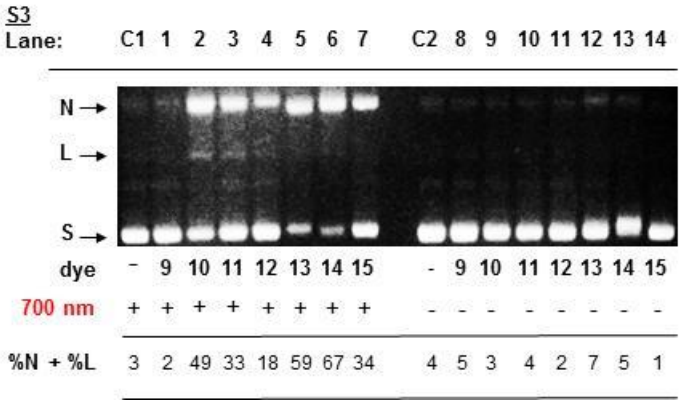

Figure 5.S3. A photograph of a 1.5% non-denaturing agarose gel showing photocleavage of 38 μM bp of pUC19 plasmid DNA in the presence of 10 μM of dyes **9** through **15** (22 °C, 10 mM sodium phosphate buffer pH 7.0). **C1** and **C2** correspond to DNA without dye. Reactions in **C1** and **Lanes 1-7** were individually irradiated for 60 min with a 700 nm LED (0.20 watts). Reactions in **C2** and **Lanes 8** to **14** were kept in the dark for 60 min. S, L, and N designate supercoiled, linear, and nicked forms of pUC19 plasmid DNA.

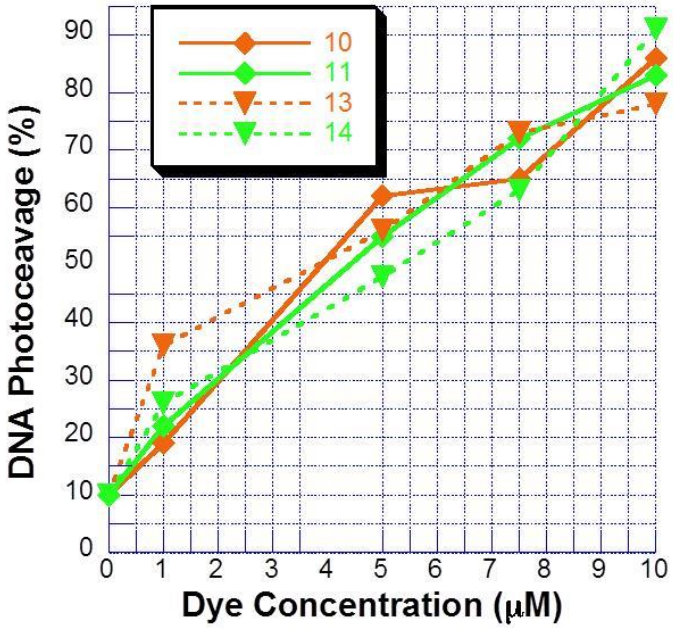

Figure 5.S4. Samples containing 38 μM bp of pUC19 plasmid DNA in the presence of 1 μM to 10 μM of dye **10**, **11**, **13**, or **14** were irradiated at 575 nm for 60 min in a ventilated Rayonet photochemical reactor with ten 575 nm fluorescent lamps (22 °C, 10 mM sodium phosphate buffer pH 7.0).

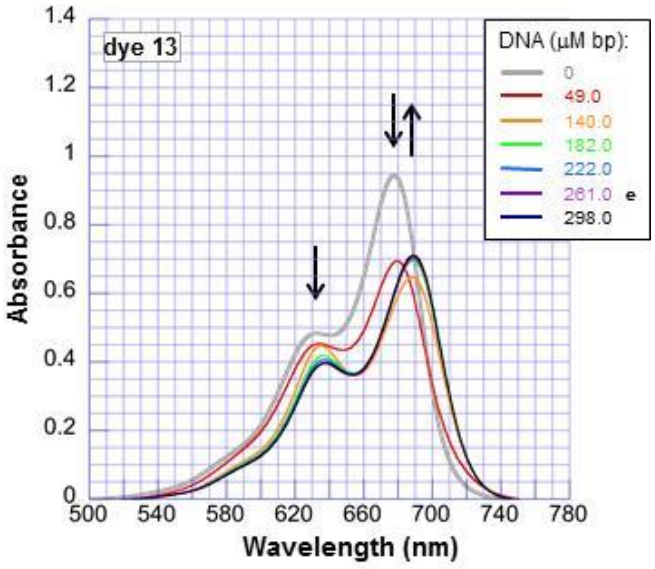

Figure 5.S5. UV-visible absorption titration spectra of 10 μM of dye **13** recorded at 22 °C. The sample contained 10 mM sodium phosphate buffer pH 7.0 and increasing concentrations of calf thymus DNA (0 μ mM bp to 298 μM bp). Following each sequential DNA addition, the solution was allowed to equilibrate for 15 min in the dark before the UV-visible spectrum were recorded. All absorption spectra have been corrected for sample dilution. The letter **e** designates titration endpoint.

5.5.1. Experimental Procedures

5.5.1.1. Materials and Methods. The chemical reagents used in the synthesis of these compounds were obtained from either Acros Organics or Alfa Aesar. The ^{1}H NMR and ^{13}C NMR spectra were recorded on a Bruker Avance (400 MHz) spectrometer using DMSO-d_6 or MeOD-d_4 containing tetramethylsilane (TMS) as an internal calibration standard. UV-Vis/NIR absorption spectra were recorded on a Varian Cary 50 spectrophotometer. High-resolution accurate mass spectra (HRMS) were obtained either at the Georgia State University Mass Spectrometry Facility using a Waters Q-TOF micro (ESI-Q-TOF) mass spectrometer or utilizing a Waters Micromass LCT TOF ES+ Premier Mass Spectrometer. Liquid chromatography utilized a Waters 2487 single wavelength absorption detector with wavelengths set between 640 and 700 nm depending on the dye's photo-physical properties. The column used in LC was a

Waters Delta-Pak 5 uM 100A 3.9 x 150 mm reversed phase C_{18} column. Evaporative light scattering detection analyzes trace impurities that cannot be observed by alternate methods; a SEDEX 75 ELSD was utilized in tandem with liquid chromatography to observe purity.

The reagents used in photocleavage and spectroscopic studies were of the highest available purity and required no further purification. Ethidium bromide, dimethyl sulfoxide (DMSO) (purity $\geq$ 99.9%), were obtained from Sigma-Aldrich. Sodium phosphate buffer was prepared using sodium phosphate dibasic salt from J.T. Baker and sodium phosphate monobasic salt obtained from Fisher Scientific. Calf thymus DNA was purchased from Invitrogen (Lot# 1128117). UV-visible spectra were recorded with a Shimadzu UV-2401 PC spectrophotometer (Shimadzu Scientific Instruments). Fluorescence spectra were recorded using a Shimadzu RF-1501 spectrofluorophotometer. Photocleavage reactions were run in an aerobically ventilated Rayonet Photochemical Reactor fitted with either ten RPR-5750 Å lamps (The Southern New England Ultraviolet Company) or irradiated individually using either a 623 nm LED (0.17 watts) or a 700 nm LED (0.20 watts). Transformation of *E. coli* competent cells (Stratagene, XL-1 blue) with pUC19 plasmid DNA (Sigma-Aldrich) and growth of bacterial cultures were performed according to established laboratory methods.[21] Purification of the plasmid DNA was accomplished using a Quiagen Plasmid Mega Kit.

5.5.1.2. Synthesis and characterization of cyanine dyes. Compound **3** was obtained commercially from Acros Organics. Salts **4** and **5** and cyanine precursors **6** and 7 were prepared using procedures previously reported by our laboratory.[22,23]

5.5.1.3. Synthetic procedure for preparing dicationic salt (8). Benz[*e*]indole (10 g) was added to acetonitrile (250 mL). The suspension was heated to reflux and 3-bromopropyl

trimethylammonium bromide (BrTMAB) was added (3 mol equiv). After 72 h, the reaction was allowed to cool and the solid product was obtained upon addition of diethyl ether. After recrystallization from methanol using reduced temperature and titration with diethyl ether, the product was filtered and thoroughly dried under high vacuum. Because their dicationic nature makes these compounds highly hygroscopic, the proceeding reactions should be anhydrous.

1,1,2-Trimethyl-3-(3-(trimethylammonio)propyl)-1H-benzo[e]indolium bromide (**8**): 52% yield. MP 95-97 ^{o}C. ^{1}H-NMR (400 MHz, DMSO-d_6), **δ**: 1.79 (s, 6H), 2.42-2.37 (m, 2H), 3.03 (s, 3H), 3.41 (s, 9H), 3.65 (t, *J* = 8.0 Hz, 2H), 4.64 (t, *J* = 8.0 Hz, 2H), 7.82-7.75 (m, 2H), 8.26 (t, *J* = 8.8 Hz, 2H), 8.33 (d, *J* = 8.8 Hz, 1H), 8.39 (d, *J* = 8.8 Hz, 1H). ^{13}C-NMR (100 MHz, DMSO-d_6), **δ**: 15.01, 21.94, 22.09, 45.32, 53.09, 56.13, 62.41, 113.90, 123.89, 127.70, 127.78, 128.93, 130.20, 131.18, 133.55, 137.33, 138.89, 198.10.

5.5.1.4. Synthetic procedure for preparing the highly hydrophobic pentacyanine dye 9 and monocationic pentacyanine dyes 10 to 12. Benz[*e*]indole salt **6** or **7** was added to acetic anhydride (15 mL) and sodium acetate (3 mol equiv). The mixture was heated to 50 ^{o}C and malonaldehyde bisphenylimine **3** or corresponding derivative **4** or **5** (1 mol equiv) was added to the stirring mixture, which caused an instant color change from light pink to deep blue-green. The reactions were monitored using TLC and UV-visible-NIR absorption spectroscopy. After 2 to 4 h, the reactions were stopped, allowed to cool to room temperature, and placed in the freezer. Diethyl ether was added to the reaction mixtures to precipitate monocationic compounds **9** to **12**. The products were isolated using silica gel column chromatography and a gradient elution ranging from 1:1 EtOAC:DCM to 2% MeOH in DCM as eluting solvents.

2-((1E,3Z,5E)-3-chloro-5-(1,1-dimethyl-3-(3-phenylpropyl)-1H-benzo[e]indol-2(3H)-ylidene)penta-1,3-dien-1-yl)-1,1-dimethyl-3-(3-phenylpropyl)-1H-benzo[e]indol-3-ium bromide

(**9**): 47% yield. MP 165-168 ^{o}C ^{1}H-NMR (400 MHz, DMSO-d_6), **δ:** 1.98 (s, 12H), 2.04 (t, *J* = 4.0 Hz, 4H), 2.82 (t, *J* = 4.0 Hz, 4H), 4.31 (t, *J* = 8.0 Hz, 4H), 6.235 (d, *J* = 16.0 Hz, 2H), 7.23-7.36 (m, 10H), 7.57 (t, *J* = 8.0 Hz, 2H), 7.72 (t, *J* = 8.0 Hz, 2H), 7.82 (d, *J* = 8.0 Hz, 2H), 8.12 (t, *J* = 8.0 Hz, 4H), 8.28 (d, *J* = 8.0 Hz, 2H), 8.58 (d, *J* = 12.0 Hz, 2H). ^{13}C-NMR (100 MHz, DMSO-d_6), **δ:** 27.65, 29.77, 33.39, 44.93, 52.44, 100.59, 112.99, 123.47, 123.60, 126.49, 127.42, 128.68, 129.17, 129.55, 129.80, 131.22, 131.73, 132.90, 135.16, 140.62, 141.89, 147.75, 176.31. TOF HRMS *m/z* (M^+) calculated for $C_{51}H_{50}N_2Cl$ 725.3663 found 725.3663.

2-((1E,3Z,5E)-3-bromo-5-(1,1,3-trimethyl-1H-benzo[e]indol-2(3H)-ylidene)penta-1,3-dien-1-yl)-1,1,3-trimethyl-1H-benzo[e]indol-3-ium iodide (**10**)**:** 90% yield. MP 229-230 ^{o}C. ^{1}H-NMR (400 MHz, DMSO-d_6), **δ:** 1.97 (s, 12H), 3.80 (s, 6H), 6.345 (d, *J* = 12.0 Hz, 2H), 7.53 (t, *J* = 8.0 Hz, 2H), 7.69 (t, *J* = 8.0 Hz, 2H), 7.83 (d, *J* = 8.0Hz, 2H), 8.12-8.07 (m, 4H), 8.26 (d, *J* = 8.0 Hz, 2H), 8.635 (d, *J* = 12.0 Hz, 2H). ^{13}C-NMR (100 MHz, DMSO-d_6), **δ:** 25.91, 31.56, 50.78, 101.49, 111.54, 115.27, 121.88, 124.78, 127.01, 127.51, 129.61, 129.95, 131.27, 133.26, 139.85, 147.91, 175.31. TOF HRMS *m/z* (M^+) calculated for $C_{35}H_{34}N_2Br$ 561.1905 found 561.1914.

2-((1E,3Z,5E)-3-chloro-5-(1,1,3-trimethyl-1H-benzo[e]indol-2(3H)-ylidene)penta-1,3-dien-1-yl)-1,1,3-trimethyl-1H-benzo[e]indol-3-ium iodide (**11**)**:** 53% yield. MP 206-208 ^{o}C. ^{1}H-NMR (400 MHz, DMSO-d_6), **δ:** 2.00 (s, 12H), 3.83 (s, 6H), 6.365 (d, *J* = 12.0 Hz, 2H), 7.56 (t, *J* = 8.0 Hz, 2H), 7.72 (t, *J* = 8.0 Hz, 2H), 7.85 (d, *J* = 8.0 Hz, 2H), 8.08-8.15 (m, 4H), 8.29 (d, *J* = 8.0 Hz, 2H), 8.60 (d, *J* = 16.0 Hz, 2H). ^{13}C-NMR (100 MHz, DMSO-d_6), **δ:** 26.73, 32.36, 51.50, 99.98, 112.27, 122.58, 122.67, 125.59, 127.80, 128.34, 130.39, 130.77, 132.05, 134.10, 140.61, 146.66, 175.96. TOF HRMS *m/z* (M^+) calculated for $C_{35}H_{34}N_2Cl$ 517.2411, found 517.2401.

1,1,3-Trimethyl-2-((1E,3E,5E)-5-(1,1,3-trimethyl-1H-benzo[e]indol-2(3H)-ylidene)penta-1,3-dien-1-yl)-1H-benzo[e]indol-3-ium iodide (**12**)**:** 80% yield. MP >260 ^{o}C. ^{1}H-NMR (400 MHz, DMSO-d_6), **δ:** 1.95 (s, 12H), 3.73 (s, 6H), 6.325 (d, *J* = 12.0 Hz, 2H), 6.59 (t, *J* = 12.0 Hz, 1H), 7.52 (t, *J* = 8.0 Hz, 2H), 7.67 (t, *J* = 8.0 Hz, 2H), 7.74 (d, *J* = 8.0 Hz, 2H), 8.06 (t, *J* = 8.0 Hz, 4H), 8.24 (d, *J* = 8.0 Hz, 2H), 8.465 (t, *J* = 12.0 Hz, 2H). ^{13}C-NMR (100 MHz, DMSO-d_6), **δ:** 26.61, 31.47, 50.58, 102.98, 111.53, 122.09, 124.65, 125.26, 127.48, 127.66, 129.87, 130.12, 131.23, 132.90, 140.39, 152.77, 174.114. TOF HRMS *m/z* (M^+) calculated for $C_{35}H_{35}N_2$ 483.2800, found 483.2818.

5.5.1.5. Synthetic procedure for preparing tricationic pentacyanine dyes 13 to 15. A mixture of dicationic salt **8** (2 mol equiv), individual reagent **3**, **4** or **5**, and sodium acetate (3 mol equiv) were refluxed for 6 h in anhydrous acetic anhydride under a nitrogen atmosphere and then cooled to room temperature. The reaction mixture was concentrated *in vacou*. The crude product was dissolved in deionized distilled water and the target compound was isolated by open column chromatography on reversed phase 40-63 μm 90 Å C_{18} silica gel (methanol:water 1:5).

2-((1E,3Z,5E)-3-bromo-5-(1,1-dimethyl-3-(3-(trimethylammonio)propyl)-1H-benzo[e]indol-2(3H)-ylidene)penta-1,3-dien-1-yl)-1,1-dimethyl-3-(3-(trimethylammonio)propyl)-1H-benzo[e]indol-3-ium bromide (**13**): 71% yield. MP 227-230 ^{o}C. ^{1}H-NMR (400 MHz, MeOD-d_4), **δ:** 2.05 (s, 12H), 2.46 (s, 4H), 3.28 (s, 18H), 3.84 (t, *J* = 8.0 Hz, 4H), 4.51 (s, 4H), 6.54 (d, *J* = 13.2 Hz, 2H), 7.49 (t, *J* = 7.2 Hz, 2H), 7.67 (t, *J* = 7.2 Hz, 2H), 7.89 (d, *J* = 8.8 Hz, 2H), 7.99 (d, *J* = 8.0 Hz, 2H), 8.09 (d, *J* = 8.8 Hz, 2H), 8.27 (d, *J* = 8.0 Hz, 2H), 8.62 (d, *J* = 13.2, 2H). ^{13}C-NMR (100 MHz, MeOD-d_4), **δ**: 21.17, 25.99, 39.07, 41.27, 51.65, 52.54, 63.18, 102.23, 110.94, 117.03, 122.14, 125.20, 127.57, 127.96, 129.73, 130.67, 132.43, 134.42, 138.94, 149.36, 176.29.

ESI HRMS calculated *m/z* for $[C_{45}H_{58}BrN_4]^{3+}$ 244.4610 found 245.0591; calculated *m/z* for $[C_{45}H_{58}BrN_4]^{2+}$ 366.6917, found 367.0858.

2-((1E,3Z,5E)-3-chloro-5-(1,1-dimethyl-3-(3-(trimethylammonio)propyl)-1H-benzo[e]indol-2(3H)-ylidene)penta-1,3-dien-1-yl)-1,1-dimethyl-3-(3-(trimethylammonio)propyl)-1H-benzo[e]indolium bromide (**14**): 62% yield. MP 222-224 ^{o}C. ^{1}H-NMR (400 MHz, MeOD-d_4), **δ:** 2.04 (s, 12H), 2.264 (s, 4H), 3.15 (s, 18H), 3.70 (t, *J* = 8.0 Hz, 4H), 4.42 (s, 4H), 6.40 (d, *J* = 13.2 Hz, 2H), 7.56 (d, *J* = 7.6 Hz, 2H), 7.73 (t, *J* = 7.6 Hz, 2H), 7.96 (d, *J* = 9.2 Hz, 2H), 8.17-8.11 (m, 4H), 8.28 (d, *J* = 8.8 Hz, 2H), 8.73 (d, *J* = 13.2 Hz, 2H). ^{13}C-NMR (100 MHz, MeOD-d_4), **δ**: 20.89, 26.50, 40.58, 49.35, 52.57 63.05, 104.20, 111.92, 122.72, 127.75, 128.49, 130.54, 140.59, 143.15, 155.05, 173.28. ESI HRMS calculated *m/z* for $[C_{45}H_{58}N_4Cl]^{3+}$ 229.8111, found 229.7517; calculated m/z for $[C_{45}H_{58}N_4Cl]^{2+}$ 344.7170, found 344.6516.

2-((1E,3E,5E)-5-(1,1-dimethyl-3-(3-(trimethylammonio)propyl)-1H-benzo[e]indol-2(3H)-ylidene)penta-1,3-dien-1-yl)-1,1-dimethyl-3-(3-(trimethylammonio)propyl)-1H-benzo[e]indolium bromide (**15**): 60% yield. MP 232-234 ^{o}C. ^{1}H-NMR (400 MHz, MeOD-d_4), **δ:** 2.04 (s, 12H), 2.39 (m, 4H), 3.23 (s, 18H), 3.80 (s, 4H), 4.38 (s, 4H), 6.65 (t, *J* = 12.8 Hz, 2H), 7.17 (m, 1H), 7.49 (m, 2H), 7.62 (m, 2H), 7.73 (t, *J* = 9.2 Hz, 2H), 8.08-7.97 (m, 4H), 8.26 (t, *J* = 9.2 Hz, 2H), 8.41 (m, 2H). ^{13}C-NMR (100 MHz, MeOD-d_4), **δ:** 21.30, 26.32, 40.7, 51.02, 52.62, 63.10, 103.28, 110.79, 121.97, 124.68, 126.55, 127.35, 128.06, 129.63, 130.46, 132.02, 132.02, 133.70, 139.16, 153.57, 174.48. ESI HRMS calculated *m/z* for $[C_{45}H_{59}N_4]^{3+}$ 218.4908, found 218.4383; calculated *m/z* for $[C_{45}H_{59}N_4]^{2+}$ 327.7365, found 327.1663.

5.5.1.6. Photocleavage at 575 nm, 588 nm, 623 nm, and 700 nm. Chromophores **9** – **15** at 10 μM final concentrations were added to solutions containing 38 μM bp pUC19 plasmid

DNA and 10 mM sodium phosphate buffer, pH 7.0. All samples were then equilibrated in darkness for 60 min at 22 °C, (no hν). Each sample series was irradiated at either: 575, 588, 623, or 700 nm for 60 min at 22 °C. Duplicate control samples were equilibrated in darkness for 60 min at 22 °C, (no hν).

For each series of photocleavage experiments, following irradiation, the extent of cleavage was measured by gel electrophoresis. Following the addition of 3.0 μL of electrophoresis loading buffer (15% (w/v) Ficoll and 0.025% (w/v) bromophenol blue) to the reaction mixtures, cleavage products were separated on ethidium bromide stained 1.5% non-denaturing agarose gels (Sigma-Aldrich) (0.50 μg/mL EtBr final concentration) in 1X TAE buffer, using an OWL* A1 Large Gel System electrophoresis box (Thermo Scientific). To determine the percent conversion of supercoiled plasmid DNA to its nicked and linear forms, the gels were visualized and digitally photographed on a transilluminator set at 302 nm. The DNA bands on the digital images were quantitated using Image Quant v.5.0 software. Supercoiled bands were adjusted using a correction factor of 1.22. Photocleavage yields were calculated using Formula 1. For inhibition of photocleavage experiments, the percent photocleavage inhibition was calculated using Formula 2.

$$\% \text{ Photocleavage} = [(\text{Linear} + \text{Nicked}) / (\text{Linear} + \text{Nicked} + \text{Supercoiled})] \times 100 \quad (1)$$

$$\text{Percent Photocleavage Inhibition} = [(\%\ \text{Total of Linear and Nicked DNA}_{\text{without scavenger}} - \%\ \text{Total of Linear and Nicked DNA}_{\text{with scavenger}})/(\%\ \text{Total of Linear and Nicked DNA}_{\text{without scavenger}})] \times 100. \quad (2)$$

5.5.1.7. DNA Photocleavage Concentration Titrations. To each in a duplicate series of Eppendorf tubes were added 10 mM sodium phosphate buffer pH 7.0 and **10, 11, 13** and **14** at final concentrations of 10 to 1.0 μM (total volume 40 μL). Parallel dark controls were prepared.

Reaction mixtures were irradiated at 575 nm for 60 min at 22 °C, while the controls remained in darkness for 60 min at 22 °C.

5.5.1.8. Inhibition of DNA Photocleavage. Samples containing carbocyanines **10** – **15** were prepared following the same procedures as described above for the 575 nm photocleavage reactions. Before irradiation, final concentrations of 100 mM of sodium azide or of sodium benzoate were added to all samples.

5.5.1.9. UV-visible Spectrophotometric Analysis. In a total volume of 500 μL, solutions contained a final concentration of 10 μM of cyanine dye (**9 – 15**) in the presence of 38 μM bp CT DNA and 10 mM sodium phosphate buffer pH 7.0. After a pre-equilibration period of 1 h (22 °C, no hν), UV-visible spectra were then collected from 900 to 200 nm.

5.5.1.10. Fluorescence Emission Spectra. Samples contained 10 μM of compounds **9** to **15**, 10 mM sodium phosphate buffer pH 7.0 and 38 μM bp CT DNA in a 2000 μL total volume. Following equilibration in darkness for 60 min at 22 °C, the samples in 3.0 mL quartz cuvettes (Starna), were excited at: 731 nm (**9**); 689 nm (**10**); 695 nm (**11**), 695 nm (**12**); 689 nm (**13**); 692 nm (**14**), and 690 nm (**15**), the wavelengths in the absorption spectra of the cyanine dyes that did not change in intensity upon the addition of DNA. Emission spectra were recorded from 800 - 200 nm at 22 °C.

5.5.1.11. Absorption Titration. In absorption titrations experiments, samples of 10 μM cyanine dye (**10**, **11**, **12**, **13**, **14**, or **15**) contained 10 mM sodium phosphate buffer pH 7.0 and increasing concentrations of calf thymus DNA (0 μ mM bp to 300 μM bp) in a 500 μL total volume. Following each sequential addition of CT DNA, the solutions were allowed to equilibrate for 15 min in darkness at 22 °C before the UV-visible spectra were recorded from 800 – 200 nm. All absorption spectra were corrected for sample dilution.

5.6 References

1. Rye, H. S.; Yue, S.; Wemmer, D. E.; Quesada, M. A.; Haugland, R. P.; Mathies, R. A.; Glazer, A. N., Stable fluorescent complexes of double-stranded DNA with bis-intercalating asymmetric cyanine dyes: properties and applications. *Nucleic Acids Res.* **1992,** *20* (11), 2803-2812.

2. Armitage, B. A., Cyanine Dye–DNA Interactions: Intercalation, Groove Binding, and Aggregation. In *DNA Binders and Related Subjects*, Waring, M.; Chaires, J., Eds. Springer Berlin Heidelberg: 2005; Vol. 253, pp 55-76.

3. Armitage, B., Cyanine dye–nucleic acid interactions. In *Heterocyclic Polymethine Dyes*, Strekowski, L., Ed. Springer Berlin Heidelberg: 2008; Vol. 14, pp 11-29.

4. Kawabe, Y.; Kato, S., Spectroscopic study of cyanine dyes interacting with the biopolymer, DNA. *Dyes and Pigments* **2012,** *95* (3), 614-618.

5. Mahmood, T.; Paul, A.; Ladame, S., Synthesis and Spectroscopic and DNA-Binding Properties of Fluorogenic Acridine-Containing Cyanine Dyes. *J. Org. Chem.* **2009,** *75* (1), 204-207.

6. Josefsen, L. B.; Boyle, R. W., Unique diagnostic and therapeutic roles of porphyrins and phthalocyanines in photodynamic therapy, imaging and theranostics. *Theranostics* **2012,** *2* (9), 916-966.

7. Ormond, A. B.; Freeman, H. S., Dye sensitizers for photodynamic therapy. *Materials* **2013,** *6* (3), 817-840.

8. Juzeniene, A.; Moan, J., The history of PDT in Norway Part one: Identification of basic mechanisms of general PDT. *Photodiagn. Photodyn.* **2007,** *4* (1), 3-11.

9. Gorman, A.; Killoran, J.; O'Shea, C.; Kenna, T.; Gallagher, W. M.; O'Shea, D. F., In vitro demonstration of the heavy-atom effect for photodynamic therapy. *J Am Chem Soc* **2004,** *126* (34), 10619-10631.

10. Sovenyhazy, K. M.; Bordelon, J. A.; Petty, J. T., Spectroscopic studies of the multiple binding modes of a trimethine-bridged cyanine dye with DNA. *Nucleic Acids Res.* **2003,** *31* (10), 2561-9.

11. Garoff, R. A.; Litzinger, E. A.; Connor, R. E.; Fishman, I.; Armitage, B. A., Helical Aggregation of Cyanine Dyes on DNA Templates: Effect of Dye Structure on Formation of Homo- and Heteroaggregates. *Langmuir* **2002,** *18* (16), 6330-6337.

12. Wang, M.; Silva, G. L.; Armitage, B. A., DNA-Templated Formation of a Helical Cyanine Dye J-Aggregate. *J. Am. Chem. Soc.* **2000,** *122* (41), 9977-9986.

13. Cao, R.; Venezia, C. F.; Armitage, B. A., Investigation of DNA binding modes for a symmetrical cyanine dye trication: Effect of DNA sequence and structure. *J. Biomol. Struct. Dyn.* **2001,** *18* (6), 844-857.

14. Biver, T.; De Biasi, A.; Secco, F.; Venturini, M.; Yarmoluk, S., Cyanine dyes as intercalating agents: Kinetic and thermodynamic studies on the DNA/Cyan40 and DNA/CCyan2 systems. *Biophys. J.* **2005,** *89* (1), 374-383.

15. Beckford, G.; Owens, E.; Henary, M.; Patonay, G., The solvatochromic effects of side chain substitution on the binding interaction of novel tricarbocyanine dyes with human serum albumin. *Talanta* **2012,** *92*, 45-52.

16. Akerman, B.; Tuite, E., Single- and double-strand photocleavage of DNA by YO, YOYO and TOTO. *Nucleic Acids Res* **1996,** *24* (6), 1080-90.

17. Verhoeven, J. W., Glossary of terms used in photochemistry (IUPAC Recommendations 1996). *Pure Appl. Chem.* **1996,** *68* (12), 2223 - 2286.

18. Larsson, A.; Carlsson, C.; Jonsson, M.; Albinsson, B., Characterization of the Binding of the Fluorescent Dyes Yo and Yoyo to DNA by Polarized-Light Spectroscopy. *J. Am. Chem. Soc.* **1994,** *116* (19), 8459-8465.

19. Da Ros, T.; Spalluto, G.; Boutorine, A. S.; Bensasson, R. V.; Prato, M., DNA-photocleavage agents. *Curr Pharm Design* **2001,** *7* (17), 1781-1821.

20. Di Mascio, P.; Wefers, H.; Do-Thi, H. P.; Lafleur, M. V.; Sies, H., Singlet molecular oxygen causes loss of biological activity in plasmid and bacteriophage DNA and induces single-strand breaks. *Biochim. Biophys. Acta* **1989,** *1007* (2), 151-7.

21. Sambrook, J., Fritsch, E.F., and Miniatis,T., *Molecular Cloning: A Laboratory Manual* Second ed.; Cold Springs Harbor Laboratory Press: Cold Springs Harbor, NY, 1989.

22. Owens, E. A.; Hyun, H.; Kim, S. H.; Lee, J. H.; Park, G.; Ashitate, Y.; Choi, J.; Hong, G. H.; Alyabyev, S.; Lee, S. J.; Khang, G.; Henary, M.; Choi, H. S., Highly charged cyanine fluorophores for trafficking scaffold degredation. *Biomed Mater* **2013,** *8* (1).

23. Sinha, S. H.; Owens, E. A.; Feng, Y.; Yang, Y.; Xie, Y.; Tu, Y.; Henary, M.; Zheng, Y. G., Synthesis and evaluation of carbocyanine dyes as PRMT inhibitors and imaging agents. *Eur. J. Med. Chem.* **2012,** *54* (0), 647-659.

CHAPTER 6. SUMMARY

In Chapter 2, we examined the copper(II)-dependent photocleavage enhancement of supercoiled pUC19 plasmid DNA by a bis-acridine chromophore in the presence of 150 mM NaCl and 260 mM KCl, salt concentrations that mimic those found in the cell nucleus where genomic DNA is located.[1] Under the high ionic strength conditions, and one mol equivalent of Cu(II), a bis-acridine chromophore linked by a 2,6-bis(aminomethyl)pyridine unit (**3**) generated higher levels of photocleavage than the previously studied bis-acridine **4**, linked by a 2,6-bis{[(methoxycarbonlyamino)-ethyl]methylaminomethyl}pyridine bridge. UV-visible spectral analyses showed a relationship between chromicity changes produced upon the addition of DNA and observed photocleavage yields. For **3**, the combination of **3**/Cu(II)/KCl produced strong cleavage and 40 % hyperchromicity compared to **4**/Cu(II)/KCl, which generated moderate cleavage and 4% hypochromicity. Thermal melting experiments showed that in the presence and absence of one mol equiv of Cu(II), compound **3** binds to DNA with significantly higher affinity than compound **4**. Thus, the data are consistent with our observation that compound **3** generates higher levels of photocleavage.

Chapter 3 describes the salt dependent enhancement in photo-degradation of supercoiled, nicked circular and linear forms pUC19 plasmid DNA to high mobility fragments by a 9-aminomethyl anthracene chromophore, **4**.[2] UV-visible, thermal melting analysis and circular dichroism results showed that, in the absence of physiological concentration of 150 mM NaCl and 260 mM KCl, the chromophore forms an intercalative complex with calf thymus DNA. In the presence of the combination of salts, circular dichroism data indicate a correlation between salt induced unwinding of the DNA duplex and the photocleavage enhancement. UV-visible and

fluorescence spectral data show that binding mode of the anthracene changes from intercalation to external interactions that facilitate the production of DNA damaging singlet oxygen and hydroxyl radicals.

Chapter 4 described the results of photocleavage studies at physiological nuclear concentrations of NaCl and KCl of a 9-aminomethyl bis anthracene (**2**) and its mono anthracene analogue (**4**).[3] The studies found that at high anthracene to DNA molar ratios, both the bis and mono anthracenes generated photocleavage under ionic strength concentrations that mimic those found in the cell nucleus. Under these conditions, pUC19 plasmid DNA was converted from its nicked circular and linear forms to high mobility DNA fragments. UV-visible, circular dichroism, thermal melting and viscometric titration data indicate that this enhancement in photocleavage can be attributed to a change in binding mode from intercalation under low ionic strength to a groove binding mode of interaction in the presence of the salts.

In Chapter 5, a series of pentamethine linked carbocyanine dyes (**9** – **15**) were synthesized and examined for their DNA binding affinity and photonuclease properties.[4] UV-visible spectroscopic studies support the formation of groove or externally bound carbocyanine DNA complexes that support and facilitate the efficient photocleavage of the supercoiled plasmid DNA. Photocleavage studies show that the halogenated methyl and TMAB analogues (**10**, **11**) and (**13**, **14**), respectively, efficiently convert supercoiled plasmid DNA to its nicked circular and linear forms following irradiation at wavelengths of light in the PDT phototherapeutic window. Photocleavage inhibition studies using the singlet oxygen scavenger sodium azide and the hydroxyl radicals scavenger sodium benzoate show that both ROS are generated during the photocleavage process.

The overall goals of this dissertation were elucidate the mechanisms of photo-induced DNA damage and DNA binding interactions of three classes of chromophores: acridine, anthracene, and carbocyanine. By using a combination of photochemical experiments and various spectroscopic techniques we were able to characterize these compounds with the intention that the insights gained from this work could be used in an effort to create second generation PDT agents.

6.1 References

1. Grant, K. B.; Terry, C. A.; Gude, L.; Fernández, M.-J.; Lorente, A., Synthesis and DNA photocleavage by a pyridine-linked bis-acridine chromophore in the presence of copper(II): Ionic strength effects. *Bioorg. Med. Chem. Lett.* **2011,** *21* (3), 1047-1051.

2. Terry, C. A.; Fernández, M.-J.; Gude, L.; Lorente, A.; Grant, K. B., Physiologically Relevant Concentrations of NaCl and KCl Increase DNA Photocleavage by an N-Substituted 9-Aminomethylanthracene Dye. *Biochemistry* **2011,** *50* (47), 10375-10389.

3. Grant, K., B.; Sawoo, S.; Mapp, C. T.; Williams, D. E.; Gude, L.; Fernández, M.-J.; Lorente, A., Bis- and Mono-9-aminomethylanthracene Dyes: The Effects of Chloride Salts on DNA Interactions and Photocleavage. *Eur. J. Med. Chem.* **2013**.

4. Mapp, C. T.; Owens, E. A.; Henary, M.; Grant, K. B., The Oxidative Cleavage of DNA using Pentamething-linked Cyanine Dyes as Sensitizers. *Bioorg. Med. Chem. Lett.* **2013**.